# DESIGN AND TESTING OF A DEFLECTOR INTEGRATED CROSS AXIS WIND TURBINE

WAN KHAIRUL MUZAMMIL BIN ABDUL RAHIM

FACULTY OF ENGINEERING
UNIVERSITY OF MALAYA
KUALA LUMPUR

2018

# DESIGN AND TESTING OF A DEFLECTOR INTEGRATED CROSS AXIS WIND TURBINE

**WAN KHAIRUL MUZAMMIL BIN ABDUL RAHIM**

**THESIS SUBMITTED IN FULFILMENT OF THE REQUIREMENTS FOR THE DEGREE OF DOCTOR OF PHILOSOPHY**

**FACULTY OF ENGINEERING**
**UNIVERSITY OF MALAYA**
**KUALA LUMPUR**

**2018**

**UNIVERSITY OF MALAYA**

**ORIGINAL LITERARY WORK DECLARATION**

Name of Candidate: **Wan Khairul Muzammil bin Abdul Rahim**

Matric No: **KHA120136**

Name of Degree: Doctor of Philosophy

Title of ~~Project Paper/Research Report/Dissertation~~/Thesis ("this Work"):

**Design and Testing of a Deflector Integrated Cross Axis Wind Turbine**

Field of Study: **Energy**

I do solemnly and sincerely declare that:

(1) I am the sole author/writer of this Work;
(2) This Work is original;
(3) Any use of any work in which copyright exists was done by way of fair dealing and for permitted purposes and any excerpt or extract from, or reference to or reproduction of any copyright work has been disclosed expressly and sufficiently and the title of the Work and its authorship have been acknowledged in this Work;
(4) I do not have any actual knowledge nor do I ought reasonably to know that the making of this work constitutes an infringement of any copyright work;
(5) I hereby assign all and every rights in the copyright to this Work to the University of Malaya ("UM"), who henceforth shall be owner of the copyright in this Work and that any reproduction or use in any form or by any means whatsoever is prohibited without the written consent of UM having been first had and obtained;
(6) I am fully aware that if in the course of making this Work I have infringed any copyright whether intentionally or otherwise, I may be subject to legal action or any other action as may be determined by UM.

Candidate's Signature Date:

Subscribed and solemnly declared before,

Witness's Signature Date:

Name:

Designation:

**DESIGN AND TESTING OF A DEFLECTOR INTEGRATED CROSS AXIS WIND TURBINE**

## ABSTRACT

The consequences of global modernisation have increased the demand for energy, which led to the interests for alternative energies, such as wind energy. However, in unfavourable wind conditions, factors such as low wind speed, high turbulence and wind direction variations can reduce the performance of horizontal axis wind turbines (HAWT). Certain vertical axis wind turbine (VAWT) design perform well under these harsh operating conditions, but these wind rotors typically have low power coefficients. To overcome these problems, a novel design of deflector integrated cross axis wind turbine (CAWT) is proposed. This is achieved through improved design of the wind rotor via harnessing wind energy from both the horizontal and vertical components of the oncoming wind by using the deflector. Experiments using deflectors to guide the oncoming airflow upward were designed to test the CAWT performance with various inclination angles. Different horizontal blade pitch angles CAWT were also fabricated to ascertain their characteristics. A conventional Darrieus VAWT was tested under the same experimental conditions for benchmarking purposes. It was found that the CAWT's peak power coefficients, $C_P$ integrated with the 45° deflector were increased significantly by 103, 154, 172 and 175% at tip speed ratios, TSRs of 0.70, 0.87, 0.92 and 0.93 for horizontal blade pitch angles, $\beta$ of 0°, 5°, 10° and 15°, respectively. The same configuration CAWTs recorded the highest improvement of rotor rotational speeds amongst the other configurations with 363.1 rpm (78.0%), 433.1 rpm (112.3%), 412.5 rpm (102.2%) and 347.5 rpm (70.3%), respectively. Several unique characteristics of the CAWT and VAWT were observed. Firstly, the CAWTs in bare configurations produced higher power output compared to the VAWT, except for the 15° pitch angle CAWT. Then, the use of deflectors enhanced the performance of the CAWTs. However, the

performance of the VAWT was observed to decline by 19% after the deflectors were integrated. Lastly, the data from the experiments showed that the torque coefficient, $C_Q$ of the 15° pitch angle CAWT integrated with the deflector is 87% higher than the VAWT, suggesting that the CAWT has a better ability to self-start in low wind speed and skewed wind conditions. A semi-empirical approach was also developed to analyse the performance of the CAWT. The aerodynamic behaviour of the CAWT was determined by combining the blade element momentum (BEM) and double multiple stream tube (DMST) models. The approach emphasised on the blade aerodynamics, inflow distribution, and torque distribution around the rotor. Moreover, the approach showed notable agreement between the experimental and analytical results. Finally, the feasibility of wind augmenting device as a compact on-site renewable energy generation system was explored with the omni-direction-guide-vane (ODGV) and a VAWT. The ODGV acts as a wind concentrator, whereby the wind energy output was increased by 3.48 times in comparison to a conventional rotor. By integrating the ODGV with a VAWT, the annual operating hours and energy generated from the system in Sepang and Subang can be increased by 41% and 438%, and 25% and 305%, respectively.

Keywords: Cross axis wind turbine; Wind energy; Renewable energy; Urban energy system; On-site energy generation system.

***DESIGN AND TESTING OF A DEFLECTOR INTEGRATED CROSS AXIS WIND TURBINE***

## ABSTRAK

Permintaan tenaga yang tinggi akibat daripada pemodenan global telah membawa kepada kepentingan tenaga alternatif, contohnya tenaga angin. Tetapi, dalam keadaan angin yang tidak menentu, faktor-faktor seperti kelajuan angin yang rendah, pergolakan tinggi, dan perubahan berterusan arah angin mengurangkan prestasi turbin angin paksi mendatar (HAWT). Reka bentuk turbin angin paksi menegak (VAWT) yang tertentu boleh beroperasi dengan baik di bawah keadaan angin yang tidak menentu itu. Tetapi, turbin angin jenis VAWT biasanya mempunyai pekali kuasa yang rendah. Untuk mengatasi masalah ini, satu reka bentuk novel turbin angin bersilang paksi (atau CAWT) digabungkan dengan pemesong telah dicadangkan. Ini dicapai melalui reka bentuk turbin angin yang lebih baik melalui penggunaan tenaga angin dari dua komponen angin yang berlainan, iaitu mendatar dan menegak yang terhasil daripada pemesong. Eksperimen menggunakan pemesong menghalakan aliran udara ke arah menegak direka untuk menguji prestasi CAWT dengan sudut kecenderungan yang berbeza. Eksperimen juga dijalankan dengan bilah bersudut condong berbeza untuk mengenal pasti ciri-ciri bilah mendatar CAWT tersebut. VAWT jenis Darrieus telah dipilih dan diuji di bawah keadaan eksperimen sama sebagai penanda aras. Berdasarkan keputusan eksperimen, pekali kuasa puncak bagi CAWT yang terintegrasi dengan pemesong 45° telah meningkat dengan ketara sebanyak 103, 154, 172 dan 175% pada nisbah kelajuan hujung (atau TSR) 0.70, 0.87, 0.92 dan 0.93 untuk bilah bersudut condong, $\beta$ daripada 0°, 5°, 10°, dan 15°, masing-masing. Konfigurasi yang sama turut menunjukkan peningkatan yang ketara dalam kelajuan pusingan dengan 363.1 rpm (78.0%), 433.1 rpm (112.3%), 412.5 rpm (102.2%) and 347.5 rpm (70.3%), masing-masing. Beberapa ciri unik CAWT dan VAWT telah berjaya diperhatikan. Pertama, CAWT dalam konfigurasi tanpa pemesong

menghasilkan kuasa yang lebih tinggi berbanding dengan VAWT, kecuali bagi CAWT dengan bilah mendatar bersudut 15°. Kemudian, penggunaan pemesong meningkatkan prestasi CAWT. Tetapi, prestasi VAWT didapati telah menurun sebanyak 19% selepas digabungkan dengan pemesong. Terakhir, data daripada eksperimen menunjukkan bahawa pekali tork bagi CAWT dengan bilah mendatar bersudut 15° terintegrasi dengan pemesong adalah 87% lebih tinggi daripada VAWT. Ini menunjukkan bahawa CAWT mempunyai keupayaan yang lebih baik untuk mula berputar di kawasan kelajuan angin rendah dan dalam keadaan aliran condong. Pendekatan separa empirikal juga dibangunkan untuk menganalisa prestasi CAWT. Ciri-ciri aerodinamik CAWT ditentukan dengan menggabungkan model momentum unsur bilah (BEM) dan model aliran tiub dwiganda (DMST). Pendekatan ini mengenalpasti kepentingan aerodinamik turbin dan pemodelan dalam pendekatan bersepadu, menekankan keperluan aerodinamik bilah lokal, pengedaran aliran masuk, serta tork di sekitar turbin. Selain itu, pendekatan ini menunjukkan persetujuan yang baik antara keputusan eksperimen dan model yang dibangunkan. Akhirnya, kebolehlaksanaan peranti penambahan angin sebagai sistem penjanaan tenaga diterokai melalui penggunaan *omni-direction-guide-vane* (ODGV) dengan VAWT. ODGV bertindak sebagai penumpu angin, di mana output tenaga angin meningkat sebanyak 3.48 kali ganda berbanding dengan VAWT tanpa ODGV. Penggunaan ODGV dengan VAWT menunjukkan jam operasi tahunan dan tenaga yang dihasilkan oleh sistem di Sepang dan Subang boleh ditingkatkan masing-masing sebanyak 41% dan 438%, dan 25% dan 305%.

Kata kunci: *Cross axis wind turbine*; Tenaga angin; Tenaga boleh diperbaharui; Sistem tenaga bandar; Sistem penjanaan tenaga di tapak.

## ACKNOWLEDGEMENTS

All praises and thanks be to God for strength and protection during my journey to the completion of this thesis. I would like to say my thanks to my supervisor, Assoc. Prof. Dr. Chong Wen Tong, and co-supervisors, Dr. Ong Hwai Chyuan and Prof. Dato' Dr. Kamaruzzaman Sopian; without their guidance, critics, and persistent help this thesis would not have been possible. I also would like to thank all the researchers and staff in the Faculty of Engineering, University of Malaya, especially my laboratory mates with their assistance and advice through many brainstorming sessions for conducting this research. I also would like to seize this opportunity to thank the University of Malaya for their financial support granted through the PPP research grant (PG052-2014A). To my dear friend Deanna Beryl Majilang, I would be forever thankful to you, without whom I shall never find my muse all those years ago. It is my greatest honor and joy to mention Farida Hanum Rasip, my beloved wife, whose constant support, encouragement, and love has been my source of energy and motivation. You never cease to amaze me with your strength and passion, and your positivity have carried me through, in times of happiness and sorrow. Finally yet importantly, to my family and my in-laws who have supported me throughout the entire process, by granting me a harmonious and joyous life, and helping me to put all the pieces together, I shall be forever grateful for your love.

## TABLE OF CONTENTS

## LIST OF FIGURES

## LIST OF TABLES

## LIST OF SYMBOLS AND ABBREVIATIONS

| | | | |
|---|---|---|---|
| $A$ | : | Swept area | [m$^2$] |
| $a$ | : | Axial induction factor | [-] |
| $a'$ | : | Radial induction factor | [-] |
| $B$ | : | Number of horizontal blades | [-] |
| BIWT | : | Building integrated wind turbine | [-] |
| BEM | : | Blade element momentum | [-] |
| $c$ | : | Chord length of vertical blade | [mm] |
| $c_b$ | : | Chord length of horizontal blade | [mm] |
| CAWT | : | Cross axis wind turbine | [-] |
| $C_n$ | : | Normal coefficient; $C_n = C_L \cos\alpha + C_D \sin\alpha$ | [-] |
| $C_t$ | : | Tangential coefficient; $C_t = C_L \sin\alpha - C_D \cos\alpha$ | [-] |
| $C_L$ | : | Lift coefficient | [-] |
| $C_D$ | : | Drag coefficient | [-] |
| $C_T$ | : | Thrust coefficient | [-] |
| $C_Q$ | : | Torque coefficient; $C_Q = C_P/\lambda = Q/(0.5\rho ARV_\infty^2)$ | [-] |
| $C_P$ | : | Power coefficient; $C_P = P/(0.5\ \rho AV_\infty^3)$ | [-] |
| $d$ | : | Diameter of rotor | [m] |
| DMST | : | Double multiple stream tube | [-] |
| $F_D$ | : | Drag force; $F_D = \frac{1}{2}\rho U_T^2 C_D c$ | [N] |
| $F_L$ | : | Lift force; $F_L = \frac{1}{2}\rho U_T^2 C_L c$ | [N] |
| $h$ | : | Height of vertical blade | [m] |
| HAWT | : | Horizontal axis wind turbine | [-] |
| $l_b$ | : | Length of horizontal blade | [mm] |

| | | | |
|---|---|---|---|
| $\dot{m}$ | : | Mass flow rate | [$m^3/s$] |
| $N$ | : | Number of vertical blades | [-] |
| NACA | : | National Advisory Committee for Aeronautics | [-] |
| ODGV | : | Omni-direction-guide-vane | [-] |
| $P$ | : | Wind turbine power; $P = 0.5C_P\rho AV_\infty^3$ | [W] |
| $p$ | : | Pressure | [Pa] |
| $Q$ | : | Torque; $Q = 0.5C_Q\rho ARV_\infty^2$ | [Nm] |
| $R$ | : | Rotor radius | [m] |
| $\Delta S$ | : | Speed-up factor; $\Delta S = (V_Z - V_\infty)/V_\infty$ | [-] |
| $T$ | : | Thrust force | [N] |
| $U_T$ | : | Effective velocity | [m/s] |
| $V$ | : | Wind velocity | [m/s] |
| VAWT | : | Vertical axis wind turbine | [-] |

*Greek letters*

| | | | |
|---|---|---|---|
| $\beta$ | : | Vertical blade pitch angle | [°] |
| $\beta_b$ | : | Horizontal blade pitch angle | [°] |
| $\rho$ | : | Density | [$kg/m^3$] |
| $\omega$ | : | Angular velocity | [-] |
| $\alpha$ | : | Angle of attack (AOA) | [°] |
| $\theta$ | : | Azimuth angle | [°] |
| $\lambda$ | : | Tip speed ratio (TSR) | [rad/s] |
| $\sigma$ | : | Wind turbine solidity | [-] |
| $\zeta$ | : | Torque contribution at selected span locations | [%] |
| $\gamma$ | : | Skew angle | [°] |
| $\varphi$ | : | Inflow angle | [°] |

*Subscripts*

| | | | |
|---|---|---|---|
| $\infty$ | : | Free stream | [-] |
| $a$ | : | Induced velocity | [-] |
| $b$ | : | Horizontal blade components | [-] |
| $d$ | : | Downstream | [-] |
| $e$ | : | Equilibrium | [-] |
| $i$ | : | Instantaneous | [-] |
| $o$ | : | Vertical component of wind velocity | [-] |
| $R$ | : | Relative velocity | [-] |
| $t$ | : | Transformed vectors | [-] |
| $u$ | : | Upstream | [-] |
| $z$ | : | Location above the local deflector surface | [-] |

## LIST OF APPENDICES

# CHAPTER 1: INTRODUCTION

## 1.1 Overview

Harnessing wind energy provides a means to reduce dependencies on fossil fuel reserves. With the rapid growth of the global human population, the demand for energy also increases. Therefore, many countries around the world have adopted renewable energy technology to generate clean and inexhaustible energy to fulfil their ever-increasing electricity demands. In some places, i.e. Mecklenburg-Vorpommern, Germany; Aspen, Colorado, United States; and Schleswig-Holstein, Germany; 100% of their average yearly demand is provided by renewable energy resources (MacPherson, 2014; Reuters, 2014; Robbie, 2015). As one of the fastest growing renewable energy resources in the world today (Gipe, 2004), the global cumulative installed wind capacity has been increased significantly since 1996. The total wind power capacity at the end of the year 2017 was about 539 GW (Global Wind Energy Council, 2018) (Figure 1.1). It is projected to reach 2000 GW by the year 2030, supplying between 17-19% of global electricity demand.

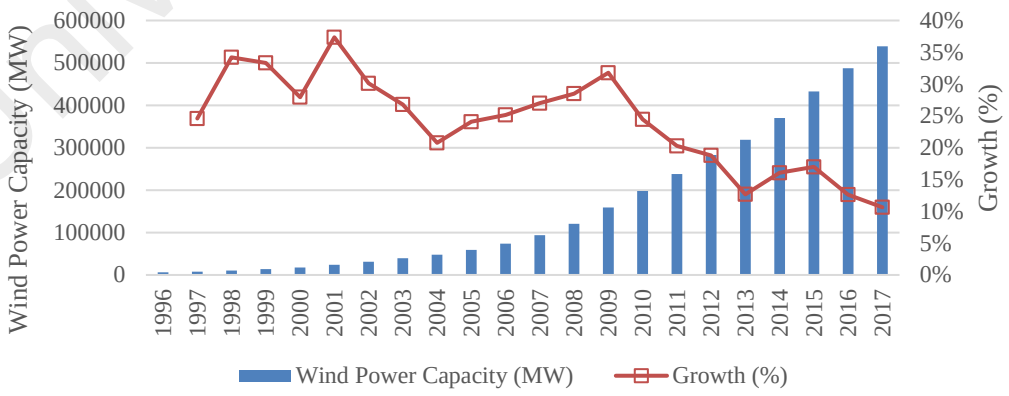


**Figure 1.1: Total installed wind power capacity (MW) and market growth rate (%) from the year 1996 to 2017**

(Global Wind Energy Council, 2018)

Several classes of wind energy have been recognised by the National Renewable Energy Lab (NREL) based on the potential wind power density (WPD). The WPD signifies the region's potential for wind energy based on the mean wind speed at predetermined heights. As shown in Table 1.1, areas of Class 7 have the highest power density with a range of 400-1000 W/m$^2$ (mean wind speed: 7-9.4 m/s at 10 m height). Whereas, areas of Class 1 have the lowest power density with a range of 0-100 W/m$^2$ (mean wind speed: 0-4.4 m/s). As logic dictates, the implementation of wind energy devices must be prioritised for areas with the higher average wind speed. Current commercial wind turbines are also limited to regions with Class 3 or higher WPDs. However, due to the on-site energy demand of future cities, the placement of wind energy devices would be nearer to or in the urban areas. Lower WPD class regions are usually found in the urbanised areas, and therefore the installed wind turbines in cities or towns are smaller. Recently, there is an increasing trend of small and medium scale wind turbines installed in the urban areas due to many factors, such as the wind conditions, noise pollution, aesthetic and structural safety issues. Therefore, small wind turbines in the context of integration in an urban environment are considered one of the most promising technologies for the efficient diffusion of renewable energy sources.

**Table 1.1: Wind power density regional classes at heights of 10 m and 50 m**

| Class | 10 m | | 50 m | |
|---|---|---|---|---|
| | Wind power density (W/m$^2$) | Wind speed (m/s) | Wind power density (W/m$^2$) | Wind speed (m/s) |
| 1 | 0-100 | 0-4.4 | 0-200 | 0-5.6 |
| 2 | 100-150 | 4.4-5.1 | 200-300 | 5.6-6.4 |
| 3 | 150-200 | 5.1-5.6 | 300-400 | 6.4-7.0 |
| 4 | 200-250 | 5.6-6.0 | 400-500 | 7.0-7.5 |
| 5 | 250-300 | 6.0-6.4 | 500-600 | 7.5-8.0 |
| 6 | 300-400 | 6.4-7.0 | 600-800 | 8.0-8.8 |
| 7 | 400-1000 | 7.0-9.4 | 800-2000 | 8.8-11.9 |

(Elliot, Holladay, Barchet, Foote, & Sandusky, 1986)

In the wind energy industry, there are two major types of wind turbines; the horizontal axis wind turbine (HAWT) and the vertical axis wind turbine (VAWT). In general, the HAWTs are better at extracting wind energy than the VAWT. Therefore, the HAWT machines dominate most wind turbines in the commercial market today. However, new interests in the VAWT technology from researchers and manufacturers have reignited significant development efforts for this wind turbine (Mohamed, 2012; Tjiu, Marnoto, Mat, Ruslan, & Sopian, 2015a, 2015b). In some situations, the VAWT has superior advantages over the HAWT, including its ability to extract wind energy from almost every direction, easier to maintain, has less visual impact, produce low noise emissions and can work with improved performance in skewed wind flow conditions (Balduzzi, Bianchini, Carnevale, Ferrari, & Magnani, 2012; Eriksson, Bernhoff, & Leijon, 2008b; Mohamed, 2014; Peacock, Jenkins, Ahadzi, Berry, & Turan, 2008). The complex characteristic of urban winds involves erratic, insubstantial and inconsistent wind flow due to the many obstacles (i.e. buildings). The distinctive characteristic of urban wind requires wind turbines that suit this phenomenon well. As such, the VAWT is deemed more suitable for the urban context compared to the large and more common HAWT (Balduzzi et al., 2012).

### 1.1.1 Energy scenario in Malaysia

Before the 1980s, the primary energy source in Malaysia was oil with an energy share of up to 71.9% (see Figure 1.2 and Table 1.2). During the international energy crisis of 1973-1974 (oil embargo by Arab nations), the interest on wind turbines and other alternative energy technologies were renewed. In 1981, the Malaysian government introduced the Four-Fuel Diversification Strategy to reduce dependencies on oil as a source of energy. Oil, natural gas, coal and hydropower were identified as the four fuel types to diversify the nation's energy supply mix. Figure 1.2 shows the trend of energy supply mix in Malaysia from 1978 to 2013. Since the introduction of the Four-Fuel

Diversification Strategy in 1981, natural gas has gradually become the primary source of energy supply for the country. In 2013, natural gas contributed about 47.1% of the total energy mix in Malaysia. The government of Malaysia in its Eighth Malaysian Plan (2001-2005) has included renewable energy as the nation's Fifth Fuel. The plan to include renewable energy as one of the fuel mixes in Malaysia energy supply was further established in the Ninth Malaysia Plan (2006-2010). In the Ninth Malaysia Plan, the government aimed to deliver 350 MW of renewable energy generation capacity connected with the national grid. However, the current renewable energy capacity contribution is still insignificant when compared to the total power generation in the country. Referring to Table 1.2, hydropower contributed less than 5% in the electrical generation since 1978. Since then, there are still no significant changes to tackle the high usage of fossil fuel reserves in the country. Moreover, the now defunct Small Renewable Energy Power (SREP) programme introduced in 2001 has failed to intensify the renewable energy industry in Malaysia. In 2011, a new Feed-in Tariff (FiT) system was announced with a plan to create 2080 MW grid-connected renewable energy or 11% share of the total national energy generation by 2020. The projection of the renewable energy mix translates to an estimated cumulative of 45.7 million tonnes of CO2 equivalent emission mitigated by 2020 (Umar, Jennings, & Urmee, 2013). The success of the plan remained to be unseen if the current trend of energy production is still unchanged.

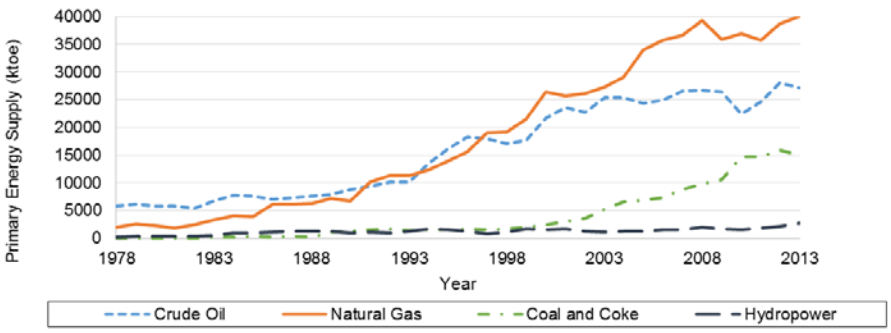


**Figure 1.2: Primary energy supply in Malaysia from 1978 to 2013**

(Malaysia Energy Information Hub, n.d.)

**Table 1.2: Summary of Malaysian primary energy supply share**

| Year | Crude Oil (%) | Natural Gas (%) | Coal and Coke (%) | Hydropower (%) |
|---|---|---|---|---|
| 1978 | 71.9 | 24.8 | 0.3 | 3.0 |
| 1990 | 49.3 | 38.2 | 7.4 | 5.1 |
| 2000 | 41.6 | 50.6 | 4.8 | 3.0 |
| 2010 | 29.7 | 48.7 | 19.5 | 2.1 |
| 2011 | 32.0 | 46.4 | 19.2 | 2.4 |
| 2012 | 33.2 | 45.6 | 18.7 | 2.5 |
| 2013 | 32.0 | 47.1 | 17.8 | 3.2 |

(Malaysia Energy Information Hub, n.d.)

The installations of renewable energy systems in Malaysia can be mainly found in rural areas to increase the country's electrification coverage rate (Hossain, Hasanuzzaman, Rahim, & Ping, 2015). From 2004 to 2010, the total installed capacity of renewable hybrid energy systems in Malaysia was 5520 kW (Ministry of Rural and Regional Development, 2012). Out of the total, 85% of the installed capacity was contributed by hybrid solar systems (integration of solar and other power sources). The rest was contributed by a wind-solar-diesel hybrid power generation system installed in Perhentian Kecil, which is an island located on the northeastern coast of Peninsular Malaysia, near Terengganu. In 2013, a solar-diesel hybrid plant having a capacity of 1.5 MW was installed on an island in East Malaysia and is distributed across nine islands (IBC Solar, 2013). The statistics have shown that the remote and sparsely populated islands in some parts of Malaysia are more suitable for renewable power plants instead of the island-wide power grid, particularly the use of wind-solar hybrid systems. A feasibility study conducted on the optimum green energy systems for island resorts in Malaysia found that the use of a renewable energy system (200 kW solar energy and 40 kW wind energy) can supply the load demands of all villagers and tourists (Ashourian et al., 2013). Another existing study shows that the combination of the wind-solar-battery hybrid renewable energy system is a cost-effective power source for villages in Malaysia (Fadaeenejad, Radzi, Ab Kadir, & Hizam, 2014). Based on the review, implementation

of wind energy generation systems in Malaysia is often overlooked. This is because Malaysia experiences relatively low wind speed of less than 4 m/s throughout the year, which is much lower than the required rated wind speed for conventional wind turbines (Kamaruzzaman & Tamer, 2013). In another study, it was found that Mersing has the highest monthly wind speed in the country with a wind speed of 5.4 m/s and capacity factor of 4.39%. However, by using numerical weather prediction (NWP) models for mesoscale winds to forecast wind characteristics, it was found that there is economic potential for wind energy in Malaysia (Nor, Shaaban, & Abdul Rahman, 2014). Therefore, it is hopeful that the diffusion of wind energy can be more recognised in the country for its potential.

### 1.1.2 Global status of small wind turbine

Small wind world market is growing at a slow pace in terms of installations. A report published in 2017 showed that there was a shortfall of small wind turbine installations back in 2013 (Gsänger & Pitteloud, 2017). However, the market was recovered in 2014 and was growing slowly. As of the end of 2015, the cumulative total of installed wind turbines in the world is at least 990,000 units, which was an increase of 5% compared with the previous year (as shown in Figure 1.3).

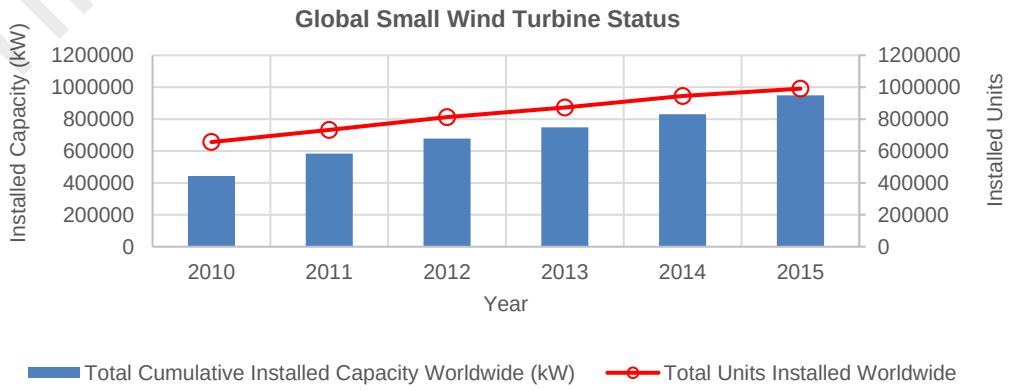


**Figure 1.3: Status of small wind turbine in terms of installed capacity and units**

(Gsänger et al., 2017)

Based on another report by Gsänger and Pitteloud (2014) and shown in Figure 1.4, there is no commercial manufacturer of wind turbine operating in the South-East Asian region. China and the USA are the only two countries that have more than 50 manufacturers of wind turbine technology. Five countries (the USA, the UK, Germany, China, and Canada) account for more than 50% of small wind manufacturers. Developing countries, such as in the South-East Asian region continue to be left behind in terms of the manufacturing of wind turbines. Moreover, the mean wind speed potential in this region is low as shown in Figure 1.5 (< 4 m/s), with wind power density of approximately less than 40 W/m$^2$. This would indicate that the South-East Asian countries are suitable for Class 1 wind turbine installations. Apart from having low wind speeds, due to the difference in temperature between the land and sea (and therefore creating a pressure difference), the winds in this region experience frequent direction changes and turbulent.

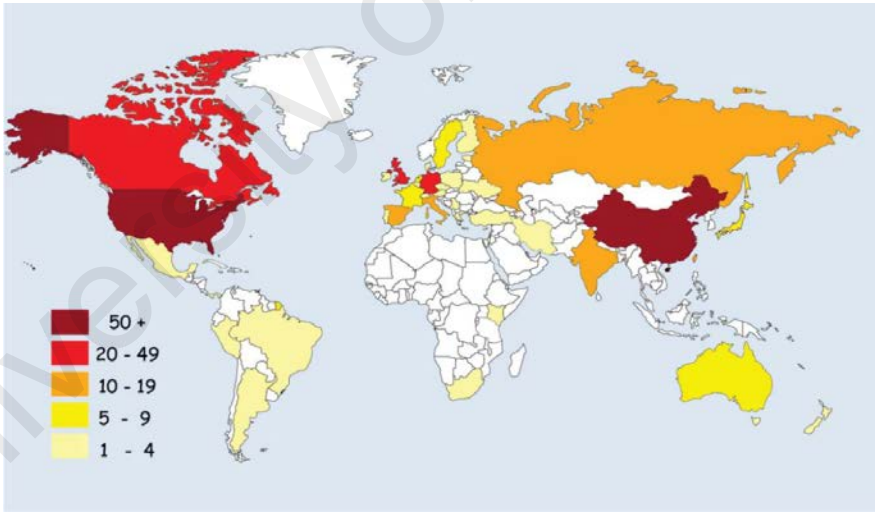


**Figure 1.4: Distribution map of small wind turbine manufacturer**

(Gsänger et al., 2014)

The characteristics of wind in Malaysia and her neighbouring countries require a wind turbine that can self-start and omnidirectional. Therefore, the vertical axis wind turbine is more suitable to be deployed in this region than the horizontal axis wind turbine.

However, the HAWT technology has been dominating the wind energy market for over 30 years. At the end of 2011, out of 327 small wind turbine manufacturers, 74% invested in the HAWT technology, while only 18% adopted the VAWT. Even when the majority of the current VAWT models were developed in the past seven years, the market share for the small wind turbine technology remains insignificant. This is due to the lower capacity of the turbine, and much of the large-scale wind turbines are adopted in wind farms.

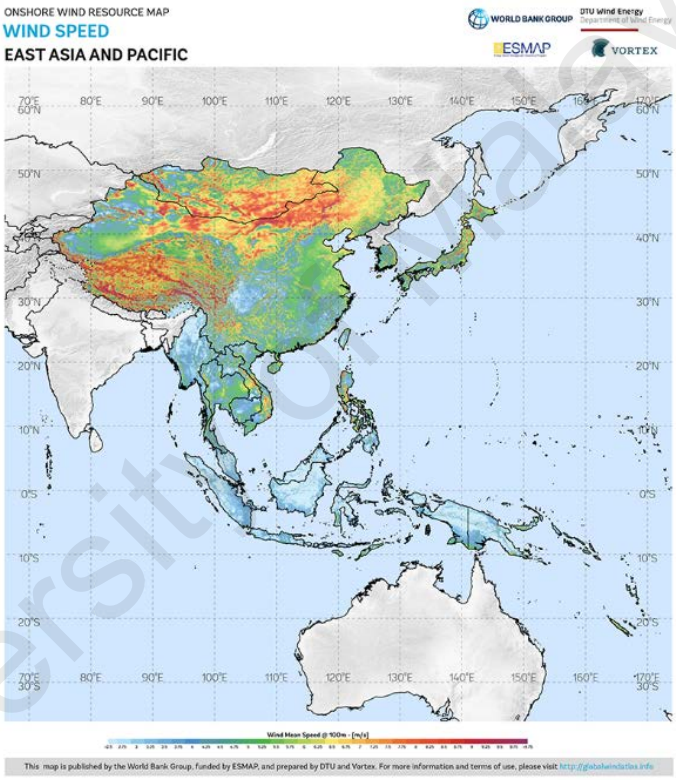


**Figure 1.5: Wind atlas in East-Asia and Pacific**

(Global Wind Atlas, n.d.)

## 1.2 Problem Statement

As mentioned, the characteristics of wind in tropical countries, such as Malaysia requires a wind turbine that is able to self-start in low wind speed areas. The wind turbine must also be designed for areas with gusty and turbulent winds. Based on these criteria, the VAWT has the better potential for maximum exploitation of wind energy in this

region. The VAWT has two basic types according to the aerodynamic force characteristics that act upon their blades, i.e. lift and drag-based wind turbines (Islam, Ting, & Fartaj, 2008b). Savonius wind turbine is one type of a drag-based wind rotor. The Savonius turbine relies on the drag force to move two cups affixed to a shaft in opposite rotations. Meanwhile, the Darrieus wind rotor is a lift-type vertical axis wind turbine that uses lift forces generated by the interaction of wind on the airfoil to rotate. A lift-type wind turbine has better performance output and efficiency compared to the Savonius turbine (Ricci, Romagnoli, Montelpare, & Vitali, 2016; Roy & Saha, 2015). However, issues such as poor self-starting characteristic affect the overall performance of the turbine (Mohamed, Janiga, Pap, & Thévenin, 2010). Nevertheless, new studies have shown that the modern Darrieus VAWT design can ensure self-starting by optimising the number of blades, exploiting new and improved airfoil shape, or by implementing minimum loading on the rotor (Bianchini, Ferrari, & Magnani, 2011; Dominy, Lunt, Bickerdyke, & Dominy, 2007; Worasinchai, Ingram, & Dominy, 2015).

As mentioned, the significant disadvantage of the VAWT is in terms of its efficiency in extracting power from the wind. The lower efficiency of the VAWT is due to the unstable operating conditions of the turbine at all wind speeds, caused by the periodic variation of the rotor and the direction of the apparent wind velocity perceived by the blades (Brahimi, Allet, & Paraschivoiu, 1995). Moreover, as the VAWT rotates, the interactions between wakes shed by the blades rotating in the upwind and downwind regions of the rotor causes dynamic and reliability issues in which the blades have to go through a dynamic stall in every revolution (Simao Ferreira, van Zuijlen, Bijl, van Bussel, & van Kuik, 2010). Intrinsically, the aerodynamic phenomena manifested in VAWTs present challenging tasks for researchers to understand the complex fluid mechanics of such devices to estimate their performances (Almohammadi, Ingham, Ma, & Pourkashan, 2013; Daróczy, Janiga, Petrasch, Webner, & Thévenin, 2015; Salvadore, Bernardini, &

Botti, 2013). New concepts of vertical axis wind energy devices are being introduced to overcome the disadvantages of the conventional design of VAWTs. Some of these wind turbine concepts are being adopted in the design of the building (Li, Shu, & Chen, 2016; Meinhold, 2010; Sharpe & Proven, 2010), augmented with shrouds (Allaei & Andreopoulos, 2014; Chong et al., 2013a; Chong, Fazlizan, Poh, Pan, & Ping, 2012a; Chong et al., 2013c; Park, Chung, & Park, 2016; Ying, Chen, Xu, & Tian, 2015), or mounted on top of a building for maximum utilisation of wind energy (Chong et al., 2013a; Yang et al., 2016). The pertinent question then becomes; at the forefront of conventional wind turbine technology, particularly the VAWT–how do we innovate the conventional design to make it more efficient and to possess superior performance characteristics in any wind condition? For wind turbine designers, the critical knowledge lies in the thorough understanding of the workings of a wind turbine, which includes aerodynamics of wind rotors, the geometrical aspects of the wind rotors, the importance of airfoil profiles, and the design of the wind rotor. Hence, this study aims to introduce a novel type of wind turbine that can maximise the energy potential of oncoming wind. Called the cross axis wind turbine (CAWT), the rotor design takes advantage of the qualities of both the HAWT and the VAWT while overcoming their respective drawbacks. The design of the CAWT is well suited for the unpredictable nature of complex wind flows in an urban environment. The airfoil-shaped struts of the CAWT enable the rotor to extract wind energy from the vertical and horizontal components of the oncoming winds (skewed airflow). The airfoil-shaped struts incorporated in the CAWT design improve the performance of the rotor by fully utilising the undisturbed portion of the skewed flow both in the downwind and upwind regions of the turbine. The disadvantages of HAWT and VAWT in comparison to the CAWT are based on their utilisation of wind energy from the velocity components of the oncoming wind. The HAWT relies on one horizontal wind direction, therefore requiring a yaw mechanism to

rotate the wind turbine. The VAWT, however, is an omnidirectional device that primarily accepts wind from any horizontal wind direction. Also, the HAWT's nacelle houses all the generating components of the wind turbine, which includes the generator, drive train, gearbox, and brake assembly. Hence, the HAWT's centre of gravity is usually located high above the ground, which would create some stability issues in offshore applications.

## 1.3 Research Objectives

The main objective of this research is to study the feasibility of the concept of the deflector integrated cross axis wind turbine. Since the innovation in the concept is novel, and no recorded works on the particular design are found, the study explores the experimental and theoretical principal of the design. Therefore, the objectives of the research are listed as follows:

i. To investigate the performance of the cross axis wind turbine system with various pitch angles of the turbine's horizontal blades by experimental analysis.
ii. To analyse the effects of the deflector with various inclination angles on the performance of the cross axis wind turbine system.
iii. To determine the aerodynamic characteristics of the horizontal and vertical blades of the cross axis wind turbine by combining blade element momentum and double multiple stream tube models.
iv. To investigate the application of a wind-augmentation device called the omni-direction-guide-vane as a renewable energy generation system for the vertical axis wind turbine.

## 1.4 Research Scope

Research in wind turbine aerodynamics are very complex and involve sophisticated methods. In the main research study, there are a few major components involved in the design, i.e. deflector, airfoil, and connector. These three elements can affect the rotor's

performance due to many parameters, and for each change made to one component would affect the others. Therefore, due to the nature of the research, there are several limitations in conducting the study:

i. For benchmarking purposes, a conventional, straight-bladed Darrieus VAWT with a common airfoil profile with a low peak tip speed ratio, TSR is selected. The chosen conventional VAWT has three NACA0015 blades operating with a low range of TSR (0 to 2). This rotor performance was benchmarked against the performance of the CAWT, and both of these two rotors have the same external blade geometrical properties.
ii. The performance of the rotors is the central aspect of the study to attain some insights into the characteristics of the cross axis wind turbine. Therefore, specific design parameters are not the focus of the current study, such as the design of the connectors, and the materials used for the rotors.
iii. The aerodynamic properties of the connectors and their effects are not within the scope of the current study.
iv. The pressure distribution profile of the oncoming winds will not be determined in the current study.
v. The features of the cross axis wind turbine are limited to various aspects, such as:
    - Similar external geometrical elements of the conventional Darrieus wind turbine, such as the size, the blade shape, and the airfoil profile.
    - Due to the limitation of the working area and the experimental rig, the study was conducted on small-scale turbines having the dimensions of 0.35 m (diameter) x 0.30 m (height).
    - Aerodynamic losses due to the end blades of the rotors (vertical and horizontal blades) will not be considered.

- Straight blade rotors are preferred due to simplicity in fabricating the prototypes and in calculating the aerodynamic forces from the blades.
- The symmetrical NACA0015 airfoil profile is used for the design of the cross axis wind turbine blades. This follows the airfoil blades of the conventional Darrieus VAWT.
- The vertical blades of the CAWT are fixed at 0º pitch angle. This configuration is the same for the VAWT.

vi. The case study of the omni-direction-guide-vane as a power generation system is limited to the analysis of the Darrieus VAWT. Further analysis involving the experimental works of ODGV with the CAWT is required to ascertain the wind rotor's performance integrated with ODGV.

## 1.5 Thesis Outline

Research in wind energy and aerodynamics are complex and involves sophisticated experimental design and theoretical studies. The deflector integrated cross axis wind turbine system can be considered as the first step in creating a better wind turbine with higher outputs than the conventional vertical axis wind rotor with the same size and external geometrical features. The study aims to show the concept of harnessing energy from both the vertical and horizontal directions of oncoming wind flows. To present the findings from the study clearly, the organisation of the thesis is as follows:

Chapter 1 introduces the research with an overview and some background of this research. Then, the problem statement and the objectives of the research follow them.

Chapter 2 presents the literature review where the state-of-the-art reviews of related studies regarding wind turbines are presented. The analytical and mathematical formulation of the aerodynamic study of wind turbines is shown in this Chapter. The

comprehensive review is done to justify and define the novelty of the current research works.

Chapter 3 covers the methodology of the study. Initially, the design of the cross axis wind turbine is described. This includes the fabrication of the wind turbine and the test rig. The methodologies, i.e. experimental steps and the theoretical procedures used in the research are then discussed. The application of a wind-augmentation device as a renewable energy generation system and its research parameters are also described.

Chapter 4 presents the discussions based on the results from the methodology presented in Chapter 3. This chapter includes the analysis of the cross axis wind turbine performance based on the configurations of the pitch angle of the horizontal blades and the effects of the deflector with various inclination angles. The evaluation of the theoretical performance of the cross axis wind turbine based on the proposed approach is then presented. The Chapter ends with some evaluation of the wind-augmentation device as a power generation system.

Chapter 5 concludes the thesis with a summary of the present work with recommendations for future studies.

## 1.6 Summary

The depletion of natural resources has increased the prices of fuel commodities to meet the demand for energy in the world. Since some countries and regions experience low wind speed with high variability and turbulent winds, it is imperative for wind turbine researchers to design wind turbines that can meet these extreme requirements to alleviate dependencies on fossil fuels. This chapter has discussed some introductory backgrounds of global wind energy status and types of wind turbines and their characteristics. Moreover, the research objectives, scope and limitations have also been established. The

following chapters offer more in-depth discussion, exploration and investigation of the novel wind turbine that would benefit the environment.

# CHAPTER 2: LITERATURE REVIEW

## 2.1 Introduction

Over the past few hundred years, wind energy technology has progressed from the use of bundles of straw to composite materials, and traditional calculations to computational techniques. Wind turbine shapes and efficiencies, however, have evolved very slowly. This chapter introduces the basic concepts and characterisation of the wind, wind energy and classification of wind turbines. Also, a review of the current development of wind turbine, skewed wind flow, and the aerodynamics of wind turbine are presented in this chapter.

## 2.2 Characteristics of Wind

The underlying driving force for air to move is due to the air pressure. The mass of overlying air in the atmosphere reduces with altitude. This reduction of air mass causes air pressure to decrease. Hence, the difference in air pressure between two regions (higher altitude and lower altitude) causes the air to move from higher to lower pressure regions. However, these vast regions of having alternately high and low-pressure gradients are formed by complex mechanisms. The movement of air masses can be interrelated with three different properties: pressure, density and temperature. This relationship is called the Equation of State, which can be expressed as:

$$p = R\rho\tau \tag{2.1}$$

where $p$ is pressure, $\rho$ is density, $\tau$ is temperature (in Kelvin), and $R$ is the specific gas constant. This relationship is vital in explaining the movement of air, in which any changes of a variable will cause changes to the others.

The atmosphere receives energy from the sun (short-wave radiation, including ultraviolet light) and also from the short-wave and long-wave radiations that are reflected off from the Earth's surface. This phenomenon creates a distinctive temperature profile within the atmosphere, which influences the densities of air. To further explain this relationship, Equation (2.1) can be rearranged as follows:

$$\rho = {}^{p}/_{R\tau} \tag{2.2}$$

where the density of air, $\rho$ is isolated. As shown in Equation (2.2), when pressure decreases, so does the density (for any given temperature). The reduction in air pressure causes the temperature to reduce as well. As the temperature is inversely proportional to density, a decrease in temperature would increase the density. However, the pressure-density relationship overwhelms this effect. Thus, as pressure decreases with height, so does the air density.

Apart from differences in pressure, the different heating between the Earth's poles and the equator, and the effect of the Earth's rotation influence global winds. The effect of friction closer to Earth's surface causes the wind to be slower than in higher altitudes. Furthermore, local turbulence decreases with altitude due to the increase of wind momentum and the height above obstacles (less surface contact). For these reasons, turbine hub heights have increased as high as 100 m for the past few decades to capture more energy from the wind (Livingston & Anderson, 2004). The taller wind turbines are economically advantageous and can compensate for the increased tower cost, due to the increased energy production (National Renewable Energy Laboratory, 2004). However, taller wind turbines require a large area to harvest wind energy.

The vertical variations of wind speed are called the wind shear profile. The measured wind resource at a site (which is usually at the lower height compared to the hub height

of the turbine) needs to be extrapolated. The power law is one of the most commonly used analytical models to extrapolate wind speeds to various heights, and its relationship is shown as follows (Manwell, McGowan, & Rogers, 2002; Twidell, 1987):

$$V(z) = V_r(Z/Z_r)^{\alpha} \quad \textbf{(2.3)}$$

where *V(z)* is the wind speed at height *Z*, $V_r$ is the wind speed at the reference height $Z_r$ above the surface (measuring hub), and $\alpha_f$ is the wind friction coefficient or the terrain index. The wind friction coefficient depends on the roughness and type of the terrain, density of the built environment, wind direction and the stability of the atmosphere. Table 2.1 shows the variation of the wind friction coefficient depending on locations.

**Table 2.1: Selected terrain types and their typical wind friction coefficients, $\alpha_f$**

| **Type of Terrain** | **Wind Friction Coefficient, $\alpha_f$** |
|---|---|
| Ice | 0.07 |
| Snow on Flat Ground | 0.09 |
| Mudflats | 0.10 |
| Coast with onshore winds | 0.11 |
| Hedges | 0.21 |
| Scattered trees and hedges | 0.24 |
| Trees, hedges and few buildings | 0.29 |
| Suburbs | 0.31 |
| Woodlands | 0.43 |

(Gipe, 2004; Twidell, 1987)

The impacts of obstacles and terrain features on the wind characteristics are illustrated in Figure 2.1. The terrain and surrounding buildings may affect the wind speed and cause turbulence. Ideally, the best location for a wind turbine is at the top of a smooth hill where the slope of the terrain speeds up the wind speed. Turbulence occurs where obstacles are blocking the wind. This blockage effect of an upwind obstacle is significant and reduces the ability of a wind turbine to capture energy from the wind. As shown in Figure 2.1, any wind turbines within the distances of 10 times the height of the obstacle will be

affected by the turbulence. As an added precaution, the hub for the wind turbine should be twice the height of the obstacle to reducing the adverse effects that the turbulent winds may cause.

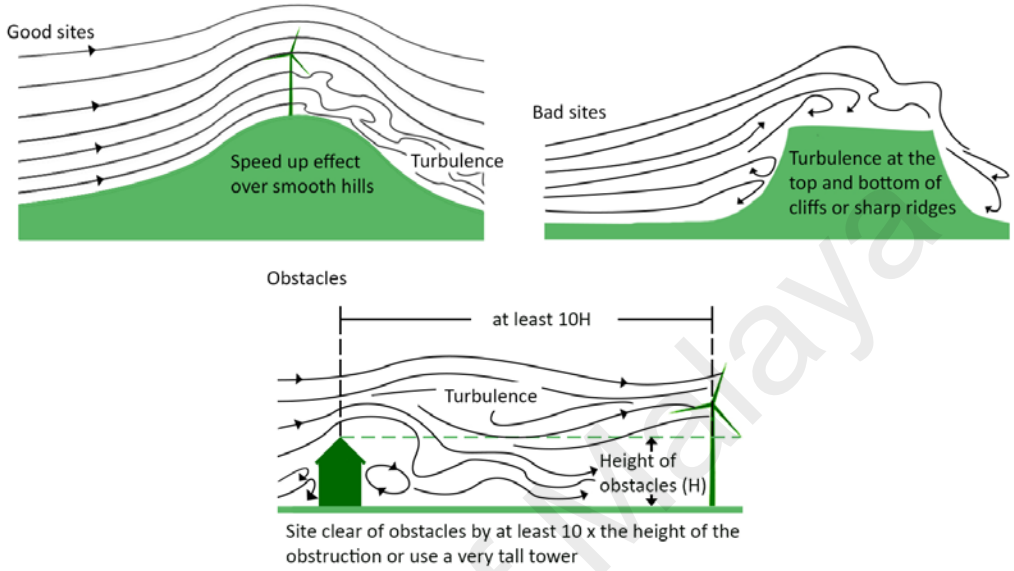


**Figure 2.1: Effects of terrain features and obstacles on wind characteristics**

(Twidell, 1987)

In European cities, organisations involved in the planning are urged to place wind turbines closer to populated areas due to the decreasing number of economic sites (Wagner, Bareiss, & Guidati, 1996). It was reported that on-site energy generation using wind turbines and solar energy systems in urban areas have high potentials (Knight, 2004). However, as discussed, the presence of high-rise buildings generates weak and turbulent wind conditions. Moreover, the skewed wind flow over the obstacles presents an untapped potential of wind energy for wind turbines to benefit from.

## 2.3 Power in the Wind

The transformation of wind energy into electricity using wind turbines is often called wind power (Gipe, 2004). During the ancient time, wind energy was utilised to propel ships and boat. However, from the early 20$^{th}$ century until the 1970s, the interest in wind

energy focused on the charging of batteries for distant dwellings, which was replaced when the electricity grid was introduced. During the energy crisis of 1973-1974, the interests on wind turbines and other alternative energy technologies were renewed. In 1990, the global wind power installed capacity was just approximately 2.4 GW. After two and a half decades, the wind energy based power generation has increased by about 180 times to 433 GW in 2015 (Global Wind Energy Council, 2018).

The availability of wind power for extraction depends not only on altitude, air density and wind friction coefficient but with wind velocity as well. As such, wind power is fundamentally a type of kinetic energy for air that travels from one location to another:

$$P_w = \frac{1}{2}\dot{m}v^2 \quad \textbf{(2.4)}$$

where $v$ is the air velocity at turbine hub height and $\dot{m}$ is the mass flow rate of air which can be expressed as:

$$\dot{m} = \rho A v \quad \textbf{(2.5)}$$

where $A$ is the swept area of the turbine and $\rho$ is the air density at the turbine hub height. By relating Equations (2.4) and (2.5):

$$P = \frac{1}{2}\rho A v^3 \quad \textbf{(2.6)}$$

Equation (2.6) is the availability of power in the wind. However, there exists a theoretical limit known as the Betz limit that sets an extractable limit of about 59.3% of the total wind power (refer to Figure 2.2).

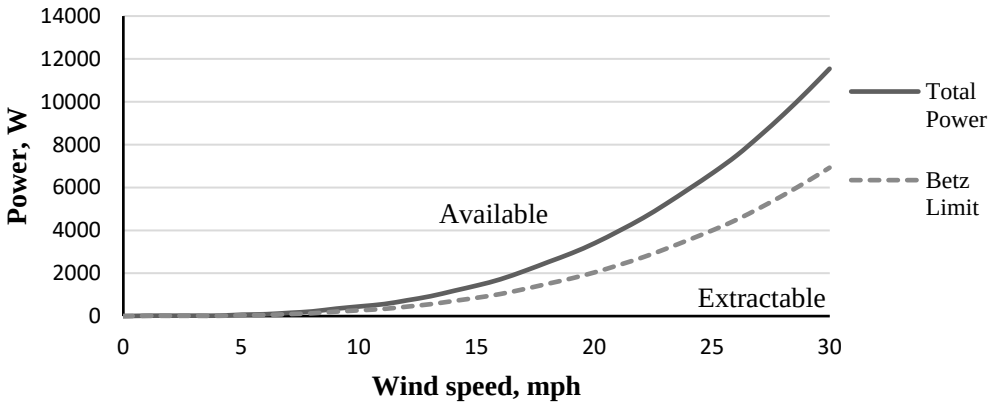


**Figure 2.2: Betz limit for a typical wind turbine**

(Jamieson, 2011)

## 2.4 Wind Turbine

A wind turbine converts the kinetic energy from the motion of the wind into mechanical energy. In the modern era, the mechanical energy is converted into electricity through the use of a generator (Gipe, 2004). To harness wind energy in large scale, wind farms were erected and connected to large utility grids. Figure 2.3 shows an example of a wind farm, i.e. Alta Wind Energy Center located in Tehachapi Pass, California, USA.

**Figure 2.3: The Alta Wind Energy Center**

(California Energy Commission, n.d.)

Wind power technology has improved in the past few decades in which the capacity of a wind turbine has increased from the classical 250 W to 5 MW. Wind turbines can also be classified into two different categories based on its axis of rotation, i.e. horizontal axis or vertical axis. Figure 2.4 shows the typical efficiencies of HAWTs in comparison with VAWTs at different tip speed ratios.

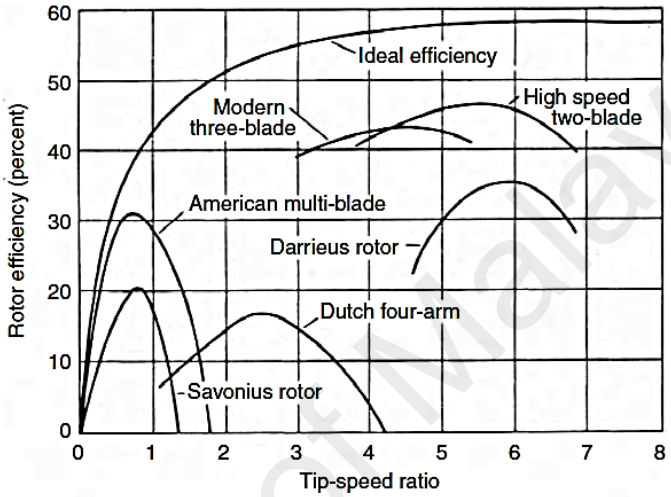


**Figure 2.4: Performance curves of major wind turbine designs as a function of tip speed ratio**

(Patel, 2006)

### 2.4.1 Types of vertical axis wind turbine

As discussed in Chapter 1, the vertical axis wind energy conversion systems are classified based on the characteristics of their aerodynamic forces (i.e. lift or drag-based wind rotors, refer to Figure 2.6). The Savonius wind rotor uses the force of the wind to push its surface (drag force), as an open sail. For modern wind turbines, the Darrieus lift-based wind devices are more common. This type of wind turbine uses specially shaped airfoil blades, and the lift force is more dominant when the air stream passes over the airfoil (refer to Figure 2.5).

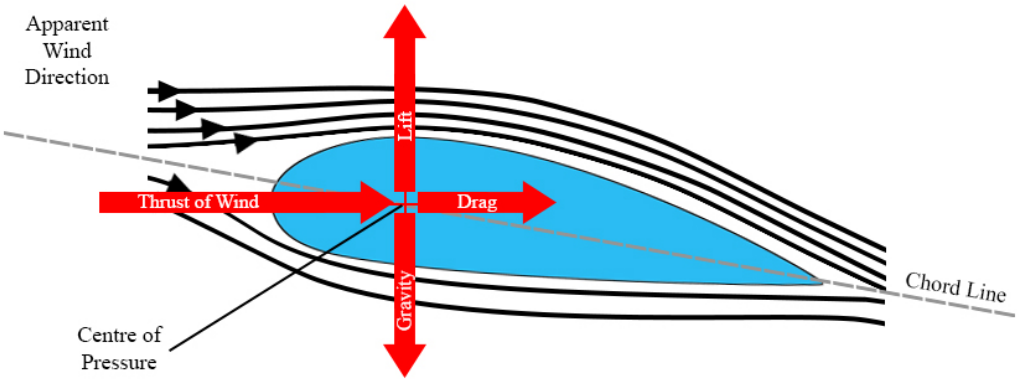


**Figure 2.5: The net lift force caused by the differential pressure of flow over the airfoil blade**

(Aerodynamic Lift and Drag and the Theory of Flight, n.d.)

S.J. Savonius in 1922 invented the Savonius rotor where there are two cups affixed to a shaft (Savonius, 1931). The two cups would form an "S" viewed from above. The oncoming air stream would come in contact with the inner surfaces of the cups, creating a differential drag to spin the turbine. However, the Savonius turbine suffers from poor efficiency.

The Darrieus wind turbine is another popular design of VAWT. The turbine was proposed by a French engineer, G.J.M. Darrieus in 1931 and relies on airfoil blades to generate lift forces for rotation. Different than the Savonius turbine, the Darrieus wind turbine performs poorly in low wind speed areas but has higher efficiency (Mathew, 2006). In this literature review, the focus of the study will be mainly based on the design of the lift-based Darrieus VAWT. The following subsection discusses the development of the wind turbine.

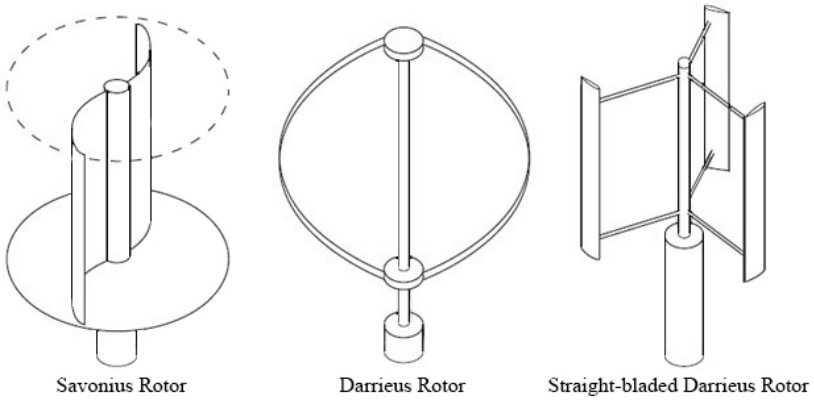


**Figure 2.6: Savonius and Darrieus rotors**

(Eriksson et al., 2008b)

### 2.4.2 Development of the lift-type Darrieus wind turbine

Since the energy crisis in the 1970s, development in wind turbines was recognised for its clean and inexhaustible potential in power generation, therefore much of the renewed interest in wind turbines emanated from our knowledge and concern that the dependencies on fossil fuel reserves alone can lead to future world economic crisis. At the time, an already proven technology in wind energy generation was the HAWT (Hau, 2006). The use of the VAWTs for large electricity generation projects was mainly ignored due to their lack of efficiencies compared to the HAWTs. Nevertheless, the introduction of variable-pitch Darrieus VAWT configuration known as giromill that has a coefficient of power, $C_P$ of about 0.5 is considered comparable to the HAWT (Brulle, 1977, 1980; Moran, 1977). Moreover, it was reported that the cost to generate power by the Darrieus wind turbine was 18-39% less than the HAWT, depending on the size and mean wind speed of the site (Brulle, 1977). Unlike the more stable HAWT, the blades of the VAWT experience rapid changes of angle of attack (AOA) as the blades rotate in the upwind and downwind regions which relates to complex aerodynamic issues that are not experienced by the HAWT blades. Recent developments on Darrieus vertical axis wind energy devices, however, have contributed to better performance and reliability of the turbine.

Mimicking the wings of birds, the airfoil profile adopted in the Darrieus wind turbine has minimum resistance in forwarding motion and capable of exploiting maximum available amount of energy by using the traversing thrust of the blades (Darrieus, 1931). Patented in 1931, Darrieus described two major configurations for the wind turbine, curved- and straight-blades (Figure 2.7). The airfoil-shaped blades use the aerodynamic lift forces created by the wind flow over them to rotate. Compared to the Savonius turbine, the Darrieus rotor generates less torque (difficult to self-start) but rotates much faster (Jin, Zhao, Gao, & Ju, 2015; Mathew, 2006). However, it was reported that the Savonius rotor utilised 20% less flow energy utilised from the oncoming wind flow compared to that of Darrieus rotor (Gorelov & Krivospitsky, 2008), with the maximum theoretical efficiency of $C_P = 0.18$ (Mohamed et al., 2010).

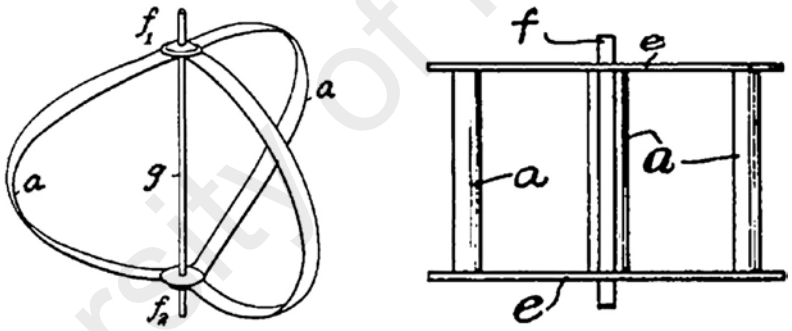


**Figure 2.7: Illustrations in the original patent by Darrieus. The left image is known as the curved-blade wind turbine, whereas the right image illustrates the straight-blade wind turbine**

(Darrieus, 1931)

Over the years, the original two configurations of a lift-type wind turbine have evolved into several variations. The development of the curved-blade configuration has evolved into phi-rotor or also known as the egg-beater rotor due to its similarity in geometry. Various investigations involving different analytical tools, experimental methods, and numerical models to assess its performance have been carried out since the 1970s (Loth & McCoy, 1983; Paraschivoiu, 1981, 1988, 2002; Rajagopalan & Fanucci, 1985;

Strickland, 1975; Strickland, Smith, & Sun, 1981; Templin, 1974; Wilson & Lissaman, 1974). It was reported that Sandia National Laboratories (SNL) built a 34 m diameter phi-rotor in 1988 which achieved a peak power coefficient, $C_P$ of 0.409 at TSR, $\lambda$ of 6.34 (Ashwill, 1992). However, the phi-rotor faced a couple of failures during its early development stages due to the many disadvantages of the turbine (Johnson, 2006; Templin, 1979), such as uneven wind velocity across rotor height (high height-to-diameter ratio) (Ashwill, 1990; Owens, Hurtado, Paquette, Griffith, & Barone, 2013; Popelka, 1982), wake due to large rotor column (Paraschivoiu, 2002), gravity-induced bending stress on the troposkien blades (Paraschivoiu, 2002; Sutherland, Berg, & Ashwill, 2012), and high axial load on support bearings (usage of guy-wires and large rotor assembly) (Sutherland et al., 2012). Recently, many innovations and new design of the phi-rotor were introduced in particularly to address the issues plaguing the phi-rotor. A couple of examples are the use of fixed-on-tower and cantilevered design (shown in Figure 2.8) offering a more durable and more straightforward system than the guy-wired system, foldable blades that can be remotely controlled to reduce the risks of blade ejection at high wind speeds, and tailoring airfoil profile to a particular section of the blade for aerodynamic performance and structural strength (Vertical Wind Turbine Info, 2012).

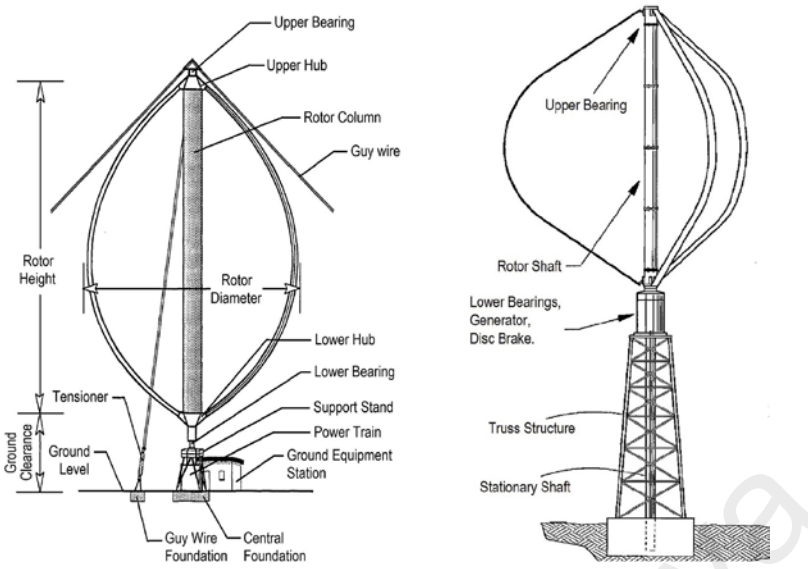


(a) (b)

**Figure 2.8: Illustrations of (a) the guy-wired phi-rotor, and (b) the cantilevered phi-rotor**

(a) (Spera, 2009); (b) (Nigam & El-Sayed, 2011)

In the case for the straight-blade Darrieus turbine, two different variations of the design were developed during the 1970s: the variable-geometry (Musgrove-rotor) rotor and variable-pitch (Giromill) rotor (shown in Figure 2.9). The Musgrove-rotor employed a blade-reefing mechanism to limit the speed of the rotor in high wind speed conditions (Mathew, 2006; Musgrove, 1978). Supported on each end of an airfoil-shaped horizontal beam, two sets of straight-blades were positioned. In strong winds, the rotor feathers about the beam and the blades furled horizontally due to the centrifugal force (Mathew, 2006; Musgrove, 1978). In its early development, the Musgrove rotor showed good potentials, which led to the building of several large-scale rotors (rated 100 kW) (Price, 2006). However, due to the complexity of the blade-reefing mechanism and large concrete structure needed to support the rotor result in a high cost in production and maintenance of the turbine. On the other hand, the giromill is an H-rotor Darrieus wind turbine with variable pitch blades to maintain the AOA of the wind interacting with the blades relatively constant in the upwind and downwind regions of the rotor. The method

of controlling the pitch blade (either by using hydraulic, cam and push-rod, or motor-driven timing belt mechanisms) produced comparable power coefficient as the HAWT (McConnel, 1979; Moran, 1977). Nevertheless, the mechanism that controls the pitch angle proves costly and unreliable which was challenging to maintain. Therefore, the giromill was abandoned for the much simpler and cost-effective H-rotor (Eriksson, Solum, Leijon, & Bernhoff, 2008c; Sjokvist & Eriksson, 2013). The H-rotor is a fixed-pitch straight-blade wind turbine that uses a direct-drive generator to provide better cost efficiency since it is positioned near to the ground. However, due to the large-scale cyclic torque of the fixed-pitch blade, the rotor shaft is exposed to torsional stress due to vibration. Therefore, the rotor requires a stronger and lighter shaft.

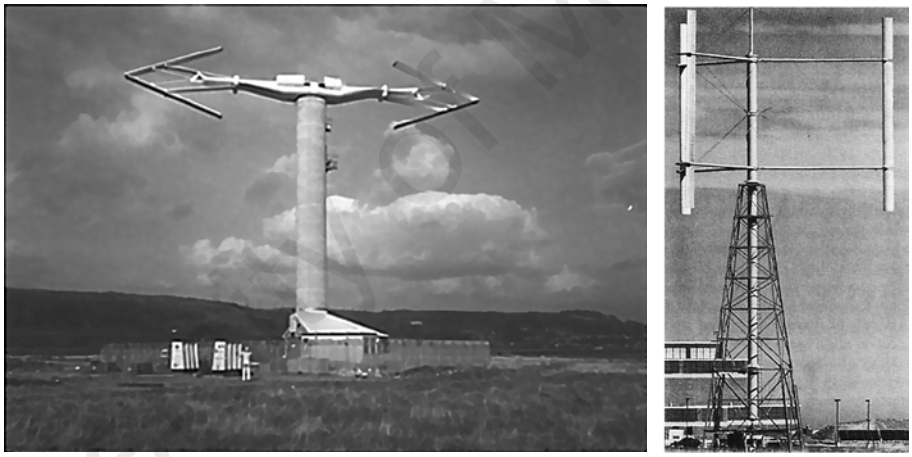

(a) (b)

**Figure 2.9: (a) The Musgrove rotor, and (b) the giromill**

(a) (Price, 2006); (b) (Spera, 2009)

Later, the helical H-rotor was first developed as a water turbine with thicker and longer hydrofoil to form a stronger structure as shown in Figure 2.10(a) (Gorlov, 1995). Then, the helical design was adopted in another wind turbine. For example, the Turby wind turbine was reported to have a power coefficient of 0.3 at $\lambda$ of 3 (van Bussel, Mertens, Polinder, & Sidler, 2004a). As shown in Figure 2.10, there is a clear difference between the water turbine and the wind turbine. For the helical water turbine, the rotor's solidity

is much higher compared to the wind turbine. Solidity is the ratio of blade area to the total swept area of the turbine. In doing so, the water turbine has a reduced rotational speed which helps to minimise the effect of cavitation. There are a few advantages of the helical rotor design in the context of wind energy device, such as the blade profile of the helical H-rotor is uniformly distributed around the border, therefore reducing cyclic torque, producing better performance output, and lower noise emission. In the urban context, the helical H-rotor is gaining popularity due to its aesthetic value, hence the visual impact of mounting the wind turbine in an urban environment is lessened.

(a) (b)

**Figure 2.10: (a) The Gorlov helical turbine, and (b) the Turby wind turbine**

(a) (Rourke, Boyle, & Reynolds, 2010); (b) (van Bussel et al., 2004a)

### 2.4.3 Recent innovations in wind turbines – uncommon geometries to enhance the turbine power output

Many researchers have explored new designs of the wind turbine. These innovations in wind turbines were designed to tackle the common issues of vertical axis wind turbines, which include low rotor efficiency and poor self-starting characteristic, among others. Firstly, with a similar concept of using the skewed flow to enhance the performance of wind turbine, Batista, Melício, Mendes, Calderón, and Ramiro (2015) introduced an

innovative blade profile design incorporated into a VAWT. Called the EN0005, the blade ends are specially designed as new lift-capable blades that extend the main blade body. These blade ends can be placed parallel to the main body, or be placed at an angle to the outside or inside of the rotor. Field tests of the new VAWT shown that the design is capable to self-start even at the low wind speed of 1.25 m/s. However, no further discussions were provided in terms of the power performance, torque output or the rotor rotational speed of the turbine in regards to the position of the end blades. A vertical axis wind turbine with airfoil-shaped cross-sections, mounted as the inclined arms of the rotor were introduced by De Marco, Coiro, Cucco, and Nicolosi (2014). By employing numerical simulations, and validated against experimental data, the use of inclined airfoil-shaped arms increases the average power coefficient of the turbine by up to 289%.

There exists a unique innovation of the Darrieus VAWT called the Aerogenerator X which was designed under the novel offshore vertical axis (NOVA) project. As shown in Figure 2.11, the turbine is a V-shaped structure mounted on an offshore platform with a rotor diameter of 270 m and height of 130 m. It was reported that the wind turbine could generate up to 10 MW of power (Quilter, 2013). The wind turbine has two extended arms to form a V-shape with airfoils mounted on their ends, where the approaching wind interacts with the foils. In its early stages, the turbine was designed with several blades along the arms with guy wires at each half of the support arm to enhance structural strength. However, through feasibility studies, it was found that by designing a simpler rotor with only two blades at the end of the arms, the rotor weight can be reduced to half of the early design. Through this process, the bending stress on the two tilted arms is reduced significantly and therefore removing the use of guy wires (Wind Power Ltd., 2010).

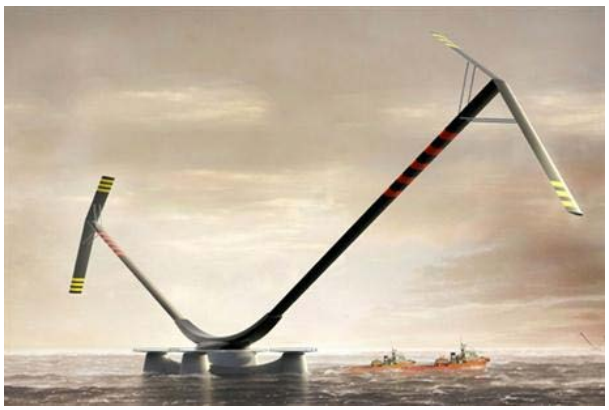

**Figure 2.11: An artist's impression of the Aerogenerator X, a Darrieus design with unique V-shape rotor**

(Quilter, 2013)

Another recent innovation of the Darrieus design is the articulating H-rotor called the Blackhawk wind turbine, shown in Figure 2.12. The turbine is a passive control rotor that automatically adjusts the tilt of its vertical blades for a better angle of attack (Boatner, 2010). The wind turbine idea is based on the concept of helicopter rotor which mechanically regulates the blades to the difference in wind pressure to reduce mechanical and vibrational stresses. The horizontal component of the oncoming wind interacts with the vertical blade, and in turn, the mechanical system of the turbine tilts the vertical blades accordingly. This is done by using a gimbal mechanism, which allows the blades to oscillate around the rotor hub freely. To prevent over-tilting, dampeners are incorporated into the design. The pitch angles of the blades are changed via the linkages from the hub to the blades, depending on the orthogonal wind force that pushes the blades. The passive pitch-control mechanism enables the Blackhawk wind turbine to self-start even at low wind speed despite having low solidity. However, there were no further recorded experimental and practical analyses of the Blackhawk wind turbine found in the literature.

**Figure 2.12: The 1.5 kW Blackhawk wind turbine prototype (3 m diameter and 2.1 m height)**

(Boatner Consulting, n.d.)

There is a unique strategy proposed by Govind (Govind, 2017) to integrate a vertical axis wind turbine with a horizontal axis wind turbine as illustrated in Figure 2.13(a). From the study, the combination of torque from those two subsystems increased the operational ability of the turbine. During operation, the excess torque from the horizontal axis wind turbine is transferred to the vertical axis wind turbine using a continuously variable transmission. The energy output from this design has been shown to exceed the energy outputs from both independent subsystems under different wind conditions. However, additional maintenance works on the turbine is expected due to the complexity of the transmission system. Researchers have also explored the use of double blade design. This was proposed in the Butterfly-rotor consists of closed-loop blades as shown in Figure 2.13(b). It was mainly designed to improve the self-starting properties of the vertical axis wind turbine with the addition of airfoil blades within the external airfoil blades. Furthermore, the design of the Butterfly-rotor can provide higher efficiency with reduced cyclic vibration due to the direct linkage of the looped blades to the hub. By using the blade element momentum model, it was estimated that the Butterfly-rotor (diameter: 2.06 m; height: 0.8 m) could generate 330 W of power at a wind speed of 12 m/s (Hara et al., 2014). In another research, a high solidity Tulip-shaped vertical axis wind turbine was

designed for low visual impact and cost-efficient system in suburban environments (van de Wiel, 2015). Shown in Figure 2.13(c), the Tulip is a bio-inspired wind turbine with a high solidity rotor. High solidity turbines commonly experience aerodynamic phenomena such as flow curvature and high angles of attack (dynamic stall). By optimising the airfoil based on aerodynamic and structural characteristics of the rotor, the correction for flow curvature and wake effects manage to reduce the aerodynamic phenomena. From the tests, the wind turbine could produce a power coefficient of 0.368 at a tip speed ratio of 2.5.

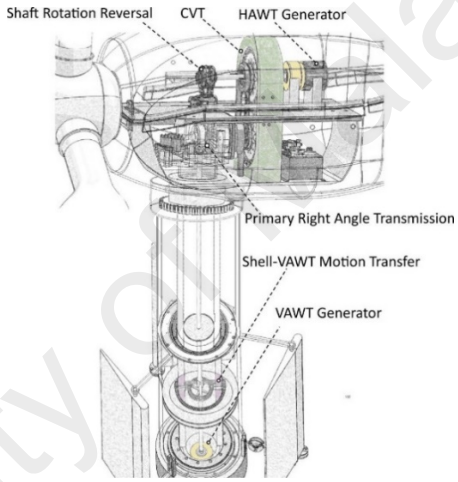


(a)

(b)

(c)

**Figure 2.13: (a) Illustration of the primary drivetrain of the hybrid horizontal axis wind turbine and vertical axis wind turbine subsystems, (b) the Butterfly-rotor with closed-loops, (c) the bio-inspired Tulip wind turbine**

(a) (Govind, 2017); (b) (Hara, 2012); (c) (van de Wiel, 2015)

### 2.4.4 Enhancing the performance of the wind turbine by augmenting the oncoming wind flows

Traditional methods of extracting power from the wind in urban areas using wind turbine alone may not be efficient due to the uncertainty of wind speed and the turbulence generated from the surrounding buildings. Moreover, for a wind turbine to be used in an urban area, issues such as the structural strength of the wind turbines, failures of blades, acoustic pollution and electromagnetic interference should be addressed (Oppenheim, Owen, & White, 2004). Besides focusing on improving the performance of wind turbine by the aerodynamic study of the turbine blades, increasing the oncoming wind speed before it interacts with the wind turbine also provides a significant result in increasing the potential power output. The power in the wind is proportional to the cubic power of the wind speed, in which a 10% increase in wind speed will produce 33% more power. To increase the speed of the wind, one of the most economical and efficient way is to build a shroud or guide vanes surrounding the wind turbine (Wong et al., 2017). The use of a dual turbine setup can also be employed to enhance the flow velocity surrounding the turbines (Chen, Chen, Huang, & Hwang, 2017). In this subsection, the method of augmenting wind turbine and its many designs and ideas are discussed.

#### 2.4.4.1 Improvement of wind turbine performance by using deflectors

In investigating the method of power enhancement of wind turbines, researchers have employed the use of simple deflectors to augment the oncoming winds. Kim and Gharib (2013) investigated two counter-rotating Darrieus VAWT with the straight-plate deflector. By placing a single deflector plate in the upstream position to increase the local wind velocity surrounding the turbines, the VAWT's maximum power coefficient was increased by three times depending on the ratio of the width of the deflector to the diameter of the rotor. Wong et al. (2018b) performed lab tests and numerical computations to investigate the aerodynamic effects and the flow field around a flat plate

deflector as an augmentation device. It was found that the power coefficient was increased by 7.4% compared to the bare turbine configuration in the lab tests. From the simulations, the average power coefficient can be increased by up to 33% depending on the position of the deflector relative to the turbine. In another study, Wong et al. (2018a) carried out three-dimensional simulations to investigate the effects of a flat plate deflector placed at the upwind side of a VAWT. Based on the results, the cycle-averaged torque coefficient was increased by 47.1% compared to a bare VAWT.

#### 2.4.4.2 Vertical flow augmentation

Many researchers have explored studies in vertical flow induced by augmenting devices to direct the approaching wind vertically towards the rotor by the use of ducts, deflectors or shrouds. The design basically varies from one another and can be categorised as single intake or omnidirectional in which the approaching wind flows into the device and exits out through an outlet after interacting with the rotor blades. A study by Hu and Cheng (2008) proposed a bucket-shape ducted wind turbine in which a 'sucking effect' can be produced in the duct. The duct structure has a single inlet facing the approaching wind to increase the airspeed by up to 60% by optimising the duct's interior. Results from field tests have shown that the proposed system increases the power extraction efficiency of the rotor by 80%, higher than the standard of a conventional wind turbine based on the Betz limit (Hu et al., 2008). Ahmed (2013) used the same principle by employing a cowling structure to enclose the rotor and relied on guide vanes to direct the approaching wind downward. By optimising the cowling diameter, outlet angle and gap of the guide vane, the study reported an increase of wind speed by up to 30-60% (Ahmed, 2013). For a more practical application of these vertical flow devices, capturing wind from every direction is vital. Sureshan (2008) designed an omnidirectional, vertical discharge wind turbine consisting of a shroud that captures wind from any direction and directs it to flow vertically through a throat section where an airfoil multi-bladed rotor is mounted. The

design, called the IMPLUX, used airfoil shaped deflectors to guide the oncoming wind upward towards a vertically mounted wind turbine as shown in Figure 2.14(a) (Sureshan, 2008). Allaei et al. (2014) proposed the INVELOX as shown in Figure 2.14(b). The INVELOX captures the approaching wind through an omni-directional intake, accelerates the flow through a shrouded Venturi section and finally passes through a diffuser where a wind turbine is mounted. The authors claimed that the INVELOX could increase the average wind speed ratio by 1.8, and the electrical energy generated by the system is about 80-560% more than a conventional wind turbine.


(a) (b)

**Figure 2.14: (a) The illustration of flow vectors inside and around the IMPLUX wind turbine, and (b) the INVELOX wind turbine prototype**

(a) (Nguyen, 2011); (b) (Allaei et al., 2014)

Another unique design that focuses on the unpredictable nature of wind conditions in urban areas was proposed by Zhang, Chen, and Calay (2013) who performed CFD analyses and experiments on a shroud structure as shown in Figure 2.15(a). Consisting of five chambers along the circumference of the shroud, the system can receive approaching wind from every direction and direct the wind flow upward where a wind turbine is placed. The authors reported that the shroud was able to significantly increase the approaching wind speed by up to 1.3 times at the outlet, which is equivalent to 2.5 times

increase in wind energy (Zhang et al., 2013). Further investigations by Ying et al. (2015) by employing an impulse turbine placed at the outlet of the shroud have shown that under a non-uniform flow, the maximum power coefficient of the turbine reaches 0.06-0.12, which is lower than that under uniform flow by 29-65%. However, a good self-starting ability was reported with wind speed as low as 1.6 m/s. In another study, a small wind power system integrated with an exhaust air duct was proposed by Park et al. (2016) as shown in Figure 2.15(b). The system functions by inducing the outside airflow in the exhaust air duct by installing a small wind power system on the outlet of the structure. The authors estimated that the generated electricity of the system is approximately 1.7-1.9 times higher than other wind turbine systems (Park et al., 2016).

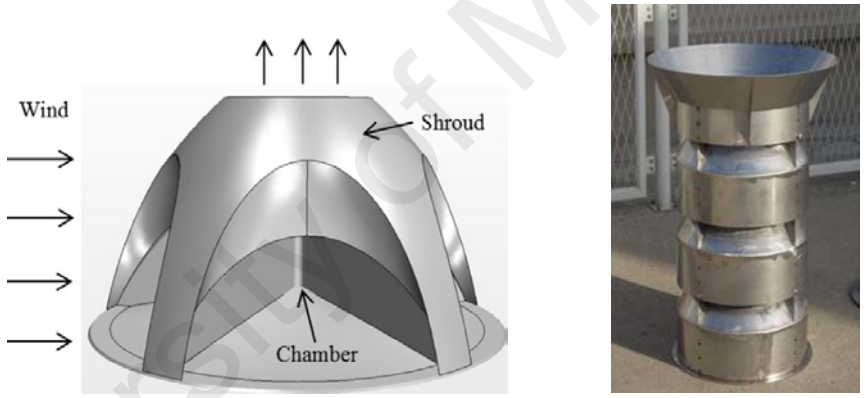


(a) (b)

**Figure 2.15: (a) The omni-flow shroud wind energy system, and (b) the Venturi exhaust air duct caps**

(a) (Zhang et al., 2013); (b) (Park et al., 2016)

#### 2.4.4.3 Horizontal flow augmentation

Besides the method of changing the direction of the airflow from horizontal to vertical through the use of external devices, the method of augmenting the oncoming horizontal wind flow to increase its wind speed has been commonly used with vertical axis wind turbines. There have been many studies on different designs of ducted or diffuser augmented wind turbines to increase the oncoming wind speed. To achieve the maximum

ratio of lift force to the drag force ($L/D$ ratio) of a wind turbine blade, the wind stream must be directed towards the optimum angle of attack of the blade.

Takao, Maeda, Kamada, Oki, and Kuma (2008) researched the effect of guide vane geometry on the performance of a straight-bladed VAWT. The angle and gap between the rotor blade and guide vane were varied to study the effects on the VAWT power output. From the study, the power coefficient of the VAWT was 1.5 times higher than a wind turbine that has no guide vane (Takao et al., 2008). In another study, CFD analysis and experiments on a varying stator vane geometries of a Zephyr VAWT (ZVWT) was conducted. As shown in Figure 2.16(a), the turbine features a unique design that incorporates stator vanes with reverse winglets, which are also called stator tabs. The high solidity of the turbine ensures better performance in low operational TSRs, but limit the turbine's peak power output in high wind speeds. The authors found that the stator tabs that were designed to reduce turbulence produce an overall improvement for the wind turbine by 13.5% (Pope et al., 2010). A study by Yao, Tang, and Wang (2013) presents a novel VAWT design consists of a wind rotor and a tower cowling. The tower cowling consists of eight baffle plates distributed axially to direct the wind towards the wind rotor as shown in Figure 2.16(b). The basic concept of the design of the tower forces the oncoming wind to be directed towards the blade. This would increase the oncoming wind speed, and more positive torque can be produced while preventing negative torque by restricting the wind force on the outer side of the blades. In doing so, the self-start characteristics of the VAWT can be improved. The simulation results showed that with the optimal configuration of the tower (800 mm diameter, eight arc-shaped baffles tilted at angle 15°, and two VAWT blades) can produce 2.4 times higher in power coefficient compared to a bare turbine.

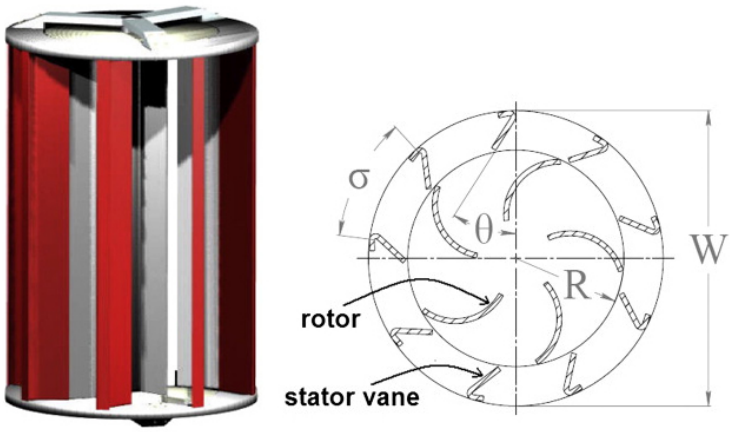


(a)

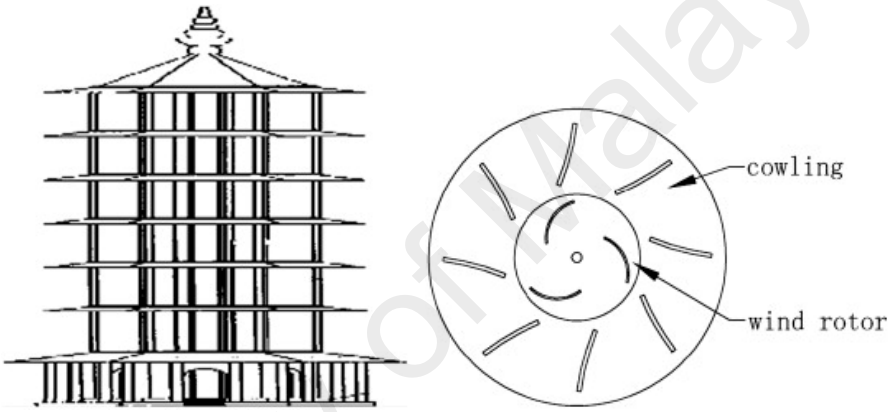


(b)

**Figure 2.16: (a) Illustration of the Zephyr VAWT prototype (left) and its geometrical variables (right), (b) Illustration of the cowling tower (left) and the cross section of the tower with its main features (right)**

(a) (Pope et al., 2010); (b) (Yao et al., 2013)

To address the low wind speed condition in Malaysia, Chong et al. (2013c) designed an innovative device called the power-augmentation-guide-vane (PAGV) to increase the wind speed and guide it before interacting with the rotor blades. The PAGV is a device consisting of several guide vanes used to increase the energy generation of the wind turbines in low wind speed areas. From the experimental analysis, it was found that the power output for VAWT with PAGV increased by 5.8 times, and the self-start wind speed of the turbine is lowered to 1.5 m/s from the initial wind speed of 3.0 m/s. By improving

the design of the PAGV, Chong et al. (2013a) designed the wind-augmentation device called the omni-direction-guide-vane (ODGV). As shown in Figure 2.17, the guide vanes concentrate the oncoming wind velocities and guide the wind flow to the VAWT blades for an optimum angle of attack. The venturi effect created by the channels can induce a higher wind speed into the VAWT, which allows for smaller and lighter rotating wind turbine parts to be used to produce a similar power output.

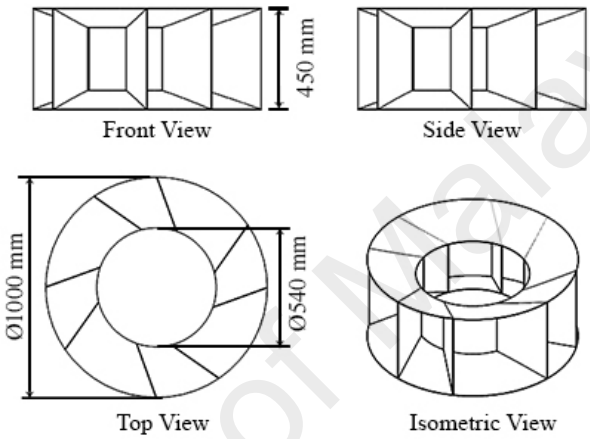


**Figure 2.17: The omni-direction-guide-vane**

(Chong et al., 2013a)

A wind tunnel study using a Wortmann FX 63-137 5-bladed VAWT was enclosed by an ODGV model with dimensions shown in Figure 2.17. Evaluations on the power generated and the rotational speed of the wind turbine for the VAWT was carried out. At a fixed wind speed of 6 m/s, the data from the experiment for load assessment of the wind turbine for bare and ODGV integrated VAWTs are tabulated in Table 2.2. The shrouded VAWT shows significant improvements over the bare VAWT where the maximum torque and steady rotational speed was recorded to achieve 23.64 mN.m and 144.40 rpm respectively. Further calculations show that the power generated by the shrouded VAWT increased by about 350% when compared to a bare VAWT, after calculating the losses

due to bearing friction. This proves that the ODGV has positive effects on the wind turbine performance.

**Table 2.2: Performance of bare and ODGV integrated VAWT**

| Parameter | ODGV integrated VAWT | Bare VAWT | Augmentation Ratio |
|---|---|---|---|
| Power generated (W) | 0.4352 | 0.1252 | 3.48 |
| Maximum torque (mN.m) | 23.64 | 11.25 | 2.10 |
| Rotor speed (rpm) | 144.40 | 77.40 | 1.87 |

(Chong et al., 2013a)

Similar to the ODGV, Nobile et al. also used an omnidirectional stator around an H-rotor Darrieus VAWT as shown in Figure 2.18. The stator has eight guide vanes with two conical surfaces at the top and bottom of the device to reduce the back pressure by enhancing turbulent flows inside the stator. The use of the guide-vane in the shape of NACA0018 airfoil profile helps to accelerate and deaccelerate the oncoming wind flow by converging and diverging the airflow stream at specific regions. Although the stator incorporates the use of conical surface to concentrate wind to the VAWT, the skewed wind flow deflected by the surface was not part of the design element. The guide vanes of the stator in the upstream region restrict some flows to the downstream region that may produce negative torque, hence improving the performance of the VAWT. By using ANSYS CFX software, the performance of the VAWT at three different guide vane blade pitch angles (-30°, 0°, and +30°) was simulated. The study showed that the average power and torque coefficients of the VAWT with stator were increased up to 35% compared to the bare VAWT with an optimum pitch angle of 0° (Nobile, Vahdati, Barlow, & Mewburn-Crook, 2014).

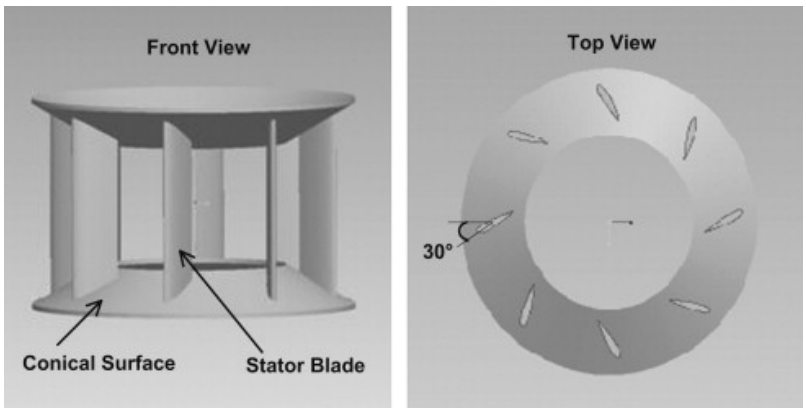


**Figure 2.18: The design of the omnidirectional stator**

(Nobile et al., 2014)

From the review, a summary of the augmentation devices is shown in Table 2.3. These external devices are used to guide the oncoming wind flow to a better angle of attack, thus enhancing the lift-to-drag ratio of the rotating blades. The augmentation devices are also employed to promote positive torque by concentrating most of the wind flows to the upstream region of the turbine. Moreover, the acceleration of the oncoming wind speed by using the concept of Venturi effect before it interacts with the wind turbine blades enhances the performance of the VAWT. Furthermore, these devices can be used to improve the aesthetic values of a wind turbine for urban wind energy application. Therefore, in this study, the application of deflector as a mean to augment the oncoming wind flow could significantly enhance the performance of the wind rotor. The novelty of the current study is in the use of the deflector to not only augment the oncoming wind flow but to create skewed wind flows for the CAWT, harnessing the potential wind energy of the horizontal and vertical wind components.

**Table 2.3: Summary of augmentation devices based on their descriptions, types, methodologies and results.**

| No. | Reference | Description | Type | Methodology | Research Results |
|---|---|---|---|---|---|
| 1 | Ying et al. (2015) | Studied an omni-direction shroud through the use of CFD simulation and experimental works. | Vertical flow augmentation – Shroud | VAWT – Simulation and experiment | The design showed good self-starting ability with low noise. However, non-uniform wind distribution was observed. |
| 2 | Loganathan, Chowdhury, Mustary, and Alam (2015) | Developed a cowling device for a cyclonic type VAWT. The half of the frontal area of the outer shell is closed to prevent the wind interact with the returning convex blade, whereas the inner shell allows the discharging of the wake to the vertical outlet. | Vertical flow augmentation - Cowling | VAWT - Experiment | The rotor rotational speed increases by 26% for the 16-bladed VAWT. Meanwhile, the 8-bladed VAWT recorded an increase of 40%. |
| 3 | Allaei et al. (2014) | Designed the INVELOX wind turbine. It captures the approaching wind, accelerates the flow and passes through a diffuser before finally, a wind turbine that is oriented horizontally harnesses the wind energy. | Vertical flow augmentation – Shroud with Venturi section | Horizontally mounted wind turbine – Simulation and field test experiment | Wind speed augmentation of 1.58 to 1.80 was achieved through CFD simulation. The electrical energy from field tests showed an increase in performance compared to the conventional wind turbine (80-560%). |
| 4 | Ahmed (2013) | Developed a cowling system for small-scale power generation. Employed an air guide vane cowling integrated with a vertically mounted wind turbine. The cowling assembly guides the oncoming | Vertical flow augmentation - Cowling | Vertically mounted wind turbine – Simulation and experiment | Wind speed increases by 30-40% for the inlet wind speed of 5 m/s. |

| | | | | | |
|---|---|---|---|---|---|
| | | wind flow vertically and downward to the wind turbine. | | | |
| 5 | Ali, Golde, Alam, and Moria (2012) | Developed a cowling device with a tail-end section that allows for even flows at both sides of the device. Also, the tail-end section functions as a yawing device to direct the opening of the cowling to the direction of the oncoming flow. The chimney of the cowling allows for the wake to be exhausted vertically. | Vertical flow augmentation - Cowling | Multi-bladed drag-type VAWT – Simulation and experiment | The rotor rotational speed increases by more than two times compared to a bare VAWT. |
| 6 | Hu et al. (2008) | Designed a bucket-shape ducted wind turbine to increase the oncoming wind speed. Divided into two sections, the upper duct is an axis-symmetric outlet, and the lower duct is the flow entrance compartment. The oncoming wind flow is directed upwards toward the vertically mounted wind turbine in the upper duct. | Vertical flow augmentation – Bucket-shaped duct | Vertically mounted wind turbine – CFD simulation and field text experiment | The oncoming wind speed was shown to increase by 60% in simulation studies. From field tests, the power generation was increased by 80%. |
| 7 | Sureshan (2008) | Designed the Implux wind turbine. An omnidirectional, vertical discharged shroud to capture wind and divert it vertically to a wind rotor oriented vertically at the outlet. | Vertical flow augmentation - Shroud | Vertically mounted wind turbine – Simulation | Simulations showed that the guide vanes of the shroud directed the oncoming wind flow vertically. However, there is a lack of experimental information provided by the author. |

| | | | | | |
|---|---|---|---|---|---|
| 8 | Tartuferi, D'Alessandro, Montelpare, and Ricci (2015) | Designed a complex curtain system with airfoil-shaped Savonius blades wind turbine. The curtain system has two aerodynamic appendages that partially enclose the wind rotor | Horizontal flow augmentation – Curtain system | Savonius VAWT – Simulation and experiment | The power coefficient of the wind turbine increased by 20% compared to the bare turbine. |
| 9 | El-Askary, Nasef, AbdEl-hamid, and Gad (2015) | Innovative deflectors were designed to be integrated with Savonius wind rotor. In general, there are three plates of the system, in which the first one directed the wind to the concave advancing blades of the wind rotor. The other two plates are to reduce the negative torque created when the wind interacts with the convex returning blade of the rotor. | Horizontal flow augmentation – Guide plates | Savonius VAWT – Simulation | Maximum power coefficient of 0.52 at TSR value of 1.1 was simulated. An increment of 1.6 times compared to the conventional wind turbine. However, the design of the guide plates creates strong vortex shielding and turbulent wakes. |
| 10 | Chen and Chen (2015) | An omni-direction vortical stator assembly (VSA) was designed to improve a drag-type VAWT with six half-tube blades. The guide vanes allow wind flow to tangentially enter the VSA, hence creating a vortex flow inside the VSA assembly. | Horizontal flow augmentation – Vortical stator assembly | Drag-type VAWT – Experiment | The VSA increased the rotor rotational speed, torque output and maximum power by 318%, 200%, and 910%, respectively at a 6 m/s wind speed. |
| 11 | Burlando, Ricci, Freda, and Repetto (2015) | Designed an omni-direction airfoil-shaped stator vane for a three-bladed Savonius rotor. | Horizontal flow augmentation – Airfoil-shaped stator | Savonius VAWT – Simulation and experiment | 10% increased wind speed. Through simulation of wind flows, the stators enhanced the convergence of the wind flow |

| | | | | | |
|---|---|---|---|---|---|
| | | | | | through the gaps between the vanes. |
| 12 | Wang and Zhan (2015) | Designed a barchan dune guide blades integrated with the lotus-shaped micro-wind turbine. | Horizontal flow augmentation – Barchan dune guide blades | Drag-type lotus-shaped wind turbine – Simulation | Average torque and power coefficients increased by up to 120% compared with wind turbine without guide vanes. |
| 13 | Nobile et al. (2014) | Designed an omni-directional stator to shroud an H-rotor VAWT. The stator comprises of eight straight vertical blades with two conical surfaces at the top and bottom to promote turbulent mixing. | Horizontal flow augmentation - Shroud | Darrieus VAWT - Simulation | Average torque and power coefficients were increased by 30-35% compared with a bare turbine at TSR of 2.75. |
| 14 | Kim et al. (2013) | Carried out a study on the straight-plate deflector for two counter-rotating Darrieus VAWT. A single deflector plate was placed in the upstream position to increase the local wind velocity surrounding the turbines. | Horizontal flow augmentation – Straight-plate deflector | Two counter-rotating Darrieus VAWT - Experiment | The maximum power coefficient was increased by three times when the ratio of the width of the deflector to the rotor diameter is 0.33. When the deflector was placed inside the streamline near to the VAWT, the performance of the wind turbines reduces and worse than the bare wind turbines. |
| 15 | Yao et al. (2013) | Designed a tower-shaped cowling to surround a drag-type VAWT. Eight baffles are distributed evenly around a cylindrical space to force more wind to | Horizontal flow augmentation – Tower cowling | Drag-type VAWT – Simulation | Maximum power coefficient of 0.48 for a two-bladed rotor having a chord length of 210 mm tilted at 10° was achieved. This is |

| | | | | | |
|---|---|---|---|---|---|
| | | the inner part of the rotor blades. This is to promote positive torque and reduce negative torque. | | | approximately 2.4 times higher than the value of the bare wind turbine. |
| 16 | Chong et al. (2013a) | Designed an omni-direction-guide-vane ODGV to surround a lift-type Darrieus VAWT to enhance the power output of the system. The ODGV comprises four pairs of guide vanes with upper and lower wall ducts. | Horizontal flow augmentation - Shroud | Darrieus VAWT – Simulation and experiment | The rotor rotational speed and the torque output were increased by 182% and 58% (TSR = 2.5), respectively. Meanwhile, the power output was improved by 3.48 times compared to the bare VAWT. |
| 17 | Chong et al. (2012a) | Designed a power-augmentation-guide-vane (PAGV) for a drag-type Sistan wind turbine. | Horizontal flow augmentation - Shroud | Sistan VAWT – Simulation and experiment | The rotor rotational speed was improved by 73.2%. Whereas, the power output was increased by 5.8 times at a wind speed of 3 m/s. |
| 18 | Mohamed, Janiga, Pap, and Thévenin (2011) | Carried out a study of using a straight plate as an obstacle shield for two and three-bladed Savonius VAWT. | Horizontal flow augmentation – Straight plate deflector | Savonius VAWT – Simulation | The power coefficient of the two-bladed and three-bladed Savonius VAWT was increased by 27.3% and 27.5%, respectively. From the simulation, the straight plate managed to deflect the oncoming flow towards the concave side of the wind rotor, while reducing the negative torque at the convex side of the rotor. |

| | | | | | |
|---|---|---|---|---|---|
| 19 | Pope et al. (2010) | Designed the Zephyr VAWT. Comprises of nine stator vanes surrounding the VAWT with reverse winglets. | Horizontal flow augmentation - Shroud | 5-bladed VAWT – Simulation and experiment | Improved the maximum power coefficient by 22%. |
| 20 | Altan, Atılgan, and Özdamar (2008) | Designed a wind curtain plate system for a Savonius wind turbine. Two curtains are placed at the upstream of the wind rotor to concentrate the flow of the oncoming wind. | Horizontal flow augmentation – Curtain plate system | Savonius VAWT – Simulation and experiment | The Savonius VAWT rotor integrated with the curtain plate system recorded an increase in the maximum power coefficient by 38.5%. |

### 2.4.5 Building Integrated Wind Turbine (BIWT)

Due to the diminishing of economic areas for wind turbines, interests in utilising wind energy in urban areas has increased over the years, with the government of UK provided attractive schemes to encourage the application of micro-wind turbines in urban areas (Peacock et al., 2008). As such, high-rise buildings have been retrofitted or designed with wind turbines as part of the architectural feature of the building to harness urban wind energies. These systems are commonly known as the building-integrated wind turbines (BIWTs). In the urban environment, the wind flows are usually highly turbulent. As the wind passes through or around a building, positive pressure is created on the windward position, and negative pressure is created at the side and leeward positions due to the wake and vortices. These zones having different pressure gradients accelerates the wind flow. Therefore, most of the wind turbines in urban areas are sited at the parapet, ridge, corner, edge or in specially designed architectural passages for wind augmentation (Ayhan & Saglam, 2012).

#### 2.4.5.1 Retrofitting existing buildings with wind energy systems

The process of retrofitting wind energy system unto existing high-rise buildings involves in physically linking the wind turbines to the building as a tower (Dutton, Halliday, & Blanch, 2005). Retrofitting many small rotors of various types which are commercially available instead of a few large-sized wind turbines on high-rise buildings is considered as the more economical and convenient method (Bahaj, Myers, & James, 2007). However, the conventional design of small rotors for BIWT systems may not be appealing and could pose dangerous risks due to blade failures. Moreover, the total output power from the system might be considerably lower than that from the large-sized wind turbines due to the limited installation sites at the edges of the buildings and rooftops.

Sharpe et al. (2010) have shown that for a specially designed wind turbine for urban areas, the visual impact of the wind energy system can be lessened (Figure 2.19a). Called the Crossflex, the modular form of the Darrieus wind turbine system can be easily integrated to any buildings. The Boston Logan airport building has ingeniously designed the BIWT system to be at a location on top of the building where the wind speed is accelerated to enhance the performance of the wind turbines (Figure 2.19b). Another example of using the form of building to promote concentrated wind streams over retrofitted wind turbines is shown in Figure 2.19(c). Designed by "Waugh Thistleton", a British bureau of architectural projects, the building can be represented as a sail that collects air stream around the façade of the building, accelerating the wind flow and directs them to the wind turbines located on all heights on one side (Bobrova, 2015).

Krishnan and Paraschivoiu (2016) proposed a building-mounted diffuser device to accelerate wind flow inside the channel (Figure 2.20a). A Savonius turbine is placed inside the diffuser shroud to extract energy from the accelerated flow. By using computational fluid dynamics simulation, the optimisation of the shroud and the location of the turbine can be optimised. It was found that the power coefficient of the turbine is improved from 0.135 to 0.340. In another study, Park, Jung, Lee, and Park (2015) proposed an innovative BIWT system by directly utilising the building façade, which is mostly unused in conventional BIWT systems. The idea of the concept is to fill the empty façade with wind turbines, and mounting guide vanes to concentrate and accelerate oncoming wind to the wind turbines. As shown in Figure 2.20(b), the high static pressure from the wind blowing to the building flows through the guide vanes, creating a low static pressure area, and therefore augmenting the wind flows. The simulation data showed that the wind speed was increased to more than 300% for a range of wind speeds.

(a)

(b) (c)

**Figure 2.19: (a) Architectural integration of wind turbines on the ridge of a building, (b) Logan Airport deployed some horizontal axis wind turbines, and (c) A high-rise building in London with retrofitted wind turbines**

(a) (Sharpe et al., 2010); (b) (Yu, 2008); (c) (Bobrova, 2015)

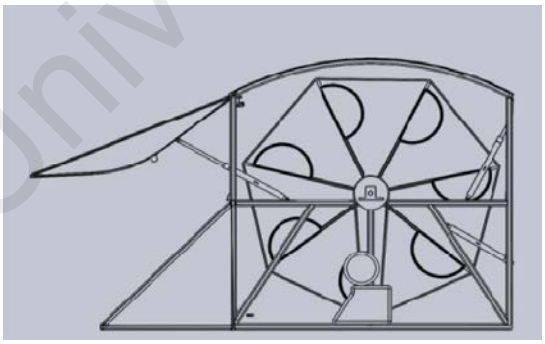

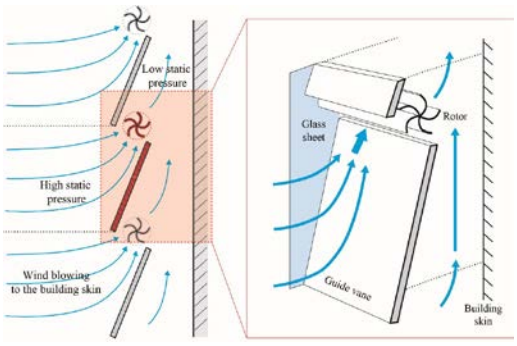


(a) (b)

**Figure 2.20: (a) 2D view of the building-mounted diffuser, (b) Schematic diagram of the BIWT system utilising the building façade**

(a) (Krishnan et al., 2016); (b) (Park et al., 2015)

#### 2.4.5.2 Architectural design with the integration of wind turbines

The most iconic building that pioneers the incorporation of large rotors in the design of high-rise building is the World Trade Centre building in Bahrain (BWTC) as shown in Figure 2.21(a). The BWTC comprises of the twin-tower building with three integrated 29 m diameter, 250 kW HAWTs (Smith & Killa, 2007). Uniquely designed wind passages on top of the London's Strata Tower concentrate oncoming wind to three wind rotors on top of the building. The three 19 kW HAWTs are designed to produce energy of approximately 8% of the total energy required by the high-rise building (Figure 2.21b).

(a) (b)

(c)

**Figure 2.21: (a) Bahrain World Trade Center, (b) The Strata Tower in London, and (c) The V-shaped roof of the hybrid solar-wind-rain eco-roof system**

(a) (Shockley, 2011); (b) (Glancey, 2010); (c) (Chong et al., 2016)

With further consideration of building architecture and the integration of renewable energy, Chong et al. (2016) proposed a new eco-friendly roof design with the hybrid solar

and wind energies generation system (Figure 2.21c). Apart from the VAWT mounted horizontally, the system is an integration of rainwater harvester, daylight and roof ventilation systems. The V-shaped roof design enhances the wind power generation due to the Venturi effect. Based on the techno-economic analysis of the system, it was found that the payback period is eight years with a total of 21205.65 kWh/year of energy generated from the hybrid wind-solar systems.

The strategy of fully implementing wind turbine into the design of the building presents futuristic and sustainable outlooks; however, there are some concerns when considering these large-scale building-integrated turbines. Vibrational issues that might affect the comfort level of building occupants must be considered in the initial design of the building. Moreover, the design of the horizontal axis BIWT systems require the blades to be fixed facing one direction. Therefore, a complete and thorough study of the proposed sites must be carried out to determine the best position to site the building.

## 2.5 Wind Turbine Theory

The wind turbine theory strongly relates to the aerodynamic study. Aerodynamic deals with the motion of air or other gaseous fluids and the forces acting on bodies moving through them. In order to design and develop a wind energy device, understanding and interpreting the aerodynamic principles is necessary. In this sub-section, the theoretical model and basic parameters of wind turbines are presented.

### 2.5.1 Theoretical models of wind turbines

In this sub-section, a one-dimensional wind turbine model is presented. The model is based on the axial momentum theory analysed by Betz in 1926. The momentum theory describes the control volume integrals for conservation of mass, axial and angular momentum balances and energy conservation (Sørensen, 2012). It is from this theory that the Betz limit was derived. According to Betz limit, no turbine can capture more than

59.3 percent of the kinetic energy in the wind. Rankine and Froude originally develop the simple axial momentum theory. The analysis assumes a control volume, in which the control volume boundaries are the surface of a stream tube and two cross-sections of the stream tube. The turbine is represented by a uniform actuator disk which creates a discontinuity of pressure in the stream tube of air flowing through it. The stream tube is visualised in Figure 2.22. The analysis uses the following assumptions:

- Homogenous, axisymmetric, incompressible, steady-state fluid flow;
- No frictional drag (inviscid flow);
- An infinite number of blades;
- Uniform thrust over the disk or rotor area;
- A non–rotating wake region; and
- The static pressure far upstream and far downstream of the rotor is equal to the undisturbed ambient static pressure.

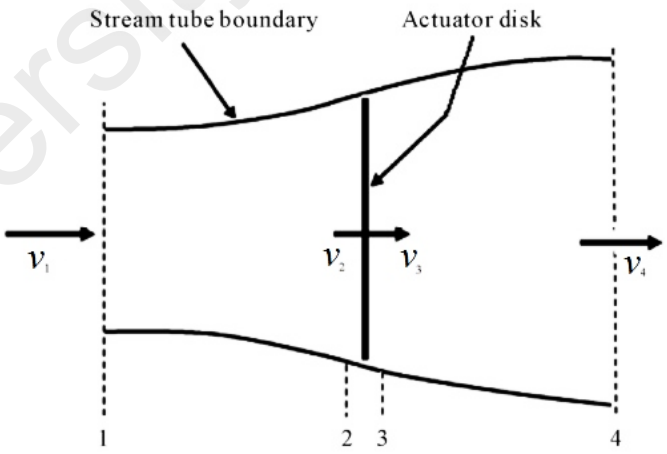


**Figure 2.22: Actuator disk model of a wind turbine. Mean air velocity is represented by $v$ while 1, 2, 3, and 4 indicate locations**

(Beri & Yao, 2011)

Applying the conservation of linear momentum to the control volume enclosing the whole system, one can find the net force on the contents of the control volume. That force is equal and opposite to the thrust, *T*, which is the force of the wind on the wind turbine. From the conservation of linear momentum for a one-dimensional, incompressible, time-invariant flow, the thrust is equal and opposite to the rate of change of momentum of the air stream (Manwell et al., 2002):

$$T = v_1(\rho AV)_1 - v_4(\rho AV)_4 \quad \textbf{(2.7)}$$

where $\rho$ is the air density, $A$ is the cross-sectional area, $V$ is the air velocity, $v$ is the mean air velocity, and the subscripts indicate values at numbered cross-sections in Figure 2.22. For a steady state flow, the equation of continuity entails that the rate of mass flow is constant in each cross-section. Thus, $(\rho AV)_1 = (\rho AV)_4 = \dot{m}$, where $\dot{m}$ is the mass flow rate. Therefore, substituting $\dot{m}$ into Equation (2.7):

$$T = \dot{m}(v_1 - v_4) \quad \textbf{(2.8)}$$

Taking into account that the thrust must be positive, the velocity behind the rotor, $v_4$, should be less than the free stream velocity, $v_1$. The pressure difference can be estimated using the Bernoulli's function by applying it in the two control volumes on either side of the actuator disc. Firstly, in the stream tube upstream of the disk (Manwell et al., 2002):

$$p_1 + \frac{1}{2}\rho v_1^2 = p_2 + \frac{1}{2}\rho v_2^2 \quad \textbf{(2.9)}$$

Then, in the stream tube downstream of the disk:

$$p_3 + \frac{1}{2}\rho v_3^2 = p_4 + \frac{1}{2}\rho v_4^2 \quad \textbf{(2.10)}$$

where it is assumed that the far upstream and far downstream pressures are equal ($p_1 = p_4$) and that the velocity across the disk remains the same ($v_2 = v_3$). The thrust can also be expressed as the net pressure difference across the actuator disk:

$$T = A_2(p_2 - p_3) \tag{2.11}$$

Solving $(p_2 - p_3)$ using Equations (2.9) and (2.10), and substituting it into Equation (2.11), the following thrust expression is obtained (Manwell et al., 2002):

$$T = \frac{1}{2}\rho A_2(v_1^2 - v_4^2) \tag{2.12}$$

Equating the thrust values from Equations (2.8) and (2.12), and recognising that the mass flow rate equals to $\rho A_2 v_2$, thus the mean air velocity at the front side of the disk:

$$v_2 = \frac{1}{2}(v_1 + v_4) \tag{2.13}$$

Hence, the wind velocity at the rotor plane, using this simple model, is the average of the upstream and downstream wind speeds. If one defines the axial induction factor, $a$ (in some literature it is called the axial interference factor) as the fractional decrease in wind velocity between the free stream and the rotor plane, then:

$$a = \frac{v_1 - v_2}{v_1} \tag{2.14}$$

Therefore, by using Equations (2.13) and (2.14) and performing various substitutions:

$$v_2 = v_1(1 - a) \tag{2.15}$$

$$v_4 = v_1(1 - 2a) \tag{2.16}$$

From Equation (2.16), the maximum value of the axial induction factor is 0.5. Else, the value of the wake velocity will be negative. By substituting Equation (2.16) into Equation. (2.12), the axial thrust on the disk is simplified as (Manwell et al., 2002):

$$T = 2\rho A v_1^2 a(1 - a) \tag{2.17}$$

Also, the power extraction is equal to $v_2 T$, hence using Equations (2.15) and (2.17):

$$P = 2\rho A v_1^3 a(1 - a)^2 \tag{2.18}$$

The non-dimensional thrust and power coefficients of the wind turbine can be characterised as follows:

$$C_T = \frac{T}{\frac{1}{2}\rho A v_1^2} \tag{2.19}$$

$$C_P = \frac{P}{\frac{1}{2}\rho A v_1^3} \tag{2.20}$$

Therefore, by applying Equations (2.17) and (2.18) into Equations (2.19) and (2.20), respectively:

$$C_T = 4a(1 - a) \tag{2.21}$$

$$C_P = 4a(1 - a)^2 \tag{2.22}$$

Then, by differentiating Equation (2.22) with respect to the axial induction factor, $a$, and setting the derivative to zero, the maximum value of the power coefficient is as follows:

$$\frac{dC_P}{da} = \frac{d(4a - 8a^2 + 4a^3)}{da} = 4 - 16a + 12a^2 = 0 \quad \textbf{(2.23)}$$

Solving Equation (2.23) produced two solutions; $a$ = 1 and $a$ = 1/3. Applying the former will give the minimum value of power coefficient, $C_P$ = 0. Hence, substituting $a$ = 1/3 in Equation (2.22), the maximum power coefficient (Manwell et al., 2002):

$$C_{P,max} = C_{P,Betz} = 4 \times \frac{1}{3} \times \left(1 - \frac{1}{3}\right)^2 = \frac{16}{27} = 0.593 \quad \textbf{(2.24)}$$

which is the value for the Betz limit. Note that this value does not include the losses for the rotation of the wake. Hence, the extractable amount of power obtained from any wind turbines will be much less than this value.

### 2.5.2 Wind turbine power output

The extraction of power from the wind by the wind rotor causes the wind to slow down. After the oncoming wind interacts with the rotor blades, the wind speed behind the rotor is lower than its initial speed. The value given in Equation (2.24) represents the maximum fraction that an ideal wind turbine can extract power from the wind. The power coefficient of a real turbine, $C_{P,real}$ is therefore less than the value given in Equation (2.24). To estimate the power output of real wind turbines, the following relationships can be used:

$$P_{turbine,real} = C_{P,real} \frac{\rho A v^3}{2} \quad \textbf{(2.25)}$$

$$P_{turbine,real} = P_{turbine,Betz} \frac{C_{P,real}}{C_{P,Betz}} \quad \textbf{(2.26)}$$

The value of $C_{P,real}$ is an empirically measured characteristics of a real wind turbine.

### 2.5.3 Tip speed ratio, $\lambda$ (TSR)

To obtain a maximum or an optimal efficiency of the wind rotor, it is necessary to match the angular velocity of the rotor to the oncoming wind speed in the design of a wind turbine. If the rotor of the wind turbine turns too slowly, most of the winds will pass undisturbed through the gap between the rotor blades with a small amount of power extraction. On the other hand, if the rotor turns too fast, the rotating blades act as a solid wall obstructing the wind flow and hence reducing the power extraction. It is also interesting to note that the TSR of a wind turbine can also be correlated with its solidity. The tip speed ratio (TSR) is defined as the ratio of the speed of the rotor tip to the free stream wind speed as the following non-dimensional equation:

$$TSR: \lambda = \frac{\text{Tip speed of rotor blade}}{\text{Wind speed}} = \frac{v_{tip}}{V} = \frac{\omega r}{V} \qquad \textbf{(2.27)}$$

where $v_{tip}$ is the speed of the rotor blade tip, $V$ is the wind speed, $\omega$ is the angular velocity of the rotor and $r$ is the radius of the rotor. The tip speed of the rotor blade is the tangential velocity of the rotor blade tip. However, the theory of TSR is only applicable to the lift type turbine, since the drag type turbine depends only on the drag force from the wind flow, which means the blade speed will either be the same as the wind speed or lower.

### 2.5.4 Wind turbine solidity

The solidity of a wind turbine is usually defined as the percentage of the circumference area of the rotor which contains material rather than air. The solidity of a wind turbine is defined as the ratio of blade surface area ($nch$) to the frontal swept area ($2Rh$) that the rotor passes through. From the literature review, the solidity of a wind turbine can be either expressed as $nc/R$, or $nc/d$ ($d$ represents the diameter of the rotor, $R$ is the radius, and $h$ is the height of the rotor). It has been found from the literature that most researchers

have used $nc/R$ as the definition of the solidity (Islam, Fartaj, & Carriveau, 2011; Kirke, 1998). Therefore, the solidity, $\sigma$ can be expressed as:

$$\sigma = \frac{nc}{R} \tag{2.28}$$

where $n$ is the number of blades, and $c$ is the chord length. High-solidity wind turbines carry a lot of material and have coarse blades. They generate much higher starting torque and have a lower tip speed ratio than low-solidity wind turbines. Moreover, the high-solidity turbines are inherently less efficient than low-solidity machines. Figure 2.23 depicts the example of torque that can be achieved by turbines with high, medium and low solidity. The calculation for solidity for the VAWT is much more complex than the HAWT. This is due to the varying geometry with respect to the projected frontal area as the VAWT rotates (French, 2010). Table 2.4 shows the solidity values for different types of VAWTs. Note that the solidity of the Darrieus turbine is the lowest.

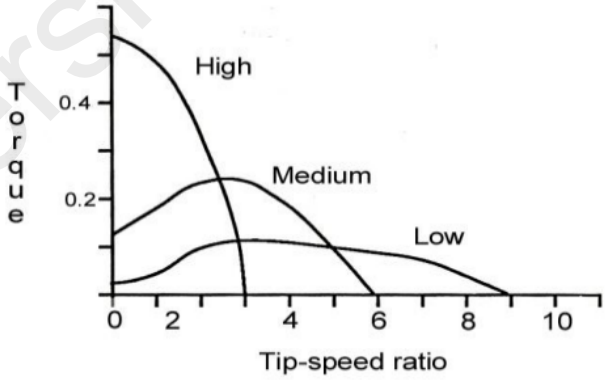


**Figure 2.23: Example of torque versus tip speed ratio for wind turbines with high, medium and low solidity**

(Noble & Sanchez, 2008)

**Table 2.4: Solidity of different types of VAWTs and their other characteristics**

| Type | Speed | Torque | $C_p$ | Solidity, % |
|---|---|---|---|---|
| Panemone | Low | Medium | > 0.10 | 50 |
| Savonius | Moderate | Medium | 0.15 | 100 |
| Darrieus | Moderate | Very low | > 0.25 | 10-20 |
| Variable geometry | Moderate | Very low | 0.20-0.35 | 15-40 |

(Noble et al., 2008)

### 2.5.5 Angle of attack

The angle of attack (AOA), $\alpha$ is a term used in wind turbine design to describe the angle between the chord line of an airfoil and the oncoming wind flow as shown in Figure 2.24. Lift type turbine depends completely on the shape of the airfoil blades and the angle of attack. The AOA for the VAWT is a function of wind velocity, turbine rotational speed and position around the rotational axis. Hence, throughout each revolution, the AOA is continuously changing for each blade (Blackwell, 1974).

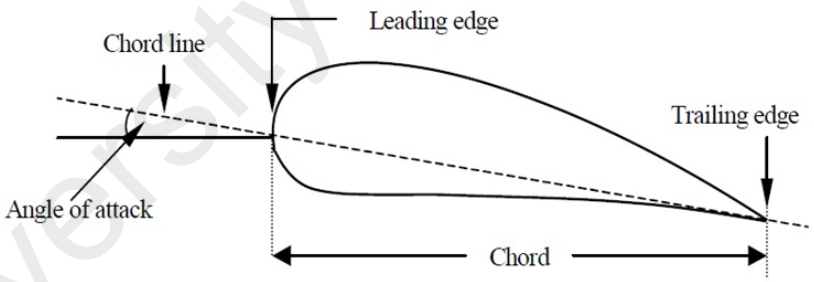


**Figure 2.24: Parameters of an airfoil**

(Mathew, 2006)

The lift and drag coefficient of an airfoil blade varies with every angle of attack. Lift coefficient, $C_L$ is the factor that contributes to the elevation of the blade (lift is always perpendicular to the wind flow). Drag coefficient, $C_D$ is used to quantify the drag, i.e. the resistance of an object in the air. These dimensionless units are expressed in the following equations:

$$C_L = \frac{F_L}{\frac{1}{2}\rho A v^2} \quad \textbf{(2.29)}$$

$$C_D = \frac{F_D}{\frac{1}{2}\rho A v^2} \quad \textbf{(2.30)}$$

where $F_L$ and $F_D$ is the lift and drag force respectively. Figure 2.25 shows the pressure distribution on an airfoil. The AOA of an airfoil controls the distribution of pressure above and below it. An airfoil at positive AOA develops negative pressure on its upper surface and positive pressure below it. The result of this pressure difference creates lift. Whereas, an airfoil at negative AOA develops negative pressure on the upper and lower surfaces of the airfoil, and positive pressure at its leading edge. This leads to the separation of flow at its trailing edge resulting in higher resistance or drag.

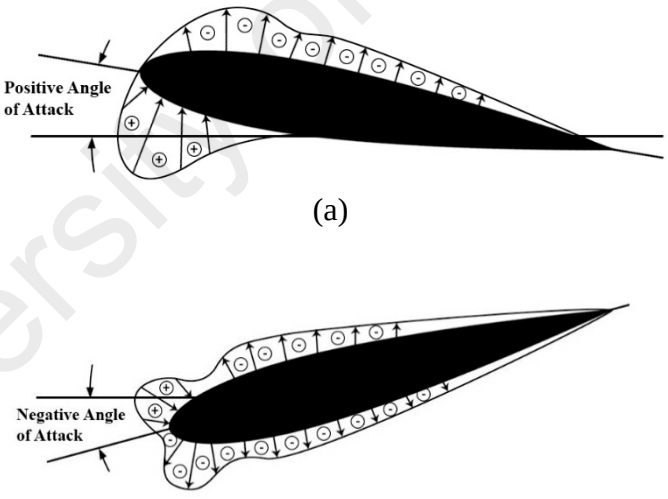


**Figure 2.25: (a) An airfoil at a positive angle of attack, (b) an airfoil at a negative angle of attack**

### 2.5.6 Lift-to-drag ratio

Aerodynamic performance is fundamental for efficient rotor design (Maalawi & Badr, 2003). The ratio is the amount of lift generated by the airfoil over the aerodynamic drag that it creates while moving through the air. A higher value of $C_L/C_D$ ratio is more

favorable as the higher lift with lower drag leads to a better performance of wind turbine. Although the coefficient for the lift and drag of airfoil is difficult to predict mathematically, freely available software such as XFOIL (Drela, 2013) or QBlade (Marten, 2016) model results accurately for wind turbine applications. Figure 2.26 shows an example of the $C_L/C_D$ ratio of NACA0015 airfoil generated using the QBlade software at Reynolds number of 20000. Traditionally, airfoil is tested experimentally with tables correlating lift and drag at given angles of attack and Reynolds numbers (Abbott & Doenhoff, 1949). Wind turbine airfoil designs have been borrowed from aircraft technologies with similar Reynolds numbers and section thicknesses that are suitable for conditions at the blade tip. However, due to the differences in operating conditions and mechanical loads, special considerations should be made for the design of wind turbine specific profiles. Such as post-stall extrapolation techniques, i.e. Viterna (Viterna & Corrigan, 1982) or Montgomerie (Montgomerie, 2004).

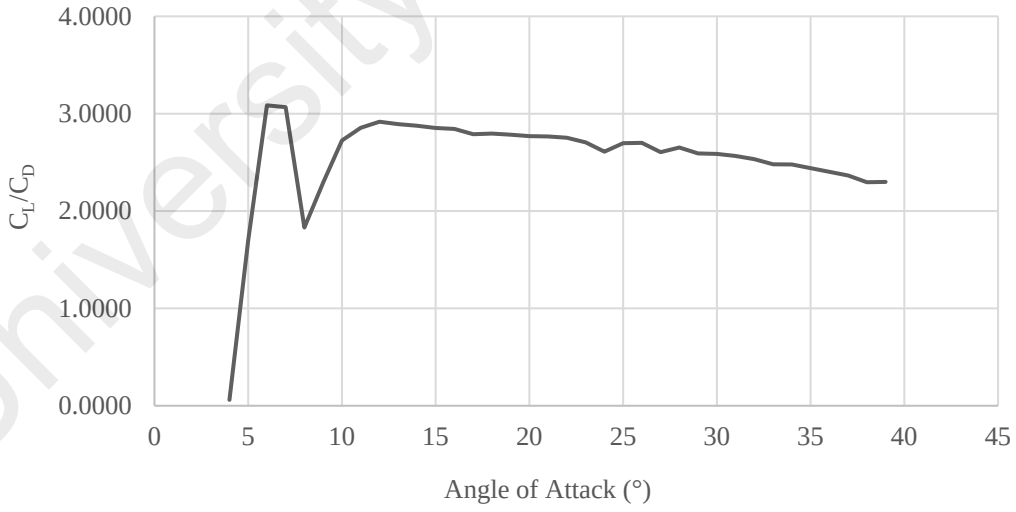


**Figure 2.26: $C_L/C_D$ graph of the NACA0015 airfoil at Re = 20000**

### 2.5.7 Blade element theory

The conservation equations of fluid mechanics were used in section 2.5.1 to derive equations for the power output and thrust for a turbine modelled as an actuator disk. The

conservation theory assumed that there is no radial dependence in the flow or over the disk, which leads to the Betz limit on wind turbine performance. However, the theory does not consider forces acting on the individual blades which produce thrust and torque, and hence power. This subsection serves as a brief introduction to the blade element theory. The forces acting on a blade element is shown in Figure 2.27. The velocity in the wind direction is given as (Manwell et al., 2002):

$$U_1 = (1 - a)U_0 \quad \textbf{(2.31)}$$

where $a$ is the axial induction factor and $U_0$ is the free-stream velocity. The circumferential velocity is given by:

$$U_2 = \Omega r + a'\Omega r \quad \textbf{(2.32)}$$

where Ω is the rotational speed of the turbine, $r$ is the turbine radius, and $a'$ is the radial induction factor. By using vector, the effective velocity is the sum of these velocities and can be given by:

$${U_T}^2 = (1 - a)^2 + [(1 + a')\lambda_r]^2 \quad \textbf{(2.33)}$$

where $\lambda_r$ is the local speed ratio of the blade element:

$$\lambda_r = \Omega r / U_0 \quad \textbf{(2.34)}$$

Meanwhile, the axial and radial induction factors can be defined as:

$$a = \left(\frac{4\ \sin^2\phi}{\sigma C_N} + 1\right)^{-1} \quad \textbf{(2.35)}$$

$$a' = \left(\frac{4\ \sin\phi\cos\phi}{\sigma C_T} - 1\right)^{-1} \quad \textbf{(2.36)}$$

with the inflow angle $\phi$, the tangential and normal force coefficients $C_T$ and $C_N$ and the rotor solidity $\sigma$, which is given by Equation (2.28). As shown in Figure 2.27, if the induction factors are known, the inflow angle can be easily computed. The inflow angle then can be used to find the angle of attack, $\alpha$. From the geometry, the inflow angle can be given as:

$$\phi = \theta_P + \alpha \quad \textbf{(2.37)}$$

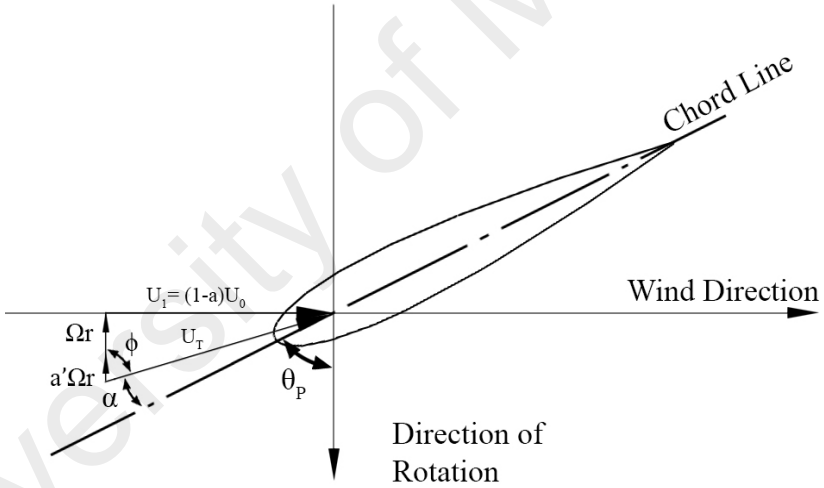


**Figure 2.27: Forces acting on a blade element**

Figure 2.28 shows the resulting lift and drag forces of a blade element. By definition, the lift force acts at right angles to $U_T$ and the drag acts in the direction of $U_T$. As the primary aim of the forces on the blade element is to produce a torque about the axis of rotation, it is necessary to maximize the lift and minimize the drag. As the drag force acts to reduce the torque produced by the lift, it is imperative that the ratio of lift-to-drag is as high as possible to indicate optimal turbine performance.

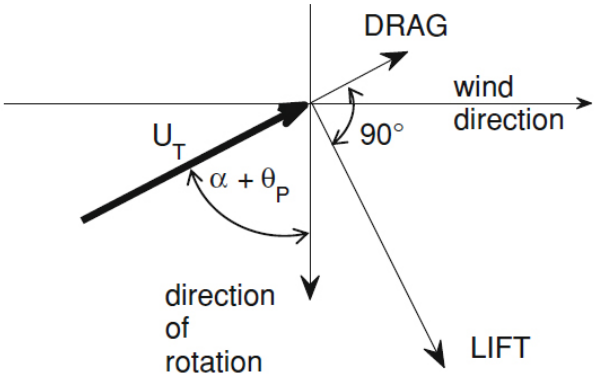


**Figure 2.28: Lift and drag forces on a blade element**

The basic assumption is that the lift and drag forces acting on the blade element are the same as those on an airfoil of the same section, the angle of attack, and effective velocity. Modifying Equations (2.29) and (2.30), the lift and drag forces in terms of the effective velocity are given by:

$$F_L = \frac{1}{2}\rho U_T^2 C_L c \tag{2.38}$$

$$F_D = \frac{1}{2}\rho U_T^2 C_D c \tag{2.39}$$

where $c$ is the chord length of the airfoil.

### 2.5.8 Darrieus vertical axis wind turbine: aerodynamic analysis

The mathematical formulation and aerodynamic analysis of Darrieus vertical axis wind rotor are complex due to the varying vectors to match the rotation of the blades based on their azimuth angles. The general mathematical expressions are first described before continuing to the main aerodynamic models of the vertical axis wind turbine. Figure 2.29 shows the illustration of velocities and forces acting on an airfoil.

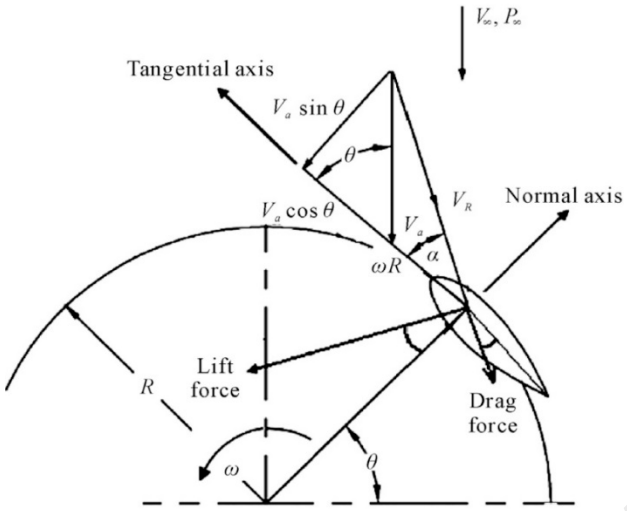


**Figure 2.29: Illustration of force and velocity vectors for straight bladed vertical axis wind turbine**

(Beri et al., 2011)

Based on the vector velocity triangle, $V_R$ can be expressed as (Beri et al., 2011):

$$V_R = \sqrt{(V_a \sin\theta)^2 + (\omega R + V_a \cos\theta)^2} \quad \textbf{(2.40)}$$

where $V_R$ represents the relative velocity, $\omega$ is the rotational velocity in rad/s, $\theta$ is the azimuth angle, $R$ is the radius of the rotor, and $V_a$ is the induced velocity. The ratio of the relative velocity and free-stream wind velocity can be acquired by:

$$\frac{V_R}{V_\infty} = \sqrt{\left(\frac{V_a}{V_\infty}\sin\theta\right)^2 + \left(\frac{\omega R}{V_\infty} + \frac{V_a}{V_\infty}\cos\theta\right)^2} \quad \textbf{(2.41)}$$

Replacing $V_2$ with $V_a$ and $V_1$ with $V_\infty$; based on Equation (2.15), the ratio of relative velocity and free-stream wind velocity (Equation (2.41)) can be modified as:

$$\frac{V_R}{V_\infty} = \sqrt{((1-a)\sin\theta)^2 + [(1-a)\cos\theta + \lambda]^2} \quad \textbf{(2.42)}$$

which is basically similar to Equation 2.33. Therefore, referring to the illustration in Figure 2.29, the expression of the angle of attack, $\alpha$ can be represented by:

$$\tan\alpha = \frac{V_a \sin\theta}{V_a \cos\theta + \omega R} \tag{2.43}$$

Non-dimensionalizing the equation:

$$\tan\alpha = \frac{\frac{V_a}{V_\infty}\sin\theta}{\frac{V_a}{V_\infty}\cos\theta + \frac{\omega R}{V_\infty}} \tag{2.44}$$

$$\alpha = \tan^{-1}\left[\frac{(1-a)\sin\theta}{(1-a)\cos\theta + \lambda}\right] \tag{2.45}$$

The aerodynamic forces and their respective components are shown in Figure 2.30. The coefficient of normal force, $C_n$ can be expressed as the difference between the drag and lift forces in their normal components. Whereas, the coefficient of tangential force, $C_t$ is the difference between the drag and lift forces in their tangential components (Beri et al., 2011):

$$C_t = C_L \sin\alpha - C_D \cos\alpha \tag{2.46}$$

$$C_n = C_L \cos\alpha + C_D \sin\alpha \tag{2.47}$$

Based on the azimuth angle, $\theta$, the thrust force, $T_i$ (the subscript $i$ refers to the instantaneous location of the rotor blades) can be described as:

$$T_i = \frac{1}{2}\rho V_R^2 (hc)(C_t \cos\theta - C_n \sin\theta) \tag{2.48}$$

where $c$ is the chord length of the blade, and $h$ is rotor blades' height. Therefore, the torque, $Q_i$ can be written as:

$$Q_i = \frac{1}{2}\rho V_R^2 (hc) C_T R \quad \textbf{(2.49)}$$

where $C_T$ is the thrust coefficient.

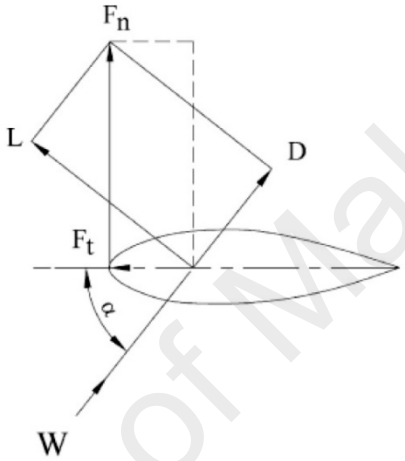


**Figure 2.30: Forces acting on an airfoil blade**

(Islam et al., 2008b)

### 2.5.9 Aerodynamic prediction model for vertical axis wind turbine

Aerodynamic prediction models have been developed throughout the decades to determine the performance of the straight bladed Darrieus VAWTs. The main purpose of all of these aerodynamics models is to evaluate the induced velocity fields of the rotating turbine. By calculating the velocity vectors, researchers are able to determine all the blade forces and hence the power output by the turbine (Brahimi et al., 1995). The basics of these models are based on the Blade Element Momentum (BEM) theory which is the prediction of flow velocity through turbine by calculating the streamwise aerodynamic forces on the blades with the rate of change in momentum of air flow (Islam et al., 2008b). Applying the Bernoulli's equation in the stream tubes, the average pressure difference

across the turbine is calculated to find the forces acting on the rotor disk (Paraschivoiu, 2002). The application of the model, however breakdowns for a rotor with large solidities with high TSRs due to inadequate momentum equations for these specific cases. Several other models have been proposed to predict the performance of vertical wind rotors, including the single stream tube model (Templin, 1974) and the multiple stream tube model (Strickland, 1975). In this thesis, the double multiple stream tube model developed by Paraschivoiu (1988) will be used to account for the vertical blades of the cross axis wind turbine.

In the double multiple stream tube (DMST) model, the area of the turbine is divided into two regions, upstream and downstream regions as shown in Figure 2.31 where the rotor area is further divided into smaller stream tubes with equal angular size (Paraschivoiu, 1981). For each tube, the one-dimensional momentum theory is used to relate the upstream and downstream blade velocities by defining an axial induction factor. Here, the wake from the upwind pass is assumed to be fully expanded, and the ultimate wake velocity has been reached before the interaction with the blades in the downwind pass (Bedon, Castelli, & Benini, 2013). Therefore, in the downwind position, the blades interact with reduced wind velocities. The DMST model states that the blades interact with the wind vectors in the upstream and downstream positions to account for the varying flow across the rotor. The subscripts $au$ and $ad$ denote the upstream and downstream positions of the induced velocity vectors.

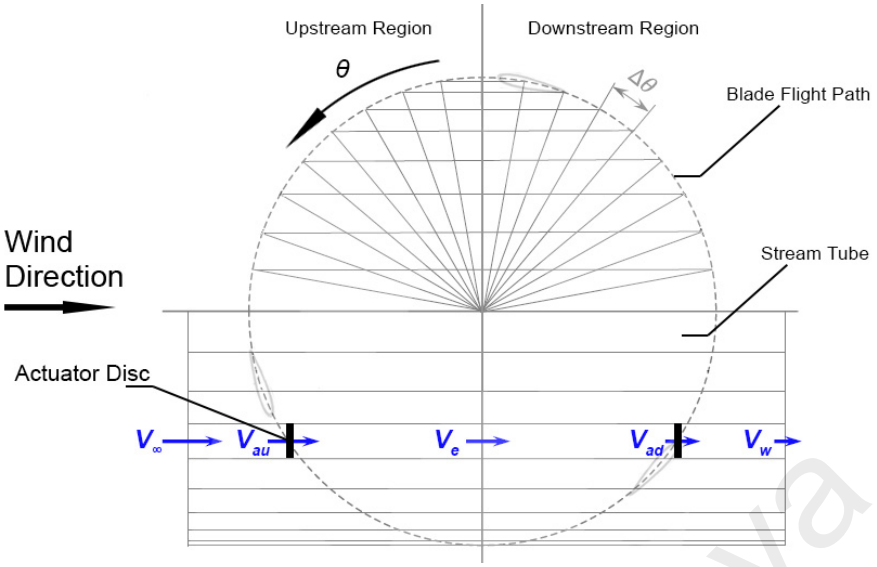


**Figure 2.31: Illustration of the upstream and downstream regions with stream tubes**

Adopted from: (Paraschivoiu, 2002)

Based on the actuator disk theory, the induced velocity, $V_{au}$ is the average of the oncoming air velocity, $V_\infty$ and the equilibrium air velocity, $V_e$. Hence:

$$V_{au} = \frac{1}{2}(V_\infty + V_e) \quad \textbf{(2.50)}$$

$$V_e = 2(V_{au} - V_\infty) \quad \textbf{(2.51)}$$

## 2.6 Wind Turbine in Skewed Wind Flow

There is increasing attention to the performance of wind turbines in skewed wind flow. Normally, the expected flow conditions are parallel to the rotor axis of the HAWTs or perpendicular to the VAWTs. The behaviour of wind turbines in the skewed flow conditions are still not fully understood. For HAWTs in skewed flow, experimental investigations and theoretical studies have shown that there is a reduction in power output when compared to the HAWTs exposed to aligned wind condition (Burton, Sharpe, Jenkins, & Bossanyi, 2001) (see Figure 2.32). This is due to the different swept area (the

area described by the diameter of the rotor and perpendicular to the oncoming wind direction) generated by the blades during rotation. In parallel flow conditions (i.e., wind direction aligned with the horizontal axis), the blades produce a planar surface area according to the circumference of the rotor, providing a perpendicular plane to the axial line of the rotor. However, the projected plane area in skewed flow conditions is reduced according to the cosine of the skewed angle as shown in Figure 2.33.

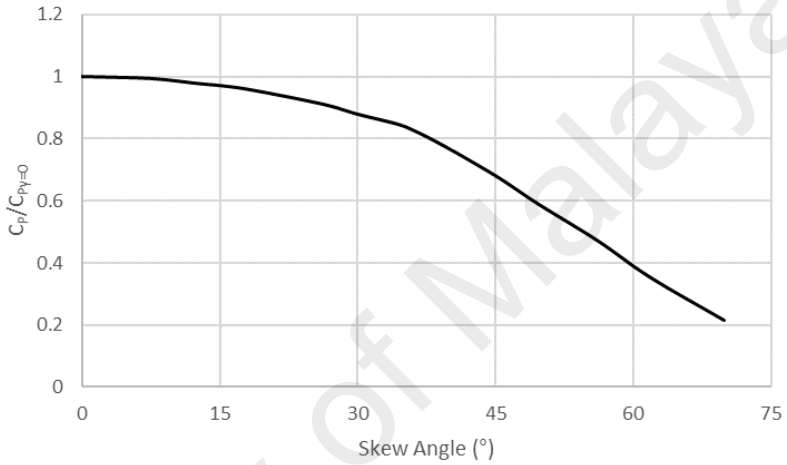


**Figure 2.32: Reduced HAWT power coefficient in skewed flow conditions**

(Burton et al., 2001)

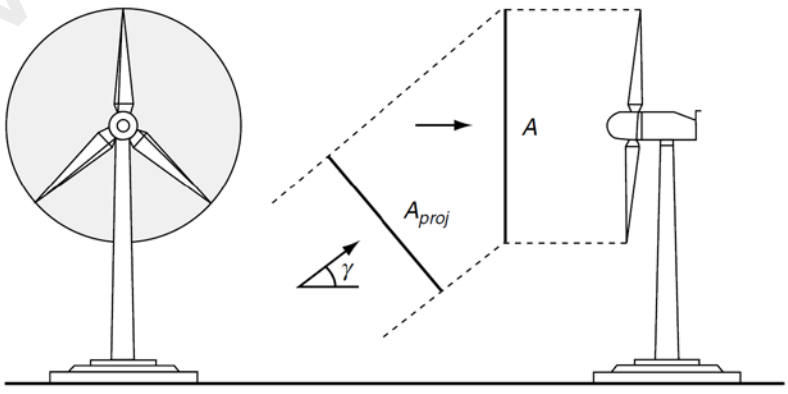


**Figure 2.33: Projected swept area as a function of the cosine of oncoming flow skew angle**

(Bianchini, Ferrara, Ferrari, & Magnani, 2012)

Experimental investigations on VAWTs showed an opposite behaviour in skewed flow conditions, in which the studies have shown that the power output was increased for relatively small skew angles, depending on the geometrical ratios of the rotor (Scheurich & Brown, 2011). In the varying interaction between the blades and the oncoming flow volume, the blades of the vertical rotor describe a cylindrical volume, different from the planar surface generated by the horizontal rotor (Bianchini et al., 2012). Therefore, the total swept area of the vertical rotor is increased, mostly due to the contribution of the skewed flow in the downwind region that balances the decrease of the projected upwind area. Hence, the misaligned flow interacts with an increased available surface area of the rotor (see Figure 2.34). Also, the increased swept area may be due to the expanded airflow in the downwind region of the rotor. If the aspect ratio of the vertical rotor is sufficiently small, the skewed convection of the wake could cover a larger surface area in the downwind and upwind regions of the rotor. Therefore, the interaction between the skewed airflow and the blades of the vertical rotor could potentially generate more lift, hence producing higher torque and better power output.

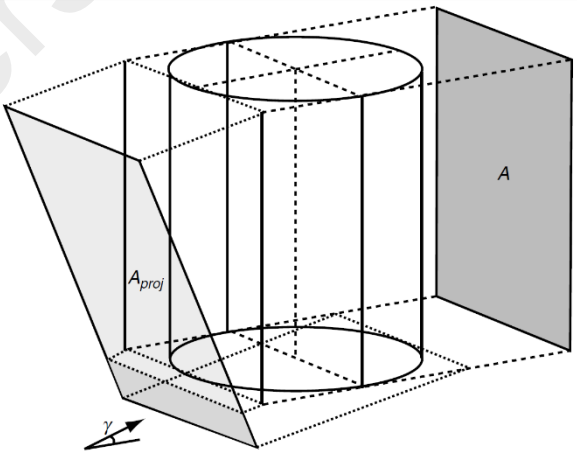


**Figure 2.34: Increased projected swept area for a VAWT in skewed flow condition**

(Bianchini et al., 2012)

During normal operation, the vertical axis wind turbine blades encounter the wake of the vertical rotor as they move to the downwind zone of the rotor's azimuthal cycle. In normal flow, the whole length of each blade is exposed to the wake of the turbine in the downwind region of the rotor as shown in Figure 2.35(a). In skewed wind flow conditions, the convection of the wake follows the skew angles of the oncoming flow (Figure 2.35b), therefore allowing the undisturbed wind of the skewed flow to interact with some areas of the downwind blades (Scheurich et al., 2011). The resultant effects, and by comparing these two different flows, are in the tangential force produced by each of the blades. In normal flow, the interaction between the wake and the blades in the downwind region suppresses the potential torque due to the turbulent and low wind speed condition of the downwind wake. Therefore, much of the torque output is produced by the blades in the upwind region of the rotor (i.e., contributes to the fluctuation of torque as the turbine rotates). In skewed flow, however, the undisturbed portion of the downwind wake that interacts with each of the blades can contribute to the overall increase in the rotor power output. For a horizontal axis wind turbine in skewed flow, experimental investigations and theoretical studies have shown that there is a reduction in electrical energy output compared to the HAWT in normal wind condition due to a reduced swept area (Burton et al., 2001). Hence, the skewed flow phenomenon has shown the advantage of the VAWT over the HAWT with respect to the behaviour of the rotor under varying airflow angle conditions which are common in urban settings.

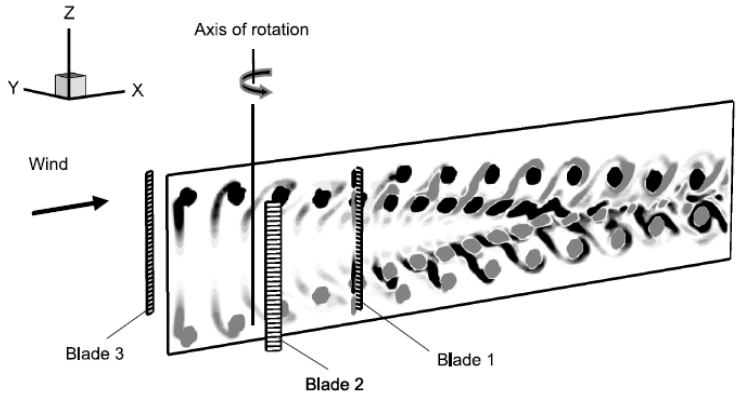


(a)

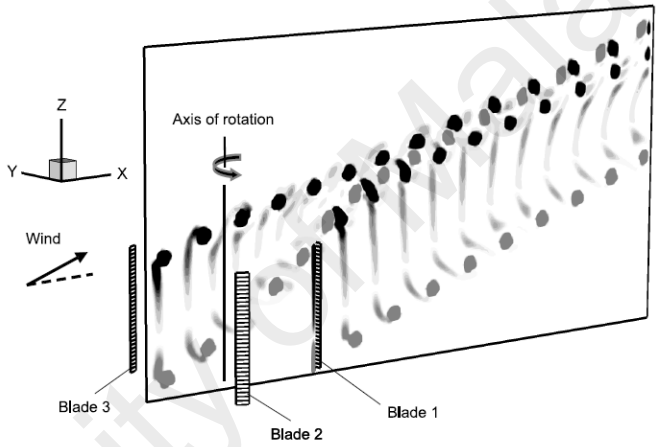


(b)

**Figure 2.35: (a) Wake characteristics during normal flow, (b) Wake characteristics during skewed flow**

(Scheurich et al., 2011)

Recent studies have shown that the progress of wind turbine design should be focused on optimisation of the struts' shape and configuration, as the supporting structures can influence the performance of wind turbine rotors, particularly in small wind turbines (Bianchini, Ferrara, & Ferrari, 2015). Airfoil-shaped struts, as with the current study, can reduce the parasitic drag commonly found in normal struts and produce additional torque from the lift force of the airfoil struts. Some suggest that the airfoil struts in skewed flow conditions can further increase the performance of the wind turbine (Islam, Fartaj, &

Carriveau, 2008a). However, many of the current research work only deal with the conventional wind turbine in skewed wind flow conditions.

By measuring the flow and the wake shed by the VAWT in normal and skewed flow, Ferreira (Ferreira, 2006) showed that with normal flow, the characteristics of the flow in and around the rotor, and in the wake, are mostly influenced by the upwind passage of the blades. Therefore, the downwind region of the VAWT operates in the wake of the upwind half of the rotor which results in reduced energy potential. The stronger vorticity in the upwind area of the VAWT (due to higher lateral wind loading) generates wake and alters the downwind stream which saw the loss of energy potential in the downstream position (Worasinchai et al., 2015). Similar observations were made by Balduzzi et al. (2012) who carried out computational fluid dynamics (CFD) studies on different roof shapes with different geometrical proportions. The results showed that the power output from the VAWT increased by up to 12% for skew angles between 15° to 30°. In another study, Orlandi, Collu, Zanforlin, and Shires (2015) developed an unsteady RANS 3D approach to predict the performance of an H-rotor VAWT in skewed flow conditions. Comparable observations were made, in which the improvement of power potential produced by the VAWT in skewed flows are due to the reduced disturbance in the wake generated during the upwind phase.

In the urban context, wind turbines operate close to the wakes induced by buildings that may cause skewed flow conditions. In investigating the performance of an H-Darrieus performance on a roof, Mertens et al. (Mertens, van Kuik, & van Bussel, 2003) had shown that the rotor power output increased by 30% when the rotor was exposed to 10°-40° skewed angle wind flow. The experimental data were also compared with improved momentum models that were modified based on the evaluation of both the aerodynamic efficiency of the airfoils and the turbine swept area. Mertens et al. suggested

that in skewed flow conditions, the lift and drag forces generated by the airfoils depend only on the orthogonal component of the oncoming wind velocity, whereas the parallel component contributes to the zero effect on the surface of the airfoils. This is known as the cross-flow principle (Hoerner, 1965; Hoerner & Borst, 1985), which describes the wind speed interacting with the blades of the vertical rotor in skewed flow to become a function of both the induction factor of a stream tube and the skew angle. To accommodate the different energy extraction of each azimuthal section of the turbine, Mertens et al. (2003) divided the rotor into three separate sectors of height, to represent single and double stream tube zones of the skewed flow through the rotor, as shown in Figure 2.36.

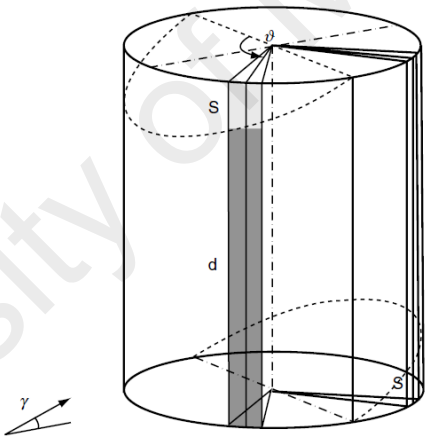


**Figure 2.36: A proposed rotor model divided into different zones based on heights to account for the skewed flow**

(Mertens et al., 2003)

In another study, Simão-Ferreira, van Bussel, and van Kuik (2006) developed a model to predict the effect of the skewed flow on the performance of an H-rotor wind turbine. Based on the behaviour of the turbine in skewed flow and the variation of the projected swept area, a correction to the power coefficient was applied using the ratio of inflow momentum between the turbine in normal and skewed flow conditions. The method

showed good agreement between the experimental and the estimated data. However, the rotor information in normal flow condition is required before any approximation is made using this method. Therefore, Bianchini et al. (2012) proposed an improved model to estimate the performance of the H-rotor in skewed flows. The analytical method focuses on the cross-flow principle in skewed flow and evaluating the turbine projected swept area in the upwind and downwind portions of the rotor. The method describes the zonal evaluation of torque output by considering either a single or double flow-rotor interaction (i.e., single actuator disk theory and double multiple stream tube model) in both the upwind and downwind regions (as shown in Figure 2.37). Notable agreement between the experimental and analytical data was shown, with an increase in accuracy over the method proposed by Simão-Ferreira et al. (2006). However, the model's validity is limited to a range of skew angles based on the aspect ratio of the turbine.

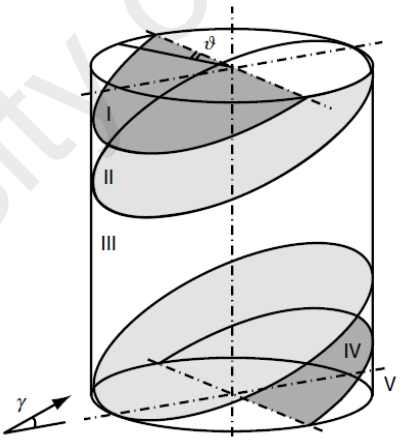


**Figure 2.37: A proposed rotor model divided into different skewed zones**

(Bianchini et al., 2012)

## 2.7 Summary

This chapter has introduced the research and development of the wind turbine technology. From the basic design and type of wind turbines, the flow augmentation devices, to the more complex aerodynamics fundamentals. As discussed, the research and

development on the use of this technology are still on-going. Researchers explored novel designs of wind turbines to enhance their performances. Based on the literature, the remarkable features shown by the new wind turbines have demonstrated the importance of innovative design towards improving the vertical axis wind turbine technology. However, to the best of the author's knowledge, none of the design goals had focused on the harnessing of the vertical component of the oncoming wind, which is the essence of the current research aim. The novel cross axis wind turbine was conceptualised to capture the maximum potential of wind energy in the vertical component of the oncoming wind, which is often overlooked.

Findings from the literature showed that the performance of the VAWT in skewed flow conditions could be further improved. However, this depends on the design and geometry of the rotor, and a limited range of skew angles. Studies on the geometrical aspects of the VAWT and their relations in skewed wind flow were explored have also shown that in a skewed airflow, and if the VAWT aspect ratio (AR) is sufficiently small ($H/R$ ratio less than 2.1), the rotor could generate a higher power output compared to the VAWT operating in normal flow condition due to the skewed convection of the wake. Therefore, the improved performance of the VAWT in skewed airflow is due to the wake convection that covers a larger area in the downstream and upstream regions of the rotor (Scheurich et al., 2011). This study seeks to take advantage of this phenomenon, where the cross axis wind turbine was designed to capture the skewed wake of the oncoming airflow by using airfoil struts with various pitch angles.

# CHAPTER 3: METHODOLOGY

## 3.1 Introduction

There are two research works presented in the thesis. The main research seeks out to design and analyse a new type of wind turbine that can take advantage of the misaligned flow of wind. As discussed in the literature review, many research works have been carried out to improve the design of the vertical axis wind turbine. In this study, a new type of wind turbine with airfoil-shaped struts have been designed to take advantage of the kinetic energy of skewed airflows. In order to produce the skewed airflow, deflectors are integrated into the design to enhance the oncoming flow and interact with the airfoil-shaped struts. Moreover, the applicability of a wind-augmentation device as a renewable energy generation system is also presented in this thesis. The potentiality of the device in low wind speed regions was carried out through the case study to assess the integration of a wind-augmentation device called the omni-direction-guide-vane (ODGV) with a vertical axis wind turbine (VAWT) in an urban environment. The ODGV was designed to surround the VAWT to create a venturi effect and increases the oncoming wind speed before it interacts with the turbine blades.

## 3.2 Design Concept and Description of the Cross Axis Wind Turbine

Figure 3.1 shows the flowchart of the cross axis wind turbine research. By using CAD software, the design of the cross axis wind turbine is developed based on the concept. Prototypes are fabricated for laboratory testing and characterisations, and then theoretical development is carried out for further analysis. As mentioned, the cross axis wind turbine design takes advantage of the qualities of both the HAWT and the VAWT while overcoming their respective drawbacks. The design of the novel turbine has the benefit of better turbine performance in the unpredictable nature of the wind since it can extract

wind energy from both the horizontal and vertical wind components. The CAWT has the potential to replace the conventional vertical axis wind turbine for urban wind energy system due to its ability to extract wind energy irrespective of the direction of the wind, thereby enhancing the power performance output. The disadvantages in terms of oncoming wind directions for HAWT and VAWT are illustrated in Figure 3.2. The HAWT shown in Figure 3.2 relies on one horizontal wind direction, therefore requiring a yaw mechanism to rotate the wind turbine. The VAWT, being an omnidirectional device, interacts with winds from any horizontal direction.

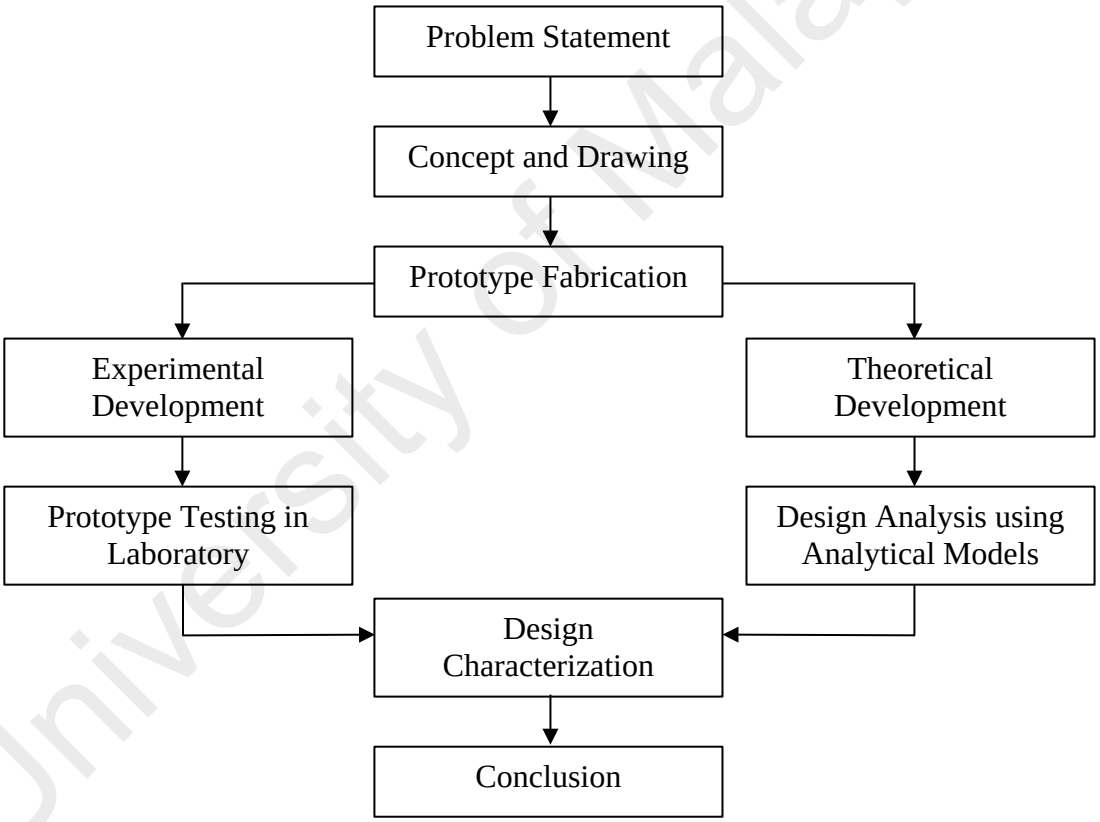


**Figure 3.1: Research flowchart of deflector integrated cross axis wind turbine**

Unlike the conventional vertical axis wind turbine, the CAWT structure is made of three main vertical blades that are connected to the six untwisted horizontal blades via specially designed connectors. The three vertical blades criteria call for the six horizontal blades to be arranged evenly. Therefore, at each of the upper and lower rotors, the blades

are arranged at a 120º angle between each other. Also, the upper horizontal rotor of the CAWT is at an offset angle of 60° relative to the bottom struts to attain a well-distributed force along the horizontal blades to reduce vibration. Besides, the concept creates a sufficient area for the skewed wind to pass through in between the blades. This arrangement forms the cross axis wind turbine, and it differs from the conventional H-rotor VAWT where the airfoil-shaped struts can produce lift from the interaction of the vertical airflows, therefore maximising the wind energy potential. The CAWT occupies the same space as the VAWT but can create more lift generation forces due to the larger swept areas, owing to the vertical and horizontal blade arrangement. Moreover, it is inferred that the airfoil-shaped struts might induce aero-levitation forces that can be useful in reducing frictions in the generator and therefore prolonging its life cycle.


**Figure 3.2: Wind direction for the VAWT and HAWT**

The concept of using deflectors stems from the fundamental knowledge that when wind approaches an object, its speed will be slowed down by the obstacle. However, based on the conservation of momentum, the wind flows around the object, and its speed will be accelerated by some magnitude. Therefore, at the lowest pressure point around the object, the wind speed is the highest, and vice versa. This creates a transitory accelerated region around the object, as shown in Figure 3.3. This phenomenon is able to

enhance the kinetic energy with increased Reynolds number required by the CAWT to improve the lift force generated by the airfoils. Therefore, the performance of the CAWT can be enhanced for low wind speed region, owing to the speed-up effect of wind around obstacles.

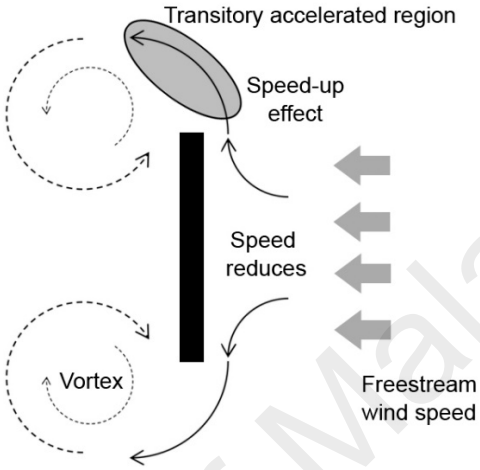


**Figure 3.3: Transitory accelerated region**

The wind characteristics in urban areas are significantly influenced by the roughness of urban terrain where there are large densities of high-rise buildings. These bluff bodies produce complex wind characteristics where the separation of wind flow is influenced by the buildings in response to the high multi-directional wind in urban environments. The CAWT has superior turbine performance in multi-directional wind conditions found in urban areas, as it can extract wind energy from the horizontal and vertical components. These unpredictable wind conditions in urban areas require specially designed wind turbines to maximise the potential of wind power. Hence, the new cross axis wind turbine design is proposed.

### 3.2.1 The general arrangement of the cross axis wind turbine

Shown in Figure 3.4, the cross axis wind turbine is a combination of six horizontal blades and three vertical blades. The CAWT rotor assembly is mounted on a support

frame and rotates on its vertical axis. The shaft in the centre of the CAWT is directly fixed to the generator. The horizontal blades act as the connecting struts of the CAWT, linking the hub to the vertical blades via the connectors. The upper and lower hubs are attached to a central shaft. In total, the fabricated model has six connectors to link the vertical and horizontal blades together.

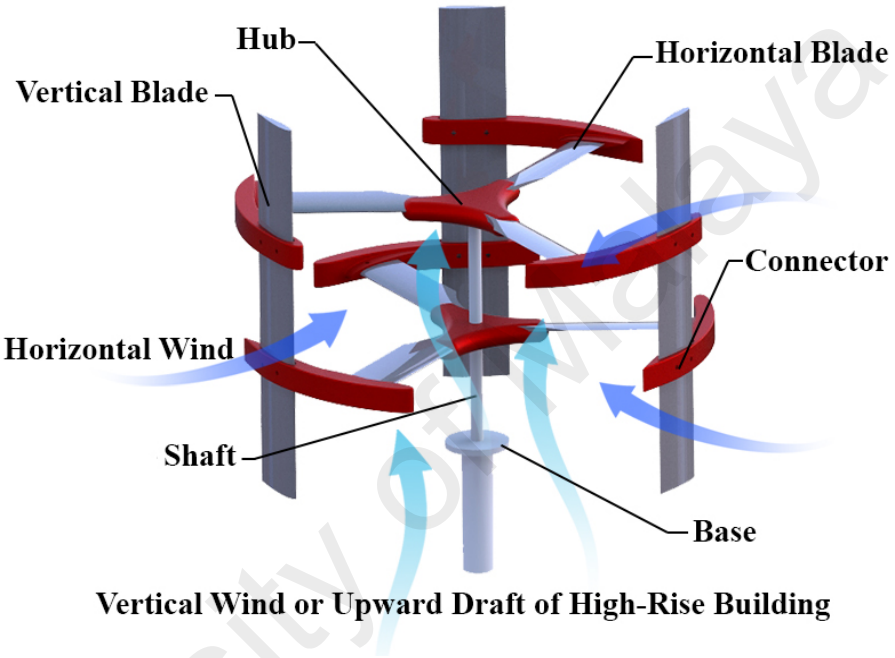


**Figure 3.4: The cross axis wind turbine's general arrangement**

In Darrieus wind rotor, the struts provide support by connecting the central rotating column to the blades. The struts are crucial in transferring torque to the central shaft, stabilising the rotor during extreme wind speed conditions, reducing fatigue stresses in the blades and can influence some natural frequencies in the rotor (Islam et al., 2008a). Typically, the connecting struts are made of flat plates with no aerodynamic characteristics. Therefore, in some cases, the connecting struts can become detrimental to the turbine overall performance due to the parasitic drag generated by the flat plates. By using airfoils (i.e. streamline-shaped objects), the parasitic drag can be reduced significantly and thus improving the performance of the VAWT. In this study, the

connecting struts for the CAWT are airfoil-shaped, and these horizontal blades are pitched at different angles to investigate the pitch angle effect on the performance of the wind turbine.

### 3.2.2 Working principle of the cross axis wind turbine

As discussed, the concept of the novel cross axis wind turbine (CAWT) is to extract wind energy from the oncoming wind by creating a larger interaction area between the winds and the airfoils. By utilising the vertical component of the skewed airflow, the horizontal blades can interact with the oncoming wind vector to create lift (i.e., HAWT-like rotor). The potential energy in the normal oncoming flow orthogonal to the vertical blades can still be extracted at the same time. Therefore, the airfoil-shaped struts can enhance the self-starting ability of the CAWT, and improve the performance of the entire wind turbine by extracting most of the available energy from the oncoming wind. The significant advantage of the CAWT is that it can function with airflow that is omnidirectional from the sides for the vertical blades, and from the bottom of the turbine through the horizontal blades (see Figure 3.5). The vertical wind component, either created by the building or a guide vane structure, interacts with the airfoil-shaped struts. The primary function of the connectors is to link the horizontal blades to the vertical blades. The upper and lower horizontal blades can be pitched at different angles to allow for optimisation of the CAWT performance. The rotational kinetic energy from the spinning of the CAWT is converted into mechanical energy at the central shaft. The direct coupling of the shaft to the generator ensures that the energy loss during the conversion of mechanical to electrical energy is minimal.

(a) (b)

**Figure 3.5: Artist's impressions of (a) CAWT on top of a high-rise building, and (b) CAWT with a guide vane structure with illustrations of the wind flow**

### 3.2.3 Shape of airfoil

A proper choice of a suitable airfoil profile for the prototype can aid in the improvement of the turbine performance. For this study, the symmetrical NACA0015 airfoil profile (National Advisory Committee for Aeronautics) with a 15% thickness to chord ratio was chosen. In some studies, the cambered airfoil is preferable for the VAWT due to virtual camber effect that may be detrimental to the turbine's efficiency in energy extraction (Migliore, Wolfe, & Fanucci, 1980; Rainbird et al., 2015). However, the symmetrical NACA airfoils have been a popular choice for VAWT researchers due to the availability of well-documented data. Therefore, the process of validation of numerical and theoretical predictions can be made faster and easier. Moreover, symmetrical airfoils can provide lift from both sides of the airfoil due to having the same aerodynamic characteristics of lift and drag on the upper and lower surfaces of the airfoil (Hameed & Afaq, 2013). As such, the NACA0015 airfoil blades were used throughout the study.

### 3.3 Wind Turbine Prototype

Tests were carried out to investigate the capability of the CAWT compared to a conventional straight-bladed VAWT. In carrying out the study, lab-scale experiments were conducted in which a small CAWT prototype was built as per the design parameters as shown in Table 3.1. A VAWT was also constructed with the same dimensions and tested under similar experimental conditions as the CAWT for benchmarking. In the current study, the rotor diameter of the CAWT, *d*, is 350 mm. The vertical blade chord length and height are 50 mm and 300 mm, respectively, and the horizontal blade chord length is 34 mm (refer to Figure 3.6). The pitch angle, $\beta_b$ of the CAWT horizontal blades was varied from 0° to 15° (in incremental value of 5°) to determine its effect on the performance of the turbine. Therefore, four different CAWT configurations were fabricated and tested for the lab-scale study. The materials used for the fabrication of the wind turbines are shown in Table 3.2 while the lab-scale models of the CAWT and VAWT used in the experiment are shown in Figure 3.7.

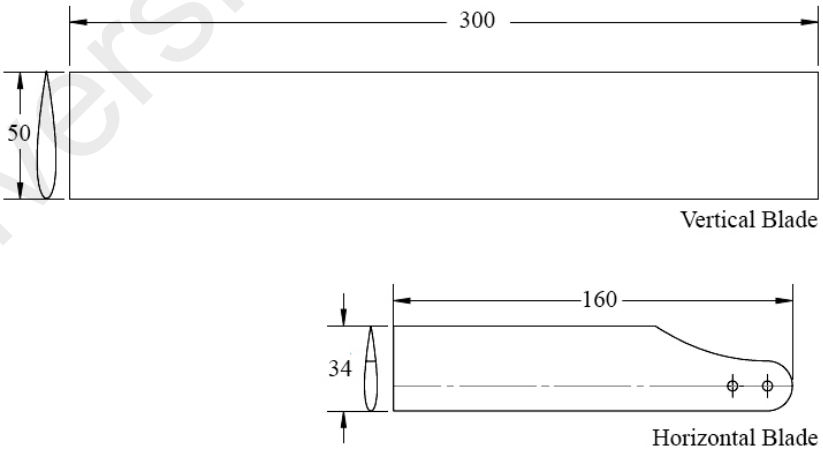


**Figure 3.6: Blade dimensions (in mm)**

**Table 3.1: Design parameters of the wind turbines**

| Parameters | CAWT | VAWT |
|---|---|---|
| Diameter of rotor, $d$ (mm) | 350 | 350 |
| Height of vertical blade, $h$ (mm) | 300 | 300 |
| Chord length of vertical blade, $c$ (mm) | 50 | 50 |
| Number of vertical blades, $N$ | 3 | 3 |
| Connecting struts of the VAWT | - | Radius = 150 mm (flat plate: thickness = 2.03 mm, width = 25 mm) |
| Pitch angle of vertical blade, $\beta$ (°) | 0 | 0 |
| Length of horizontal blade, $l_b$ (mm) | 150 | - |
| Chord length of horizontal blade, $c_b$ (mm) | 34 | - |
| Pitch angle of horizontal blade, $\beta_b$ (°) | 0, 5, 10, 15 | - |
| Number of horizontal blades, $N_b$ | 6 | - |
| Profile of airfoils | NACA0015 | |

**Table 3.2: Materials selection**

| Components | CAWT | VAWT |
|---|---|---|
| Horizontal blades | Carbon fibre | - |
| Vertical blades | Carbon fibre | |
| Connecting struts | - | Mild steel |
| Connectors | Rapid prototyping material, ABS (Acrylonitrile Butadiene Styrene) | - |
| Shaft | Mild steel | |
| Hub | ABS | - |
| Generator | 10 W | |
| Deflector | Acrylic glass | |

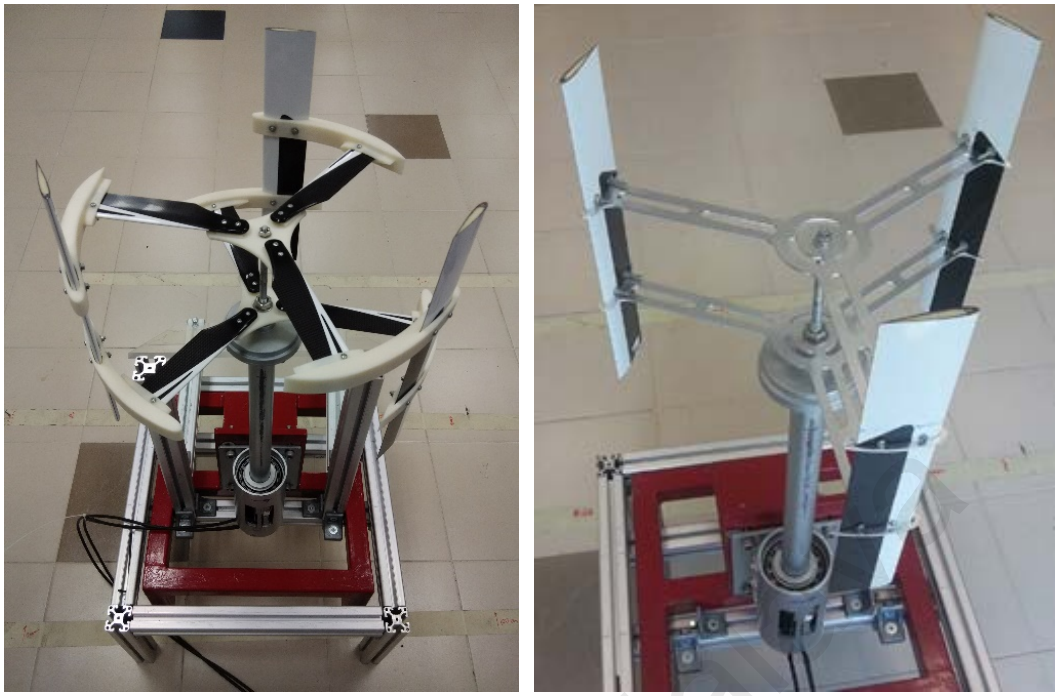

(a) (b)

**Figure 3.7: (a) The CAWT prototype, and (b) the VAWT model**

A detailed view of the CAWT configuration is shown in Figure 3.8(a), in which the illustration of one-third of the turbine is presented. The figure shows one vertical blade and two horizontal blades, linked by the bottom and top connectors. The connectors were carefully designed to support the vertical and horizontal blades of the CAWT. The basic design of the connector resembles the form of an airfoil, with leading and trailing edges on the curved outline of the connector. The aerodynamic properties of the connectors and their effects, however, are not within the scope of the current study and therefore future studies investigating the connectors are necessary. A further look into the design of the connectors shows that the top connector can be identified by the position of the vertical blade slot near the leading edge of the connector whereas the vertical blade slot for the bottom connector is positioned near the trailing edge of the connector. The vertical blades are inserted through the vertical blade slots of the connectors and fixed with screws. Whereas, the horizontal blades are inserted into the horizontal blade slots of the connectors. Note that the hubs were designed with inclined planes to accommodate the

horizontal blades with various pitch angles. Additional drawings of the CAWT can be found in Appendix A.

The use of rapid prototyping machine aids the fabrication of the connectors and the hubs (Dimension BST 1200es, as shown in Figure 3.9a). The material for the hubs and connectors is the Acrylonitrile Butadiene Styrene (ABS), with a layer resolution of 0.2540 mm. There are a few particular options available for the rapid prototyping process. Sparse double dense (high density) is chosen for the interior fill style. It is a bi-directional raster interior that creates a honeycomb grid pattern with multiple contours around the boundaries. This interior style is a good compromise between the durability of the part and the volume of material usage. In addition, there are a few support styles that can be chosen depending on the user's usage. Supports are used to support overhangs and prevent the part from collapsing while the prototyping process is in progress. For this research, the Smart support is chosen due to its practicality and easy removal. The fabricated parts are shown in Figures 3.9(b) and 3.9(c).

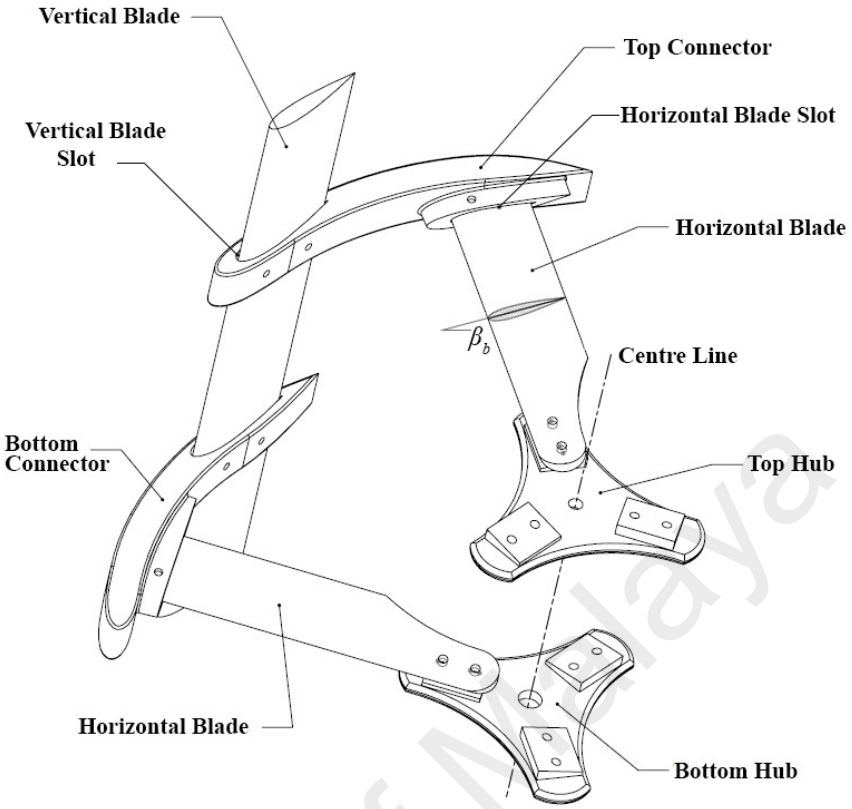


(a)

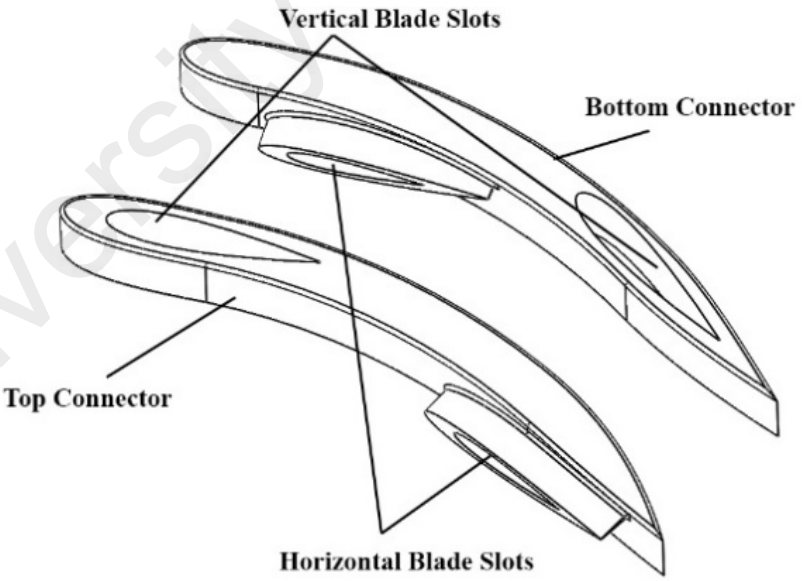


(b)

**Figure 3.8: (a) An illustration of the CAWT showing the pitch angle, $\beta_b$, of the horizontal blades. The vertical blade is linked with the horizontal blades via the connectors, and (b) the top and bottom connectors of the CAWT**

(a)


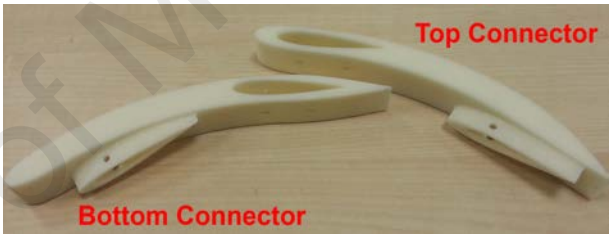


(b) (c)

**Figure 3.9: (a) The Dimension BST 1200es rapid prototyping machine, (b) the fabricated bottom and top hubs, and (c) the bottom and top connectors**

## 3.4 Experimental Setup

A small-scale experiment was conducted to investigate the performance of the CAWT, from which the results will be compared to the performance of a conventional VAWT. The current investigation was carried out using the following key configurations:

- Deflectors with inclination angles from 30° to 45° were integrated with the CAWT and the VAWT models.
- The CAWT horizontal blade pitch angle, $\beta_b$ were varied between 0° to 15°.
- Varying the deflector vertical distance below the bottom of the CAWT rotor, i.e. 5 and 10 cm.

- Similar experiments were conducted under bare rotor configuration (without deflectors).

### 3.4.1 The arrangement of the experimental setup

The specific dimensions of the experimental setup are shown in Figures 3.10 and 3.11. In wind turbine experiments, the blockage effect is a very important factor, which affects the results significantly. Different from the open environment, laboratory-scale tests require that the blockage ratio must be less than 0.05 (Wang, Wang, & Chong, 2018). The blockage effect refers to an increase in freestream velocity around the model caused by the constriction of the flow due to the walls and the model (blockage ratio = frontal area of model/cross-section of test section). If the blockage ratio is more than 0.05, blockage corrections must be determined to obtain valid test data. Vertical axis wind turbines present a unique aerodynamic obstruction in wind testing, where the flow field around these wind turbines is unsteady, periodic, separated, asymmetric, and highly turbulent. In the current tests, the room has a blockage ratio of 0.01. This indicates that the wake interference from the walls interacting with the turbine model is negligible. Furthermore, at 6.5 m downstream of the blowers, there are window openings at the wall to provide exhaust for the blowers. Therefore, the far-field wake from the downstream of the CAWT is minimal, and its influence is negligible.

The deflector, as shown in Figure 3.10 is placed at about $x_d$ = 50 mm away from the central axis of the wind turbine (radius of the generator, $r_g$ = 50 mm). To determine the effect of deflector placed below the bottom of the wind turbine, different vertical distances, $y_d$ were used (50 mm and 100 mm). At 50 mm below the generator, there was a 20 mm clearance between the deflector and the blades. Deflectors with an inclination angle of 30° to 45° were used throughout the study to investigate their effects. The horizontal length and the width of the deflectors were fixed at 350 mm, which is equal to

the diameter of the CAWT rotor. This limitation is also applied for the vertical height of the deflector, $h_d$ which varies depending on the inclined angle. As mentioned, a conventional, three straight-bladed VAWT with similar diameter, height, and blade profile as the CAWT was also tested for comparison purposes.

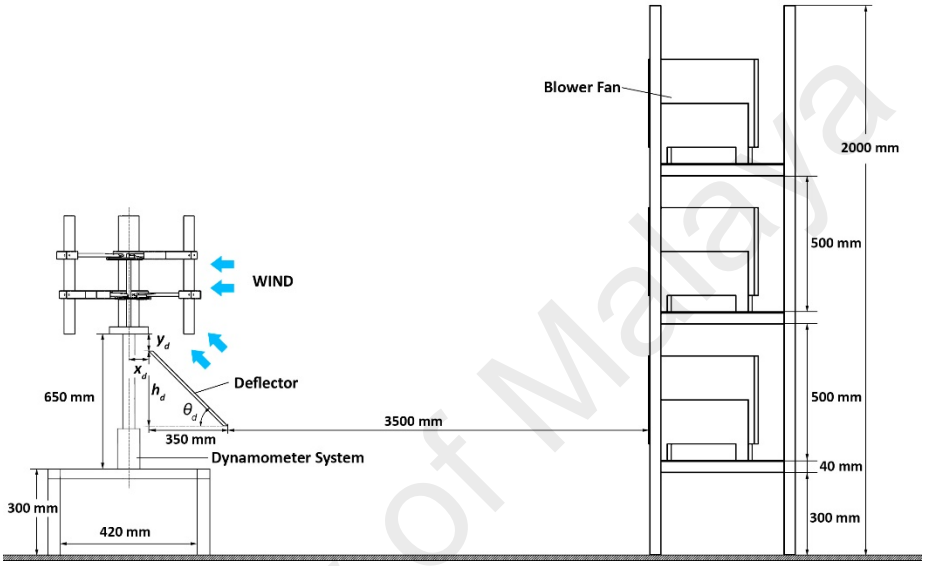


**Figure 3.10: A schematic diagram of the experimental setup**

As illustrated in Figure 3.11, the source of the wind for the tests consists of an array of nine blower fans that were arranged in a 3 x 3 configuration (also shown in Figure 3.12b). The experimental rig where the CAWT and the VAWT were fixed with a dynamometer controller system (for data logging). The experimental rig was then placed at 3.5 m downstream of the fan array. At this position, wind speed measurements were taken over a 3 x 3 grid of equally spaced points covering a 1.0 m x 1.0 m cross-section by using a vane anemometer. The wind direction is set at 0°, i.e. orthogonal to the deflector. The position of the central axis of the turbine was taken as the centre point. At each measuring point, the wind speed measurements were carefully taken using a vane anemometer over a period of 5 minutes. At each point, the measurements were repeated

for ten times to ensure repeatability and airflow uniformity is achieved. Moreover, since the flow of the blowers was unsteady, wind speeds at different positions were measured.

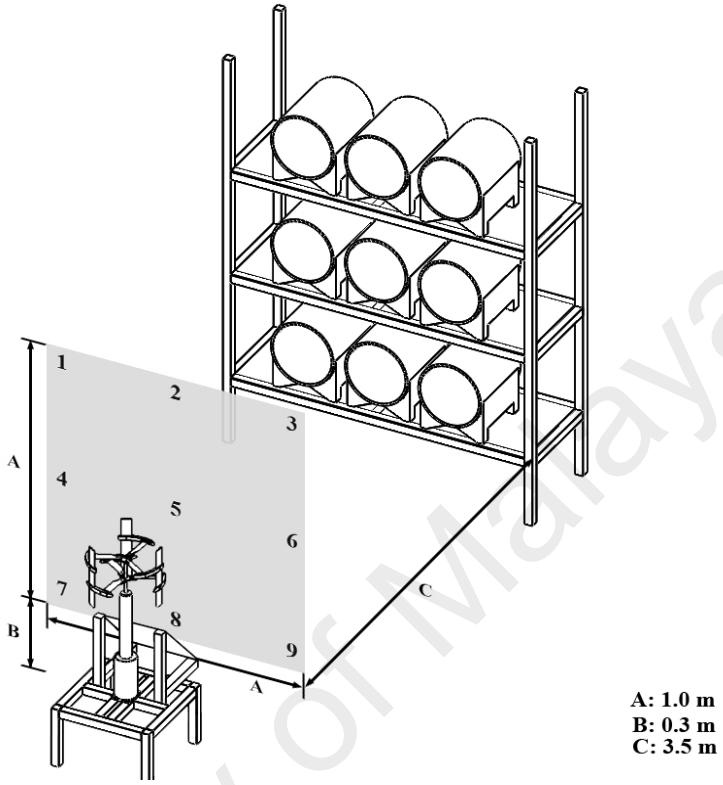


**Figure 3.11: Wind speed measurement area (shaded region)**

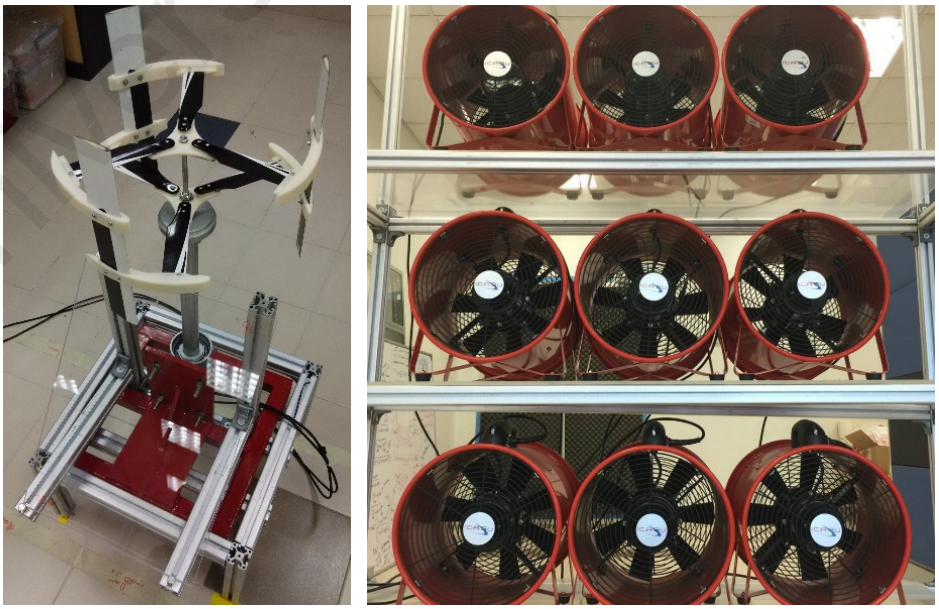

(a) (b)

**Figure 3.12: (a) The CAWT experimental prototype with a deflector, and (b) the 3 x 3 fan array setup**

The 3.5 m distance was chosen after spatial uniformity is achieved, where the uncertainty of the wind speed is the lowest. At 3.0 m distance, the wind speed measurements showed that the average wind speed was $V_\infty$ = 5.0 ± 0.8 m/s. To reduce the uncertainty of the vortex flow generated by the blowers, another distance was chosen. Hence, the average wind speed of $V_\infty$ = 4.5 ± 0.2 m/s at 3.5 m distance was obtained and the wind speed profile is shown in Figure 3.13. The following equations were used to calculate the standard deviation and SEM of the data samples throughout the experiment (Altman & Bland, 2005).

$$S_x = \sqrt{\frac{1}{n-1}\sum_{i=1}^{n}(x_i - \bar{x})^2} \quad \textbf{(3.1)}$$

$$SE_{\bar{x}} = \frac{S_x}{\sqrt{n}} \quad \textbf{(3.2)}$$

where $n$ is the number of samples, $x_i$ is the specific data in the sample, and $\bar{x}$ is the mean of the sample. The data samples are shown in Appendix B.

As illustrated in Figure 3.13, points 1 to 9 are the locations for the wind speed measurements, where point 5 is the central point of the area (Y = 0; Z = 0). Measurements at points 1-3 and 7-9 showed the closest accuracy to the mean wind speed of 4.5 m/s (0.02%, 0.25%, 0.86%, 0.92%, 1.51%, and 1.21%, respectively). Due to the combined kinetic turbulence intensity from the vortex flows of the turbine, measurement points 4-6 (at the central region of the wind speed measurement area) showed higher wind speeds. Furthermore, the wind speed measurement data for the 3.5 m distance showed that the standard error of mean (SEM) for each run is below 5% (300 wind speed samples), indicating the data has good precision. Moreover, the wind speed profiles measured across the test section can be used to determine the flow uniformity, as shown in Figure

3.14. The measured results were normalised by dividing the mean wind speed, which is the freestream velocity as follows. It can be seen that the low wind speed of the test section resulted in the unsteady wind becoming more uniform downward (repeatability between ± 0.985% to ± 0.991%). Without the flow straightener, the increase in turbulent intensity due to the vortex flows throughout the test section led to the non-uniformity of the flow field. This is one of the major limitations of the study. Therefore, a proper wind tunnel test with better flow uniformity and lower turbulence intensity is required for future studies.

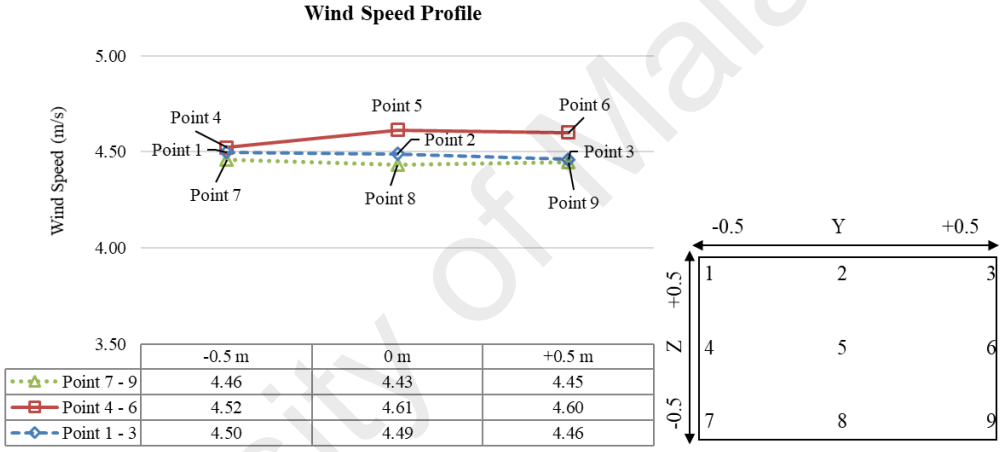


**Figure 3.13: Wind speed profile of the experiment**

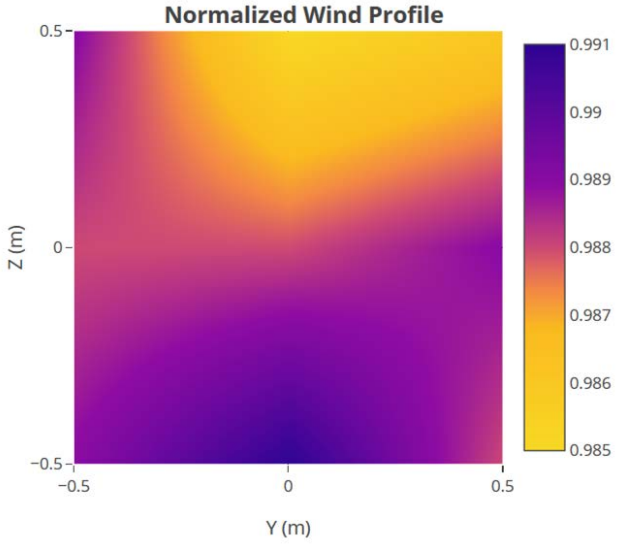


**Figure 3.14: Normalized wind profile**

### 3.4.2 Evaluating the performance of the wind turbine

The wind turbine performances were logged using a controller system in which the recorded parameters for the study are the power, current, voltage, and turbine rotational speed. The wind turbine dynamometer systems consist of a shaft (which the wind turbine is mounted on), turbine speed sensor, associated sensors for generator voltage and current measurements, data acquisition system and dynamometer controller. The dynamometer was designed for testing the mechanical and electrical performance of the wind turbine, hence providing an overall system performance and efficiency outlook for the wind turbine. Figure 3.15 illustrates the dynamometer system.

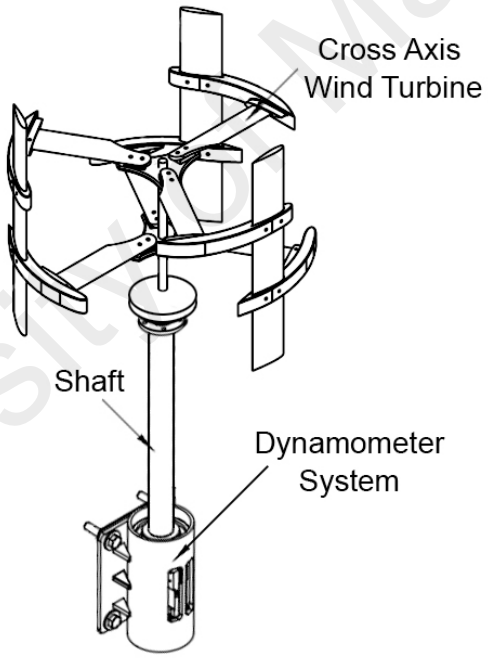


**Figure 3.15: An illustration of the cross axis wind turbine mounted on the dynamometer**

The dynamometer is directly connected to the wind turbine generator. To control the generator load, the controller varies the load duty cycle of the generator's power connection to a resistive dump load. The alternating current voltage from the generator is rectified to direct current using the dynamometer controller system as shown in Figure

3.16(a). The dynamometer controller displays the turbine rotational speed, generated torque, generated electrical power, and the percentage of electrical load application. The controller can be connected to a computer for data logging and real-time data monitoring. The controller consists of integrated sensors and serial communicated Data Acquisition System (DAQ). The integrated sensors in the controller are speed sensor using the AC frequency, load cell torque sensor, a channel for current sensor, a channel for voltage sensor, two channels of 5V analogue measurement sensor, and one additional speed channel. These sensors were read and logged by a computer data logging software. The software communicates with the controller via a serial port. This gives access to the analogue inputs, the speed input and other calculated values. Figure 3.16(b) shows a typical screenshot of the software.


(a)

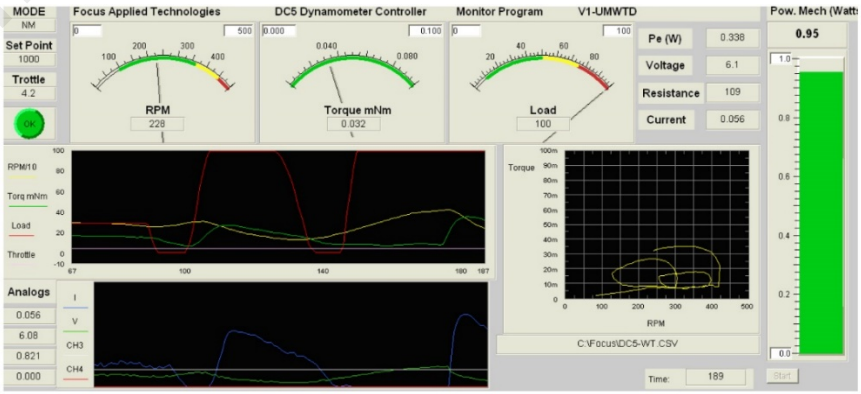


(b)

**Figure 3.16: (a) The front panel of the controller, (b) screenshot of the monitoring software**

The measurement of the rotor rotational speed was conducted during free-running conditions in which the rotors were subjected to inertia and bearing friction. No external loads were applied during this assessment. Once the rotational speed was stabilised, then the data from the controller system was recorded. To assess the performance of the wind turbines, the power coefficient and torque coefficient are presented quantitatively. The power coefficient, $C_P$ was used to evaluate the efficiency of the wind turbine, and it describes how much energy can be extracted from the wind by the rotor. The coefficient is defined as the ratio of the shaft power, $P$ generated from the wind turbine to the power available in the wind. It can be calculated by using Equation (2.20). The power coefficient varies from one wind turbine to another, depending on the type, size, airfoil shape, and other physical properties. Moreover, the power coefficient varies with the tip speed ratio, TSR (usually represented by the symbol, $\lambda$). It is defined by the ratio of the mean blade tip speed to the approaching wind velocity, and can be calculated by using Equation (2.27). Whereas, the torque coefficient, $C_Q$ is the ratio of the power coefficient, $C_P$ to the tip speed ratio, $\lambda$ (Beri et al., 2011):

$$C_Q = \frac{C_P}{\lambda} = \frac{Q}{0.5\rho A R V_\infty^2} \quad \textbf{(3.3)}$$

### 3.4.3 The effect of deflector on wind speed-up factor

Wind speed-up factor has been widely used to describe the variation of wind speed in complex terrains (Bo & Zheng, 2013; Lubitz & White, 2007) and wind flow over rooftops (Chong et al., 2016; Ozmen, Baydar, & van Beeck, 2016). The speed-up factor is crucial to determine wind turbine sites in areas of complex topography. The speed-up factor can also be used to understand the impact of wind flow over inclined slopes in terms of its wind speed, direction and turbulence. In this study, the speed-up factor, $\Delta S$ for the deflectors with different slopes is defined as:

$$\Delta S = \frac{V_z - V_\infty}{V_\infty} \tag{3.4}$$

where $V_z$ is the speed at height $z$ above the local deflector surface and $V_\infty$ is the measured wind speed. In addition, the pressure distribution profile is not considered for this study. Meanwhile, Figure 3.17 shows the location of measurement points over the deflector's inclined surface. In this experiment, nine measurement points were selected and positioned at the middle of the deflector along the center line of the prototype. A total of 70 wind speed data were collected at each measurement point. These data were averaged, and the speed-up factor at each location was calculated by using Equation (3.3) to describe the variation of wind speed over the deflectors. The location of each point was described using the ratio $z/h$, where $z$ is the distance from the local deflector surface, and $h$ is the local height at each point.

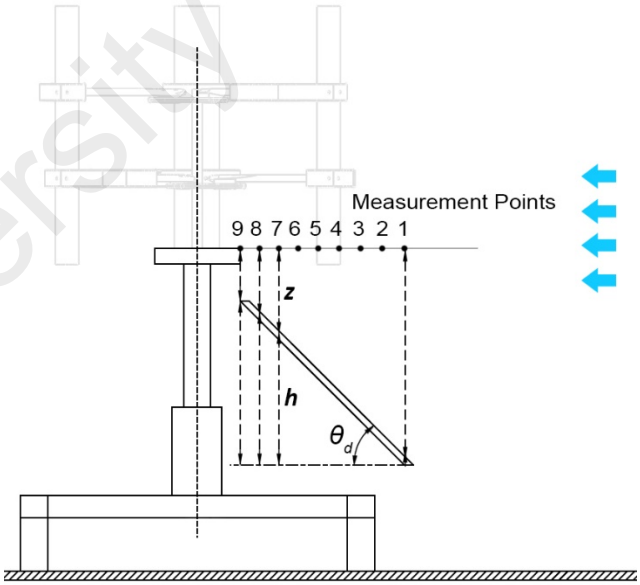


**Figure 3.17: Measurement points for the speed-up factor calculation**

## 3.5 Theoretical Method

In this section, the process of the CAWT design analysis is carried out based on the aerodynamic theories (as mentioned in Section 3.2, Figure 3.1). In general, the aerodynamics of wind turbines consist of modelling and prediction of the aerodynamic forces on the rotor blades of the turbine. In the process of predicting the performance and loading on the blades, the aerodynamic model normally requires additional input such as structural dynamics and wind conditions. Typically, the aerodynamic operation of a wind turbine can be characterised by its rotor angular velocity, $\Omega$; torque, $Q$; power output, $P$; and the rotor thrust, $T$. By using a simple model, considering axial momentum and energy, Betz and Joukowsky (Manwell et al., 2002; Okulov & van Kuik, 2012) in the 1920s predicted that for an ideal wind turbine, the maximum power output cannot exceed 59.3%. In 1935, using the foundation of Betz' law, Glauert formulated the blade element momentum (BEM) model which became the basis for all the wind turbine design procedure (Glauert, 1935). However, to analyze the aerodynamic behavior of vertical axis wind turbines, the BEM model alone is not sufficient. Several aerodynamic prediction models have been proposed throughout the decades for the Darrieus vertical axis wind turbines, including the double multiple stream tube (DMST) theory which has been briefly discussed in Chapter 2.

As the focus of the study relates to the investigation of H-rotors in misaligned flow conditions, the proposed approach considers that the approaching winds, either skewed or aligned to the rotor, are analysed independently based on their respective plane orthogonal to the wind direction. It is also assumed that in both cases, the flow from the horizontal and vertical directions will not be interacting with each other in terms of mass and energy transfers. In this study, to determine the aerodynamic behaviour of the cross axis wind turbine, an approach of combining power generated by the horizontal and vertical blades using the blade element and double multiple stream tube models is

proposed. These two models are applied independently to determine the contribution of torque for each of the vertical and horizontal blades of the CAWT. Moreover, the flow characteristics and the forces acting on the blades can be adequately described. However, the current approach is limited in terms of how the wake from the vertical blades affects the performance of the horizontal blades and vice versa. Therefore, the proposed analysis in this section uses the following assumptions:

- No aerodynamic interaction between the blade elements
- No wake interaction between the vertical and horizontal blades
- The tip loss from the blades are not considered in the analysis, particularly the effect of the connectors on the wake of the wind flows
- The swept areas orthogonal to the approaching wind from the horizontal and vertical directions are analysed independently, in which the vertical blades are analysed using the DMST model, whereas the horizontal blades are analysed based on the BEM model with some modifications
- The forces on the blades are determined solely by the lift and drag characteristics of the airfoil shape of the blades

### 3.5.1 Modelling the vertical blades of the CAWT

The vertical blades of the CAWT can be modelled by the DMST theory. As briefly discussed in Chapter 2, by using the momentum theory to relate the blade velocities in the upstream and downstream regions, the downwind blades will interact with the wind having a reduced velocity compared to the free-stream velocity for the upstream blades. Therefore, mathematically, the DMST model can precisely describe the changes in the wind flow throughout the rotor. However, for the current study, the effect of the deflected airflow on different sectors of the vertical blades is neglected, in which the approaching wind ($V_\infty$) is assumed to interact with all the elements of the vertical blade

perpendicularly. By assuming the stream tube stretches from the upstream to the downstream region of the rotor, where at each intersection between the blades and the stream tubes, the wind flow exerts aerodynamic forces at certain azimuthal positions of the rotor. The induced velocities for the upstream, $V_{au}$ and downstream, $V_{ad}$ differ from the free-stream velocity, $V_\infty$ and the equilibrium velocity, $V_e$ by (Beri et al., 2011):

$$V_{au} = (1 - a)V_\infty \quad \textbf{(3.5)}$$

$$V_{ad} = (1 - 2a)V_\infty \quad \textbf{(3.6)}$$

$$V_e = 2V_{au} - V_\infty \quad \textbf{(3.7)}$$

where $V_e$ was taken as the oncoming freestream velocity for the downstream region. The subscripts $u$ and $d$ denote the upstream and downstream positions of the velocity vectors. The expressions for the analysis on the turbine airfoil blade is shown in Figure 3.18. Some useful derived general expressions have been discussed in detailed by Beri et al. (2011) and have been given in Equations (2.40) to (2.47). Similarly, Equation (2.49) can be described as the moment of the tangential component of the resultant force about the rotor's centre for each stream tube, or the instantaneous torque at azimuthal positions, $\theta$ for each blades, reiterated as follows:

$$Q_{a,\theta} = \frac{1}{2}\rho V_R^2 (hc) C_t R \quad \textbf{(3.8)}$$

Assuming the wind velocity profile is uniform for all the stream tubes, the average wind speed measured at the 3.5 m downstream of the fan array is used for the DMST model ($V_\infty = 4.5$ m/s). For each of the CAWT configuration, the turbine is divided into 18 stream tubes (each stream tube is further divided into the upwind and downwind regions, thus 36 in total) where the size of each tube is 10° angular distance (analysis starts at an azimuth

angle of 5°). As mentioned, the stream and induced velocity is assumed perpendicular to the turbine swept plane.

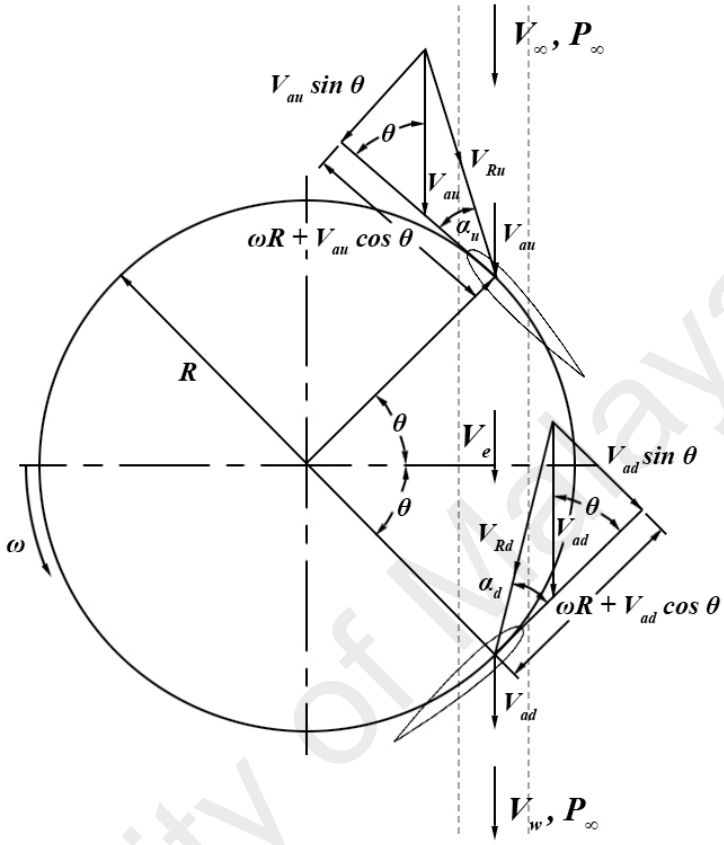


**Figure 3.18: Velocity and force diagram of the vertical blade in the upstream and downstream regions**

### 3.5.2 Modelling the horizontal blades of the CAWT

The deflected wind velocities approaching the rotor near the horizontal blades of the CAWT are measured at different azimuth angles and span locations of the rotor (refer Figure 3.19). In this study, local points are defined as the centre positions of the blade elements of the horizontal blades. The model analysis here uses momentum theory and blade element theory. Momentum theory refers to a control volume analysis of the forces at the blade based on the conservation of linear and angular momentum. Whereas, blade element theory refers to an analysis of forces at a section of the blade as a function of blade geometry (Manwell et al., 2002). The local points along the span of the blades were

selected to cover the range of flows encountered by the horizontal blades during the use of deflectors in the experiment. Three different rotor spans were selected to investigate the distribution of torque and thrust along the horizontal blade. The blade elements were divided based on the radial and azimuthal positions of the horizontal blades. Starting from the azimuth angle of 5° and ends at 355° ($\Delta\theta$ = 10° increment) covering different blade span locations. These span locations are located at radiuses $r$ = 160 mm, 120 mm and 80 mm from the centre of the CAWT (hub radius, $r_h$ = 50 mm, CAWT radius, $R$ = 175 mm), i.e. the length of the available surface area of the horizontal blades before the connectors and hubs. These locations correspond to the ratio $r/R$ = 91%, 69% and 46% span of the blade. In total, for each configuration, there are 108 different local points. By using this method, the skewed angle of the deflected airflow near the horizontal blades can be effectively estimated.

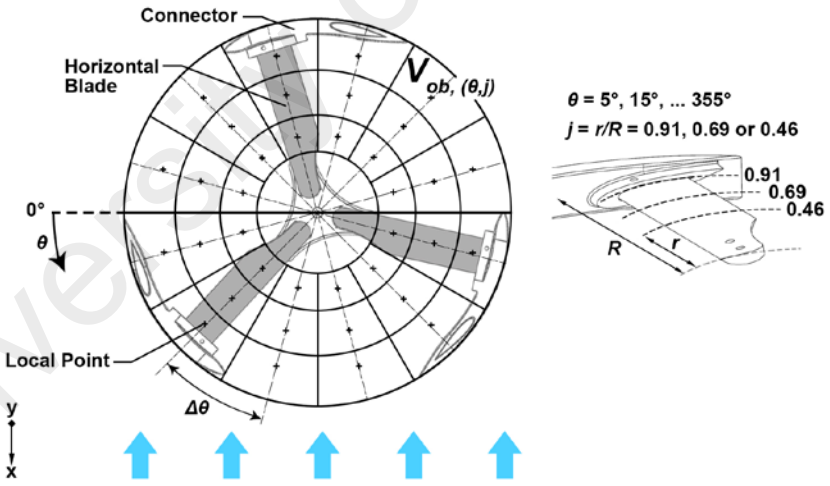


**Figure 3.19: Illustration of the CAWT from the top view showing all the local points on the horizontal blades at different azimuth angles and span locations**

Careful consideration and measurements have been taken to reduce the uncertainties arising from the use of the instrument in the study. The mean velocities at each local point are repeatedly measured to quantify for repeatability. The standard error of the mean for all the measurements is calculated using Equations (3.1) and (3.2) (Altman et al., 2005).

The measured wind velocities are then treated as vectors, and the resultant wind velocities, $V_{ob}$ at each of the local points are resolved using the mean horizontal and vertical wind velocities, $V_{ob,x}$ and $V_{ob,y}$, respectively. From the calculations, the deflected airflow skewed angle, $\gamma$ and the resultant wind flow velocity, $V_{ob}$ can be obtained at each azimuth angle. The objective of this method is to ultimately estimate the induced velocity, $V_{ab}$ apparent to the blade and thus the horizontal blade local angle of attack, $\alpha_b$ in order to determine the lift and drag forces exerted on the local point of the horizontal blade element. In blade element momentum method, the aerodynamic loads are calculated on the coordinate of the revolution surface. Due to the rotational axis of the horizontal blade, the blade orientation changes as the CAWT rotates. To analyse the aerodynamic load based on the local coordinate during the rotation, the local skewed wind flow is expressed in the form of vector and its transformation is based on the principle of trigonometry. A schematic of the local blade and wind velocity vector is shown in Figure 3.20. Due to the rotation of the horizontal blade, the airfoil plane angular position changes according to the azimuth angle. At each instantaneous angular position, the airfoil planes along the different blade elements are parallel to one another. In addition, the velocity vector at each local position perceives a different alignment of the airfoil plane based on the azimuth angle of the blade. Therefore, to estimate the drag and lift forces on the blade element at the local coordinate, the skewed wind vectors must be transformed (or projected) upon the airfoil plane for each azimuthal position. The velocity vectors are projected in parallel with the airfoil plane along the length of the blade to determine their aerodynamic loads. This proposed approach can shed some information on how the blade element, the momentum, and the skewed wind flow can influence the angle of attack of the relative wind at different span locations of the blade. Moreover, the distribution of torque along the blade length based on the horizontal blade pitch angle can be estimated for further analysis.

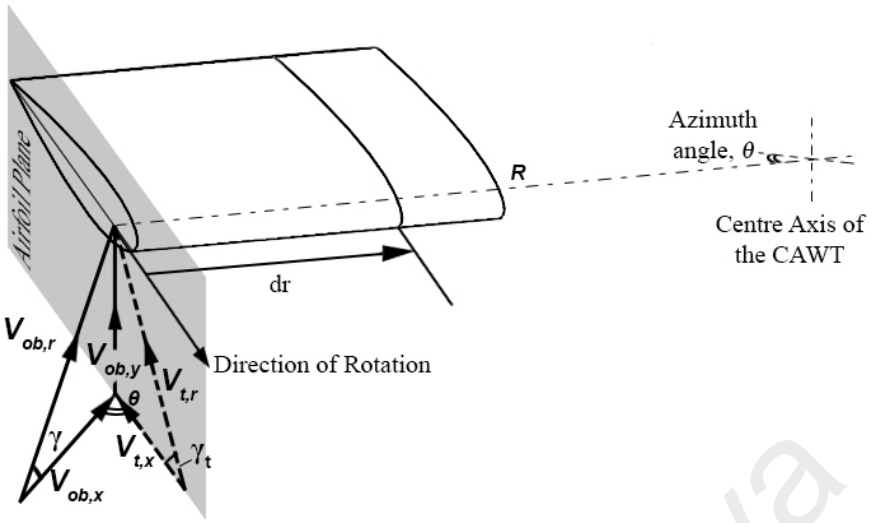


**Figure 3.20: Transformation of skewed wind vector based on the local blade coordinate**

Firstly, the resultant skewed wind velocity is calculated by using the following equation:

$$V_{ob,r} = \sqrt{{V_{ob,x}}^2 + {V_{ob,y}}^2} \quad \textbf{(3.9)}$$

where the oncoming wind velocities from the horizontal ($V_{ob,x}$) and vertical ($V_{ob,y}$) direction at each local azimuth position are measured. The skewed angle, $\gamma$ is therefore can be calculated by:

$$\gamma = \tan^{-1}\frac{V_{ob,y}}{V_{ob,x}} \quad \textbf{(3.10)}$$

The horizontal wind velocity is then projected onto the airfoil plane based on the instantaneous azimuth angle, $\theta$ and can be estimated with the following equation:

$$V_{t,x} = V_{ob,x}\cos\theta = V_{ob,r}\cos\gamma\cos\theta \quad \textbf{(3.11)}$$

where $V_{t,x}$ is the transformed horizontal velocity at the local position. Assuming that the vertical wind velocity is parallel to the airfoil plane (i.e. $V_{t,y} = V_{ob,y}$ ), the apparent wind velocity perceived by the blade at the local position is given by:

$$V_{t,r} = \sqrt{{V_{t,y}}^2 + {V_{t,x}}^2} = \sqrt{\left(V_{ob,r} \sin\gamma\right)^2 + \left(V_{ob,r} \cos\gamma \cos\theta\right)^2} \quad \textbf{(3.12)}$$

In addition, the apparent skewed angle projected onto the local plane is therefore defined as:

$$\gamma_t = \tan^{-1} \frac{V_{t,y}}{V_{t,x}} \quad \textbf{(3.13)}$$

where the induced wind speed at the local coordinate is defined based on the axial induction factor, $a$:

$$V_{ab} = V_{t,r}(1 - a) \quad \textbf{(3.14)}$$

The axial induction factor, $a$ is a parameter that indicates the degree with which the wind velocity is slowed down as it approaches the blades. It can be determined iteratively to find the most suitable value for each case. However, in this study, the induction factor is assumed as 1/3 for all conditions. It is an optimum value where the flow is decelerated by 1/3 and 2/3 of its original velocities at the far-field wake and in the vicinity of the blades, respectively. By using the cosine and sine rules, the relative velocity apparent to the horizontal blade at the instantaneous azimuth position must be corrected in terms of the transformed skewed angle, $\gamma_t$ and can be given by:

$$V_{Rb} = \sqrt{[\omega r(1 + a')]^2 + {V_{ab}}^2 - [(2\omega r(1 + a')V_{ab} \cos(180° - \gamma_t)]} \quad \textbf{(3.15)}$$

where $a'$ is the angular (or tangential) induction factor. In this study, the angular induction factor is assumed to be zero, as the radial induction factor is commonly found to be close to zero in the outer parts of the rotor, but increase significantly near the hub (Manwell et al., 2002). Similarly, the relative angle for the horizontal blades is defined based on the induced velocity vector and the relative velocity:

$$\varphi_b = \sin^{-1}\left[\left(\frac{V_{ab}}{V_{Rb}}\right)\sin(180° - \gamma_t)\right] \quad \textbf{(3.16)}$$

Note that the term $(180° - \gamma_t)$ must be replaced with $(\gamma_t)$ for azimuth positions 90° to 270°. The general relationships between the various velocity vectors, forces and angles at the local point of the horizontal blade of the CAWT is shown in Figure 3.21. The relative wind perceived by the horizontal blade, $V_{Rb}$ is the vector sum of the wind velocity due to rotation of the blade, $\omega r(1 + a')$ and the induced wind velocity at the horizontal blade, $V_{ab}$. In addition, the angle of the relative wind velocity can be defined as the sum of the horizontal blade pitch angle, $\beta_b$ and the angle of attack of the wind flow interacting with the horizontal blade, $\alpha_b$:

$$\varphi_b = \beta_b + \alpha_b \quad \textbf{(3.17)}$$

The relationship between the angle of the relative wind and the angular speed of the horizontal blade can be determined from Figure 3.21:

$$\tan\varphi_b = \frac{V_{ab}}{\omega r(1 + a')} = \frac{V_{ob}(1 - a)}{\omega r(1 + a')} = \frac{1 - a}{(1 + a')\lambda_{rb}} \quad \textbf{(3.18)}$$

where $\lambda_{rb}$ is the local tip speed ratio. Hence, the incremental lift and drag forces are given by:

$$dF_{Lb,\theta} = \frac{1}{2} C_l \rho {V_{Rb}}^2 c_b dr \quad \textbf{(3.19)}$$

$$dF_{Db,\theta} = \frac{1}{2} C_d \rho {V_{Rb}}^2 c_b dr \quad \textbf{(3.20)}$$

If the CAWT has a number of horizontal blades, $B$ the total normal force on the horizontal blade at a distance, $r$ from the hub and at an azimuthal position of $\theta$ is:

$$\begin{aligned} dF_{Nb,\theta} &= dF_{Lb,\theta} \cos\varphi_b + dF_{Db,\theta} \sin\varphi_b \\ &= \frac{1}{2} B \rho {V_{Rb}}^2 (C_l \cos\varphi_b + C_d \sin\varphi_b) c_b dr \end{aligned} \quad \textbf{(3.21)}$$

whereas, the differential torque due to the tangential force acting at a distance, $r$, from the hub with respect to the azimuth angle, $\theta$ is given by:

$$\begin{aligned} dQ_{b,\theta} &= Brd(dF_{Lb,\theta} \sin\varphi_b - dF_{Db,\theta} \cos\varphi_b) \\ &= \frac{1}{2} B \rho {V_{Rb}}^2 (C_l \sin\varphi_b - C_d \cos\varphi_b) c_b r dr \end{aligned} \quad \textbf{(3.22)}$$

By applying the axial momentum theory to the control volume of $r$ with the $dr$ thickness, the differential contribution to the thrust is:

$$dT_{b,\theta} = \rho {V_{ob}}^2 4a(1-a)\pi r dr \quad \textbf{(3.23)}$$

where $dT_{b,\theta}$ can be equated with $dF_{Nb,\theta}$. The moment of momentum theorem can be applied to the same control volume, therefore the differential torque acting on the blade is:

$$dQ_{b,\theta} = 4a'(1-a)\rho {V_{ob}}^2 \pi r^3 \Omega dr \quad \textbf{(3.24)}$$

In order to assess the distribution to the total torque from different span locations of the horizontal blades of the CAWT rotor, the following equation can be used:

$$\zeta = Q_{b,j}/Q_b \times 100\% \quad \textbf{(3.25)}$$

where $Q_b$ is the total dynamic torque of the horizontal blades and $Q_{b,j}$ is the sectional dynamic torque based on different span locations of the blade.

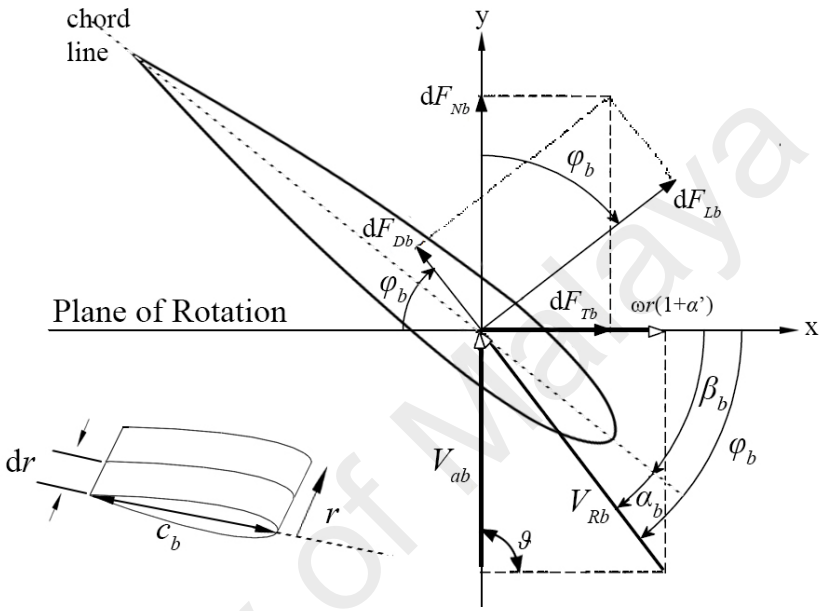


**Figure 3.21: The relationships between the various angles, forces and velocities at a blade element of the horizontal blade**

In the present study, the torque contributed by the horizontal blade can be calculated by integrating Equation (3.22) over a length, $r - r_h$. In brief, the method presented here outlines the measurement of the local deflected wind velocities, coupled with data from the experiment; the induced wind velocities apparent to the blade can be calculated. Applying the aerodynamic properties of the airfoil, the torque produced by the horizontal blade at each azimuthal position was then obtained. In the semi-empirical approach presented in the study, the data of wind velocities and rotor rotational speeds are used to obtain the induced and relative wind velocities apparent to the vertical and horizontal blades. Ultimately, the proposed approach is used to estimate the theoretical power generated by the CAWT. For a specific tip speed ratio, λ; the power from the CAWT can

be calculated through the summation of power contributions by the horizontal (BEM model) and vertical (DMST model) blades of the turbine:

$$P_{THEORETICAL} = P_{DMST} + P_{BEM} = \omega(Q_a + Q_b) \quad \textbf{(3.26)}$$

In order to proceed, the lift and drag coefficients of the NACA0015 airfoil are obtained from Sheldahl and Klimas (1981) and XFOIL (n.d.) for Reynolds number in the range between 1.5-2.5 x $10^4$. The XFOIL code was developed to predict the airfoil performance at low Reynolds numbers and is well known for its accuracy (Liu, Dong, Moschetta, Zhao, & Yan, 2014; Morgado, Vizinho, Silvestre, & Páscoa, 2016; Selig, 2003). Furthermore, it is known that the angle of attack for blades in the very low range tip speed ratio of micro-wind turbine can exceed the range in which the lift coefficient varies linearly with the angle of attack (Scheurich, Fletcher, & Brown, 2010). Therefore, requiring lift and drag coefficients data beyond the stall angle (Li, Zhu, Xu, & Xiao, 2013). The complete lift and drag coefficients for the angle of attack within the azimuth angles of ±180° were acquired through the Montgomerie extrapolation model (Montgomerie, 2004). The model predicts the characteristics of airfoils beyond the stall angle where all airfoils essentially have the same characteristics as a flat plate. In both the BEM and DMST models, the deceleration of airflow at the rotor disc generated by the interaction of the blade-flow is modelled by the variation of the induction factor. The radial wind speed of the rotor is governed by the angular induction factor, which is close to zero in the outer parts of the rotor, but increase significantly near the hub ($r/R < 0.4$) (Manwell et al., 2002). The general calculation flow procedure for the DMST and the BEM models are shown in Figure 3.22. The results and discussion for the experimental and theoretical studies of the CAWT can be found in Sections 4.1 and 4.2.

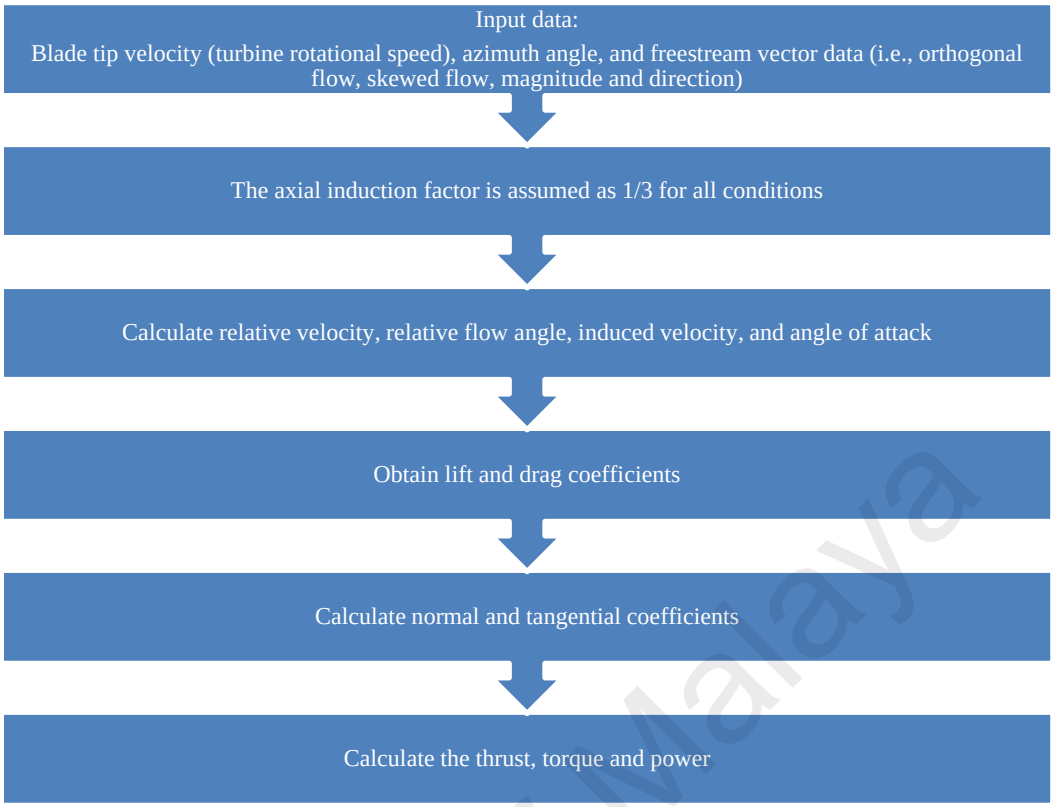


**Figure 3.22: General calculation flowchart for the theoretical models**

## 3.6 The application of a wind-augmentation device as a wind energy generation system

The potential of an augmentation device, particularly the ODGV can be illustrated by the Eco-Greenergy™ renewable energy system (Figure 3.23). The design of the system is adapted from the larger BIWT integrated ODGV (Chong, Naghavi, Poh, Mahlia, & Pan, 2011; Chong, Poh, Fazlizan, & Pan, 2012b). Originally intended to be architecturally designed as part of the high-rise building (as shown in Figure 3.23a), the design might pose serious concerns on the safety, structural, vibration and comfort issues for building occupants. Moreover, there exist issues of maintenance and high capital costs for the system this large. Hence, a smaller ODGV system with better aesthetic value was designed to become an on-site standalone energy generation system. It is then assumed that the basic theory of the larger ODGV system retains in the smaller ODGV design.

### 3.6.1 The general arrangement of the energy generation system

Figure 3.23(b) shows the overall design of the system, and Figure 3.24 shows the small-scale ODGV adopted in the system. Patented by (Chong & Kong, 2013b), the ODGV in this study can be adapted with multiple lamps at the bottom and arranged for optimum illumination. The height of the pole can be designed between 2 to 30 meters above ground level. The height and size of the system are heavily depended on the location's weather pattern and distribution of wind and solar energy resources. The system can be deployed to illuminate parks, lawns, streets or sky-gardens. In remote areas, the system can be adapted to power weather data collectors, flood monitoring systems or as emergency beacons for hikers and travellers. To harvest wind energy from all directions, the ODGV has several guide vanes that surround the VAWT. The VAWT sits in the middle of the ODGV, where its driveshaft is directly connected to a generator. Batteries in the compartment store the energy generated from the renewable energy sources. Excess energy generated from the system can be used to power other electrical appliances or fed into the grid.

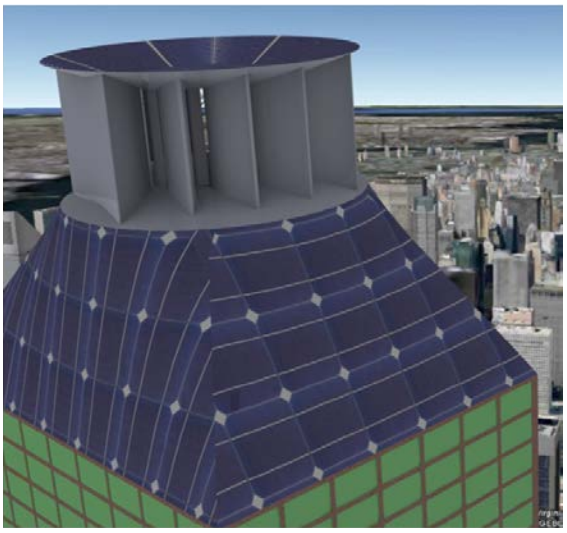

(a)

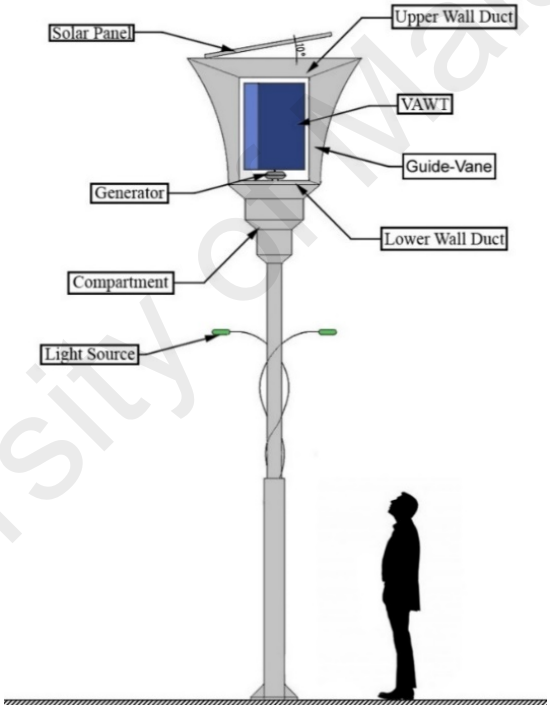


(b)

**Figure 3.23: (a) The BIWT integrated ODGV system, (b) the Eco-Greenergy™ renewable energy generation system design and general arrangement**

(a) (Chong et al., 2012a); (b) (Chong et al., 2015)

The ODGV has lower and upper wall ducts, surrounded by six guide vanes (shown in Figure 3.24). The ODGV shrouds the VAWT. The guide vanes, together with the surfaces of the upper and lower wall ducts, form the channels through which the wind stream

passes. The speed of the wind increases as it flows through a decreasing cross-sectional area according to the principle of continuity (venturi effect). Along the openings, these two different cross-sectional areas form a restriction in which the pressure at the intake is higher than the pressure at the narrow end. Thus, the wind speed entering the intake of the guide vane increases as it passes through the channel towards the exit of the guide vane. The ODGV can be fitted with any form of existing or new VAWT (Savonius, Darrieus, or CAWT). As shown in Figure 3.24, the guide vanes are used to guide the oncoming wind stream to the optimum angle of attack of the wind turbine blades. The design of the guide vanes can be adapted into various forms, i.e. curved-plates or straight-plates with constant or varied thicknesses.

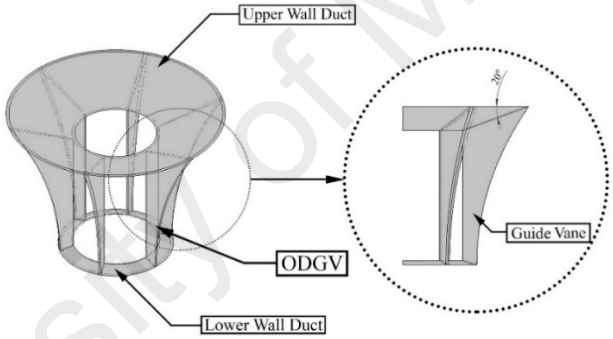


**Figure 3.24: The omni-direction-guide-vane (ODGV)**

(Chong et al., 2013b)

The cross-sectional area at the intake of the channel is preferably two times or more than the cross-sectional area at the exit. Furthermore, the upper and lower wall ducts surfaces are inclined at a fixed angle from the horizontal plane. The venturi effect created by the channels can induce a higher wind speed into the wind turbine, which allows for smaller and lighter rotating wind turbine parts to be used to produce a similar power output. Moreover, this eliminates or further minimises the electromagnetic interference issue and noise level caused by the long blades of large wind turbines. The small blades of the vertical wind rotor used in the system exert less pull compared to the blades of a

HAWT. Hence, the vertical wind rotor produces much lower levels of noise and vibration (Knight, 2004).

### 3.6.2 Assessing the energy output of the renewable energy generation system

To assess the energy output of the system, the data from the wind tunnel test of the ODGV was acquired (Chong et al., 2013a). The estimation of energy output from the system was then calculated from the acquired meteorological data from Sepang and Subang, Malaysia. As a case study, the Eco-Greenergy$^{TM}$ renewable energy system was assumed to be installed on the top of a 150 m building in an urban area. The following sub-sections describe the methodology of the wind tunnel testing, as well as the calculation of the energy output of the hybrid wind-solar system.

#### 3.6.2.1 The omni-direction-guide-vane integrated with VAWT

The effect of the ODGV on the performance of the VAWT was discussed in Chapter 2. By adopting the experimental data from the study by Chong et al. (2013a), the assessment of the ODGV as an energy generation system can be carried out. The ODGV shown in Figure 2.17 has an outer diameter of 1000 mm, the inner diameter of 540 mm and height of 450 mm. The ODGV has four pairs of guide vanes to form channels which will guide the wind stream towards the wind turbine. The guide vanes for each pair are tilted at angles of 55° and 20°. At equal spacing, each of the guide vane pairs is positioned around the tapered central cylinder. The four channels are designed to guide the oncoming wind stream towards the wind turbine at 0°, 90°, 180° and 270° positions. The placement of guide vanes at the outer radial band of the tapered cylinder permits the wind turbine to capture wind energy from every direction. Thus, the yaw mechanism can be omitted. The wind tunnel test was conducted at the Aeronautics Laboratory of University Teknologi Malaysia. There were two types of configurations, i) a bare vertical axis wind turbine without ODGV, and ii) an ODGV integrated vertical axis wind turbine. Consequently,

evaluations on the power generated and the rotational speed of the wind turbine for both configurations were carried out. An external load was applied through the use of a hysteresis brake on the shaft rotor. The brake was adjusted to increase the load exerted on the shaft. At a fixed wind speed of 6 m/s, the data from the experiment by Chong et al. (2013a) for load assessment of the wind turbine for bare and ODGV integrated VAWT configurations have been shown in Chapter 2. The data were used in the calculation of the wind energy output of the ODGV as discussed in the next subsection.

#### 3.6.2.2 Wind energy system

The acquired wind speed data from the meteorological station in Sepang and Subang, Malaysia based on the year 2007 to 2009 were used to estimate the wind energy output generated from the system. In wind studies, it is common to use historical data to investigate the weather pattern of a location (Celik-Dadaser & Cengiz, 2014; Zhang, Harff, & Schneider, 2011). However, due to the non-availability and high costs of obtaining new wind speed data, the currently available data is used for this study. The height of the sensors above ground level is 10 m. For this case study, it was assumed that the top of a 150 m tall building in an urban area was used as the site of the system. To calculate the wind speed at the height of 150 m above the ground level, the power law as shown in Equation (2.3) was used. The wind friction coefficient was taken as $a_f$ = 0.3 (Gipe, 2004; Patel, 2006) and the . In the analysis, the height of a high-rise building was taken as the reference height ($Z_r$ = 150 m). The calculated wind speed is then multiplied with the ODGV rotor rotational augmentation ratio of 1.87. Therefore, the monthly wind speeds at the height of 150 m for the selected areas for years 2007-2009 are tabulated in Figure 3.25.

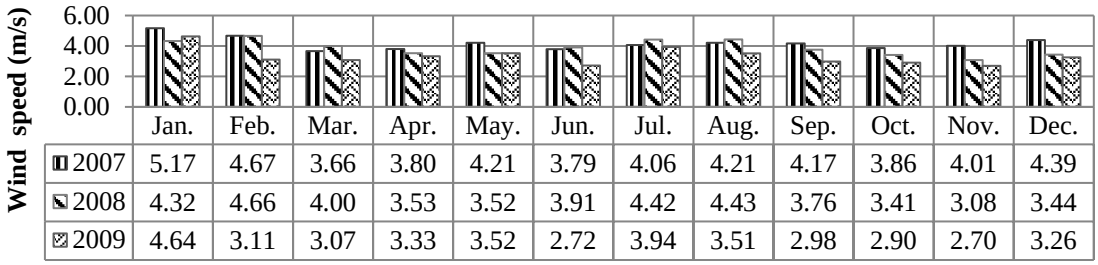


(a)

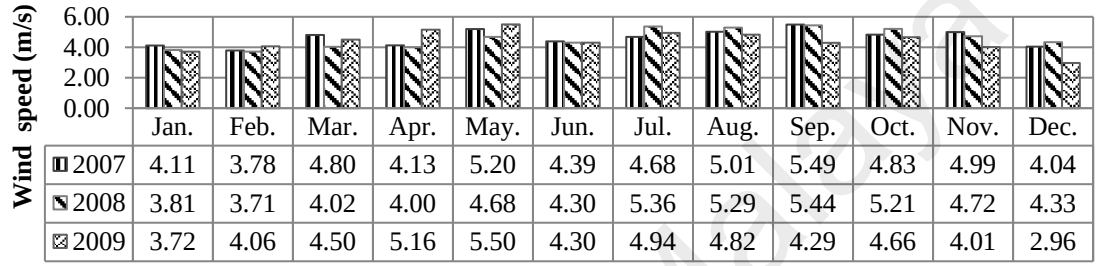


(b)

**Figure 3.25: Calculated mean wind speed from 2007 to 2009 in (a) Sepang, and (b) Subang, Malaysia at 150 m height**

The wind power is proportional to the cubic power of the wind speed approaching the ODGV. The power available in the wind was calculated using the following equation:

$$P = 0.5\rho C_P \eta_g \eta_{ODGV} A V^3 \quad \textbf{(3.27)}$$

where $\rho$ is the air density, $C_P$ is the rotor efficiency (coefficient of power), $\eta_g$ is the generator's efficiency, and $\eta_{ODGV}$ is the efficiency due to the ODGV loss. The ODGV loss parameter is the estimated efficiency due to the interaction between the wind and the ODGV structure. Some losses due to the wind-wake interference off the duct walls must also be accounted. In this study, it is estimated that 10% of the wind power is loss due to the interference. A commercially available Darrieus-type vertical axis wind turbine was

chosen for the system and its technical characteristics are shown in Table 3.3. The results and discussions for the ODGV integrated VAWT can be found in Section 4.4.

**Table 3.3: Specifications of the commercial wind turbine used in the case study**

| Parameter | Specification |
|---|---|
| Rated power | 50 W |
| Rated wind speed | 10.0 m/s |
| Starting wind speed | 2.0 m/s |
| Working wind speed | 3.0-20.0 m/s |
| Maximum wind speed | 35.0 m/s |
| Swept area (height x diameter), $A$ | 0.8 m x 0.6 m |
| Number of blades | 5 |
| Generator efficiency, $\eta_g$ | 0.8 |
| Efficiency due to ODGV loss, $\eta_{ODGV}$ | 0.9 |
| Rotor efficiency, $C_P$ | 0.4 |
| Air density, $\rho$ | 1.201 kg/m$^3$ |

(Saiam Power, n.d.)

## 3.7 Summary

This chapter provided a detailed description of this study's research methodology. Starting with the problem statement outlined in Chapter 1, the design criteria for the CAWT was established, and the turbine prototype was fabricated. To investigate the performance of the novel wind turbine, a series of experiment was carried out, with the conventional VAWT employed for benchmarking purposes. Then, analyses of the repeatability and uniformity of wind measurements were carried out to ensure the data obtained from the experiments are valid. The data was reviewed against literature and accounted for through a few calculations. Based on the *a posteriori* process, a semi-empirical method of using the double multiple stream tube theory and the blade element momentum model was discussed. Through a comparison with the experimental data, interpretations of the theoretical approach can be drawn. The intent of this study would contribute to the understanding of the element of forces happening with the blades.

Finally, a case study was presented to investigate the feasibility of power augmentation device for the use in an urban environment.

# CHAPTER 4: RESULTS AND DISCUSSIONS

## 4.1 Experimental Analysis of the Cross Axis Wind Turbine Performance

The experiments have been carried out with the utmost care. However, uncertainties are unavoidable. The expressions in Equations (3.1) and (3.2) determine the data sampling uncertainty that were obtained from the experiments. Appendix B shows all the measured data obtained from the experiments. Firstly, for wind speed measurements, since the flow of the blowers were not controlled, the intended value for the wind speed was not set. Therefore, wind speed data were taken at different distances along the upstream side of the experimental rig. By measuring the wind speed data, it was found that in order to reduce the uncertainty created by the vortex of the blowers, the distance of 3.5 m was chosen and the average wind speed of $V_\infty = 4.5 \pm 0.2$ m/s was used throughout the study. In addition, the measurement deviations in between the measured data samples from the dynamometer are well within the range of ±5%, ensuring repeatability of the experiments (Bartlett, Kotrlik, & Higgins, 2001).

### 4.1.1 Bare rotor performance

Figure 4.1 shows the performance of the CAWT in terms of power coefficient, $C_P$, for different pitch angles under bare rotor configurations. In the same figure, the performance of the bare VAWT is also shown. The graphs illustrate the peak coefficient of power, $C_P$ at different tip speed ratios (TSRs). Additionally, the varying maximum $C_P$ for the CAWT occurred at TSR values in the range between 0.53 and 0.93. From the literature, micro-wind turbines normally operate between 0 to 2 TSRs (Fazlizan, Chong, Yip, Hew, & Poh, 2015; Johnson, 2006; Kim et al., 2013; Leung, Deng, & Leung, 2010; Park, Lee, Sabourin, & Park, 2007). The power, $P$, generated by the turbines was measured by a control system that consists of a rectifier and a resistive dump load. The

generator used in the experiment is similar to those in experiments found in (Fazlizan et al., 2015; Kim et al., 2013) in which low power generation is expected where the turbine generator produced less than 1 W at wind velocity lower than 8.5 m/s. In the graphs, the lines represent the polynomial fit of order two of the obtained experimental data. The results in Figure 4.1 showed that most of the bare CAWTs with different pitch angle configurations outperform the conventional VAWT, in which the highest power coefficient was recorded by the CAWT having the pitch angle of 5° ($C_P$ = 0.042 at a TSR of 0.69). This is true except for the CAWT with the pitch angle of 15°. The reason for this outcome is still unknown. However, the author infers that the high pitch angle of the horizontal blades may contribute to the additional drag force that occurred along the airfoil, therefore reducing the power output from the CAWT. This may also contribute to the smaller range of TSR as shown in the figure. In a study to investigate the effects of blade pitch on the performance of a small HAWT in urban environments, Costa Rocha et al. (2018) have shown that blades with higher pitch angle have lower power coefficient with lower range of TSR. In another study, Abdalrahman, Melek, and Lien (2017) investigated the performance of a straight-blade VAWT with variable and fixed pitch angle using numerical simulations. The study showed that the VAWT with 0º pitch angle produced higher peak power coefficient than the higher pitch angle (6º) blade configuration (up to 62% at TSR of 2). Sudhamshu et al. (2016) have also shown that the maximum value of the tangential coefficient occurred for the 5º pitch angle HAWT with NREL S809 blades. At higher pitch angle, the tangential coefficient and power become negative at steeper pitch angles of -10º and 20º due to stalling (stall angle for the NREL S809 is 9º (Mo & Lee, 2012)). In the current study, the lift coefficient of airfoil NACA0015 suffers a severe loss of lift (stalling occurs) when the angle of attack approaches 10º-15° (Gaunaa, Sørensen, & Larsen, 2002; Miller, 2008).

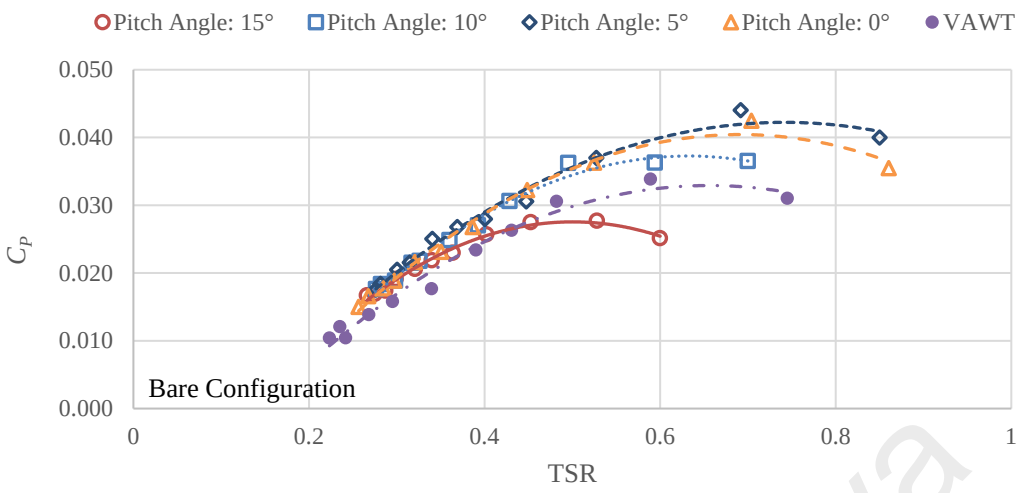


**Figure 4.1: Power coefficient against the tip speed ratio for the bare wind turbines. CAWT configurations differ in its horizontal blade pitch angles (0° to 15°)**

### 4.1.2 The effect of deflector vertical distance on the performance of the cross axis wind turbine

From the experiments, placing the deflectors further away from the central axis of the rotor ($x_d$ > 5 cm) results in undesired performance output from the turbine. Therefore, the following data presented in the current study focused on the fixed horizontal distance of $x_d$ = 5 cm, i.e. the diameter of the generator. Figure 4.2 shows the variation of peak power output for CAWT with various pitch angle integrated with deflectors fixed at different vertical distance to diameter ratios, $y_d/d$ = 0.14 and 0.29 (where $y_d$ = 5 and 10 cm). The results showed that the rotor power output decreases when the $y_d/d$ ratio between the deflector and the CAWT increases. Moreover, the data showed that there is an overall improvement between 20-34% for the ratio of 0.14. By analyzing the $C_P$ vs. TSR graphs in Figure 4.3, the effect of the deflector vertical distance can also be observed by the smaller range of TSR for every CAWT configurations. The CAWTs in the graphs were integrated with the 45° deflector and varied in the distance between the bottom plane of the CAWT and the upper plane of the deflector. By evaluating the data, there is a reduction between 15 to 36% for the TSRs when the deflector is placed further away from

the CAWT. In terms of power coefficient, a reduction between 22 to 35% were calculated depending on the horizontal blade pitch angle configuration. Similar observations were made by Kim et al. (2013). In determining the enhancement of power performance and how the stream-wise distance, $l$ of deflector affects the power output of a VAWT, the authors concluded that when the ratio of $l/d$ ($d$ is the diameter of the VAWT) is increased from 0.65 to 1.65, the maximum power coefficient and the corresponding tip speed ratio had a tendency to decrease. They attributed this reduction to the VAWT's interaction with smaller wind velocity outside the deflector wake as it moves further away from the deflector. In another study, Jin, Wang, Ju, He, and Xie (2018) carried out a study on two counter-rotating straight-bladed VAWTs with upstream deflector using experimental and three-dimensional computational fluid dynamics (CFD) methods. Comparable findings were found where when the $l/d$ ratio is increased from 0.7 to 1.3, the maximum power coefficients reduces from 0.45 to 0.39 at the TSRs of 3.3 to 2.9. Both of these findings confirmed that the power output of the turbine integrated with the deflector will always greater than that without the deflector. Furthermore, by increasing the deflector's distance from the turbine, the effect of the wake will be weakened, in which the turbines will have smaller gains from the wake. This will result in the decrease of the corresponding coefficient of power. Moreover, the flow velocity inside the deflector wake is recovered further downstream, exposing the turbines with reduced velocity. Analogous to their findings, the current study shows that the wind energy of the approaching airflow can be more efficiently extracted by the horizontal blades if the deflector is placed nearer to the bottom of the rotor. In doing so, the deflector wake can be fully utilized by the horizontal blades, and more kinetic energy can be extracted from the wind with higher wind velocity.

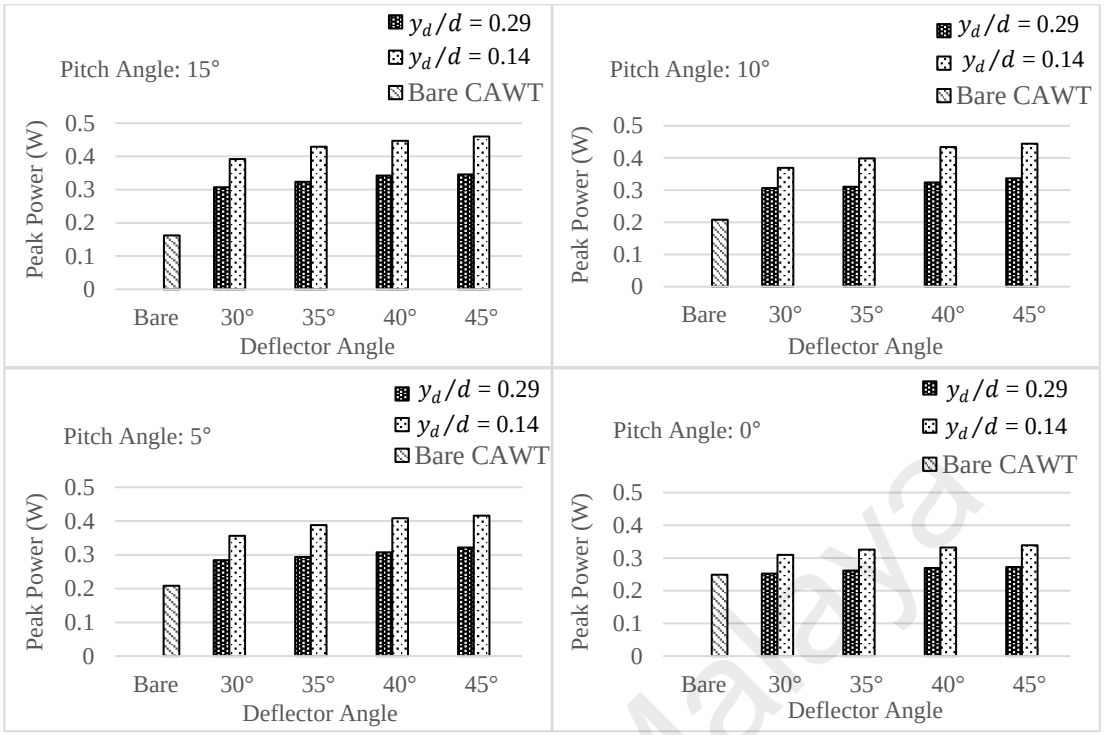


**Figure 4.2: Variation of peak power generated by the various configurations of the CAWT having various pitch angles at different $y_d/d$ ratios. Also shown, data for the bare CAWTs**

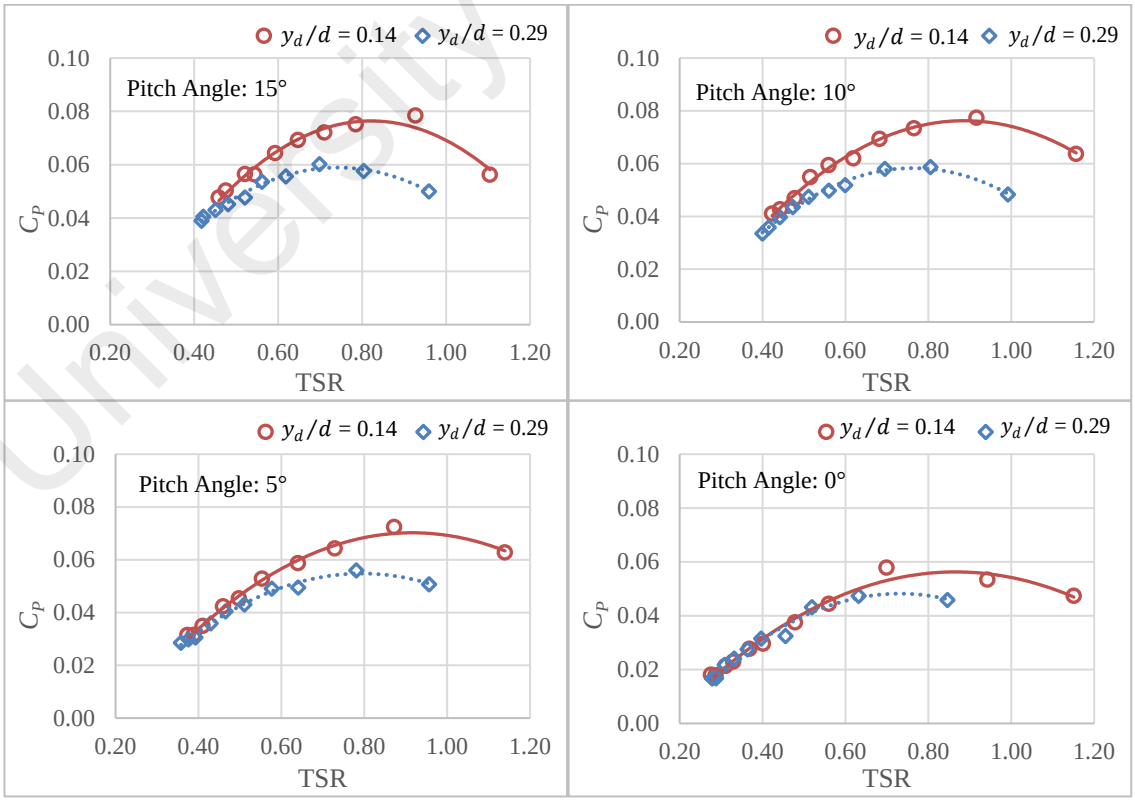


**Figure 4.3: $C_P$ against TSR for the cross axis wind turbine with various horizontal blade pitch angles integrated with the 45° deflector**

### 4.1.3 Deflector integrated wind turbine performances with varying inclination angles

The separated turbulent flow past the inclined flat plate (i.e., deflector) has been extensively studied both numerically and experimentally (Breuer & Jovicic, 2001; Fage & Johansen, 1927; Lam & Wei, 2010; Zhang, Liu, & Lu, 2009). The phenomenon has also been used in different engineering applications, such as to improve scalar mixing and to provide a flame stabilisation region in combustors, and in hovercraft's diverters to provide both vertical and horizontal thrusts. In the current study, some observations between the interaction of the deflected airflow and the CAWT could be established. By incorporating the deflectors, the performance of the CAWTs showed a significant increase across the different pitch angle configurations, as shown in Figures 4.4 to 4.8 due to the augmentation effect of the deflectors. The use of deflectors guide the oncoming wind upward and create a skewed wind flow condition. Hence, different aerodynamic effects are observed when the inclination angle of the deflectors is varied.

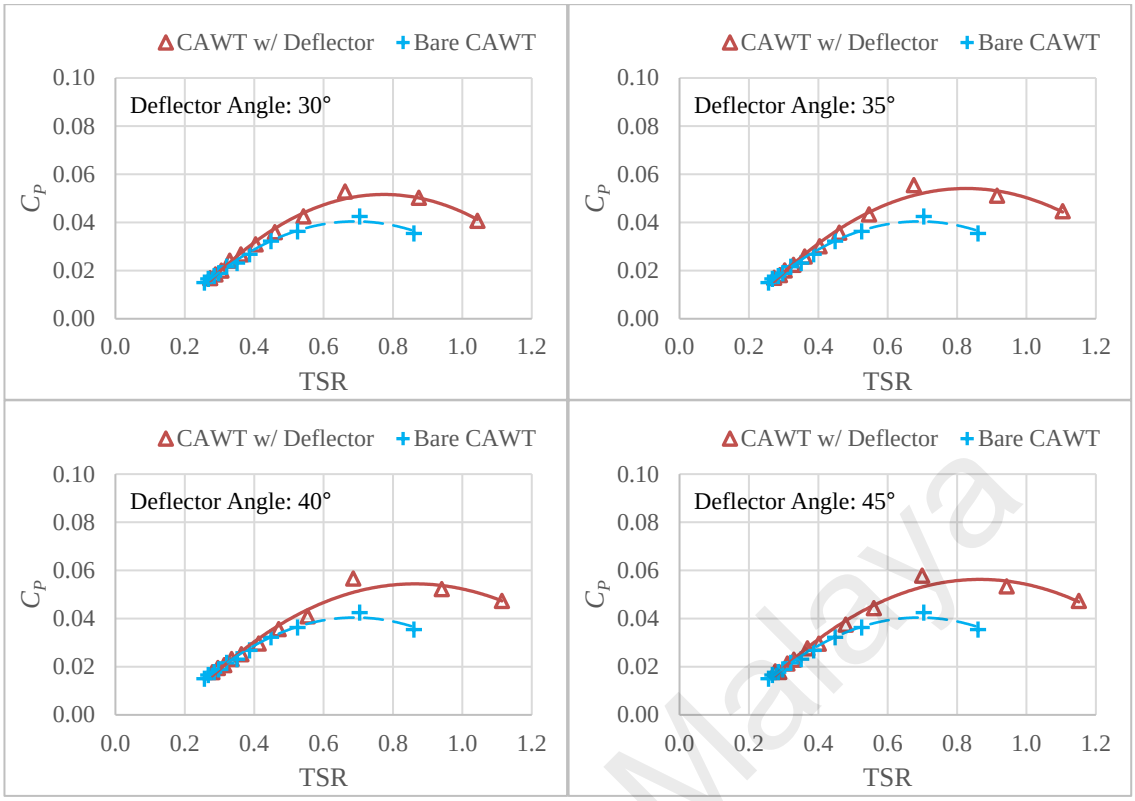


**Figure 4.4: $C_P$ against TSR for the deflector integrated and non-integrated cross axis wind turbine with horizontal blade pitch angle of 0°**

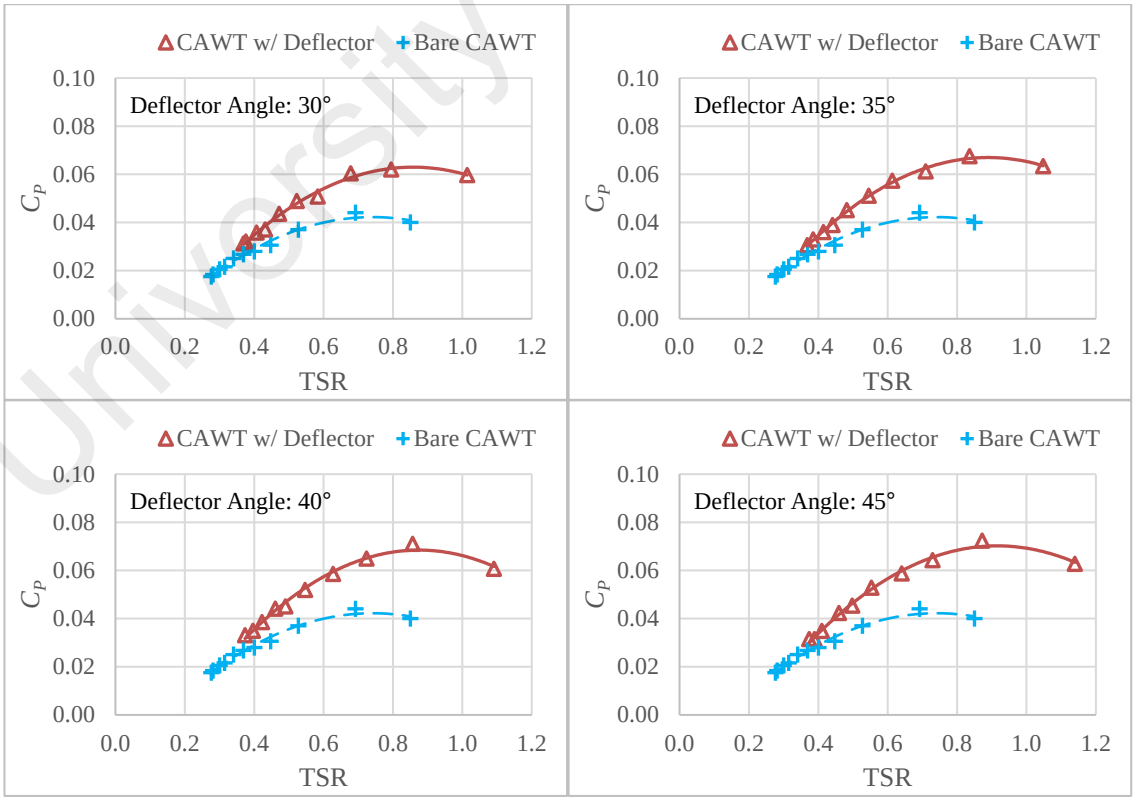


**Figure 4.5: $C_P$ against TSR for the deflector integrated and non-integrated cross axis wind turbine with horizontal blade pitch angle of 5°**

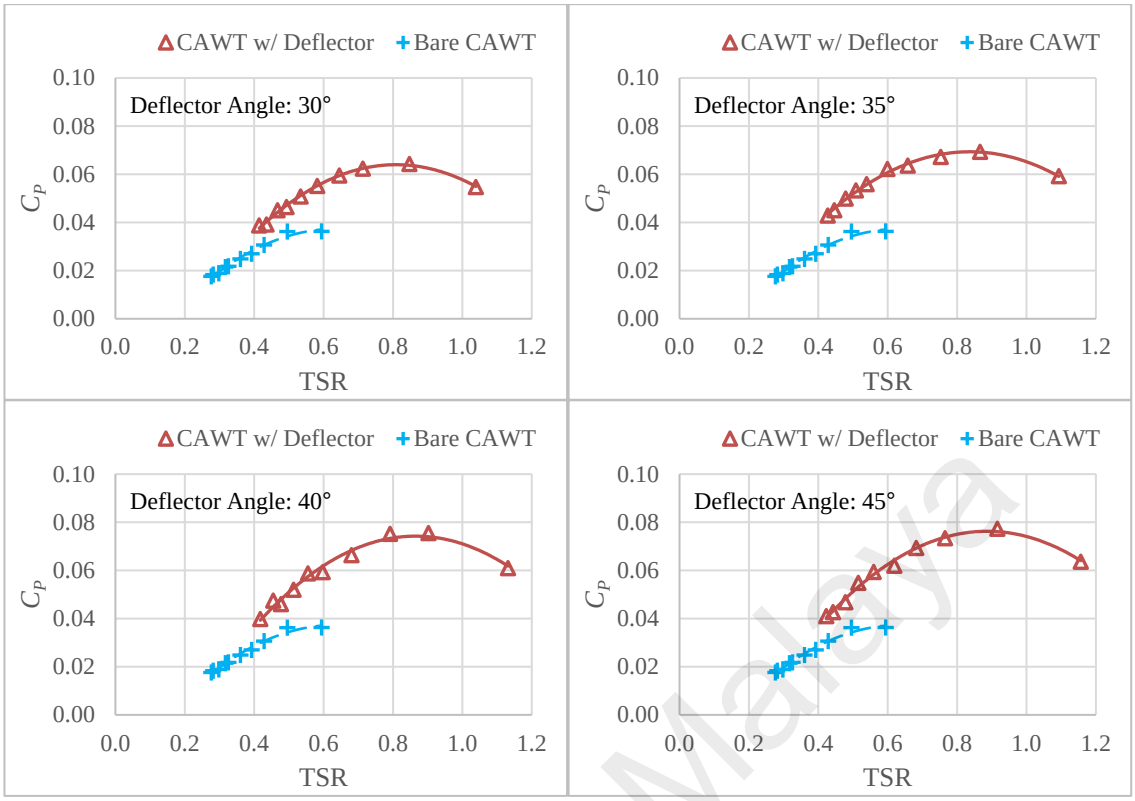


**Figure 4.6: $C_P$ against TSR for the deflector integrated and non-integrated cross axis wind turbine with horizontal blade pitch angle of 10°**

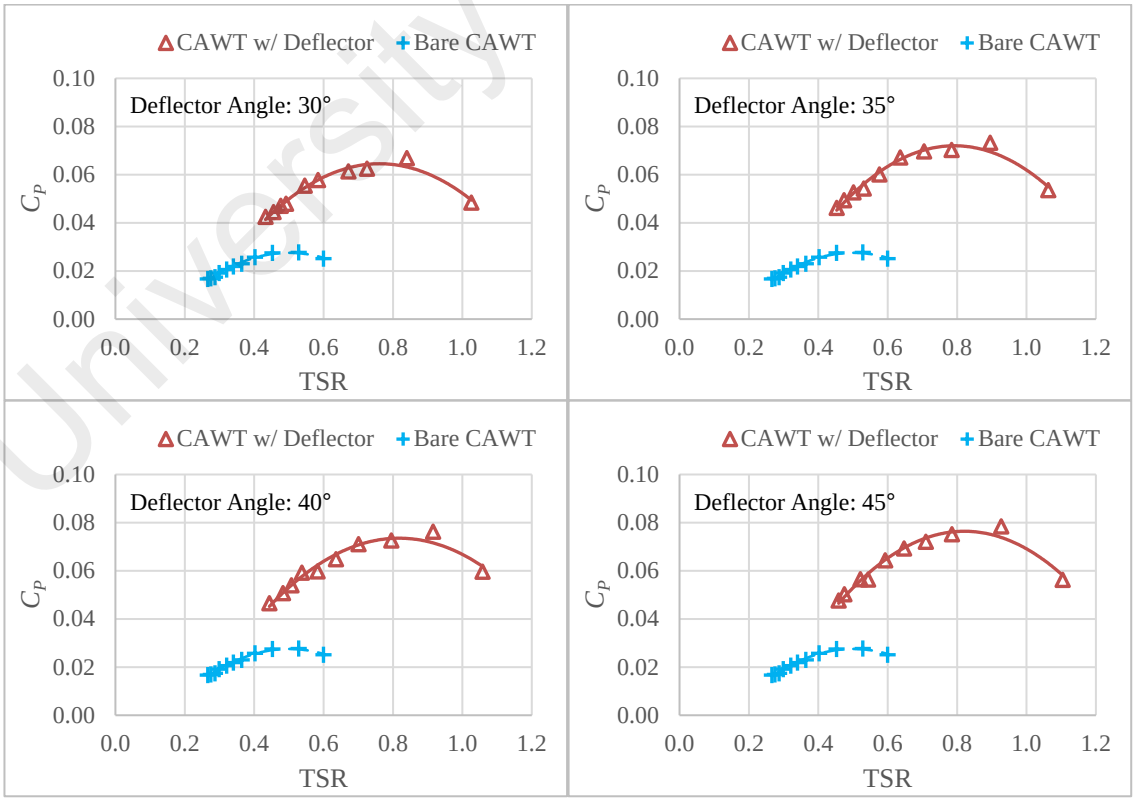


**Figure 4.7: $C_P$ against TSR for the deflector integrated and non-integrated cross axis wind turbine with horizontal blade pitch angle of 15°**

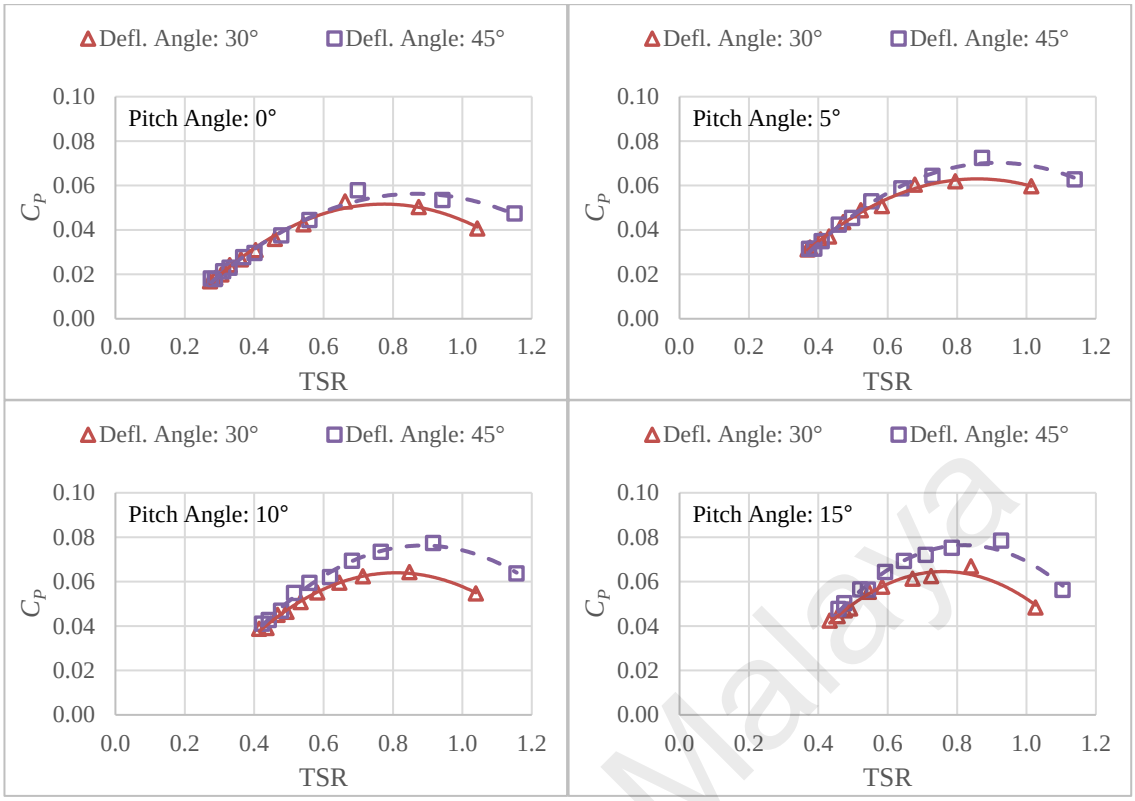


**Figure 4.8: The augmentation effect of the 30° and 45° deflectors on the cross axis wind turbine rotors with various horizontal blade pitch angles**

Quantitatively, the 45° deflector integrated CAWTs are shown to have higher peak power than the 30° deflector (as shown in Figures 4.4 to 4.8), and in general, the other deflectors. In the experiment, the peak power for the 15° pitch angle CAWT saw a 183% increase after being integrated with the 45° deflector (compared to its bare configuration). Note that the graph trend for the bare 15° pitch angle as shown in Figure 4.1 is almost analogous to that of the VAWT suggesting that without the deflector (or skewed flow), the performance of the CAWT is somewhat comparable to the conventional VAWT during operation, although the tip speed ratio range is smaller. Similar behaviours for the 40°, 35°, and 30° deflector integrated CAWTs are observed where the power outputs are increased by 175%, 164%, and 141%, respectively. The higher energy output can be related to the higher speed-up factor of the 45° deflector as illustrated in Figure 4.9. As mentioned in Section 3.4.3, to determine the speed-up factor of the deflectors, wind speed

measurements were taken without the presence of the wind turbines. Then, the factors are calculated using Equation (3.4). In analysing the speed-up factor, the wind speed at the measurement point number 9 ($z/h$ ratio of 0.04) achieved the highest speed-up ratio, with an increased wind speed of 36% due to the speed-up effect of the 45° deflector. This large increase in wind speed could indicate that the deflectors can induce strong turbulent winds on the leeward side of the deflector.

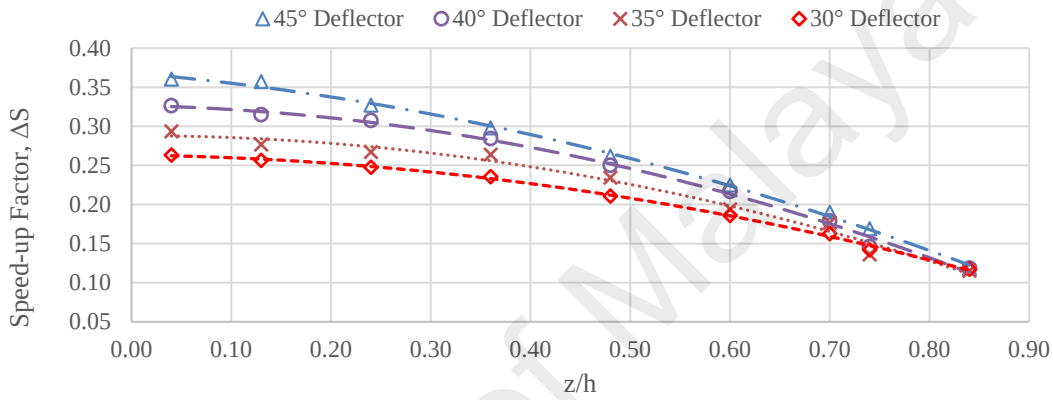


**Figure 4.9: Speed-up factor, $\Delta S$ at different measuring point locations (indicated by the $z/h$ ratio)**

In some existing studies, the vertical type wind rotors can operate efficiently in a turbulent environment (Armstron, Fiedler, & Tullis, 2012; Eriksson, Benhoff, & Leijon, 2008a; Islam, Hamza, & Dudek, 2013; Riegler, 2003; van Bussel, Mertens, Polinder, & Sidler, 2004b). Smaller wind turbines near buildings, trees, and other obstacles could take advantage of the turbulence in the oncoming winds. Cochran ( 2002) showed that high turbulence intensity in winds has a significant influence on the turbine performance due to the cubic variation of power with wind speed. Turbulent winds have larger energy potential than less turbulent winds with the same average wind speed. The capability of a vertical axis wind turbine to operate in the downstream wake of another turbine was studied by Chen et al. (2017). They conducted an optimisation study of two straight-bladed VAWTs using computational fluid dynamics and the Taguchi method. Furthermore, they observed that for a dual turbine setup, the flow velocity around and in

between the turbines was enhanced from their interaction. However, due to the harvested kinetic energy in the upstream flow, the flow velocity drops in the downstream wake. In studying small-sized wind turbines (HAWT and VAWT) in a turbulent urban environment, Pagnini, Massimiliano, and Repetto (2015) reported that the VAWT produces higher power than the HAWT during highly turbulent wind regimes blowing from the land. Moreover, the HAWT was strongly affected by the large fluctuations of wind, hence requiring frequent maintenance interventions. The VAWT however, was shown to be less affected by the strong winds and can be operational at higher wind velocities, therefore increasing the overall energy output. From the experiment, the higher wind speed and turbulent wind condition induced by the steeper slope of the 45° deflector increased the 15° pitch angle CAWT power output by 3.0%, 7.2% and 17.3%, compared to the power output of the same CAWT when integrated with the 40°, 35°, and 30° deflectors, respectively. Interestingly, the performance of the VAWT is observed to decline after being integrated with all of the deflectors as shown in Figure 4.10. Although the differences in reduction of power output are very small between the deflectors, the results from the experiment have shown that the use of deflectors for conventional VAWT is not advantageous. This can be attributed to the connecting struts of the VAWT that are known to have an aerodynamic disadvantage by disturbing the oncoming flow. The disturbed airflow adds to the resistive torque of the rotor (Li & Calisal, 2010). Geometrically, since the VAWT rotor has a high turbine aspect ratio ($H/R$ > 1.7), the skewed airflow has negatively influenced the VAWT performance. Similar observations were reported by Scheurich et al. (2011) where the generated power outputs of some VAWTs in oblique (skewed) flow are lower than those power outputs for VAWTs in normal flow (the VAWTs have high turbine aspect ratios, $H/R$ > 2.1).

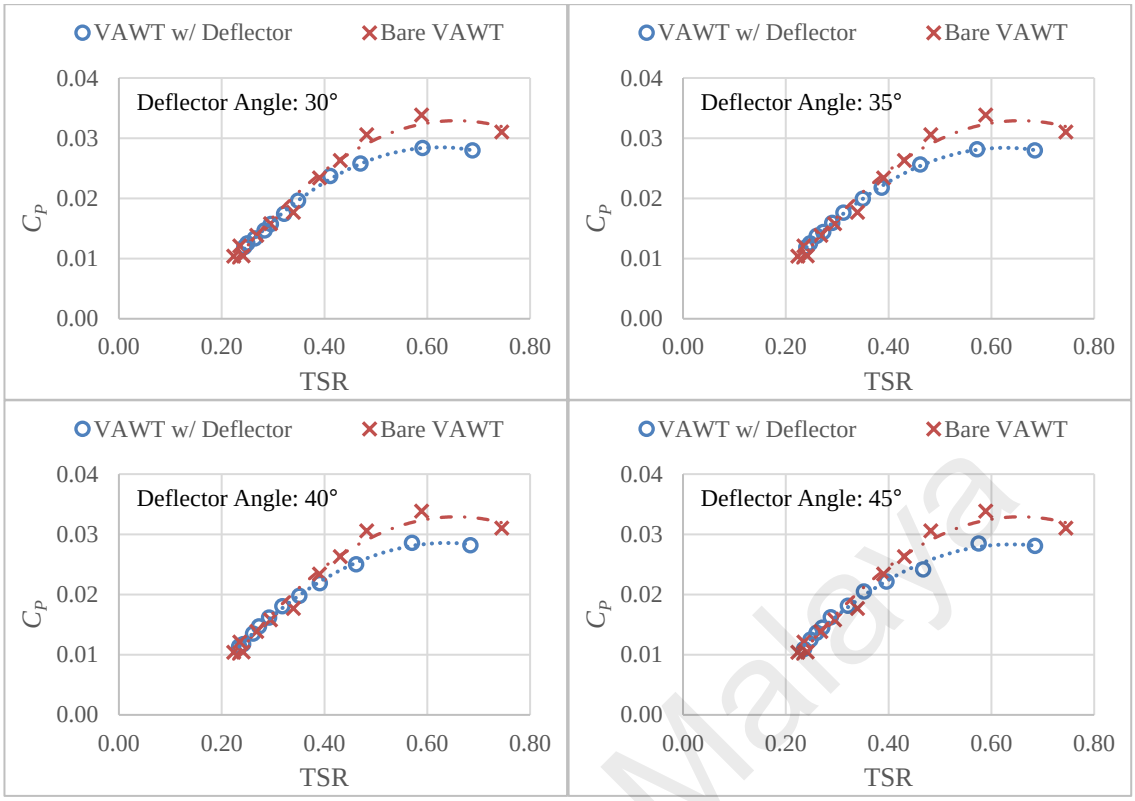


**Figure 4.10: Graphs of integrated and non-integrated VAWTs**

### 4.1.4 The effect of the horizontal blade pitch angle on the performance of the cross axis wind turbine

For brevity, Figure 4.11 shows the distribution of power coefficients versus tip speed ratio for the CAWT with horizontal blade pitch angles of 0° and 15° integrated with deflectors with inclination angles of 30°, 35°, 40° and 45°. The power output of the VAWT integrated with the various deflectors is also shown. It can be seen that even at the lower range of TSRs, the difference between the CAWTs and the VAWT caused by the pitch angles are large. Evidently, the VAWT has a smaller range of TSR compared to the CAWTs. For each configuration that was tested, the peak $C_P$ occurs at different TSRs. All the graphs show similar trends where the power coefficient of the wind turbines reach their peak values at a TSR range between 0.58 and 0.93. Improvement in the range of 27 to 36% for the maximum power coefficient is observed between the CAWT with horizontal blade pitch angles of 15° and 0°, demonstrating the effect of the pitch angle on

the CAWT's power output. By studying the geometry of these two turbines, the CAWT prototype and the VAWT model have similar external vertical blades, which contribute to a similar solidity ($\sigma = Nc/d$) value of 0.43. The high solidity value is a typical feature for a solid wind turbine that has a low efficiency compared to a lower solidity ($\sigma < 0.2$) turbine with better efficiency (Brusca, Lanzafame, & Messina, 2014). The detrimental effect of the solidity on the performance of both type of turbines in the bare configuration is evident (as shown in Figures 4.1, 4.4 to 4.7, and 4.11) where the bare rotors have lower maximum $C_P$ and a smaller range of TSRs. By introducing the 45° deflector, the horizontal blades of the CAWT interacting with the deflected airflow produced a higher $C_P$ value of 0.078 at a TSR of 0.93 (with CAWT pitch angle 15°) compared to the deflector integrated VAWT (maximum $C_P$ of about 0.028). This translates to a significant improvement in the power output of the CAWT compared to the conventional turbine. More specifically, the CAWT produced power that is 2.8 times of the power generated by the VAWT. Here, the advantage of the horizontal blades of the CAWT interacting with the deflected airflow has been demonstrated not to be affected by the high solidity of its external vertical blades.

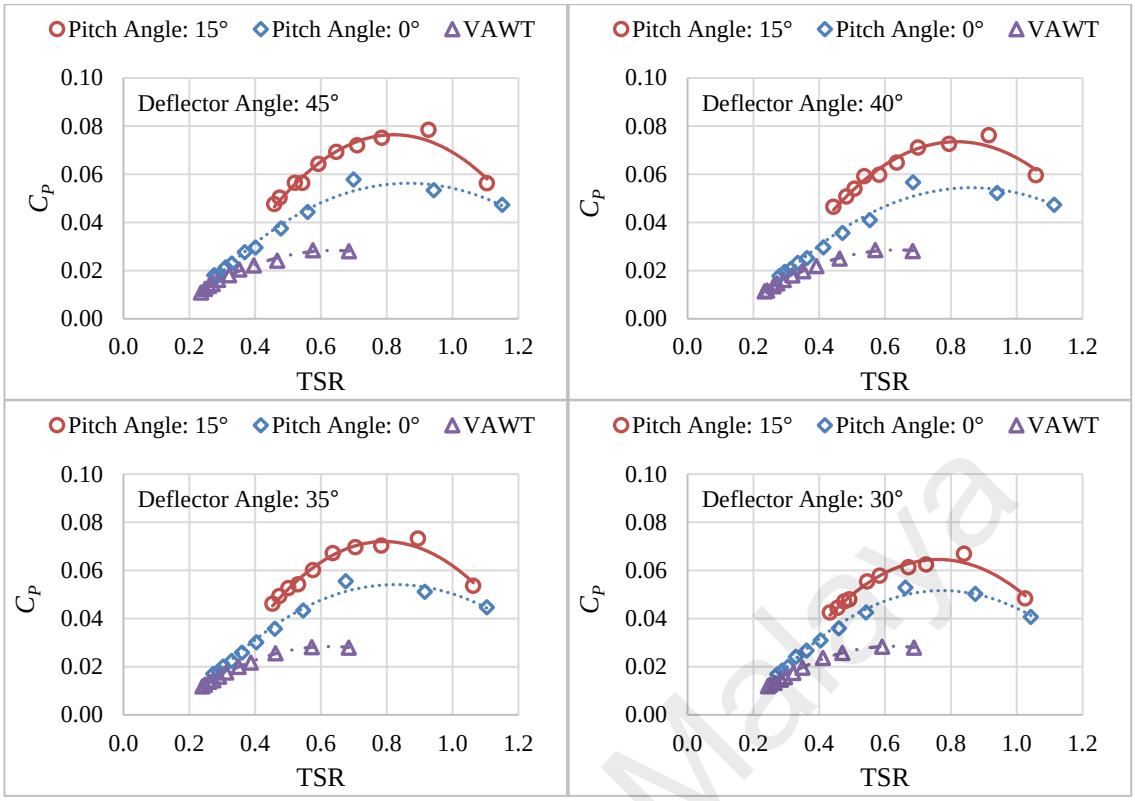


**Figure 4.11: $C_P$ against TSR for the conventional VAWT and CAWTs (horizontal blade pitch angles 15° and 0°) integrated with deflector with inclination angles of 45°, 40°, 35°, and 30°**

Further analysing the effect of the horizontal blade pitch angle within a fixed deflector configuration shown that the distribution of $C_P$ for the 10° pitch angle CAWT along the TSR values is similar to that of the 15° pitch angle CAWT (Figure 4.12). Nevertheless, the 15° pitch angle CAWT performed somewhat better in lower TSR values. By analysing the data, the effect of pitch angle on the power performance and aerodynamics of a turbine can be significant. By varying the horizontal blade pitch angle, $\beta_b$ from 0° to 15°, there is an increase of power output from 1.4 to 35.7%. Comparable to the current research work, Rezaeiha, Kalkman, and Blocken (2017) investigated the effect of varying the pitch angle of the vertical blades of a VAWT. They reported that by employing a negative pitch angle for the vertical blades (i.e. $\beta$ = -2°), the performance of the vertical axis rotor could increase by 6.6% compared to $\beta$ = 0°. It was also observed that the instantaneous moment on turbine blades for fixed pitch angle blades shifts between the upwind and downwind

regions. In the current work, however, the vertical blades of the VAWT were fixed at 0° for both the VAWT and CAWT models. This is the limitation of the current study, in which the research focus was only set by varying the pitch angle of the horizontal blades of the CAWT. Therefore, the future opportunity in research works may include investigating the effect of varying the novel turbine's vertical blade pitch angle.

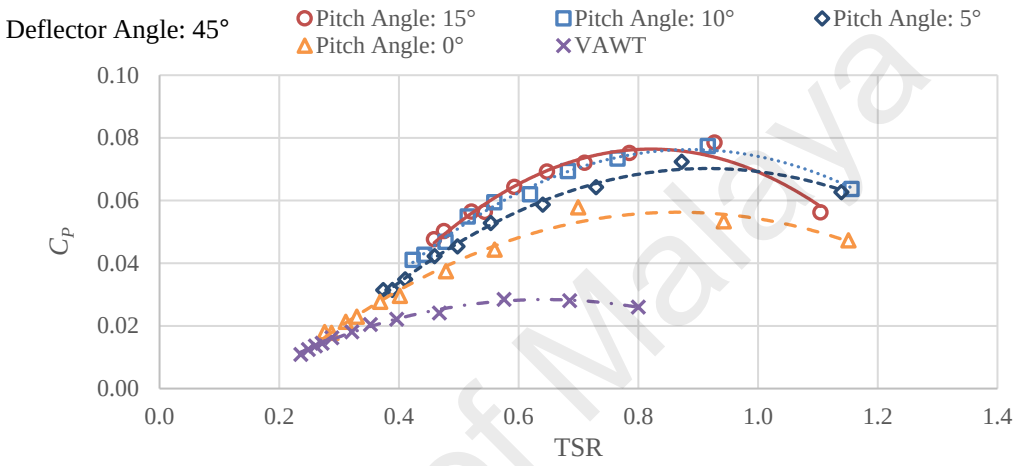


**Figure 4.12: $C_P$ against TSR for the VAWT and CAWT models integrated with the 45° deflector. The CAWT data are indicated with various pitch angles**

One of the most challenging issues associated with wind energy, in particular, the vertical axis wind turbine, is the self-starting capability of the system. For a wind turbine designed to be used in areas experiencing low wind speed, i.e. urban areas and tropical countries, it is essential to conceive a system that is able to self-start. Moreover, the increase in mechanical torque produced by wind rotors can demonstrate the possibility of the CAWT replacing the conventional VAWT for use in low wind speed application. The lift-type wind turbine has been long associated with poor self-starting characteristics compared to the drag-driven Savonius rotor. Over the years, researchers have demonstrated that a proper Darrieus VAWT design can ensure self-starting by lightly loading the turbine, ensuring an optimum number of blades or by exploiting the unsteady tangential force components along the Darrieus turbine circumference (Hill, Dominy,

Ingram, & Dominy, 2009; Worasinchai et al., 2015). Rotor geometry, i.e. chord-to-diameter ($c/d$) ratio and aspect ratio (AR), is very important in starting performance. Both the CAWT and the VAWT used in the experiment has the same $c/d$ and AR values (0.14 and 6, respectively), and therefore they are geometrically related. With a $c/d$ ratio of 0.14, Worasinchai et al. (2015) have shown that the unsteady tangential force can be generated due to a reduced frequency that drive the rotor to self-start. However, the solidity of the machines, in particularly the VAWT, can affect the rotor performances, as shown in Figures 4.11 to 4.16. Unlike the VAWT, the CAWTs have airfoil-shaped struts to take advantage of the lift forces due to the skewed wind flow. These additional lift forces are very beneficial in terms of producing higher torque output.

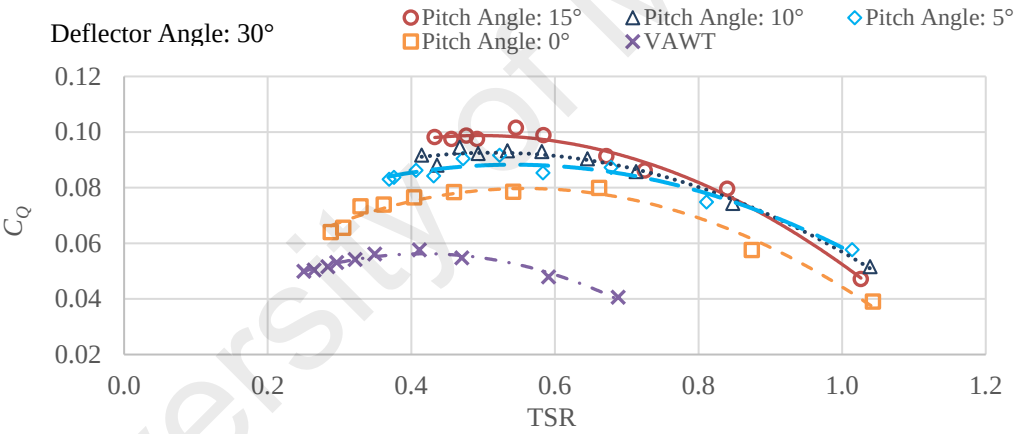


**Figure 4.13: $C_Q$ against TSR for the VAWT and various CAWT configurations integrated with 30° deflector**

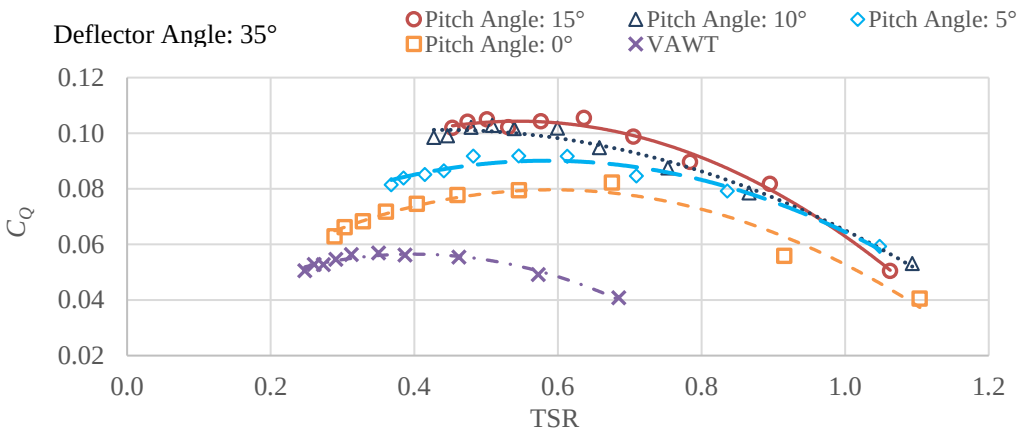


**Figure 4.14: $C_Q$ against TSR for the VAWT and various CAWT configurations integrated with 35° deflector**

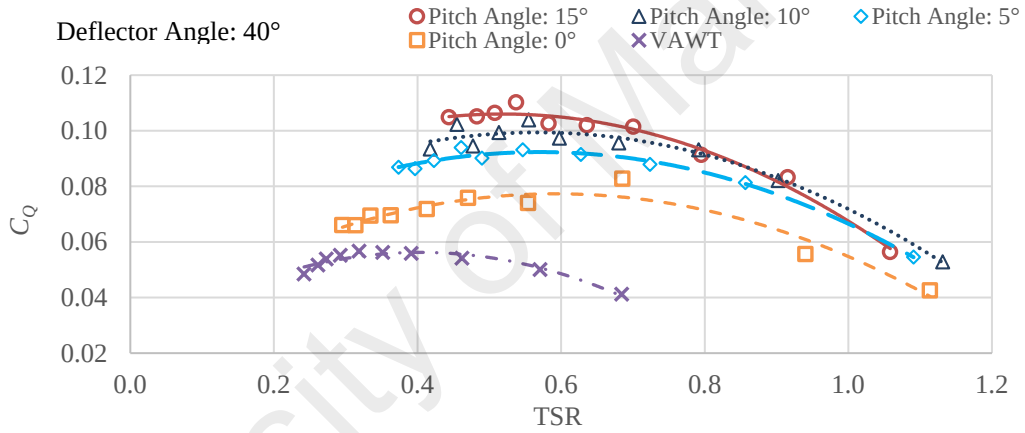


**Figure 4.15: $C_Q$ against TSR for the VAWT and various CAWT configurations integrated with 40° deflector**

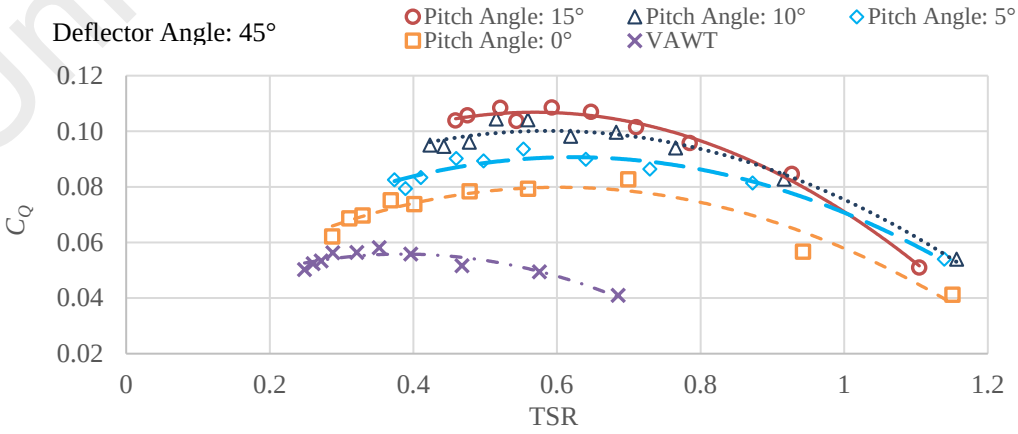


**Figure 4.16: $C_Q$ against TSR for the VAWT and various CAWT configurations integrated with 45° deflector**

The data trends in Figures 4.13 to 4.16 indicate that the torque coefficients produced by the CAWTs are significantly increased after being integrated with the deflector. Across the different deflector configurations, the torque coefficients are improved from 38.9 to 94.0%. Interesting to note that the 15° pitch angle CAWT in every deflector configurations have the highest maximum torque coefficient, and in general, produced better torque output in the lower range of the TSRs. However, at the upper range of the TSRs, the 15° pitch angle CAWT does not perform well. Based on the data, the torque coefficient for the bare 15° pitch angle CAWT suffers at higher tip speed ratios (shown in Figure 4.17a) due to the steeper pitch angle. Again, as mentioned, the phenomenon that the pitch angle of 0° has higher $C_Q$ than that of 15° for the case without deflector plate can be explained by the high pitch angle of the horizontal blades that may contribute to the additional drag force that occurred along the airfoil, therefore reducing the torque output from the CAWT. Based on the lift coefficient of airfoil NACA0015, this type of blade suffers a severe loss of lift, and the drag force becomes dominant when the angle of attack approaches 15° at low Reynolds number (<20,000). Moreover, this can be justified due to the optimum angle of attack between the inflow angle and the pitch angle of the horizontal blades (Equations 3.17 and 3.18) which will be further discussed in Section 4.2. Meanwhile, the 15° pitch angle CAWT that was integrated with the 40° deflector produced the highest torque coefficient of 0.1100, which is 94.0% higher than the VAWT integrated with the same deflector (Figure 4.17b). However, the 15° pitch angle CAWT integrated with 45° deflector has the better distribution of torque coefficients against the TSR. Nevertheless, the results from the experiment showed that the CAWT has a better ability to self-start in low wind speed regions and skewed flow conditions compared to the conventional VAWT.

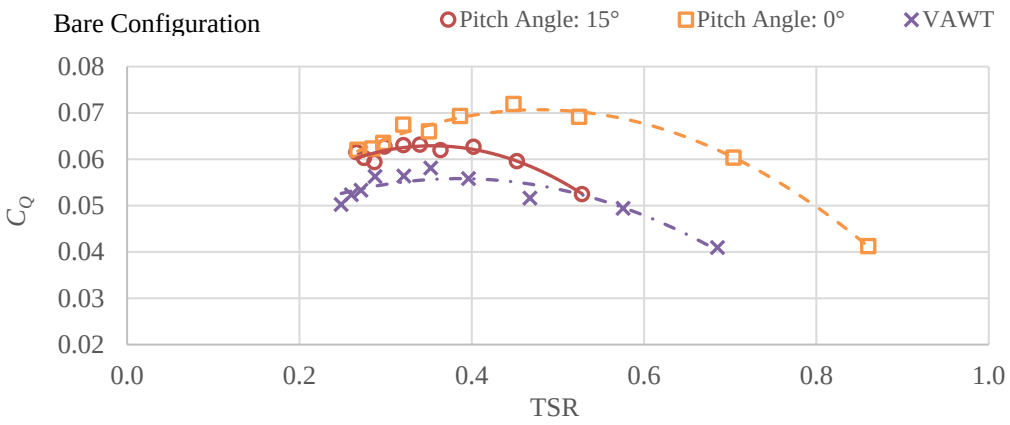


(a)

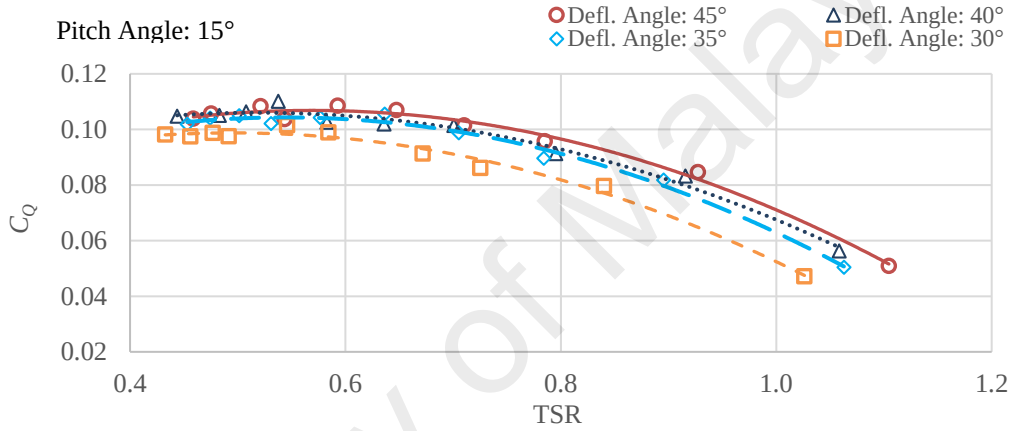


(b)

**Figure 4.17: Torque coefficient against tip speed ratio for the (a) bare configuration, and (b) the 15° pitch angle CAWT integrated with various deflectors**

The current research work has shown that the CAWT horizontal blade pitch angle and the slope of the deflectors are critical parameters in enhancing the performance of the novel cross axis wind turbine. From the experiment and as shown in Figure 4.18, the 15° pitch angle CAWT integrated with 45° deflector produced the highest peak power at 0.46 W, whereas the 0° pitch angle CAWT with the same deflector recorded a maximum peak power of 0.34 W. When the deflector angle is varied from 45° to 30°, a steady trend of decreasing peak power can be observed. In the bare configurations, however, it was observed that the 5° pitch angle CAWT achieved the best performance compared to the

other CAWTs ($C_P$ is 29.8% higher compared to the bare VAWT). Moreover, the peak power outputs for the 10° and 15° pitch angle CAWT suffered a sharp drop to 0.209 W and 0.162 W, respectively. Whereas, the peak power values of the bare 0° and 5° pitch angle CAWT are higher with a measured value of 0.249 W and 0.253 W, respectively. As discussed earlier, this is due to the steeper pitch angle of the 10° and 15° CAWTs which result in the drop of peak power for their bare configurations. It is hypothesised that this is due to the major separation of flow along the airfoil struts, therefore reducing the lift forces on the blades. Moreover, due to the symmetrical airfoil of NACA0015, it is inferred that the 0° pitch angle CAWT in the bare configuration maintains a better performance than the conventional VAWT as the airfoil-shaped struts permit the utilisation of aerodynamic lift on the blades' upper and lower surfaces. This translates to a higher torque produced by the rotor (Hameed et al., 2013; Miller, 2008).

Rezaeiha et al. (2017) suggested that to enhance the vertical axis wind turbine design, a dynamic pitch of the vertical blades is needed to improve the overall performance of the rotor. Similar observations were made by Hwang, Lee, and Kim (2009); Jing, Sheng, and Zhang (2014) and Zeiner-Gundersen (2015). In the current work, the presence of steeper pitch angles could either enhance or negatively affect the performance of the cross axis wind turbine. By analysing the bare CAWTs, there is a slight increase in the performance when the pitch angle is changed from 0° to 5° (increment by 1.6%). However, the performance declined at higher pitch angles in which the bare 15° pitch angle CAWT's power output is lower than the power out produced by the bare VAWT. It is also observed that the torque coefficient of the 15° pitch angle CAWT has a lower range of TSR compared to the other rotors in the bare configuration (Figure 4.17a). The combination of high aspect ratio and a high pitch angle of the CAWT seems to affect the performance of the rotor significantly. Using variable pitch blades and deflectors may

help in improving the CAWT performance, where the blade angle of attack can be optimised depending on the relative direction of the vertical component of the wind.

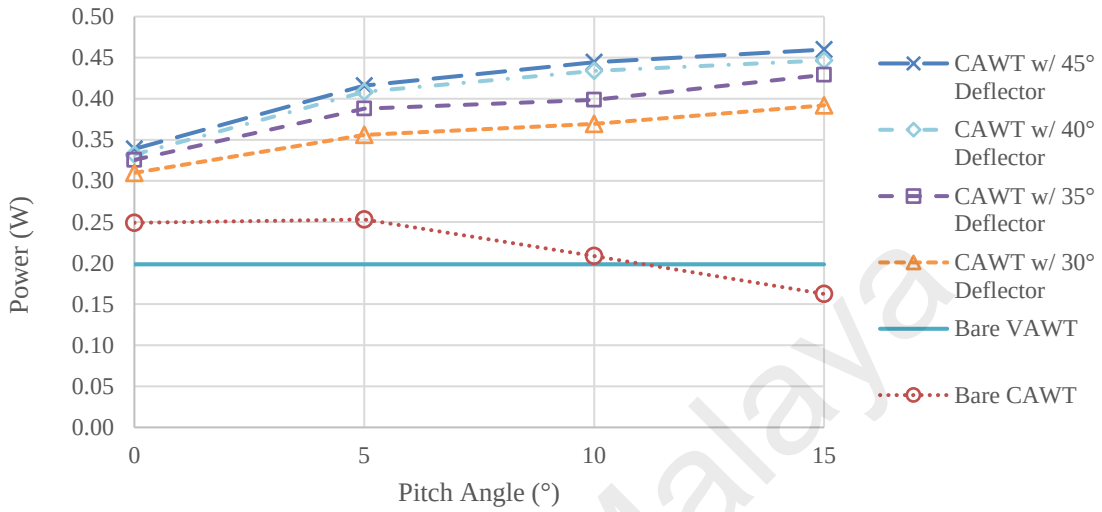


**Figure 4.18: Effect of varying the horizontal blade pitch angle with different deflectors on the performance of the CAWT**

### 4.1.5 The rotational speed of the cross axis wind turbine

To further investigate the effect of the deflected wind flow interacting with the horizontal blades of the CAWT, the graphs shown in Figure 4.19 illustrate the rotational speed performances for the wind turbines taken for a duration of 240 s at the free-running condition. During this experimental phase, the rotors are only subjected to inertia and bearing friction without external loads being applied during the assessment. For this study, the rotational speed performance of the 15° and 0° pitch angle CAWTs with the 45° deflector are chosen for further discussion. As the graphs show, the trends of the rotational speed for the wind turbines are steadily increasing and then stabilised after reaching a steady-state. Similar to the power performance output of the bare 15° pitch angle CAWT, the results in Figure 4.19(a) shown that the maximum rotational speed of the bare VAWT is higher than the bare CAWT with an approximately 35% difference. Conversely, by integrating the deflector with the CAWT, a significant increase of

rotational speed was achieved with a maximum value of 347 RPM (data were taken after the rotational speed has stabilised at the end of the 240s period).

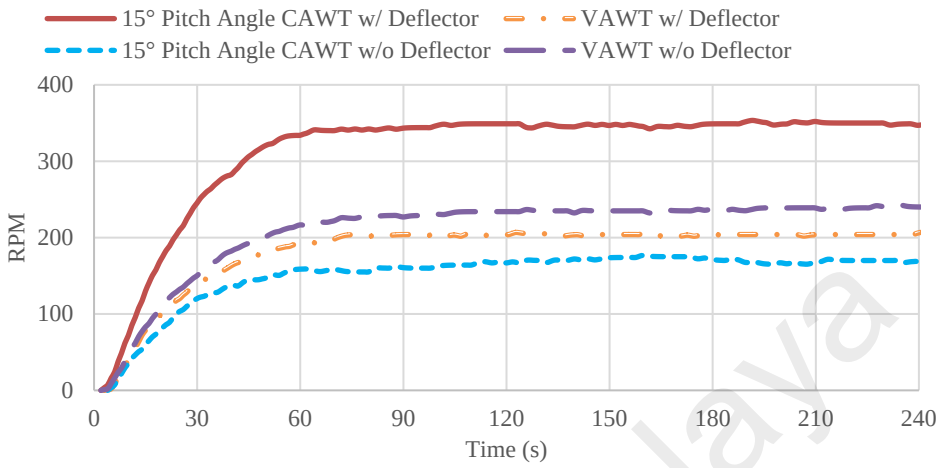


(a)

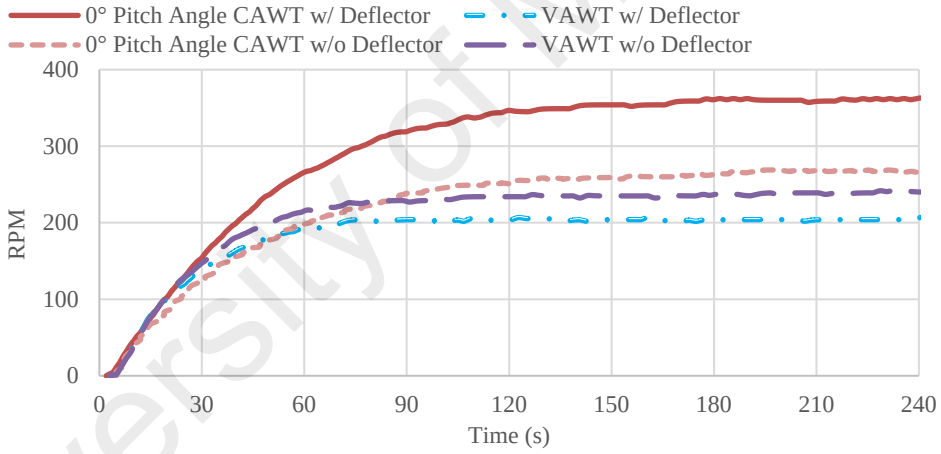


(b)

**Figure 4.19: Rotational speeds of the (a) 15°, and (b) 0° pitch angle CAWTs with the VAWT. Rotors with and without the 45° deflector are shown**

In comparison, the VAWT integrated with the deflector recorded a stabilised rotational speed of 207 RPM, lower than the results obtained from the CAWT. Based on the study of Kim et al. (2013), if the turbine is positioned near to the deflector and inside the streamlines emanating from the edge of the plate, the performance of the VAWT is reduced due to small flow velocity inside the wake. Moreover, the flat plate struts of the VAWT are unable to harness the kinetic energy of the flow velocity inside the wake.

Again, this illustrates the subpar performance of the VAWT in a highly skewed airflow. On the other hand, the rotor rotational speed of the bare 0° pitch angle CAWT shown in Figure 4.19(b) exceeds the rotor rotational speed of the bare VAWT after 90 s. This demonstrates the advantage of airfoil-shaped struts in utilising the lift forces generated by orthogonal airflow interacting with horizontal blades.

**Table 4.1: Summary of peak power coefficient, torque coefficient, and free-running RPM data for the bare and deflector integrated rotors. The values in brackets are the negative percentage change**

| Rotor | | | Parameter | | | Change (%) | | |
|---|---|---|---|---|---|---|---|---|
| | | | $C_P$ | $C_Q$ | RPM | $C_P$ | $C_Q$ | RPM |
| Bare | VAWT | | 0.0339 | 0.0634 | 240.1 | - | - | - |
| | CAWT | 0° | 0.0425 | 0.0719 | 265.8 | 25.4 | 13.4 | 10.7 |
| | | 5° | 0.0440 | 0.0721 | 258.2 | 29.8 | 13.7 | 7.6 |
| | | 10° | 0.0363 | 0.0717 | 212.0 | 7.1 | 13.1 | (11.7) |
| | | 15° | 0.0277 | 0.0631 | 167.9 | (18.3) | (0.5) | (30.1) |
| 30° Deflector | VAWT | | 0.0283 | 0.0576 | 206.6 | - | - | - |
| | CAWT | 0° | 0.0529 | 0.0800 | 328.6 | 86.9 | 38.9 | 59.1 |
| | | 5° | 0.0620 | 0.0917 | 367.6 | 119.1 | 59.2 | 77.9 |
| | | 10° | 0.0643 | 0.0946 | 338.1 | 127.2 | 64.2 | 63.6 |
| | | 15° | 0.0669 | 0.0989 | 306.0 | 136.4 | 71.7 | 48.1 |
| 35° Deflector | VAWT | | 0.0281 | 0.0569 | 205.3 | - | - | - |
| | CAWT | 0° | 0.0556 | 0.0822 | 348.7 | 97.9 | 44.5 | 69.8 |
| | | 5° | 0.0675 | 0.0918 | 384.2 | 140.2 | 61.3 | 87.1 |
| | | 10° | 0.0694 | 0.1029 | 325.5 | 147.0 | 80.8 | 71.7 |
| | | 15° | 0.0732 | 0.1050 | 333.9 | 160.5 | 84.5 | 62.6 |
| 40° Deflector | VAWT | | 0.0286 | 0.0567 | 205.0 | - | - | - |
| | CAWT | 0° | 0.0567 | 0.0827 | 350.4 | 98.3 | 45.9 | 70.9 |
| | | 5° | 0.0711 | 0.0939 | 422.0 | 148.6 | 65.6 | 105.9 |
| | | 10° | 0.0755 | 0.1040 | 383.6 | 164.0 | 83.4 | 87.1 |
| | | 15° | 0.0762 | 0.1100 | 331.5 | 166.4 | 94.0 | 61.7 |
| 40° Deflector | VAWT | | 0.0285 | 0.0581 | 204.0 | - | - | - |
| | CAWT | 0° | 0.0578 | 0.0827 | 363.1 | 102.8 | 42.3 | 78.0 |
| | | 5° | 0.0724 | 0.0936 | 433.1 | 154.0 | 61.1 | 112.3 |
| | | 10° | 0.0774 | 0.1044 | 412.5 | 171.6 | 79.7 | 102.2 |
| | | 15° | 0.0785 | 0.1085 | 347.5 | 175.4 | 86.7 | 70.3 |

In general, the CAWT has better rotational speed performance and self-starting characteristics compared to the VAWT. From the study, the effect of the deflector and the horizontal blades of the CAWT produced better power output and higher rotational

speed than the conventional VAWT. Evidently, the horizontal blades of the CAWT produced additional torque in tandem with the increase in the rotational speed of the turbine due to the interaction of the deflected vertical wind flow, hence outperforming the VAWT. A summary of the obtained data from the experiment is tabulated in Table 4.1 which shows the changes in percentage for the numerous CAWT and VAWT configurations.

## 4.2 Theoretical analysis of the cross axis wind turbine

### 4.2.1 Measured local wind velocities

An example of the local mean velocity profile (skewed flow) for all deflector configurations (and without deflector) at azimuth angles from 5° to 355° are plotted in Figure 4.20. At the upstream position, the local wind velocities gradually decrease from the azimuth angle of 5° to 85° for all deflector configurations. At an azimuth angle of 5°, the surface of the deflector is nearest to the local point where the wind velocity is high. However, changing the position of the local point from 5° to 85°, the distance between the local point and the surface of the deflector increases, thus reducing the deflected wind velocity at these local positions. At the downstream position, the wind velocities decrease from 185° to 265° azimuth angle due to the absence of deflector and the effect of the shaft. Without the deflector, the skewed wind velocities are about 2.0 m/s or lower in all azimuth angles. Even without the deflector, there exists small effect of skewed wind flow due to the vortex airflows from the blowers and the wake from the shaft. Moreover, the data showed that the wind load without the deflector is not sufficient to enhance the performance of the CAWT significantly.

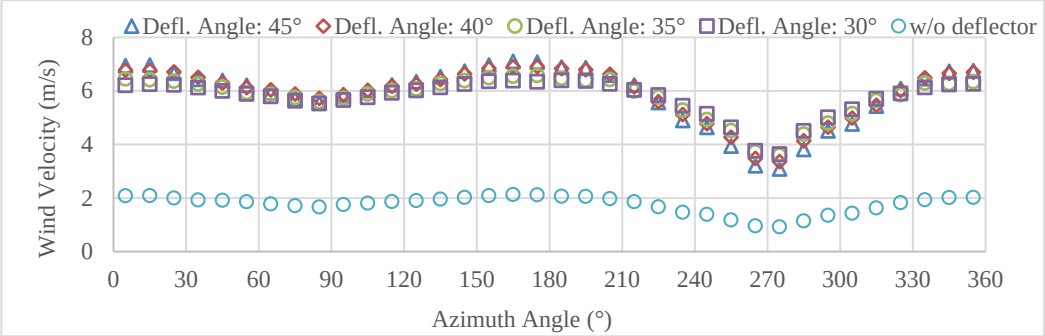


**Figure 4.20: Local mean wind velocity profile at the blade span of $r/R$ = 91%**

### 4.2.2 Validating the experimental performance of the deflector integrated cross axis wind turbine with the theoretical approach

Comparisons between the experimental and the analytical data using the approach outlined in Chapter 3 are illustrated in Figure 4.21. The graphs show the peak power from the experiments, the power contribution from the BEM and DMST models, and the calculated theoretical power produced by the CAWT using Equation (3.26). The calculations for each of the BEM and DMST models are done independently in which the aerodynamic data for low Reynolds number were used in the calculations. As mentioned, an extrapolation method was applied to predict the blade performance both near the stall region and beyond the stall point due to the low TSR of the wind turbines. In general, the trend of the graphs shows a gradual increase of power as the angle of the deflector is increased from 30° to 45°. The calculated power of the cross axis wind turbine for every deflector configuration and pitch angle shows a good agreement with the power obtained from the experiment with the difference in the range of 9.83% to 18.95%. However, power calculated from the theoretical approach is higher compared to the experimental data. This can be justified by considering that during the experiment, there are internal friction and vibration factors that lead to the power loss (Huleihil & Mazor, 2012). Moreover, due to the low tip speed ratio of the rotors, there exist aerodynamic losses at the end of the rotors, which is one of the major limitations of this study that are not taken

into account in the analytical approach. The effects of the deflector in augmenting the local flow angle, local wind velocities, and finally the rotational speed of the rotors are very important in determining the distributions of the angle of attack for each of the CAWT configurations. Utilizing the TSRs correspond to the peak power output from the experiment (as shown in Figure 4.22), both Equations (2.45) and (3.18) describe that the increase of local TSR reduces the angle of attack of the relative airflow. For example, at higher TSR, the distributions of the angle of attack are generally smaller than those configurations with lower TSR. Therefore, better lift-to-drag ratio and higher torque output can be expected.

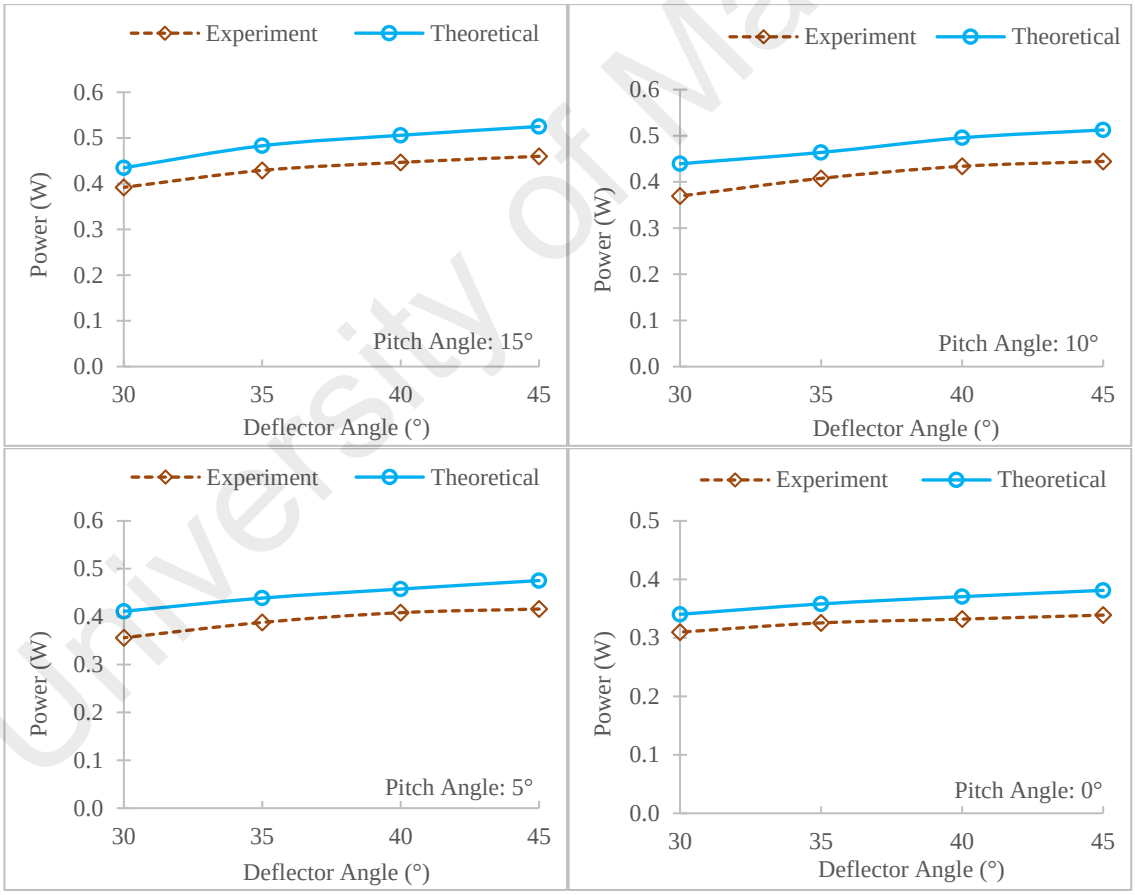


**Figure 4.21: Comparisons between the power obtained from the experiments and obtained from the proposed theoretical approach for the 15°, 10°, 5° and 0° pitch angle CAWTs integrated with various deflectors**

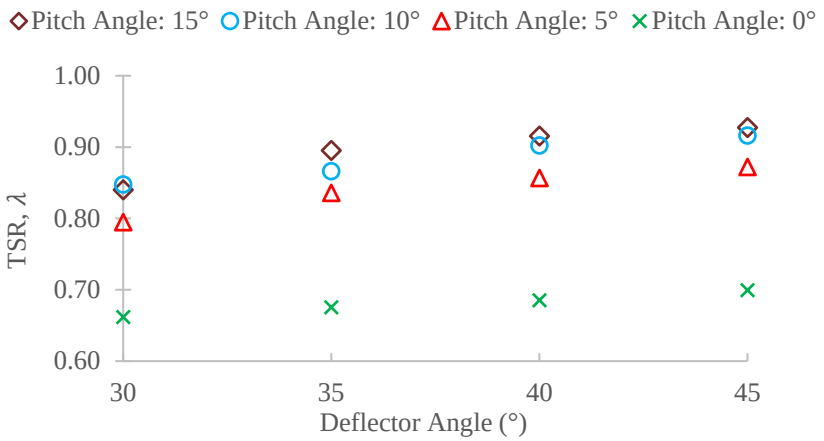


**Figure 4.22: Variation of tip speed ratio, λ associated with peak power output for different deflector and horizontal blade pitch angles**

### 4.2.3 The cross axis wind turbine blade analysis

#### 4.2.3.1 Vertical blade analysis

By using a semi-empirical approach, the rotational speed data from the experiment corresponding to the generated peak power are identified and applied in the theoretical study (Figure 4.22). To begin with, two different CAWT configurations from the experiment are selected, i.e. 15° and 0° pitch angle CAWTs integrated with the 45° deflector. The selected configurations are chosen to analyse the airflow angle of attack on the vertical blades and the corresponding torque output at different TSRs (Table 4.2).

**Table 4.2: Data for 15° and 0° pitch angle CAWT integrated with 45° deflector**

| CAWT Configuration | Peak Power, W | TSR, $\lambda$ |
|---|---|---|
| Pitch angle, $\beta_b$ = 15°; deflector angle, $\theta_d$ = 45° | 0.46 | 0.93 |
| Pitch angle, $\beta_b$ = 0°; deflector angle, $\theta_d$ = 45° | 0.34 | 0.70 |

The instantaneous torque and angle of attack against azimuth angle generated by the vertical blades are shown in Figure 4.23. Due to the geometry of the airfoil and design of the vertical rotor, the vertical airfoil's angle of attack changes from positive to negative as the turbine rotates. Moreover, as such, the fluctuation of torque occurs, which is commonly found in conventional VAWT. In Figure 4.23(a), as the vertical blades rotate,

the angle of attack is rising steadily. At an azimuth angle of 95°, the vertical blades produced the highest instantaneous torque of 0.033 Nm with the angle of attack of 37.4°. Beyond this point, the torque slowly decreases as the angle of attack continues to increase. Based on the DMST model analysis, when the blade switches to the downstream position, the angle of attack dropped almost linearly to negative in the third and fourth quadrants (downstream position). In these regions, the instantaneous torque output is low due to the significant reduction in lift coefficients. By comparing with the vertical blades experiencing low TSR of 0.70 for the 0° pitch angle CAWT configuration, the vertical blades at the higher TSR was able to mostly maintain a positive torque output in the downstream position (positive torque generated in 75.0% of overall azimuth positions). Based on the DMST analysis, the mean torque produced by the vertical blades of the 15° pitch angle CAWT rotor is 0.0066 Nm. In contrast, the vertical blades of the 0° pitch angle CAWT configuration have shown a noticeable fluctuation of torque as the rotor rotates from the upstream to downstream position. As the pitch angle of the vertical blades was not changed throughout the study, therefore the angle of attack for the vertical rotors is strictly influenced by the rotational speed and the relative velocities apparent to the vertical blades.

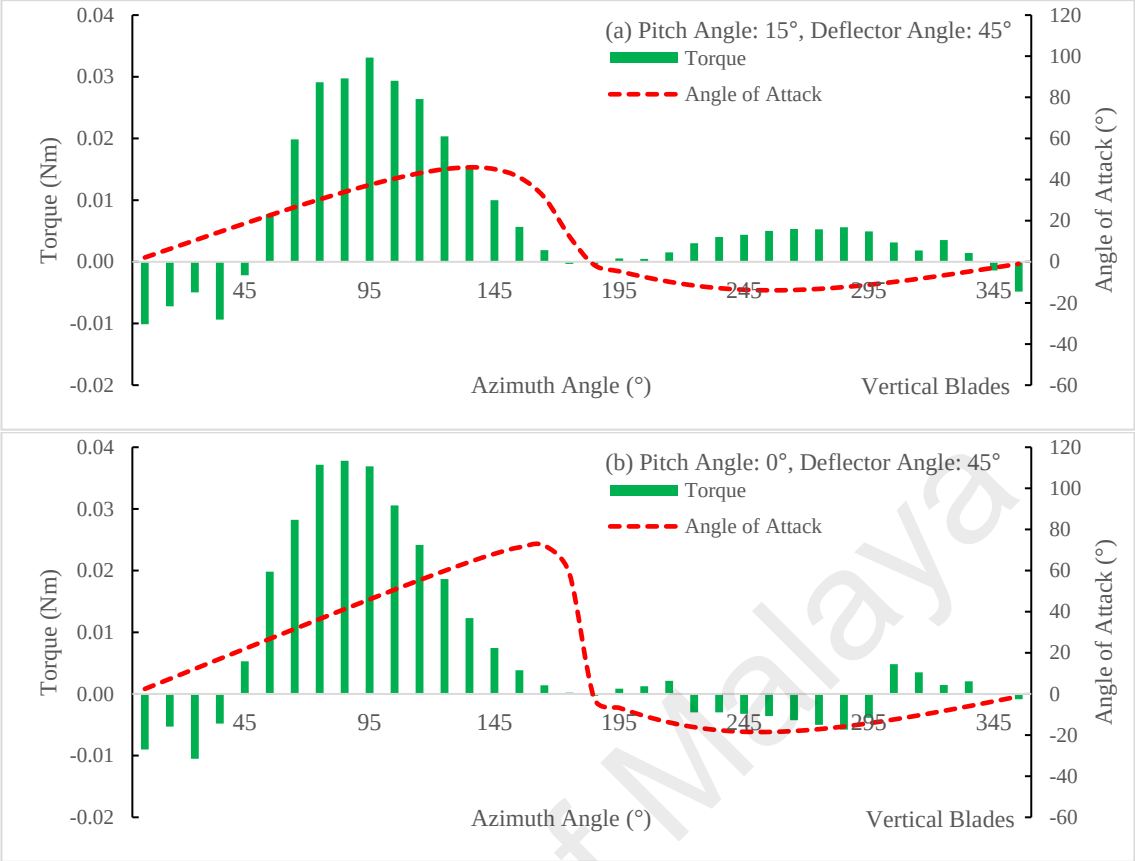


**Figure 4.23: Vertical blades analysis showing the instantaneous torque and angle of attack against azimuth angle for the (a) 15° and (b) 0° pitch angle CAWT integrated with 45° deflector rotor configurations**

From the theoretical standpoint, Equation (2.45) shows that as the TSR reduces, the local angle of attack apparent to the vertical blade increases (De Marco et al., 2014; Fazlizan et al., 2015). Similar to Fazlizan, Chong, Yip, Poh, and Muzammil (2017), wind turbines with high chord-to-radius ($c/R$) ratios ($c/R > 0.25$) exhibit very high angle of attack in the upstream position. Moreover, the high $c/R$ ratio may affect the turbine's efficiency in energy extraction. A study by Migliore et al. (1980) showed that the flow curvature effects could reduce the stall angle of a Darrieus-type wind turbine blade to some degree. Therefore, a premature stall effect may occur which results in a reduced turbine torque output. This is especially true for wind turbines with lower TSR. With lower TSR, the distribution trend of the angle of attack based on the DMST model for the 0° pitch angle CAWT is relatively higher compared with the 15° pitch angle CAWT. As

shown in Figure 4.23(b), the angle of attack for the CAWT's vertical blades is steadily rising from the first to second quarter region before it sharply declines in the third quadrant and maintains in the negative region until the fourth quadrant. With the lower TSR of 0.70 for the 0° pitch angle CAWT, the model shown that the negative torque output is generated in about 42.0% of the total azimuthal positions, with a reduction of mean torque by 9.1% compared to the 15° pitch angle CAWT.

As presented in the experimental analysis, by varying the inclination angle of the deflectors, the TSRs corresponding to the peak power output also changes. To investigate the effect of the deflector on the rotational speed of the turbine, the following Figure 4.24 depicts the instantaneous torque and angle of attack against azimuth angle for the 15° and 0° pitch angle CAWT integrated with the 30° deflector. By changing the deflector angle from 45° to 30°, the TSRs associated with the peak power for the 15° and 0° pitch angle CAWTs reduced by 9.7 and 5.7% to 0.84 and 0.66, respectively (Table 4.3). As shown in Figure 4.24(a), the DMST model illustrates that the 15° pitch angle CAWT's vertical blade torque output deteriorates at lower TSR, especially in the downstream region where there is a 3.5% increase of mean negative torque generated in the 36.0% of the total azimuthal positions (as opposed to only 22.0% of the total azimuthal positions for the 15° pitch angle CAWT with the 45° deflector). Further deterioration of torque output experienced by the vertical blades at the TSR of 0.66 can be shown in Figure 4.24(b) where the angle of attack for the 0° pitch angle CAWT increases up to 84.0° before dropping to -87.8°. This large fluctuation of angles of attack indicate that the blades fall into stalling before maintaining to generate more negative torque in the downstream position. Here, the profile of the geometrical airfoil characteristics influence the drag and lift coefficients for angles of attack beyond the stall region, especially for low Reynolds number flow regime (Camporeale & Magi, 2000).

**Table 4.3: Data for 15° and 0° pitch angle CAWT integrated with 30° deflector**

| CAWT Configuration | Peak Power, W | TSR, $\lambda$ |
|---|---|---|
| Pitch angle, $\beta_b$ = 15°; deflector angle, $\theta_d$ = 30° | 0.39 | 0.84 |
| Pitch angle, $\beta_b$ = 0°; deflector angle, $\theta_d$ = 30° | 0.31 | 0.66 |

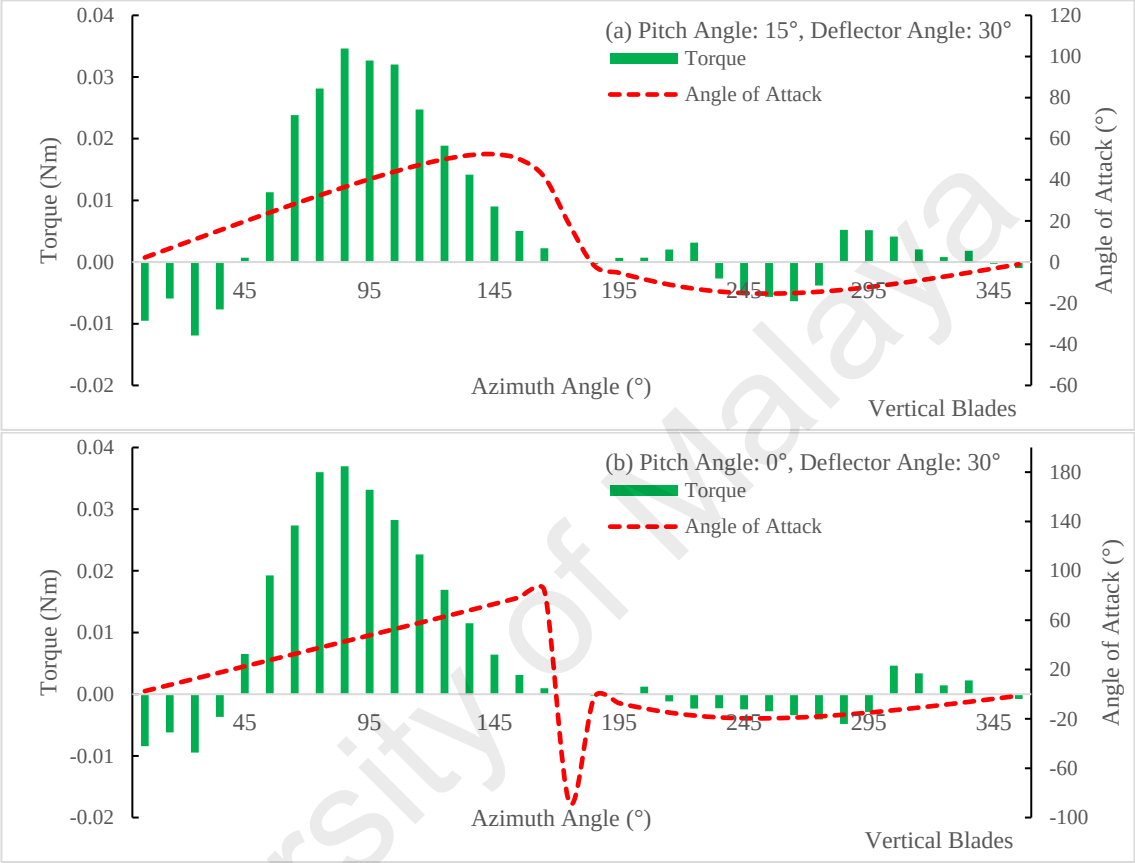


**Figure 4.24: Vertical blades analysis showing the instantaneous torque and angle of attack against azimuth angle for the (a) 15° pitch angle CAWT integrated with 30° deflector, and (b) 0° pitch angle CAWT integrated with 30° deflector**

#### 4.2.3.2 Horizontal blade analysis

The calculation sample in Appendix D showed that the induction factor of 1/3 was used for all azimuth angles. Mertens et al. (2003) stated that for induction factors of above 0.4, empirical evaluation of the thrust force to overcome the breakdown of momentum theory must be carried out to determine the local induction factor (see also Burton et al. (2001)). Following Mertens et al. (2003), these relations are not known for skew angles, and therefore an assumed value was used in the current model for the operation of the

horizontal blades in the skewed flow. Future studies should attempt to improve the model to focus on the aerodynamic loads in the wake regions of the horizontal blades. In the current study, to illustrate the aerodynamic characteristics of the horizontal blades of the CAWT, and the effect of the pitch angle on the performance of the turbine, the angle of attack and instantaneous torque against azimuth angle of rotor configurations in Table 4.2 are plotted in Figures 4.25(a) and 4.25(b). In general, the trends for the angle of attack graphs are different in the various span locations. Furthermore, the range for the local angle of attack increases from the outer span to the inner span locations (91% to 46%) due to the reduction of local TSR.

In Figure 4.25(a), the angle of attack and instantaneous torque for the 15° pitch angle CAWT are shown. At local points between azimuth angle of 5° to 75°, the torque generated by the horizontal blades are steadily increasing from negative to positive as the angle of attack approaches the stall angle ($\alpha = 9°$). After the stall point, as the turbine rotates from the azimuth angle of 75° to 125°, the torque reduces before increases to an instantaneous peak torque of 0.0025 Nm where at this point, the angles of attack are 35.9° at 91% span, 55.9° at 69% span, and 78.8° at 46% span. By analysing the data, even when the wind speed in the azimuth region between of 5° to 75° is reducing, the rotation of the blade from azimuth angle of 5° to 75° matches with the skewed flow angle and the torque output from the horizontal blade can still be generated. However, due to the steep pitch angle of the horizontal blade, the angle of attack in this region maintains lower than the required values to generate positive torque. As seen in Figure 4.25(b), the zero pitch angle horizontal blade managed to produce positive torque values much earlier than the 15° pitch angle CAWT. In the downstream position, the skewed wind velocity in the third and fourth quarter of azimuth angle (180° to 360°) significantly drops to less than 4 m/s due to the wake generated by the deflector. The reduced flow velocity affects the horizontal blades in the downstream position where the angle of attack for both the 0° and

15° CAWT integrated with the 45° deflector drop significantly as the rotation of the blade moves from the third to the fourth quarter region. Moreover, the negative angle of attack depicted in Figure 4.25(a) was due to the steep pitch angle of the horizontal blade.

In contrast to the 15° CAWT, the 0° CAWT shows the evident fluctuation of torque in the upstream and downstream positions. As depicted in Figure 4.25(b), a much higher range of angle of attack is observed. Therefore, a positive torque value occurred at an earlier azimuth angle of 25°. As the horizontal blades rotate from the azimuth angle of 5° to 145°, the angle of attack has passed beyond the stall angle of the airfoil and continued to rise. Based on the theoretical model, the range of angle of attack in the second and third quarter regions is very high which produced negative torque between azimuth angles of 155° and 195°. In this negative torque region, the instantaneous peak negative torque of -0.00062 Nm occurs at azimuth angle of 175°, in which the model predicted that the angles of attack are more than 100° (the lift coefficient is negative) 116.7° at 91% span, 128.9° at 69% span, and 138.9° at 46% span. The benefits of the higher horizontal blade pitch angle is clearly shown here in which the pitch angle helps to maintain a lower angle of attack as the turbine rotates, i.e. peak angles of attack for the 15° pitch angle CAWT are 81.0° at 91% span, 101.3° at 69% span, and 118.3° at 46% span. Therefore, the 15° pitch angle matches better with the skewed wind flow, where the torque output from the horizontal blade of the 15° pitch angle CAWT configuration is 34.8% higher than that of the 0° pitch angle CAWT.

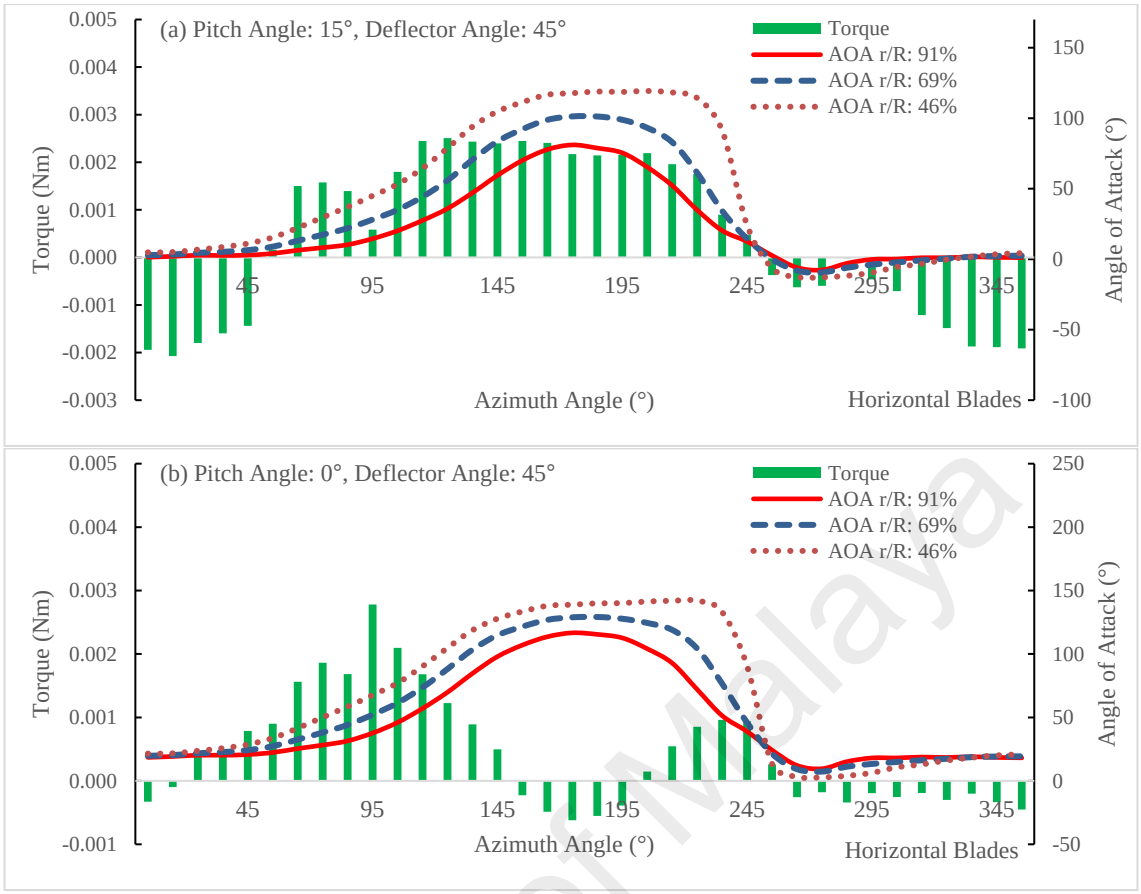


**Figure 4.25: Horizontal blades analysis showing the instantaneous torque and angle of attack against azimuth angle for the (a) 15° pitch angle CAWT integrated with 45° deflector, and (b) 0° pitch angle CAWT integrated with 45° deflector**

To further illustrate the advantage of having higher horizontal blade pitch angle for the CAWT, Figure 4.26 shows the instantaneous torque and angle of attack against azimuth angles for CAWT configurations shown in Table 4.3. By comparing Figures 4.25 and 4.26, the higher pitch angle blade helps to maintain a lower angle of attack as the turbine rotates even when the deflector angle (i.e. the skew flow angle) is reduced. Moreover, the effect of the deflector can be estimated by changing the deflector angle from 45° to 30°, the torque value of the 15° pitch angle CAWT reduced by 6.4%. In addition, the peak angles of attack of the horizontal blade for the 15° CAWT integrated with 30° deflector is 86.3° at 91% span, 109.6° at 69%, and 125.9° at 46% as compared to the very high angles of attack ($\alpha$ > 135°) for the 0° pitch angle CAWT integrated with the same deflector. Furthermore, based on the cross-flow principle (Hoerner, 1965; Hoerner et al.,

1985; Jones & Cohen, 1957), the lift and drag forces generated by the airfoil are assumed to be due only to the component of the wind velocity perpendicular to the blade. As such, without the deflectors, the horizontal component of the oncoming wind at a lower Reynolds number that is parallel to the horizontal blades in certain azimuth positions may be detrimental to the lift performance with some variations to the stall limit.

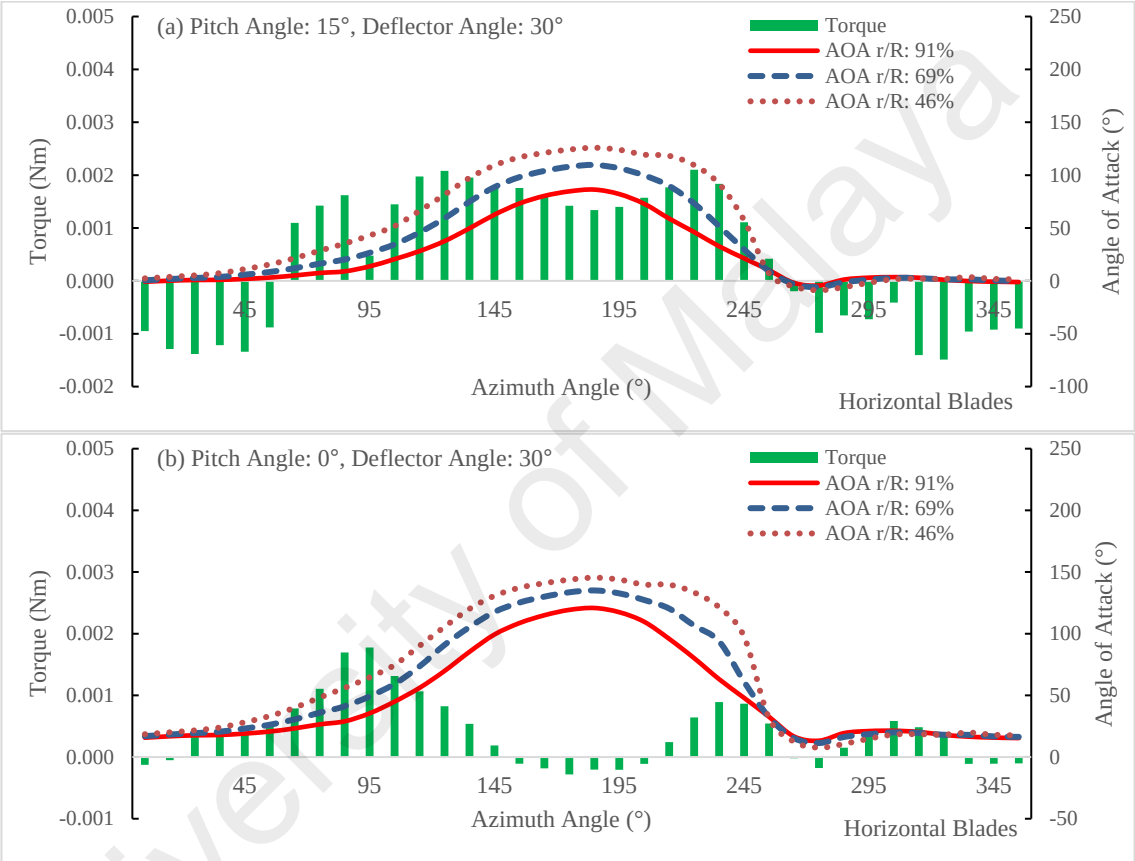


**Figure 4.26: Horizontal blades analysis showing the instantaneous torque and angle of attack against azimuth angle for the (a) 15° pitch angle CAWT integrated with 30° deflector, and (b) 0° pitch angle CAWT integrated with 30° deflector**

In conducting tests to collect lift and drag coefficients, Sandia National Labs investigated seven different airfoils up to angles of attack of 180° (Sheldahl et al., 1981). One of the airfoils is the symmetric NACA0015 where beyond the stall angle, the airfoils have the characteristics of a flat plate. The shape of the airfoil has little or no effect on its aerodynamics in the stalled region due to the separation of flow and thick boundary layers. Based on the flat plate aerodynamics, it is predicted that the lift coefficient reaches a

maximum of 1.2 at 45° angle of attack, before decreasing to 0 between 90°-100°, and then to negative lifts. From these figures, the importance of the horizontal blade pitch angle can be correlated towards reducing the angle of attack seen by the horizontal blades of the CAWT, especially in the outer span locations of the blades where most torque output is generated in this region. In extreme cases where $\alpha > 100°$, the horizontal blades will suffer negative lifts and therefore negative torque occurs, hampering the performance of the CAWT.

The thrust of the horizontal blades with different pitch angle calculated using Equation (3.21) is presented in Figure 4.27. Thrust is the axial force applied by the wind on the rotor of a wind turbine. While the power output of a wind turbine describes the amount of power transferred from the blade to the system, thrust is commonly related to all the losses of kinetic energy flow, including the energy transformed into turbulent kinetic energy. Therefore, the thrust in most aerodynamic models describes the flow in the wake of a wind turbine (Réthoré, 2006). The thrust in Figure 4.27 is generally decreasing with increase in pitch angle. Geometrically, the high pitch angle of the horizontal blade decreases its total frontal area that interacts with the approaching deflected wind, i.e. the horizontal blade becomes more parallel to the deflected wind direction. Similar observations were made by Sudhamshu et al. (2016). To investigate the effect of pitch angle on the performance characteristics of a HAWT, the authors carry out a numerical study based on the SST k-$\omega$ turbulence model. From their investigation, it is shown that the thrust decreases with an increase in pitch angle. In this study, the deflected wind flow that interacts with the horizontal blades is therefore has a better angle of attack due to the higher pitch angle, hence increases the lift force acting on the blade and simultaneously reduces the drag on its surface. Moreover, the total thrust for the 45° deflector as shown in Figure 4.28 is higher than the other deflectors at each pitch angle, suggesting that the

deflector is capable of delivering more wind to the horizontal blades of the CAWT at various pitch angle.

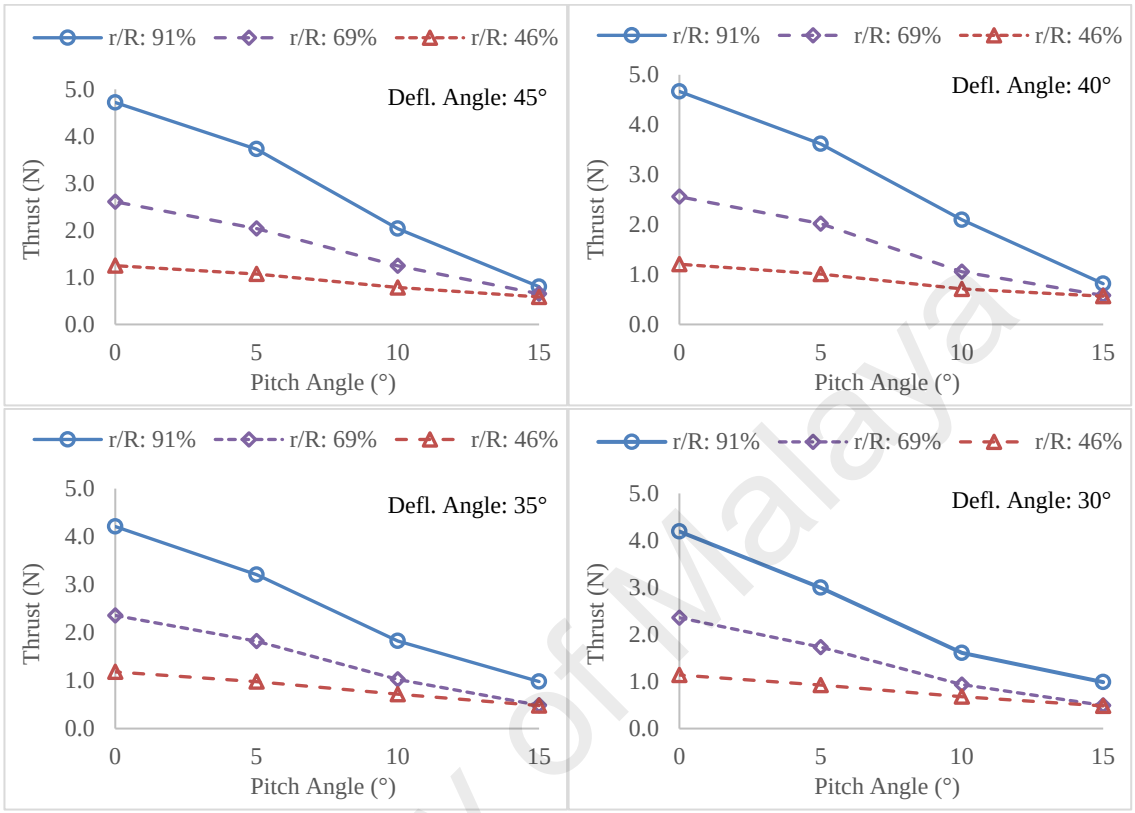


**Figure 4.27: Thrusts at different horizontal blade span locations for the various CAWT configurations integrated with different deflectors**

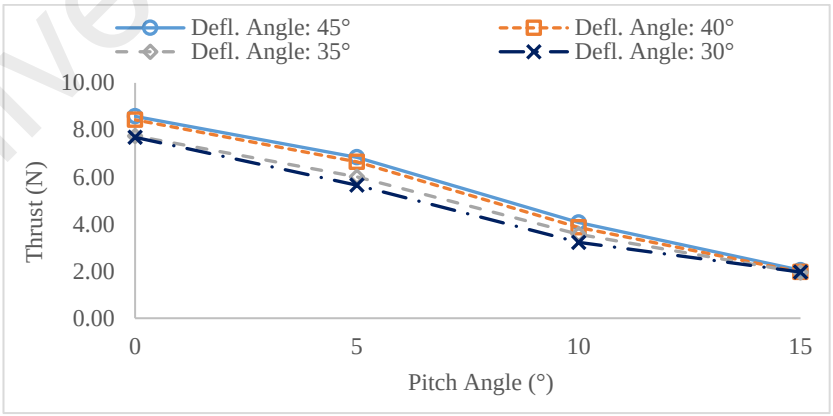


**Figure 4.28: Total thrusts for various CAWT configurations integrated with different deflectors**

The effect of the drag force can be related with the thrust and torque equations. Defined in Equations (3.21) and (3.22), an increase in the drag force on the rotor means an increase in thrust force and a decrease in torque (and therefore, the power output). As shown in Figure 4.29, there is a large number of drag forces estimated by the theoretical model for the 0° and 5° pitch angle CAWTs, especially in the outer span (91%). This can be related to the geometrical characteristics of the horizontal blade and the skewed angle of the wind flow in which as the wind flow is more parallel to the airfoil (better angle of attack), the drag force can be minimised. Hence, creating more lifts and torque output.

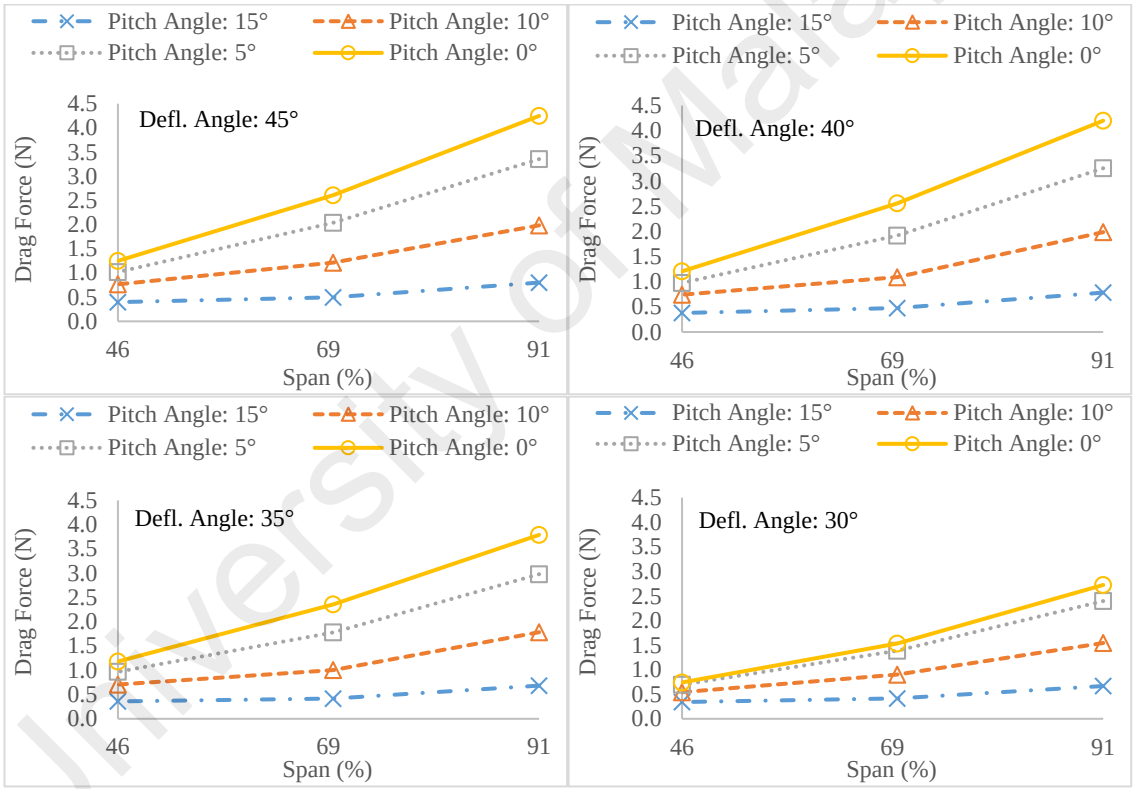


**Figure 4.29: Drag force at different horizontal blade span locations for the various CAWT configurations integrated with different deflectors**

In order to analyse the total torque contribution from each span locations of the horizontal blades, Equation (3.25) is used to define the sectional torque over the total dynamic torque of the horizontal rotor. Figure 4.30 shows the percentage of each span's dynamic torque contributing to the total torque of the horizontal blades with pitch angles

of 15°, 10°, 5° and 0° integrated with different deflectors. Interestingly, the torque contribution, $\zeta$ along the horizontal blade of pitch angle 15° CAWT integrated with the 40° and 45° deflectors drop sharply at 91% span. Moreover, at tip speed ratio of 0.93, the tangential forces component acting along the horizontal blades of the 15° pitch angle CAWT integrated with the 40° and 45° deflectors focused at the blade span of 69%.

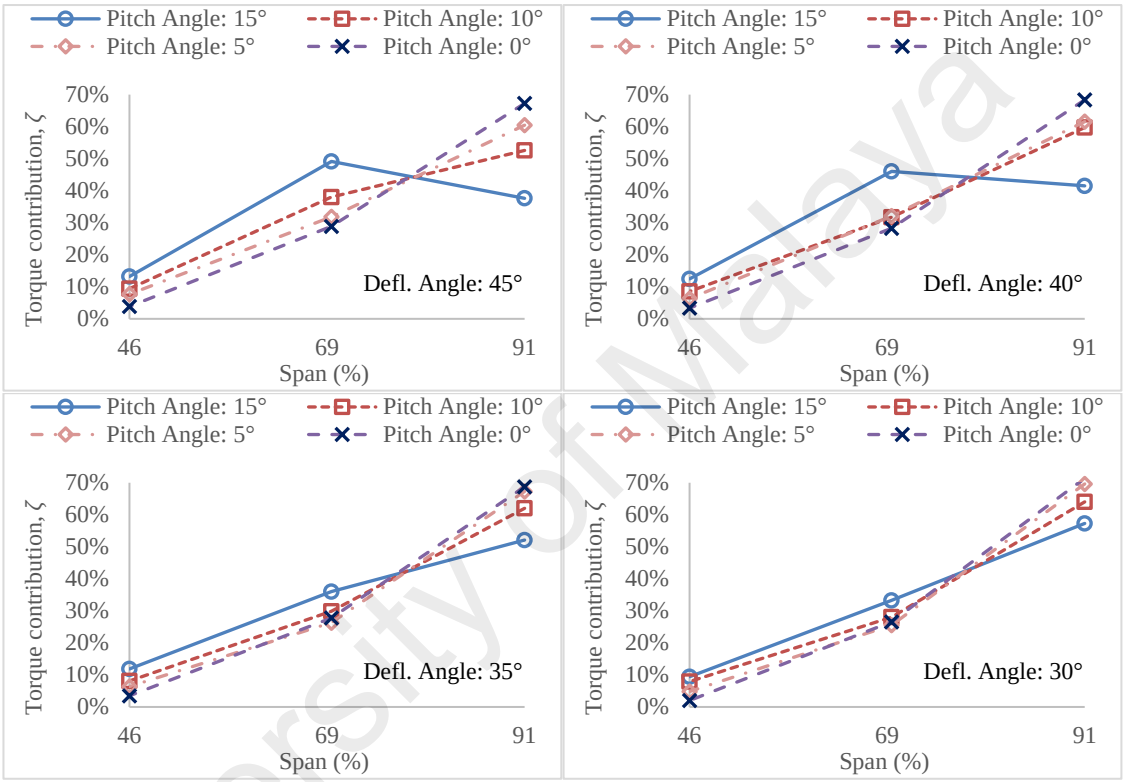


**Figure 4.30: Contribution of torque output over the different spans of the horizontal blades of the various CAWT configurations**

Further investigation of the lift-to-drag force ratio, $F_{Lb}/F_{Db}$ for different deflector configurations at 91% blade span have shown that between azimuth angles of 5° to 55°, the ratios are generally negative for the 45° and 40° deflectors which contribute to the reduction of sectional dynamic torque (as shown in Figure 4.31). This is due to the values of angle of attack in the first quarter regions approaching the stall angle (e.g., as shown in Figure 4.25a). Hence, the tangential forces acting on the horizontal blades is larger near $r$ = 12 cm (69% span).

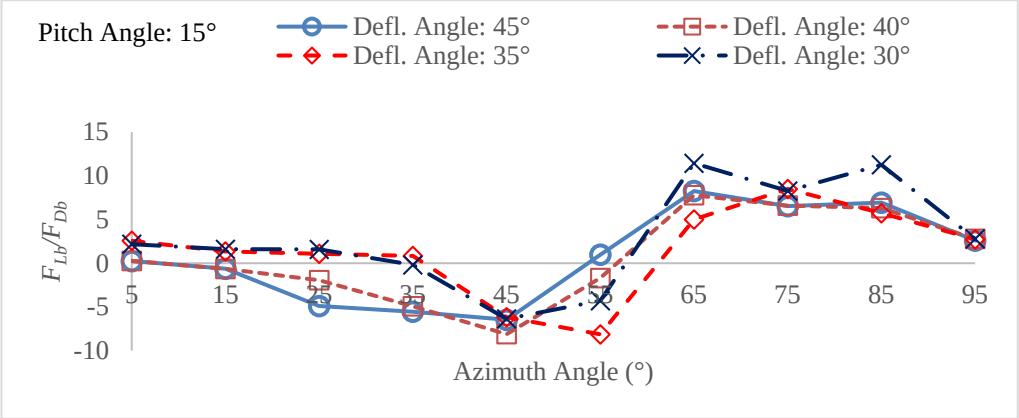


**Figure 4.31: The ratio of $F_{Lb}/F_{Db}$ against azimuth angles for horizontal blades of the 15° pitch angle CAWT integrated with various deflectors**

## 4.3 Potential application and impact of the deflector integrated cross axis wind turbine study to the wind energy industry

Based on the findings from the experiment, the deflected turbulent airflow speeds up the velocity of the oncoming wind. The turbulent kinetic energy from the skewed airflow benefits the CAWT significantly in which it outperforms the VAWT. By using the same concept shown in the experiments, the CAWT can be installed as a standalone device, integrated with a guide vane, or it can be integrated on top of building rooftops for power generation. The free-stream air on these high-rise buildings can be deflected by the building façade or the slope of the rooftops, hence creating skewed flow conditions which would enhance the performance of the wind turbine. The wind speed-up effect found in complex terrains such as hills is advantageous to the CAWT where the turbulent wind with higher wind speeds can provide better energy output than conventional wind turbines. Artist's impressions of CAWT potential applications are shown in Figure 4.32.

The CAWT has six horizontal blades and three vertical blades. Different from the conventional VAWT, the CAWT can function not only from oncoming winds from the sides of the turbine (horizontal direction) but also from the vertical direction of oncoming winds (skewed wind flow). The current study explored the use of horizontal blades with

skewed wind flow coming from the bottom of the turbine (wind flows upward) to enhance the performance of the rotor, and therefore the horizontal blade pitch angle optimisation was done according to this scenario. The CAWT works according to the lift force principle that is more dominant than the drag force when air passes over the airfoils. The lift on each blade makes the rotor turn. Once the rotor starts to rotate, the drag force is created as the blades push through the air. In normal operation of the CAWT (wind flows upward), and depending on the relationships within the velocity triangle of the blade (the inflow angle, the skewed angle, the angle of attack, the pitch angle of the airfoil, and the velocity of the oncoming wind as shown in Figure 3.20), the lift force and then the tangential force of the airfoil can be determined. This tangential force develops a rotational torque to make the blade to move forward (rotation occurs). However, when the vertical wind blows downward, the opposite reaction can occur depending on the pitch angle of the horizontal blades, which would result in slower rotational speeds or the rotor would be in a complete stop due to the opposing reactions occurred in the blades. Therefore, the application of the CAWT (with deflector or guide-vane) and the siting of the rotor are the two crucial factors in determining the performance of the rotor in a real-world scenario.

Regarding the deployment of the CAWT, the cost to produce a CAWT will be slightly higher than a VAWT due to the airfoil-shaped struts, the connectors, and the manufacturing cost of the deflector structure (its requirement depends on the location of the deployment area). However, as the results have shown, the CAWT with better performance can offset the production costs with a larger difference in energy savings compared to the VAWT in the long term. Moreover, the costs are lower than that of the HAWT as the structure is simpler, smaller, and the CAWT does not require a yawing mechanism. Moreover, without wire trenching on the ground, the installation of the CAWT is therefore, simpler and incurs less cost. The electric power generated can be

supplied to the user for any application. Such on-site power generation, especially for urban areas, remote locations and islands, represents a wide market. For example, countries such as the Phillippines and Indonesia that consist of many small islands with issues concerning the deployment of electrical grid lines are potential early adopters of the CAWT system.

(a)

(b)

**Figure 4.32: Artist's impressions of the CAWT (a) on hillsides, and (b) integrated on top of a building**

## 4.4 The potential of the wind-augmentation device for urban cities

Wind-augmentation has been shown to increase the performance of wind turbines. Based on the study with deflectors, it was found that the deflectors not only augment the

oncoming wind speed by a factor of 1.36, but the deflector can create skewed wind flows to guide the oncoming wind upward to interact with the cross axis wind turbine. Whereas, the omni-direction-guide-vane (ODGV) augments the oncoming wind flow horizontally through venturi effect by a factor of 1.87. Although not similar in design, these two share the same concept of wind augmentation. In addition, based on the experimental analysis of bare CAWTs, without the deflector, the performances of the CAWTs are lower than the deflector integrated CAWTs. Similar to the study of ODGV, the performance of the bare VAWT is lower than the performance of ODGV integrated VAWT. Hence, one can draw a similarity between these two augmentation devices based on the wind speed augmentation effect. Therefore, the results of the main study can further assist in designing a modified ODGV integrated with the CAWT. The modified ODGV can also be adopted into the design of street lights, stand-alone on-site energy generation system or for the use in offshore wind energy generation.

To illustrate the potential of the wind-augmentation device, a case study of using a vertical axis wind turbine with ODGV is presented. The system was assumed to be installed on the top of a high-rise building where the height of the building is 150 m. The power law in Equation (2.3) was used to calculate the wind speed at the height of 150 m, and the data were shown in Chapter 3 (Figure 3.25). Then, the wind speed was multiplied by the ODGV wind augmentation ratio of 1.87, which is the effect of using the ODGV. Therefore, the monthly wind speeds augmented by the ODGV at the height of 150 m in Sepang and Subang, Malaysia from 2007 to 2009 are tabulated in Figure 4.33.

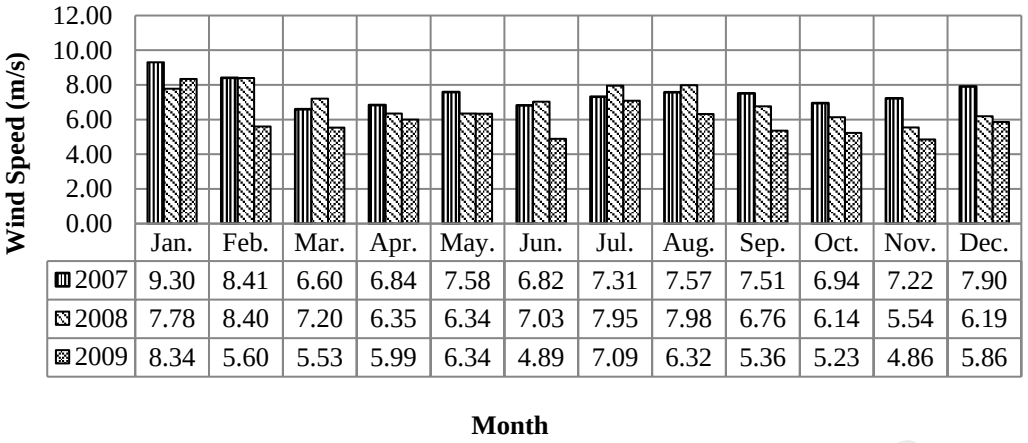


| | Jan. | Feb. | Mar. | Apr. | May. | Jun. | Jul. | Aug. | Sep. | Oct. | Nov. | Dec. |
|---|---|---|---|---|---|---|---|---|---|---|---|---|
| 2007 | 9.30 | 8.41 | 6.60 | 6.84 | 7.58 | 6.82 | 7.31 | 7.57 | 7.51 | 6.94 | 7.22 | 7.90 |
| 2008 | 7.78 | 8.40 | 7.20 | 6.35 | 6.34 | 7.03 | 7.95 | 7.98 | 6.76 | 6.14 | 5.54 | 6.19 |
| 2009 | 8.34 | 5.60 | 5.53 | 5.99 | 6.34 | 4.89 | 7.09 | 6.32 | 5.36 | 5.23 | 4.86 | 5.86 |

(a)

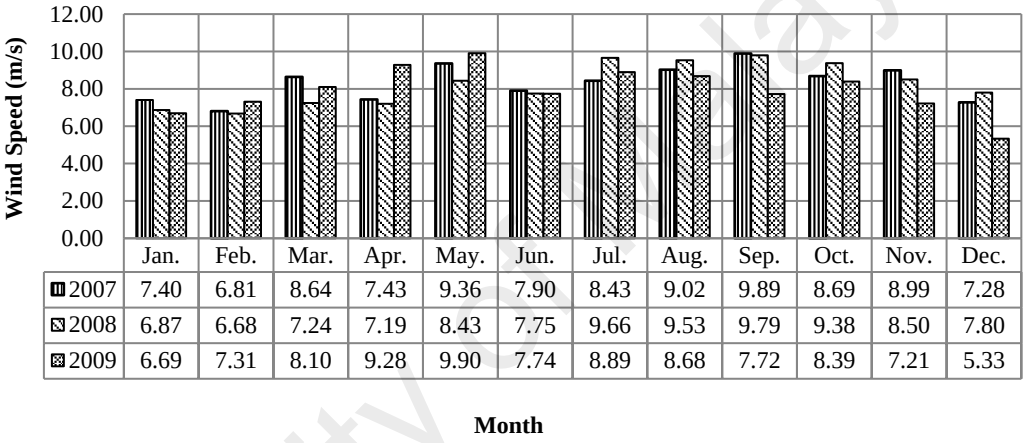


| | Jan. | Feb. | Mar. | Apr. | May. | Jun. | Jul. | Aug. | Sep. | Oct. | Nov. | Dec. |
|---|---|---|---|---|---|---|---|---|---|---|---|---|
| 2007 | 7.40 | 6.81 | 8.64 | 7.43 | 9.36 | 7.90 | 8.43 | 9.02 | 9.89 | 8.69 | 8.99 | 7.28 |
| 2008 | 6.87 | 6.68 | 7.24 | 7.19 | 8.43 | 7.75 | 9.66 | 9.53 | 9.79 | 9.38 | 8.50 | 7.80 |
| 2009 | 6.69 | 7.31 | 8.10 | 9.28 | 9.90 | 7.74 | 8.89 | 8.68 | 7.72 | 8.39 | 7.21 | 5.33 |

(b)

**Figure 4.33: Calculated mean wind speed augmented by ODGV in (a) Sepang, and (b) Subang, Malaysia from 2007 to 2009 at the height of 150 m**

Based on Equation (3.27), a small increase in the wind speed may greatly influence the output power of a wind energy device due to the cubic power of the wind speed is proportional to the wind energy. Therefore, the calculated annual wind energies generated in Sepang and Subang are 560.7 kWh/year and 1150.6 kWh/year, respectively. This shows that there is a considerable amount of renewable energy that can be generated. The advantages of integrating ODGV with the VAWT are presented and compared with similar VAWT without the ODGV in Table 4.4. The extractable energy and operational hours of the wind turbine increased with the integration of the ODGV. On average, the

number of wind turbine operating hours in Sepang and Subang increased by approximately 41% and 25% respectively when the wind-augmentation effect was considered. Moreover, the wind energy output from the system in Sepang and Subang increased by 438% and 305%, respectively. This shows that augmentation devices have great potential to be integrated into any existing wind turbine systems.

**Table 4.4: The annual operating hours and energy generation of the VAWT in Sepang and Subang, Malaysia**

| | Sepang | | Subang | |
|---|---|---|---|---|
| | Number of Annual Operating Hours | Annual Wind Energy Generated, kWh/year | Number of Annual Operating Hours | Annual Wind Energy Generated, kWh/year |
| Without ODGV | 4956 | 104.2 | 4767 | 284.0 |
| With ODGV | 6977 | 560.7 | 5934 | 1150.6 |
| Increment | 41% | 438% | 25% | 305% |

This case study introduces a renewable energy generation system designed to overcome the low wind speed conditions of urban areas through the use of the ODGV. Assessment of both of these wind turbine configuration types (bare and integrated ODGV) revealed that the ODGV integrated VAWT improved the energy output of the bare wind turbine. Furthermore, the on-site energy generation capability of the system eliminates the issues concerning conventional street lighting system such as trench wiring and landscape replacement after trenching. One such model had been installed in University of Malaya as shown in Figure 4.34. While the study focused on the application of wind energy to provide power for outdoor lighting, the system can also be used for other applications, i.e. to provide power for remote data gathering devices, flood monitoring system or emergency beacon for distress hikers.

**Figure 4.34: The Eco-Greenergy™ renewable energy system prototype in University of Malaya**

One example of incorporating the existing studies in a large scale real-world application is in the offshore wind industry. Wind turbines in offshore applications have been deployed in large-scale wind energy production (Borg & Collu, 2015; Collu, Borg, Shires, Rizzo, & Lupi, 2014; Vasel-Be-Hagh & Archer, 2017). Similarly, the CAWT has the potential to be deployed to harness offshore wind energy. In offshore application, the proposed CAWT can float on the water surface by using the assembly of guide-vanes serving as a platform. The CAWT is more stable when compared to the HAWT as its centre of gravity is expected to be located at a lower position especially during rough sea profiles in severe weather. The CAWT power extraction performance at offshore is expected to outperform the VAWT as higher torque is available from the guided wind produced by the modified ODGV, which is typically absent in most VAWT designs. Even without the guide-vanes, the CAWT has a greater potential to be deployed in the offshore application as the waves and unsteady wind speeds will induce pitching and rolling motions to the turbine axis. Consequently, a periodic tilt angle with respect to the vertical axis is induced. The CAWT may also outperform the HAWT in terms of total power extraction during rapidly changing wind direction. In particular, the CAWT is still able to continue to harness the wind energy while the HAWT loses its function momentarily

due to yaw error. The extra cost for modifying horizontal struts of the existing VAWT into airfoil blades and ODGV installation are worthy for the improvement of power extraction in wind turbine farm. Detailed techno-economic study and cost-benefit analysis of the CAWT are therefore warranted for future studies to gauge the feasibility of such applications for the cross axis wind turbine.

## 4.5 Summary

The experimental observations made for the CAWT point to interesting findings. As discussed in this chapter, the difference from the bare rotor configuration with the deflector integrated configuration is highly noteworthy. It was found that the high pitch angle of a bare CAWT (10° and 15°) can impede the overall performance of the turbine and become worse than the bare VAWT by -18.3% for the case of the 15° pitch angle CAWT. However, the use of deflectors to augment the oncoming wind, and to create skewed wind flow increase the power performance of the CAWT significantly (up to 2.8 times compared to the conventional VAWT). To further understand the function of the CAWT, a theoretical approach based on the *a posteriori* process, which requires prior knowledge of the experimental data was employed. By combining the blade element momentum model and the double multiple stream tube theory, and validated against the experimental data; it was found that the optimisation of the pitch angle helps to improve the angle of attack of the blades, and therefore the torque produced by the blades can be enhanced.

# CHAPTER 5: CONCLUSION AND RECOMMENDATIONS

## 5.1 Conclusion

The novel cross axis wind turbine presents an innovative outlook on the future of wind turbines. The cross axis wind turbine takes advantage of the simple principle of extracting oncoming wind energy from the horizontal and vertical directions. By providing a larger swept area for the wind to interact with, the power output can also be improved. Moreover, the airfoil-shaped struts incorporated in the cross axis wind turbine design to interact with the deflected airflow seems to play a major role in improving the performance of the novel turbine. The rotors used in the research have been characterised for the very low TSR response. However, with the presence of the deflectors, the interaction of dual wind flow coming for the horizontal and vertical directions creates a new possibility in the design of wind turbines, and it has been proved that the concept is feasible. Also, further research is required to draw a more comprehensive conclusion on the design concept, since the experimental prototypes are small and there are many more research opportunities can be carried out to optimise the rotor. Nonetheless, based on the results obtained in the current research work, the use of deflectors integrated with the cross axis wind turbine to enhance the performance of the rotor has been proven to be technically feasible.

The aim of the research is to determine the performance of the cross axis wind turbine system with various configurations of the horizontal blades of the turbine by experimental analysis. Also, the effects of the deflector with various inclination angles on the performance of the cross axis wind turbine system have been investigated. The four rotors of the cross axis wind turbine with different horizontal blade pitch angle have been characterised for the power output, torque value, and the rotor rotational speed. The data

from the experimental study has shown that the 15° pitch angle cross axis wind turbine integrated with the 45° deflector recorded the highest power coefficient of 0.0785 at tip speed ratio of 0.93, an increment of about 175% compared to the conventional vertical axis wind turbine. In addition, the maximum rotational speed of the 15° pitch angle cross axis wind turbine is 347.5 rpm which is 70% higher than the maximum rotational speed of the vertical axis wind turbine (204 rpm). The experiment has also been shown that this CAWT configuration yielded a torque coefficient of approximately 0.1084, an increment of about 1.7 times the torque output produced by the bare VAWT. These results indicated that the horizontal blades introduced in the cross axis wind turbine contribute additional torque by harnessing the deflected wind energy from the deflector. The effects of the deflectors on the performance of the can be illustrated by varying the deflector angle from 45° to 30°, in which the performance of all the CAWT configurations saw reductions in the power coefficient, torque coefficient and rotational speeds. For example, the peak power and torque coefficients, and the rotational performance of the 30° deflector integrated with 15° pitch angle CAWT were 0.0669, 0.0989 and 306.0 rpm, which correspond to reductions of 14.78%, 8.85%, and 11.94%, respectively. Without the deflectors, it was found that the bare CAWT configurations produced lower power output than the deflector integrated CAWTs, in which the bare 15° pitch angle CAWT performed worse than the bare VAWT by 18.3%. The steep pitch angle of the horizontal blades may be the contributing factor; where there exists a large separation of flow, which induced higher drag forces occurred along the airfoil during rotation, hence reducing the power output from the CAWT. However, further studies should be carried out to determine the exact details.

A theoretical approach to model the aerodynamic performance of the CAWT based on the blade element momentum and double multiple stream tube models is also proposed in the study. The calculated power using the proposed method gives good agreement

(9.83% to 18.95% difference) with the measured mechanical power output over the range of different deflectors and horizontal blade pitch angles. The method outlines that the performance and analysis of the vertical and horizontal blades of the CAWT are analysed independently using the two different models. Some corrections are made for modelling the horizontal blades to account for the skewed flow vectors. By evaluating each of the horizontal and vertical blades of the CAWT, the aerodynamic performance of the turbine can be better understood. In analysing the data, it was found that the pitch angle of the horizontal blade helps to maintain lower angles of attack ($\alpha < 90°$), which in turns produces higher torque output. This was demonstrated with the 15° pitch angle CAWT integrated with the 45° deflector in which along the 91% span of the blade, the turbine produces higher instantaneous torque output and better angle of attack compared to the other CAWT configurations. Furthermore, the thrusts and drag forces acting on the horizontal blades for rotors with higher pitch angles are relatively smaller than those with lower pitch angles due to the reduced frontal area of the interacting airfoil, producing better lifts. Whilst more detailed measurements are necessary to fully validate the novel approach, the method has sufficiently demonstrated that the performance of the CAWTs is heavily influenced by the pitch angle of the horizontal blades.

Finally, the potential application of an augmentation device for urban renewable energy generation system was also presented. The augmentation device or the omni-direction-guide-vane enhances the performance of the wind turbine by concentrating the oncoming wind. It was found that by employing the ODGV with a VAWT, the annual operating hours and energy generated from the system in Sepang and Subang can be increased by 41% and 438%, and 25% and 305%, respectively. The application of the wind-augmented urban renewable energy system provides a good solution for low wind speed regions where the deployment of a conventional wind turbine is not feasible.

## 5.2 Recommendations

Some limitations of the study can be proposed for further investigations:

(a) The experimental study was limited to a wind turbine of low power coefficient in a low wind speed test area. Therefore, it is necessary to examine the cross axis wind turbine in a proper wind tunnel with a higher Reynolds number flow regime, better flow uniformity, and lower turbulence intensity.

(b) Taguchi method can be considered as part of the experimental design to optimise the performance of the CAWT. Taguchi method is a robust statistical method that may be used to improve the design process.

(c) Future studies should include studies in dual flow augmentation for the modified omni-direction-guide-vane shroud and building integrated cross axis wind turbine.

(d) Flat plate aerodynamics for skewed wind flow can be considered to improve the BEM approach outlined in the thesis.

(e) Airfoil characteristics and shape can affect the angles of attack and relative speed apparent to the blades. Variations of high lift-to-drag ratio characteristics can be employed in the design to investigate the performance of the turbine, especially to suit the deflected airflow.

(f) Although the vertical and horizontal blades are responsible for the cross axis wind turbine rotor's primary drag force, the drag from the connectors also reduces the overall power output. The connectors gave structural rigidity to the blades and strengthened the overall form of the cross axis wind turbine. The connectors, however, have the disadvantage of causing aerodynamic resistive torque and requiring higher costs. For these reasons, studies should be established to investigate the effects of the connectors for which several configurations are possible.

(g) The effect of vertical blade pitch angle on power performance and aerodynamics can also be carried out to optimise the cross axis wind turbine rotor. Further investigations should be conducted to determine the loss of performance at higher pitch angle without the presence of the deflectors.

(h) Further numerical simulations are warranted to establish a complete understanding of the dual wind flow interacting with the cross axis wind turbine. It is inferred that the interaction between the oncoming skewed wind flow and the horizontal blades enhanced the coalescence between the vorticity behind the blades with the surrounding wakes shed by the blades themselves. This would, in turn, produce more load from the turbine. A 3D numerical analysis is therefore required to understand the coalescence effect completely.

(i) At low tip speed ratios, it has been shown that the range of angle of attack can reach up to more than 90° at different span locations of the blade. Therefore, in configurations with a lower angle of deflectors, the torque output generated by the outer span is larger than those at the inner spans due to these extreme angles of attack. It is interesting to note that the use of twisted horizontal blades may improve the performance of the cross axis wind turbine. In Figure 4.30, the torque contributions from the horizontal blades of the cross axis wind turbine integrated with 45° and 40° deflectors depict that the 15° pitch angle CAWT generated lower contribution of torque at the outer span of the blade, i.e. 38% and 42% compared to the middle span of the blades which contributed approximately 49% and 46% of the total torque. Using experimental and numerical methods, Hsiao, Bai, and Chong (2013) have shown that an optimum twisted blade shape performed better than untwisted blade shape in a horizontal axis wind turbine. In another study, NREL conducted field tests to characterise and compare the baseline aerodynamic performance of optimally twisted versus non-twisted HAWT blades (Simms,

Robinson, Hand, & Fingersh, 1996). The authors found that the blade twist distribution optimises power production at a single angle of attack along the span. For some modern wind turbines, the root of the blade is designed with large pitch angle and thick version of the selected airfoil for structural support. Whereas, the blade tips are designed using thin airfoil shapes for high lift-to-drag ratio. Therefore, twisted blades are recommended to enhance the effective flow velocity at the rotor blade from the blade tip to the root (Hau, 2006). However, manufacturing costs and difficulties must be taken into account as well.

In conclusion, the results of the study showed that the proposed cross axis wind turbine has the potential to give a strong impact to the development of the wind turbine industry. The advantages offered by this new wind turbine complements the strength of both vertical axis wind turbine and the horizontal axis wind turbine while diminishing their shortcomings as suggested in the previous chapters. It is expected that the study of the cross axis wind turbine will bring progress into the research on wind turbine technology.

## REFERENCES


Abbott, I. H., & Doenhoff, A. V. (1949). *Theory of wind sections*. London, UK: McGraw-Hill.

Abdalrahman, G., Melek, W., & Lien, F. S. (2017). Pitch angle control for a small-scale Darrieus vertical axis wind turbine with straight blades (H-Type VAWT). *Renewable Energy, 114, Part B,* 1353-1362.

Aerodynamic Lift and Drag and the Theory of Flight. (n.d.). Retrieved from https://www.mpoweruk.com/flight_theory.htm

Ahmed, N. A. (2013). A novel small scale efficient wind turbine for power generation. *Renewable Energy, 57*, 79-85.

Ali, A., Golde, S., Alam, F., & Moria, H. (2012). Experimental and computational study of a micro vertical axis wind turbine. *Procedia Engineering, 49*, 254-262.

Allaei, D., & Andreopoulos, Y. (2014). INVELOX: description of a new concept in wind power and its performance evaluation. *Energy, 69*, 336-344.

Almohammadi, K. M., Ingham, D. B., Ma, L., & Pourkashan, M. (2013). Computational fluid dynamics (CFD) mesh independency techniques for a straight blade vertical axis wind turbine. *Energy, 58*, 483-493.

Altan, B. D., Atılgan, M., & Özdamar, A. (2008). An experimental study on improvement of a Savonius rotor performance with curtaining. *Experimental Thermal and Fluid Science, 32*(8), 1673-1678.

Altman, D. G., & Bland, J. M. (2005). Standard deviations and standard errors. *British Medical Journal, 331*, 903.

Armstron, S., Fiedler, A., & Tullis, S. (2012). Flow separation on a high Reynolds number, high solidity vertical axis wind turbine with straight and canted blades and canted blades with fences. *Renewable Energy, 41*, 13-22.

Ashourian, M. H., Cherati, S. M., Mohd Zin, A. A., Niknam, N., Mokhtar, A. S., & Anwari, M. (2013). Optimal green energy management for island resorts in Malaysia. *Renewable Energy, 51*, 36-45.

Ashwill, T. D. (1990). *Initial structural response measurements and model validation for the Sandia 34-meter VAWT test bed*. Sandia National Laboratory.

Ashwill, T. D. (1992). *Measured data for the Sandia 34-meter vertical axis wind turbine*. Sandia National Laboratory.

Ayhan, D., & Saglam, S. (2012). A technical review of building-mounted wind power systems and a sample simulation model. *Renewable and Sustainable Energy Reviews, 16*, 1040-1049.

Bahaj, A. S., Myers, L., & James, P. A. B. (2007). Urban energy generation: Influence of micro-wind turbine output on electricity consumption in buildings. *Energy and Buildings, 39*(2), 154-165.

Balduzzi, F., Bianchini, A., Carnevale, E. A., Ferrari, L., & Magnani, S. (2012). Feasibility analysis of a Darrieus vertical-axis wind turbine installation in the rooftop of a building. *Applied Energy, 97*, 921-929.

Bartlett, J. E., Kotrlik, J. W., & Higgins, C. C. (2001). Organizational research: determining appropriate sample size in survey research. *Information Technology, Learning and Performance Journal, 19*(1), 43.

Batista, N. C., Melício, R., Mendes, V. M. F., Calderón, M., & Ramiro, A. (2015). On a self-start Darrieus wind turbine: Blade design and field tests. *Renewable and Sustainable Energy Reviews, 52*, 508-522.

Bedon, G., Castelli, M. R., & Benini, E. (2013). Optimization of a Darrieus vertical-axis wind turbine using blade element – momentum theory and evolutionary algorithm. *Renewable Energy, 59*, 184-192.

Beri, H., & Yao, Y. (2011). Double Multiple Stream Tube Model and Numerical Analysis of Vertical Axis Wind Turbine. *Energy and Power Engineering, 3*(3), 262-270.

Bianchini, A., Ferrara, G., & Ferrari, L. (2015). Pitch optimization in small-size Darrieus wind turbines. *Energy Procedia, 81*, 122-132.

Bianchini, A., Ferrara, G., Ferrari, L., & Magnani, S. (2012). An improved model for the performance estimation of an H-Darrieus wind turbine in skewed flow. *Wind Engineering, 36*(6), 667-686.

Bianchini, A., Ferrari, L., & Magnani, S. ( 2011). *Start-up behavior of a three-bladed H-Darrieus VAWT: experimental and numerical analysis.* Paper presented at the Proceedings of the ASME Turbo Expo, Vancouver, Canada.

Blackwell, B. F. (1974). The vertical-axis wind turbine. *Sandia National Laboratory, SLA-74-0160*.

Bo, T. L., & Zheng, X. J. (2013). Wind speed-up process on the windward slope of dunes in dune fields. *Computers & Fluids, 71*, 400-405.

Boatner, B. (2010). A summary overview of the blackhawk wind turbine. Retrieved from http://coen.boisestate.edu/windenergy/files/2011/10/BlackhawkOverview-BruceBoatner1.pdf

Boatner Consulting. (n.d.). What is the Blackhawk Wind Turbine. Retrieved from http://boatnerconsulting.com/blackhawk/about_bh.html

Bobrova, D. (2015). Building-integrated wind turbines in the aspect of architectural shaping. *Procedia Engineering, 117*, 404-410.

Borg, M., & Collu, M. (2015). Frequency-domain characteristics of aerodynamic loads of offshore floating vertical axis wind turbines. *Applied Energy, 155*, 629-636.

Brahimi, M. T., Allet, A., & Paraschivoiu, I. (1995). Aerodynamic analysis models for vertical axis wind turbines. *International Journal of Rotating Machinery, 2*(1), 15-21.

Breuer, M., & Jovicic, N. (2001). Separated flow around a flat plate at high incidence: an LES investigation. *Journal of Turbulence, 2*(1), 018.

Brulle, R. V. (1977). *Feasibility investigation of the giromill for generation of electrical power*. Energy Research and Development Administration.

Brulle, R. V. (1980). *McDonnell 40-kW giromill wind system. Phase II. Fabrication and test*. McDonnell Aircraft Company.

Brusca, S., Lanzafame, R., & Messina, M. (2014). Design of a vertical-axis wind turbine: how the aspect ratio affects the turbine's performance. *International Journal of Energy and Environmental Engineering, 5*(4), 333-340.

Burlando, M., Ricci, A., Freda, A., & Repetto, M. P. (2015). Numerical and experimental methods to investigate the behaviour of vertical-axis wind turbines with stators. *Journal of Wind Engineering and Industrial Aerodynamics, 144*, 125-133.

Burton, T., Sharpe, D., Jenkins, N., & Bossanyi, E. (2001). *Wind energy handbook*. Oxford, UK: John Wiley & Sons Ltd.

California Energy Commission. (n.d.). Alta wind farm powers homes. Retrieved from http://www.energy.ca.gov/tour/alta/

Camporeale, S. M., & Magi, V. (2000). Streamtube model for analysis of vertical axis variable pitch turbine for marine currents energy conversion. *Energy Conversion and Management, 41*(16), 1811-1827.

Celik-Dadaser, F., & Cengiz, E. (2014). Wind speed trends over Turkey from 1975 to 2006. *International Journal of Climatology, 34*, 1913-1927.

Chen, T. Y., & Chen, Y. Y. (2015). Developing a vortical stator assembly to improve the performance of Drag-Type vertical-axis wind turbines. *Journal of Mechanics, 31*(6), 693-699.

Chen, W. H., Chen, C. Y., Huang, C. Y., & Hwang, C. J. (2017). Power output analysis and optimization of two straight-bladed vertical-axis wind turbines. *Applied Energy, 185*, 223-232.

Chong, W. T., Fazlizan, A., Poh, S. C., Pan, K. C., Hew, W. P., & Hsiao, F. B. (2013a). The design, simulation and testing of an urban vertical axis wind turbine with the omni-direction-guide-vane. *Applied Energy, 112*, 601-609.

Chong, W. T., Fazlizan, A., Poh, S. C., Pan, K. C., & Ping, H. W. (2012a). Early development of an innovative building integrated wind, solar and rain water harvester for urban high rise application. *Energy and Buildings, 47*, 201-207.

Chong, W. T., & Kong, Y. Y. (2013b). *Outdoor light harnessing renewable energy*. WO2014126453A1.

Chong, W. T., Muzammil, W. K., Fazlizan, A., Hassan, M. R., Taheri, H., Gwani, M., . . . Poh, S. C. (2015). Urban Eco-GreenergyTM hybrid wind-solar photovoltaic energy system and its applications. *International Journal of Precision Engineering and Manufacturing, 16*(7), 1263-1268.

Chong, W. T., Naghavi, M. S., Poh, S. C., Mahlia, T. M. I., & Pan, K. C. (2011). Techno-economic analysis of a wind-solar hybrid renewable energy system with rainwater collection feature for urban high-rise application. *Applied Energy, 88*(11), 4067-4077.

Chong, W. T., Pan, K. C., Poh, S. C., Fazlizan, A., Oon, C. S., Badarudin, A., & Nik-Ghazali, N. (2013c). Performance investigation of a power augmented vertical axis wind turbine for urban high-rise application. *Renewable Energy, 51*, 388-397.

Chong, W. T., Poh, S. C., Fazlizan, A., & Pan, K. C. (2012b). Vertical Axis Wind Turbine with Omni-Directional-Guide-Vane for Urban High-Rise Buildings. *Journal of Central South University, 19*(3), 727-732.

Chong, W. T., Wang, X. H., Wong, K. H., Mojumder, J. C., Poh, S. C., Saw, L. H., & Lai, S. H. (2016). Performance assessment of a hybrid solar-wind-rain eco-roof system for buildings. *Energy and Buildings, 127*, 1028-1042.

Cochran, B. C. ( 2002). *The influence of atmospheric turbulence on the kinetic energy available during small wind turbine power performance testing*. Paper presented at the CEDER-CIEMAT, Soria, Spain.

Collu, M., Borg, M., Shires, A., Rizzo, N. F., & Lupi, E. (2014). *FloVAWT: further progresses on the development of a coupled model of dynamics for floating offshore VAWTs.* Paper presented at the ASME 2014 33rd International Conference on Ocean, Offshore and Arctic Engineering, San Francisco, USA.

Costa Rocha, P. A., Carneiro de Araujo, J. W., Pontes Lima, R. J., Vieira da Silva, M. E., Albiero, D., de Andrade, C. F., & Carneiro, F. O. M. (2018). The effects of blade pitch angle on the performance of small-scale wind turbine in urban environments. *Energy, 148*, 169-178.

Daróczy, L., Janiga, G., Petrasch, K., Webner, M., & Thévenin, D. (2015). Comparative analysis of turbulence models for the aerodynamic simulation of H-Darrieus rotors. *Energy, 90*, 680-690.

Darrieus, G. J. M. (1931). *Turbine having its rotating shaft traverse to the flow of the current.* US Patent No. 1835018.

De Marco, A., Coiro, D. P., Cucco, D., & Nicolosi, F. (2014). A numerical study on a vertical-axis wind turbine with inclined arms. *International Journal of Aerospace Engineering*.

Dominy, R., Lunt, P., Bickerdyke, A., & Dominy, J. (2007). Self-starting capability of a Darrieus turbine. *Proceedings of the IMechE Part A: Journal of Power and Energy, 221*(1), 111-120.

Drela, M. (2013). XFoil: subsonic airfoil development system [Computer Software]. Retrieved from http://web.mit.edu/drela/Public/web/xfoil/

Dutton, A. G., Halliday, J. A., & Blanch, M. J. (2005). The feasibility of building-mounted/integrated wind turbines (BUWTs): achieving their potential for carbon emission reductions.

El-Askary, W. A., Nasef, M. H., AbdEl-hamid, A. A., & Gad, H. E. (2015). Harvesting wind energy for improving performance of Savonius rotor. *Journal of Wind Engineering and Industrial Aerodynamics, 139*, 8-15.

Elliot, D. L., Holladay, C. G., Barchet, W. R., Foote, H. P., & Sandusky, W. F. (1986). *Wind energy resource atlas of the United States* (DOE/CH 10093-4). Retrieved from Department of Energy, Pacific Northwest Laboratory:

Eriksson, S., Benhoff, H., & Leijon, M. (2008a). Evaluation of different turbine concept for wind power. *Renewable and Sustainable Energy Reviews, 12*(5), 1419-1434.

Eriksson, S., Bernhoff, H., & Leijon, M. (2008b). Evaluation of different turbine concepts for wind power. *Renewable and Sustainable Energy Reviews, 12*(5), 1419-1434.

Eriksson, S., Solum, A., Leijon, M., & Bernhoff, H. (2008c). Simulations and experiments on a 12 kW direct driven PM synchronous generator for wind power. *Renewable Energy, 33*(4), 674-681.

Fadaeenejad, M., Radzi, M. A. M., Ab Kadir, M. Z. A., & Hizam, H. (2014). Assessment of hybrid renewable power sources for rural electrification in Malaysia. *Renewable and Sustainable Energy Reviews, 30*, 299-305.

Fage, A., & Johansen, F. C. (1927). On the flow of air behind an inclined flat plate of infinite span. *Proc. R. Soc. Lond. A, 116*(170-197).

Fazlizan, A., Chong, W. T., Yip, S. Y., Hew, W. P., & Poh, S. C. (2015). Design and experimental analysis of an exhaust air energy recovery wind turbine generator. *Energies, 8*(7), 6566-6584.

Fazlizan, A., Chong, W. T., Yip, S. Y., Poh, S. C., & Muzammil, W. K. (2017). Double multiple stream tube analysis of non-uniform wind stream of exhaust air energy recovery turbine generator. *International Journal of Precision Engineering and Manufacturing-Green Technology, 4*(4), 401-407.

Ferreira, C. ( 2006). *Wind tunnel hotwire measurements, flow visualization and thrust measurement of a VAWT in skew.* Paper presented at the Proceedings of the 44th AIAA Aerospace Sciences Meeting and Exhibit, Reno, Nevada.

French, J. J. (2010). *An empirical and computational method for performance evaluation of vertical axis wind energy capture systems.* (PhD), University of Tulsa.

Gaunaa, M., Sørensen, J. N., & Larsen, P. S. (2002). Unsteady aerodynamic forces on NACA 0015 airfoil in harmonic translatory motion.

Gipe, P. (2004). *Wind Power: Renewable Energy for Home, Farm, and Business*: Chelsea Green Publisher.

Glancey, J. (2010). Spin city; London's Strata tower. Retrieved from https://www.theguardian.com/artanddesign/2010/jul/18/strata-tower-london-green-architecture

Glauert, H. (1935). Airplane Propellers. division L. In W. F. Durand (Ed.), *Aerodynamic Theory, vol. IV* (pp. 169-360). Berlin: Springer.

Global Wind Atlas. (n.d.). Wind speed and wind power density in East Asia and Pacific.

Global Wind Energy Council. (2018). Global wind report (2017).

Gorelov, D. N., & Krivospitsky, V. P. (2008). Prospects for development of wind turbines with orthogonal rotor. *Thermophysics and Aeromechanics*, *15*(1), 153-157.

Gorlov, A. M. (1995). *Unidirectional helical reaction turbine operable under reversible fluid flow for power systems.* US Patent No. 5451137.

Govind, B. (2017). Increasing the operational capability of a horizontal axis wind turbine by its integration with a vertical axis wind turbine. *Applied Energy*, *199*, 479-494.

Gsänger, S., & Pitteloud, J.-D. (2014). *Small wind world report 2014*. World Wind Energy Association.

Gsänger, S., & Pitteloud, J.-D. (2017). *Small wind world report 2017*. World Wind Energy Association.

Hameed, M. S., & Afaq, S. K. (2013). Design and analysis of a straight-bladed vertical axis wind turbine blade using analytical and numerical techniques. *Ocean Engineering*, *57*, 248-255.

Hara, Y. (2012). *Proposals for butterfly wind turbine and quadruple-multiple streamtube model.* Paper presented at the Proceedings of Mechanical Engineering Congress MCEJ-12, Japan.

Hara, Y., Shiozaki, A., Nishiono, H., Saito, S., Shioya, K., Kogo, S., & Takagaki, K. (2014). Experiments of a Butterfly wind turbine with aluminium circular blades and performance predictions. *Wind Energy*, *38*(1), 16-21.

Hau, E. (2006). *Wind Turbines: Fundamentals, Technologies, Application, Economics* (2nd ed.). New York: Springer.

Hill, N., Dominy, R., Ingram, G., & Dominy, J. (2009). Darrieus turbines: the physics of self-starting. *Proceedings of the IMechE Part A: Journal of Power and Energy*, *223*(1), 21-29.

Hoerner, S. F. (1965). *Fluid-dynamic drag: practical information on aerodynamic drag and hydrodynamic resistance* (1st ed.): Hoerner Fluid Dynamics.

Hoerner, S. F., & Borst, H. V. (1985). *Fluid-dynamic lift: practical information on aerodynamic and hydrodynamic lift* (2nd ed.): Hoerner Fluid Dynamics.

Hossain, F. M., Hasanuzzaman, M., Rahim, N. A., & Ping, H. W. (2015). Impact of renewable energy on rural electrification in Malaysia: a review. *Clean Technologies and Environmental Policy, 17*(4), 859-871.

Hsiao, F. B., Bai, C. J., & Chong, W. T. (2013). The performance test of three different horizontal axis wind turbine (HAWT) blade shapes using experimental and numerical methods. *Energies, 6*, 2784-2803.

Hu, S. Y., & Cheng, J. H. (2008). Innovatory designs for ducted wind turbines. *Renewable Energy, 33*(7), 1491-1498.

Huleihil, M., & Mazor, G. (2012). Wind turbine power: the Betz limit and beyond. *Advances in Wind Power*.

Hwang, I. S., Lee, Y. H., & Kim, S. J. (2009). Optimization of cyclodial water turbine and the performance improvement by individual blade control. *Applied Energy, 86*, 1532-1540.

IBC Solar. (2013). Hybrid power supply: IBC SOLAR presents first megawatt-class photovoltaic diesel hybrid project in Malaysia. Retrieved from https://www.ibc-solar.com/corporate/press/article/news/detail/News/hybrid-power-supply-ibc-solar-presents-first-megawatt-class-photovoltaic-diesel-hybrid-project-in-m/

Islam, A., Hamza, N., & Dudek, S. (2013). Effect of roof shape, wind direction, building height and urban configuration on the energy yield and positioning of roof mounted wind turbines. *Renewable Energy, 50*, 1106-1118.

Islam, M., Fartaj, A., & Carriveau, R. (2008a). Analysis of the design parameters related to a fixed-pitch straight-bladed vertical axis wind turbine. *Wind Engineering, 32*, 491-507.

Islam, M., Fartaj, A., & Carriveau, R. (2011). Design analysis of a smaller-capacity straight-bladed VAWT with an asymmetric airfoil. *International Journal of Sustainable Energy, 30*(3), 179-192.

Islam, M., Ting, D. S. K., & Fartaj, A. (2008b). Aerodynamic models for Darrieus-type straight-bladed vertical axis wind turbines. *Renewable and Sustainable Energy Reviews, 12*(4), 1087-1109. doi:10.1016/j.rser.2006.10.023

Jamieson, P. (2011). *Innovation in wind turbine design*. London: John Wiley & Sons Ltd.

Jin, X., Wang, Y., Ju, W., He, J., & Xie, S. (2018). Investigation into parameter influence of upstream deflector on vertical axis wind turbines output power via three-dimensional CFD simulation. *Renewable Energy, 115*, 41-53.

Jin, X., Zhao, G., Gao, K., & Ju, W. (2015). Darrieus vertical axis wind turbine: basic research methods. *Renewable and Sustainable Energy Reviews, 42*, 212-225.

Jing, F., Sheng, Q., & Zhang, L. (2014). Experimental research on tidal current vertical axis turbine with variable-pitch blades. *Ocean Engineering, 88*, 228-241.

Johnson, G. L. (2006). *Wind energy systems*: Gary L. Johnson.

Jones, R. T., & Cohen, D. (1957). *Aerodynamics of wings at high speeds*. Princeton, USA: Princeton University Press.

Kamaruzzaman, S., & Tamer, K. (2013). Wind energy potential in nine coastal sites in Malaysia. *Palestine Tech Univ Res J, 1*, 10-15.

Kim, D., & Gharib, M. (2013). Efficiency improvement of straight-bladed vertical-axis wind turbines with an upstream deflector. *Journal of Wind Engineering and Industrial Aerodynamics, 115*, 48-52.

Kirke, B. K. (1998). *Evaluation of self-starting vertical axis wind turbines for stand-alone applications.* (PhD), Griffith University, Australia.

Knight, J. (2004). Breezing into town. *Nature, 430*, 12-13.

Krishnan, A., & Paraschivoiu, M. (2016). 3D analysis of building mounted VAWT with diffuser shaped shroud. *Sustainable Cities and Society, 27*, 160-166.

Lam, K. M., & Wei, C. T. (2010). Numerical simulation of vortex shedding from an inclined flat plate. *Engineering Applications of Computational Fluid Mechanics, 4*(4), 569-579.

Leung, D., Deng, Y., & Leung, M. (2010). *Design optimization of a cost-effective micro wind turbine.* Paper presented at the WCE 2010-World Congress on Engineering.

Li, C., Zhu, S., Xu, Y. L., & Xiao, Y. (2013). 2.5d large eddy simulation of vertical axis wind turbine in consideration of high angle of attack flow. *Renewable Energy, 51*, 317-330.

Li, Q. S., Shu, Z. R., & Chen, F. B. (2016). Performance assessment of tall building-integrated wind turbines for power generation. *Applied Energy, 165*, 777-788.

Li, Y., & Calisal, S. M. (2010). Three-dimensional effects and arm effects on modeling a vertical axis tidal current turbine. *Renewable Energy, 35*(10), 2325-2334.

Liu, Z., Dong, L., Moschetta, J.-M., Zhao, J., & Yan, G. (2014). Optimization of nano-rotor blade airfoil using controlled elitist NSGA-II. *International Journal of Micro Air Vehicles, 6*(1), 29-42.

Livingston, J. T., & Anderson, T. (2004). Wind shear, taller turbines, and the effects on wind farm development create a need for taller MET towers. Retrieved from

Loganathan, B., Chowdhury, H., Mustary, I., & Alam, F. (2015). An experimental study of a cyclonic vertical axis wind turbine for domestic scale power generation. *Procedia Engineering, 105*, 686-691.

Loth, J. L., & McCoy, H. (1983). Optimization of Darrieus turbines with an upwind and downwind momentum model. *J Energy, 7*, 313-318.

Lubitz, W. D., & White, B. R. (2007). Wind-tunnel and field investigation of the effect of local wind direction on speed-up over hills. *Journal of Wind Engineering and Industrial Aerodynamics, 95*, 639-661.

Maalawi, K. Y., & Badr, M. A. (2003). A practical approach for selecting optimum wind rotors. *Renewable Energy, 28*, 803-822.

MacPherson, C. (2014). In just 8 years, German State goes from 30% to 100% renewable energy. Retrieved from https://nuclear-news.net/2014/06/28/in-just-8-years-german-state-goes-from-30-to-100-renewable-energy/

Malaysia Energy Information Hub. (n.d.). Retrieved from http://meih.st.gov.my/

Manwell, J. F., McGowan, J. G., & Rogers, A. L. (2002). *Wind Energy Explained: Theory, Design and Application*: John Wiley & Sons, Ltd.

Marten, D. (2016). QBlade [Computer Software]. Retrieved from http://www.q-blade.org

Mathew, S. (2006). *Wind energy: fundamentals, resource analysis and economics*. New York: Springer.

McConnel, R. D. (1979). *Giromill Overview*: Solar Energy Research Institute. .

Meinhold, B. (2010). Chicago parking garage harvests energy from windy city gusts. Retrieved from https://inhabitat.com/chicago-parking-garage-harvests-energy-from-windy-city-gusts/

Mertens, S., van Kuik, G., & van Bussel, G. (2003). Performance of an H-Darrieus in the skewed flow on a roof. *Journal of Solar Energy Engineering, 125*, 433-440.

Migliore, P. G., Wolfe, W. P., & Fanucci, J. B. (1980). Flow curvature effects on Darrieus turbine blade aerodynamics. *Journal of Energy, 4*(2), 49-55.

Miller, S. (2008). Lift, drag, and moment of a NACA 0015 airfoil. Retrieved from http://smiller.sbyers.com/temp/AE510_03%20NACA%200015%20Airfoil.pdf

Ministry of Rural and Regional Development. (2012). Electricity. Retrieved from http://www.rurallink.gov.my/en/citizen/desa-information/infrastructure-list/infrastructure/electricity

Mo, J.-O., & Lee, Y.-H. (2012). CFD investigation on the aerodynamic characteristics of a small-sized wind turbine of NREL PHASE VI operating with a stall-regulated method. *Journal of Mechanical Science and Technology, 26*(1), 81-92.

Mohamed, M. H. (2012). Performance investigation of H-rotor Darrieus turbine with new airfoil shapes. *Energy, 47*(1), 522-530.

Mohamed, M. H. (2014). Aero-acoustics noise evaluation of H-rotor Darrieus wind turbines. *Energy, 65*(1), 596-604.

Mohamed, M. H., Janiga, G., Pap, E., & Thévenin, D. (2010). Optimization of Savonius turbines using an obstacle shielding the returning blade. *Renewable Energy, 35*(11), 2618-2626.

Mohamed, M. H., Janiga, G., Pap, E., & Thévenin, D. (2011). Optimal blade shape of a modified Savonius turbine using an obstacle shielding the returning blade. *Energy Conversion and Management, 52*, 236-242.

Montgomerie, B. (2004). *Methods for Root Effects, Tip Effects and Extending the Angle of Attack Range to ±180, with Application to Aerodynamics for Blades on Wind Turbines and Propellers*. Swedish Defense Research Agency, Stockholm, Sweden.

Moran, W. A. (1977). *Giromill wind tunnel test and analysis*. NREL.

Morgado, J., Vizinho, R., Silvestre, M. A. R., & Páscoa, J. C. (2016). XFOIL vs CFD performance predictions for high lift low Reynolds number airfoils. *Aerospace Science and Technology, 52*, 207-214.

Musgrove, P. J. (1978). *Development of the variable geometry vertical axis windmill.* Paper presented at the International Symposium on Wind Energy Systems, Amsterdam, Netherlands.

National Renewable Energy Laboratory. (2004). Global Energy Concepts. Addendum to WindPact turbine design scaling studies, technical area 3-self-erecting tower and nacelle feasibility.

Nguyen, T. (2011). New invention turns building rooftops into wind farms. Retrieved from https://www.zdnet.com/article/new-invention-turns-building-rooftops-into-wind-farms

Nigam, D. K., & El-Sayed, M. E. M. (2011). *Vertical axis wind system.* US Patent No. 7,948,111.

Nobile, R., Vahdati, M., Barlow, J. F., & Mewburn-Crook, A. (2014). Unsteady flow simulation of a vertical axis augmented wind turbine: A two-dimensional study. *Journal of Wind Engineering and Industrial Aerodynamics, 125*, 168-179.

Noble, N., & Sanchez, T. (2008). Energy from the wind. Retrieved from https://practicalaction.org/media/download/10703

Nor, K. M., Shaaban, M., & Abdul Rahman, H. (2014). Feasibility assessment of wind energy resources in Malaysia based on NWP models. *Renewable Energy, 62*, 147-154.

Okulov, V. L., & van Kuik, G. A. M. (2012). The Betz-Joukowsky limit: on the contribution to rotor aerodynamics by the British, German and Russian scientific schools. *Wind Energy, 15*, 335-344.

Oppenheim, D., Owen, C., & White, G. (2004). Outside the Square: Integrating Wind into Urban Environments. *Refocus, 5*(3), 32-35.

Orlandi, A., Collu, M., Zanforlin, S., & Shires, A. (2015). 3D URANS analysis of a vertical axis wind turbine in skewed flows. *Journal of Wind Engineering and Industrial Aerodynamics, 147*, 77-84.

Owens, B. C., Hurtado, J. E., Paquette, J. A., Griffith, D. T., & Barone, M. (2013). *Aerolastic modeling of large offshore vertical-axis wind turbines: development of the offshore wind energy simulation toolkit*. Sandia National Laboratories.

Ozmen, Y., Baydar, E., & van Beeck, J. P. A. J. (2016). Wind flow over the low-rise building models with gabled roofs having different pitch angles. *Building and Environment, 95*, 63-74.

Pagnini, L. C., Massimiliano, B., & Repetto, M. P. (2015). Experimental power curve of small-size wind turbines in turbulent urban environment. *Applied Energy, 154*, 112-121.

Paraschivoiu, I. (1981). Double-multiple streamtube model for Darrieus in turbines. Retrieved from https://ntrs.nasa.gov/archive/nasa/casi.ntrs.nasa.gov/19820015811.pdf

Paraschivoiu, I. (1988). Double-multiple streamtube model for studying vertical-axis wind turbines. *Journal of Propulsion and Power*, *4*(4), 370-377.

Paraschivoiu, I. (2002). *Wind turbine design: with emphasis on Darrieus concept*. Montreal: Polytechnic International Press.

Park, J., Jung, H. J., Lee, S. W., & Park, J. (2015). A new building-integrated wind turbine system utilizing the building. *Energies, 8*, 11846-11870.

Park, J. H., Chung, M. H., & Park, J. C. (2016). Development of a small wind power system with an integrated exhaust air duct in high-rise residential buildings. *Energy and Buildings, 122*, 202-210.

Park, J. Y., Lee, S., Sabourin, T., & Park, K. (2007). A Novel Vertical-Axis Wind Turbine for Distributed & Utility Deployment. *Dept. of Mechanical Engineering, Inha University, Korea KR Wind Energy Research Institute, Korea. KR WindPower, Inc., USA.*

Patel, M. (2006). *Wind and Solar Power Systems: Design, Analysis, and Operation*. Florida: Taylor & Francis.

Peacock, A. D., Jenkins, D., Ahadzi, M., Berry, A., & Turan, S. (2008). Micro wind turbines in the UK domestic sector. *Energy and Buildings, 40*, 1324-1333.

Pope, K., Rodrigues, V., Doyle, R., Tsopelas, A., Gravelsins, R., Naterer, G. F., & Tsang, E. (2010). Effects of stator vanes on power coefficients of a zephyr vertical axis wind turbine. *Renewable Energy, 35*(5), 1043-1051.

Popelka, D. (1982). Aerolastic stability analysis of a Darrieus wind turbine. Retrieved from https://windpower.sandia.gov/abstracts/820672A.pdf

Price, T. J. (2006). UK large-scale wind power programme from 1970 to 1990: the Carmarthen Bay experiments and the Musgrove vertical-axis turbines. *Wind Engineering, 30*(3), 225-242.

Quilter, J. (2013). Analysis: Is Aerogenerator-X going anywhere? Retrieved from https://www.windpowermonthly.com/article/1208844/analysis-aerogenerator-x-going-anywhere

Rainbird, J. M., Bianchini, A., Balduzzi, F., Peiró, J., Graham, J. M. R., Ferrara, G., & Ferrari, L. (2015). On the influence of virtual camber effect on airfoil polars for use in simulations of Darrieus wind turbines. *Energy Conversion and Management, 106*, 373-384.

Rajagopalan, R. G., & Fanucci, J. B. (1985). Finite difference model for vertical axis wind turbines. *J Propuls, 1*, 432-436.

Réthoré, P.-E. (2006). *Thrust and wake of a wind turbine: Relationship and measurements.* (M.Sc), Technical University of Denmark.

Reuters. (2014). German state able to meet power demand through renewables. Retrieved from https://www.reuters.com/article/us-germany-renewables-supplies/german-state-able-to-meet-power-demand-through-renewables-idUSKBN0GZ24I20140904

Rezaeiha, A., Kalkman, I., & Blocken, B. (2017). Effect of pitch angle on power performance and aerodynamics of a vertical axis wind turbine. *Applied Energy, 197*, 132-150.

Ricci, R., Romagnoli, R., Montelpare, S., & Vitali, D. (2016). Experimental study on a Savonius wind rotor for street lighting systems. *Applied Energy, 161*, 143-152.

Riegler, H. (2003). HAWT versus VAWT: Small VAWTs find a clear niche. *Refocus, 4*(4), 44-46.

Robbie, E. (2015). Aspen is third U.S. city to reach 100% renewable energy. Retrieved from https://www.aspentimes.com/news/aspen-is-third-u-s-city-to-reach-100-renewable-energy/

Rourke, F. O., Boyle, F., & Reynolds, A. (2010). Tidal energy update 2009. *Applied Energy, 87*, 398-409.

Roy, S., & Saha, U. K. (2015). Wind tunnel experiments of a newly developed two-bladed Savonius-style wind turbine. *Applied Energy, 137*, 117-125.

Saiam Power. (n.d.). 75W Mini VAWT. Retrieved from https://www.windsoleil.com/new-products/75w-saiam-1224v-vertical-axis-wind-turbine-generator

Salvadore, F., Bernardini, M., & Botti, M. (2013). GPU accelerated flow solver for direct numerical simulation of turbulent flows. *Journal of Computational Physics, 235*, 129-142.

Savonius, S. J. (1931). The S-Rotor and its applications. *Mech Eng, 53*(5), 333-338.

Scheurich, F., & Brown, R. E. (2011). *Vertical-axis wind turbines in oblique flow: sensitivity to rotor geometry.* Paper presented at the European Wind Energy Conference and Exhibition, Brussels, Belgium.

Scheurich, F., Fletcher, T. M., & Brown, R. E. (2010, 4-7th January 2010). *The influence of blade curvature and helical blade twist on the performance of a vertical-axis wind turbine.* Paper presented at the 48th AIAA Aerospace Sciences Meeting including the New Horizons Forum and Aerospace Exposition, Orlando, Florida.

Selig, M. S. (2003). Low Reynolds number airfoil design. Retrieved from https://pdfs.semanticscholar.org/37cd/6535639d5da933c5fdf293258f90bf50d7d5.pdf

Sharpe, T., & Proven, G. (2010). Crossflex: concept and early development of a true building integrated wind turbine. *Energy and Buildings, 42*(12), 2365-2375.

Sheldahl, R. E., & Klimas, P. C. (1981). Aerodynamic characteristics of seven symmetrical airfoil sections through 180-degree angle of attack for use in aerodynamic analysis of vertical axis wind turbines.

Shockley, J. (2011). Bahrain World Trade Center by Atkins. Retrieved from https://greenbuildingelements.com/2011/09/28/bahrain-world-trade-center-by-atkins/

Simão-Ferreira, C. J., van Bussel, G., & van Kuik, G. (2006). *An analytical method to predict the variation in performance of a H-Darrieus in skewed flow and its experimental validation.* Paper presented at the Proceedings of the European Wind Energy Conference, Athens, Greece

Simao Ferreira, C. J., van Zuijlen, A., Bijl, H., van Bussel, G., & van Kuik, G. (2010). Simulating dynamic stall on a two-dimensional vertical-axis wind turbine: verification and validation with particle image velocimetry data. *Wind Energy, 13*(1), 1-17.

Simms, D. A., Robinson, M. C., Hand, M. M., & Fingersh, L. J. (1996). *A comparison of baseline aerodynamic performance of optimally-twisted versus non-twisted HAWT blades.* Paper presented at the Fifteenth ASME Wind Energy Symposium.

Sjokvist, S., & Eriksson, S. (2013). Study of demagnetization risk for a 12 kW direct driven permanent magnet synchronous generator for wind power. *Energy Science & Engineering, 1*(3), 128-134.

Smith, R. F., & Killa, S. (2007). Bahrain World Trade Center (BWTC): the first large-scale integration of wind turbines in a building. *The Structural Design of Tall and Special Buildings, 16*(4), 429-439.

Sørensen, J. N. (2012). Aerodynamic analysis of wind turbines. In A. Sayigh (Ed.), *Comprehensive Renewable Energy* (pp. 225-240): Elsevier.

Spera, D. A. (2009). *Wind turbine technology: fundamental concepts of wind turbine engineering* (2nd ed.). New York: ASME Press.

Strickland, J. H. (1975). The Darrieus turbine: a performance prediction model using multiple streamtubes. *SAND, 75*(431).

Strickland, J. H., Smith, T., & Sun, K. (1981). *A vortex model of the Darrieus turbine: an analytical & experimental study*. Sandia National Laboratory.

Sudhamshu, A. R., Manik, C. P., Nivedh, S., Satish, N. S., Vivek, M., & Ratna, K. V. (2016). Numerical study of effect of pitch angle on performance characteristics of a HAWT. *Engineering Science and Technology, an International Journal, 19*(1), 632-641.

Sureshan, V. (2008). *Omni-directional wind turbine.* United States Patent No. US7400057 B2.

Sutherland, H. J., Berg, D. E., & Ashwill, T. D. (2012). *A retrospective of VAWT technology*. Sandia National Laboratories.

Takao, M., Maeda, T., Kamada, Y., Oki, M., & Kuma, H. (2008). A straight-bladed vertical axis wind turbine with a directed guide vane row. *Journal of Fluid Science and Technology, 3*(3), 8.

Tartuferi, M., D'Alessandro, V., Montelpare, S., & Ricci, R. (2015). Enhancement of Savonius wind rotor aerodynamic performance: a computational study of new blade shapes and curtain systems. *Energy, 79*, 371-384.

Templin, R. J. (1974). *Aerodynamic performance theory for the NRC vertical-axis wind turbine*. National Research Council. National Aeronautical Establishment Laboratory.

Templin, R. J. (1979). *Design characteristics of the 224 kW Magdalen Islands VAWT*. National Research Council of Canada. Retrieved from https://ntrs.nasa.gov/archive/nasa/casi.ntrs.nasa.gov/19800008203.pdf

Tjiu, W., Marnoto, T., Mat, S., Ruslan, M. H., & Sopian, K. (2015a). Darrieus vertical axis wind turbine for power generation I: assessment of Darrieus VAWT configurations. *Renewable Energy, 75*, 50-67.

Tjiu, W., Marnoto, T., Mat, S., Ruslan, M. H., & Sopian, K. (2015b). Darrieus vertical axis wind turbine for power generation II: challenges in HAWT and the opportunity of multi-megawatt Darrieus VAWT development. *Renewable Energy, 75*, 560-571.

Twidell, J. (1987). *A guide to small wind energy conversion systems*. New York, NY: Cambridge University Press.

Umar, M. S., Jennings, P., & Urmee, T. (2013). Strengthening the palm oil biomass Renewable Energy industryin Malaysia. *Renewable Energy, 60*, 107-115.

van Bussel, G. J. W., Mertens, S., Polinder, H., & Sidler, H. F. A. (2004a). *The development of Turby, a small VAWT for the built environment.* Paper presented at the Global wind energy conference, Chicago, USA.

van Bussel, G. J. W., Mertens, S., Polinder, H., & Sidler, H. F. A. ( 2004b). *TURBY®concept and realisation of a small VAWT for the built environment.* Paper presented at the Proceedings of the EAWE/EWEA Special Topic Conference: The Science of making Torque from Wind, Delft, The Netherlands.

van de Wiel, J. (2015). *Global and Aerodynamic Optimization of a high solidity mid-size VAWT.* Delft University of Technology.

Vasel-Be-Hagh, A., & Archer, C. L. (2017). Wind farm hub height optimization. *Applied Energy, 195*, 905-921.

Vertical Wind Turbine Info. (2012). Johnson System Inc installs vertical axis wind turbine. Retrieved from http://www.verticalwindturbineinfo.com/johnson-system-inc-installs-vertical-axis-wind-turbine/

Viterna, L. A., & Corrigan, R. D. (1982). *Fixed pitch rotor performance of large horizontal axis wind turbines*. NASA Lewis Research Center, Cleveland.

Wagner, S., Bareiss, R., & Guidati, G. (1996). *Wind turbine noise*. Berlin: Springer.

Wang, W.-C., Wang, J.-J., & Chong, W. T. (2018). The effects of unsteady wind on the performances of a newly developed cross-axis wind turbine: A wind tunnel study. *Renewable Energy*.

Wang, Y. F., & Zhan, M. S. (2015). Effect of barchan dune guide blades on the performance of a lotus-shaped micro-wind turbine. *Journal of Wind Engineering and Industrial Aerodynamics, 136*, 34-43.

Wilson, R. E., & Lissaman, P. B. S. (1974). *Applied aerodynamics of wind power machines*. Oregon State University.

Wind Power Ltd. (2010). Aerogenerator X launched by Wind Power Limited. Retrieved from https://www.offshorewind.biz/2010/07/27/aerogenerator-x-launched-by-wind-power-limited-uk/

Wong, K. H., Chong, W. T., Poh, S. C., Shiah, Y. C., Sukiman, N. L., & Wang, C. T. (2018a). 3D CFD simulation and parametric study of a flat plate deflector for vertical axis wind turbine. *Renewable Energy, 129, Part A*, 32-55.

Wong, K. H., Chong, W. T., Sukiman, N. L., Poh, S. C., Shiah, Y. C., & Wang, C. T. (2017). Performance enhancements on vertical axis wind turbines using flow augmentation systems: A review. *Renewable and Sustainable Energy Reviews, 73*, 904-921.

Wong, K. H., Chong, W. T., Sukiman, N. L., Shiah, Y. C., Poh, S. C., Sopian, K., & Wang, W. C. (2018b). Experimental and simulation investigation into the effects of a flat plate deflector on vertical axis wind turbine. *Energy Conversion and Management, 160*, 109-125.

Worasinchai, S., Ingram, G., & Dominy, R. (2015). The physics of H-Darrieus turbine starting behavior. *Journal of Engineering for Gas Turbines and Power, 138*(6).

XFOIL. (n.d.). *Xfoil subsonic airfoil development system*. Massachusetts Institute of Technology.

Yang, A. S., Su, Y. M., Wen, C. Y., Juan, Y. H., Wang, W. S., & Cheng, C. H. (2016). Estimation of wind power generation in dense urban area. *Applied Energy, 171*, 213-230.

Yao, Y. X., Tang, Z. P., & Wang, X. W. (2013). Design based on a parametric analysis of a drag drive VAWT with a tower cowling. *Journal of Wind Engineering and Industrial Aerodynamics, 116*, 32-39.

Ying, P., Chen, Y. K., Xu, Y. G., & Tian, Y. (2015). Computational and experimental investigation of an omni-flow wind turbine. *Applied Energy, 146*, 74-83.

Yu, R. (2008). Airports go for green with eco-friendly efforts. *USA Today*.

Zeiner-Gundersen, D. H. (2015). A novel flexible foil vertical axis turbine for river, ocean, and tidal applications. *Applied Energy, 151*, 60-66.

Zhang, J., Liu, N. S., & Lu, X. Y. (2009). Route to a chaotic state in fluid flow past an inclined flat plate. *Phys. Rev. E. Stat. Nonlin. Soft Matter Phys., 79*, 045306: 045301-045304.

Zhang, W., Harff, J., & Schneider, R. (2011). Analysis of 50-year wind data of the southern Baltic Sea for modelling coastal morphological evolution – a case study from the Darss-Zingst Peninsula. *Oceanologia*.

Zhang, X., Chen, Y. K., & Calay, R. (2013). Modelling and analysis of a novel wind turbine structure. *International Journal of Modelling, Identification and Control, 9*(2), 142-149.

## LIST OF PUBLICATIONS AND PAPERS PRESENTED

Journals:

1) Chong, W.T., **Muzammil, W.K.**, Wong, K.H., Wang, C.T., Gwani, M., Chu, Y.J., & Poh, S.C. (2017). Cross axis wind turbine: Pushing the limit of wind turbine technology with complementary design. *Applied Energy*, 207, 78-95.

2) Chong, W.T., **Muzammil, W.K.**, Fazlizan, A., Hassan, M.R., Taheri, H., Gwani, M., Kothari, H., & Poh, S.C. (2015). Urban Eco-Greenergy$^{TM}$ hybrid wind-solar photovoltaic energy system and its applications. *International Journal of Precision Engineering and Manufacturing*, 16(7), 1263-1268.

3) Fazlizan, A., Chong, W.T., Yip, S.Y., Poh, S.C., & **Muzammil, W.K.** (2017). Double multiple stream tube analysis of non-uniform wind stream of exhaust air energy recovery turbine generator. *International Journal of Precision Engineering and Manufacturing-Green Technology*, 4(4), 401-407.

4) Chong, W.T., Gwani, M., Tan, C.J., **Muzammil, W.K.**, Poh, S.C., & Wong, K.H. (2017). Design and testing of a novel building integrated cross axis wind turbine. *Applied Sciences*, 7(3), 251.

5) Chong, W.T., Gwani, M., Shamshirband, S., **Muzammil, W.K.**, Tan, C.J., Fazlizan, A., Poh, S.C., Petkovic, D., & Wong, K.H. (2016). Application of adaptive neuro-fuzzy methodology for performance investigation of a power-augmented vertical axis wind turbine. *Energy*, 102, 630-636.

Conferences and symposium:

1) **Muzammil, W.K.**, Wong, K.H., Chong, W.T., Gwani, M., Wang, C.T., Poh, S.C., & Wang, X.H. (2017). *Design and early development of a novel cross axis wind turbine*. Paper presented at the 8$^{th}$ International Conference on Applied Energy (ICAE 2016), 8-11 October 2016, Beijing, China.

2) Chong, W.T., **Muzammil, W.K.**, Gwani, M., Wong, K.H., Fazlizan, A., Wang, C.T., & Poh, S.C. (2016). *The development and testing of a novel cross axis wind turbine*. Paper presented at the 3$^{rd}$ AUN/SEED-Net Regional Conference on Energy Engineering and the 7$^{th}$ International Conference on Thermofluids (RCEne/THERMOFLUID 2015), 19-20 November 2015, Yogyakarta, Indonesia.

3) Chong, W.T., **Muzammil, W.K.**, Poh, S.C., Fazlizan, A., Sopian, K., & Ng, K. *Conceptual design of an innovative Eco-Greenergy$^{TM}$ hybrid wind-solar energy generation system*. Paper presented at the Renewable Energy World Asia (REWA2014), 10-12 September 2014, Kuala Lumpur, Malaysia.

4) Chong, W.T., **Muzammil, W.K.**, Fazlizan, A., Gwani, M., Julai, S., & Poh, S.C. *The design and techno-economic analysis of Eco-Greenergy$^{TM}$ outdoor lighting and charging energy generation system for urban high-rise application*. Paper presented at the World Renewable Energy Congress (WRECXIII, 3-8 August 2014, London, England.

5) Chong, W.T., **Muzammil, W.K.**, Fazlizan, A., Taheri, H., Gwani, M., Chew, L.H., & Poh, S.C. *Eco-Greenergy$^{TM}$: the future of small hybrid wind-solar energy generation system*. Paper presented at the International Green Energy Conference (IGEC-IX), 25-28 May 2014, Tianjin, China.